Award Number:
W81XWH-11-2-0218

TITLE:

Identification of New Drug Targets in Multi-Drug Resistant Bacterial Infections

PRINCIPAL INVESTIGATOR:

Andrew M. Gulick, PhD,

CONTRACTING ORGANIZATION:

Hauptman-Woodward Medical Research Institute
Buffalo, Buffalo NY 14260-7016

REPORT DATE: June 2015

TYPE OF REPORT: Final

PREPARED FOR: U.S. Army Medical Research and Materiel Command
Fort Detrick, Maryland 21702-5012

DISTRIBUTION STATEMENT:

☑ Approved for public release; distribution unlimited

REPORT DOCUMENTATION PAGE

Form Approved
OMB No. 0704-0188

1. REPORT DATE *(DD-MM-YYYY)*	2. REPORT DUE	3. DATES COVERED *(From - To)*
June 2015 16/19/2015	Final Final	26 Sept 2011 - 24 March 2015 26Sep2011 - 25Mar2015

4. TITLE AND SUBTITLE

Identification of New Drug Targets in Multi-Drug Resistant Bacterial Infections

Identification of New Drug Targets in Multi-Drug Resistant Bacterial Infections

5a. CONTRACT NUMBER

W81XWH-11-2-0218 W81XWH-11-2-0218

5b. GRANT NUMBER

N/A

5c. PROGRAM ELEMENT NUMBER

6. AUTHOR(S)

Andrew Gulick, Thomas A. Russo, MD, CM, L. Wayne Schultz, PhD, Timothy C. Umland, PhD.

Andrew M. Gulick, PhD
Thomas A. Russo, MD, CM
Timothy C. Umland, PhD

email: gulick@hwi.buffalo.edu

5d. PROJECT NUMBER

5e. TASK NUMBER

5f. WORK UNIT NUMBER

7. PERFORMING ORGANIZATION NAME(S) AND ADDRESS(ES)

Hauptman-Woodward Medical Research Institute, Inc.
700 Ellicott Street Buffalo, NY 14203-1102

Hauptman-Woodward Medical Research Institute Buffalo, Buffalo NY 14260-7016

The Research Foundation for SUNY at Buffalo Buffalo, NY 14260-7016

8. PERFORMING ORGANIZATION REPORT NUMBER

9. SPONSORING/MONITORING AGENCY NAME(S) AND ADDRESS(ES)

U. S. Army Medical Research and Material Command
Fort Detrick, Maryland 21702-5012

U.S. Army Medical Research and Materiel Command Fort Detrick, Maryland 21702-5012

10. SPONSOR/MONITOR'S ACRONYM(S)

11. SPONSORING/MONITORING AGENCY REPORT NUMBER

12. DISTRIBUTION AVAILABILITY STATEMENT

Approved for public release; distribution unlimited

Approved for Public Release; Distribution Unlimited

13. SUPPLEMENTARY NOTES

14. ABSTRACT

A. baumannii is a gram-negative bacillus (GNB) known to cause health-care associated infections. Recently, community-acquired infections, infections in wounded U.S. service members, and infections in residents of long-term care facilities have been reported. The incidence of Acinetobacter infection in all venues is increasing worldwide. The changing epidemiology and incidence of infections due to Acinetobacter establishes it as a pathogen of increasing medical importance. Further, A. baumannii has acquired an alarming number of antimicrobial resistance genes. Resistance to all aminoglycosides, cephalosporins, and fluoroquinolones is common and resistance to carbapenems and beta-lactamase inhibitor combinations is increasing. Safe, reliable agents with predictable activity against A. baumannii are presently non-existent. Improved outcomes will require the development of new therapeutics. We aim to accomplish this is by identifying and examining two biosynthetic pathways as potential antimicrobial targets in A. baumannii. Our investigation of protein targets in A. baumannii includes two goals.

A. baumannii is a gram-negative bacillus (GNB) known to cause health-care associated infections. Recently, community-acquired infections, infections in wounded U.S. service members, and infections in residents of long-term care facilities have been reported. Safe, reliable agents with predictable activity against A. baumannii are presently non-existent. Improved outcomes will require the development of new therapeutics. We aim to accomplish this is by identifying and examining two biosynthetic pathways as potential antimicrobial targets in A. baumannii. Our investigation of protein targets in A. baumannii includes two goals. First, we will validate and evaluate the druggability of enzymes from the chorismate pathway of A. baumannii. Second, we will examine and characterize a novel biosynthetic cluster that encodes non-ribosomal peptide synthetase (NRPS) enzymes that have been demonstrated to be involved in bacterial motility and to be upregulated in response to quorum signaling molecules.

15. SUBJECT TERMS

None Listed

16. SECURITY CLASSIFICATION OF:			17. LIMITATION OF ABSTRACT	18. NUMBER OF PAGES	19a. NAME OF RESPONSIBLE PERSON
a. REPORT	b. ABSTRACT	c. THIS PAGE			USAMRMC
U	U	U	UU	86 86	19b. TELEPONE NUMBER (*Include area code*) 716-898-8600

Table of Contents

Introduction

A. baumannii is a gram-negative bacillus (GNB) known to cause health-care associated infections. Recently, community-acquired infections, infections in wounded U.S. service members, and infections in residents of long-term care facilities have been reported. The incidence of Acinetobacter infection in all venues is increasing worldwide. The changing epidemiology and incidence of infections due to Acinetobacter establishes it as a pathogen of increasing medical importance. Further, *A. baumannii* has acquired an alarming number of antimicrobial resistance genes. Resistance to all aminoglycosides, cephalosporins, and fluoroquinolones is common and resistance to carbapenems and beta-lactamase inhibitors is increasing. Safe reliable agents with predictable activity against *A. baumannii* are presently non-existent. Improved outcomes will require the development of new therapeutics. We aim to accomplish this is by identifying and examining two biosynthetic pathways as potential antimicrobial targets in *A. baumannii*. Our investigation of protein targets in *A. baumannii* includes two goals.

The **first goal** focuses on validating chorismate synthase (CS) and prephenate dehydrogenase/3-phosphoshikimate-1-carboxyvinyl transferase (PD-PSCVT) as therapeutic targets in the *A. baumannii*. We will experimentally establish the prevalence and *in vivo* essentiality of these genes in multiple strains of *A. baumannii*. We will recombinantly express, purify, assay, and structurally characterize the CS and PD-PSCVT enzymes. Finally, we will evaluate the druggability of these proteins through structural and computational methods.

The **second goal** will continue our efforts to characterize the natural product biosynthetic machinery of pathogenic GNB. We will examine a novel biosynthetic cluster that encodes nonribosomal peptide synthetase (NRPS) enzymes that have been demonstrated to be involved in bacterial motility and to be upregulated in response to quorum signaling molecules. We will assay the synthetic enzymes to identify the substrate building blocks, identify the natural product through *in vitro* reconstitution and analysis of mutant strains, and assay the role of this pathway in bacterial growth and virulence.

Body

Goal 1. Validation of Chorismate Biosynthesis as an Essential Target of *A. baumannii*

Our group has developed a novel and efficient approach to identify GNB genes and their protein products that are essential for growth and/or survival during infection, which is then validated via a rat soft-tissue infection model (*1*). This method has established that chorismate synthase (CS) and the bifunctional prephenate dehydrogenase 3-phosphoshikimate-1-carboxyvinyl transferase (PD-PSCVT) are essential proteins for *A. baumannii* infection (Figure 1) (*2*). Furthermore, PSCVT is a proven druggable target in plants (*3*), and the chorismate pathway is absent in humans. Therefore, our hypothesis is that these proteins are potential therapeutic targets in GNB. The object of this goal is to validate these proteins in the chorismate biosynthesis pathway as therapeutic targets.

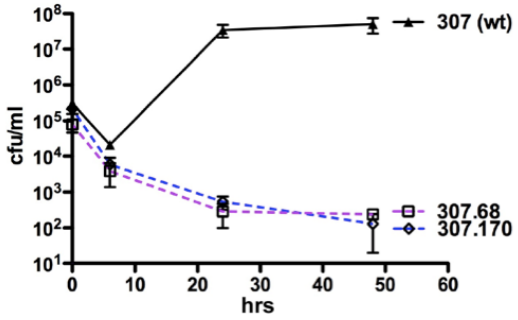

Figure 1. The mutant derivates of the *A. baumannii* wild-type strain AB307-0294, AB307.68 and AB307.170, undergo significant and durable kill in the rat soft tissue infection model. AB307-0294 (wild-type), ABV307.68 (Δpd-pscvt), and AB307.170 (Δcs). Data are mean±s.e.m. for n=3-4 for each time point.

PD-PSCVT and CS are part of the chorismate biosynthetic pathway, which is critical for the synthesis of the folate cofactors, bacterial siderophores, and aromatic amino acids (Figure 2). These enzymes from *A. baumannii* have not been studied. Moreover, inactivation of multiple enzymes within this pathway will decrease the likelihood of the development of resistance, as was done with trimethoprim-sulfamethoxazole for the folate biosynthesis pathway. Toward this end, we have extended our studies below to include shikimate kinase (SK), the enzyme that catalyzes the initial step in the shikimate pathway. A similar metabolic pathway is present in other GNB exhibiting increasing occurrences of drug resistance (e.g., *Pseudomonas aeruginosa*, *Escherichia coli*, Enterobacter species, and *Klebsiella pneumoniae*), and our studies may translate to other GNB.

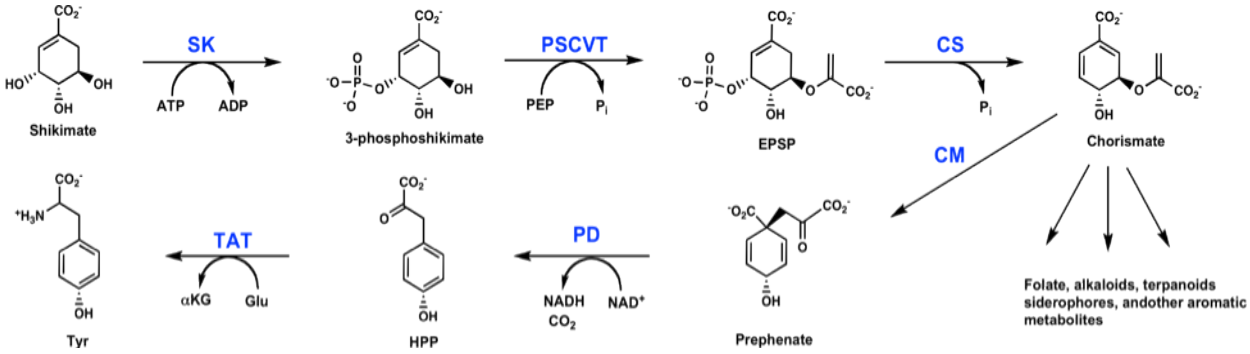

Figure 2. Chorismate biosynthesis. The biochemical steps in the synthesis of chorismate and tyrosine are shown to illustrate the enzymatic activities targeted in Goal 1. SK catalyzes the phosphorylation of the 3'-hydroxyl of shikimate to form shikimate 3-phosphate (S3P). The PSCVT activity of PD-PSCVT couples 3-phosphoshikimate with pyruvate to produce 5-enoylpyruvyl-shikimate-3-phosphate (EPSP). Chorismate synthase (CS) is a lyase that removes the 3-phosphate to produce chorismate, a key building block for the formation of many aromatic compounds. The PD of PD-PSCVT removes a hydride from prephenate to form the aromatized product hydroxyphenylpyruvate (HPP), which then serves as the substrate for tyrosine aminotransferase (TAT), the enzyme that catalyzes the final step in tyrosine synthesis.

Establish the in vivo essentiality of CS and PD-PSCVT in multiple A. baumannii strains.

To generate isogenic mutants in the genes that encode CS and PD-PSCVT required an extension of previously established methods to generate site-specific mutants. Isogenic mutant generation is more facile in strains that have lost their surface polysaccharides, which appears to be the case for a number of ATCC *A. baumannii* strains that are widely studied. For all of our work we utilized clinical isolates that possessed their full repertoire of surface polysaccharides. Although more challenging, results were clinically meaningful. Further, a number of these clinical isolates are resistant to a broad array of antimicrobials. As a result, antimicrobial cassettes that can be used in mutant construction is quite limited. Nonetheless, we were able to overcome these potential obstacles.

During the course of this proposal two methods were successfully developed. The first approach employed a modified conjugative approach. This was used for site-specific gene disruption of *aroA*, the gene encoding PD-PSCVT in *A. baumannii*. The construct we are using to achieve this goal has been generated was described in the September 2013 report. Previously, we generated *aroA* disrupted derivatives of the wild-type strain AB307-0294. Candidates with disruptions in *aroA* in AB714 and AB764 have identified and confirmed.

Next, we combined two recently described approaches. First, we obtained from Dr. Robert Shanks from the University at Pittsburgh a plasmid construct (pMQ310) that contains the hygromycin antimicrobial resistance cassette. This antimicrobial resistant determinant can be used to create constructs in kanamycin-resistant *A. baumannii* strains. Next, we used a one-step PCR-based approach to generate a linear construct that contains the hygromycin cassette flanked by a minimum of 125bp of DNA from the gene to be disrupted as described by Dr. Bryan Davies (*4*). This linear construct was introduced into the *A. baumannii* strain undergoing site-specific allelic exchange via electroporation. The efficiency of recombination was maximized by the previous introduction of the plasmid pMMB67EH (kind gift from Dr. Davies), which contains an *A. baumannii* compatible origin of replication and the *A. baumannii* RecA recombinase that is induced by IPTG. This method has proven to be more time efficient and more successful than the previously developed modified conjugal approach. It has become the standard for isogenic mutant construction in *A. baumannii* in our lab.

***In vitro* phenotypic analysis**

The *in vitro* phenotypic analysis of AB714Δ*aroA* and AB764Δ*aroA* was tested first by growth in minimal media. the growth of 2 possible mutants from each strain was evaluated in AB minimum media (Figure 3).

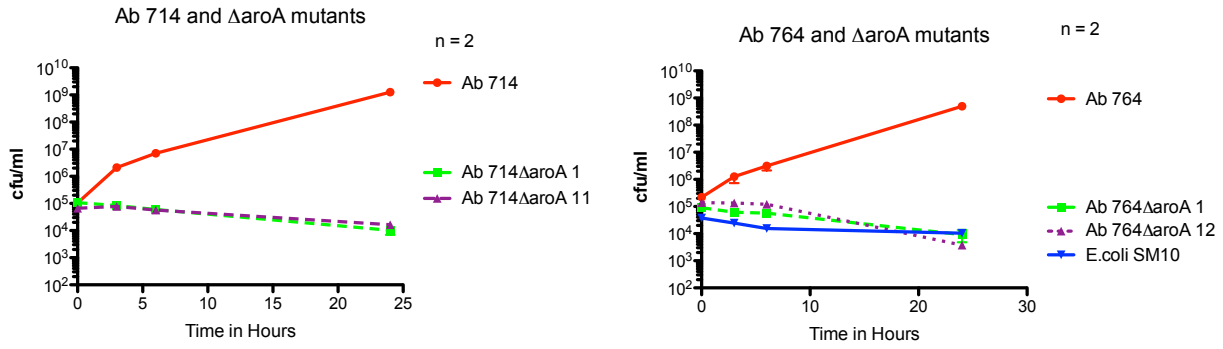

Figure 3. Growth curves of AB714, AB764 wt and respective *aroA* mutants, 2 for each strain.

The mutants all showed decreased growth, as did *E. coli* SM10 which was used as negative control.

***In vivo* phenotypic analysis**

In previous years, we have reported on the *in vivo* phenotypic analysis of the the *aroA* mutants of strain AB307. We continued our studies to demonstrate essentiality in multiple parental background strains. *In vivo* studies were performed using a starting inoculum of 2-4 x 10^8 CFU/mL to compare the growth/survival of AB714 and AB764 with AB714Δ*aroA* and AB764Δ*aroA* respectively in the rat soft-tissue infection/abscess model (Figure 4). Both AB714Δ*aroA* and AB764Δ*aroA* survived less well than their wild-type parents. The difference was greater for AB714Δ*aroA* than AB764Δ*aroA*. However, the decrease in survival, especially for AB764Δ*aroA* was not as great as anticipated. Although the reasons for this are not completely clear, it is likely due to the initial high starting inoculum that was required, since at lower inocula the wild-type parents were significantly cleared. Perhaps at this inoculum the host defenses are somewhat over-whelmed. Nonetheless these data do support our hypothesis that AroA is a viable drug target.

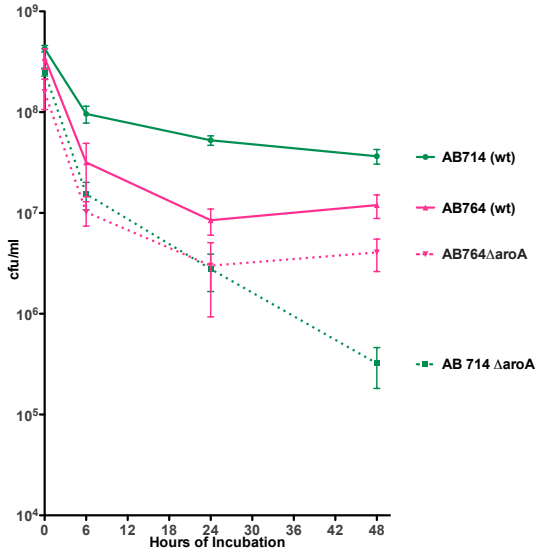

Figure 4. Survival of wild-type and *aroA* mutants *in vivo*.

A. baumannii shikimate kinase is in vivo essential.

The *A. baumannii* genes *aroA* and *aroC* encoding the two enzymes immediately downstream of SK in the chorismate pathway, PSCVT and CS, respectively, were previously determined to be *in vivo* essential. It was hypothesized that *A. baumannii aroK*, encoding *A. baumannii* SK, would be also *in vivo* essential. The *in vivo* growth and survival of the *aroK* deletion mutant AB307Δ*aroK* and its wild-type parent AB307-0294 were compared in the established rat soft tissue infection model (Fig. 5). As expected, the wild-type parent AB307-0294 grew by ~2 logs over 48 hr. By contrast, AB307Δ*aroK* underwent complete kill over the same period. Importantly, AB307Δ*aroK* is capable of growth in rich laboratory media, with an initial growth lag but similar log phase growth and plateau cell density as AB307-0294, thereby excluding a generalized growth defect.

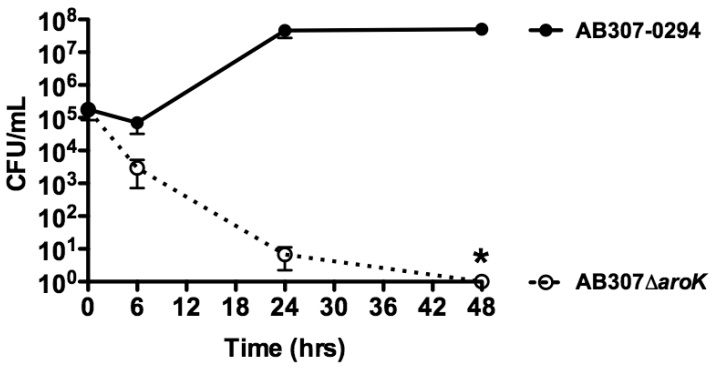

Figure 5. Survival of AB307-0294 wild-type and Δ*aroK* mutant in vivo, using the rat soft tissue

Fragment-based screening of shikimate kinase.

We have completed fragment screening of SK using differential scanning fluorimetry (DSF). DSF is a thermal-denaturation assay that measures the stability of a target protein and is used to measure the subsequent increase in protein melting temperature due to the binding of a ligand to the protein (*5, 6*). The thermal unfolding is detected using a dye (e.g., Sypro Orange) that fluoresces upon interaction with hydrophobic residues, which typically are enriched in the core of a globular protein. As the protein thermally unfolds, more hydrophobic core residues are exposed and the fluorescence of the dye increases and eventually plateaus as the protein is completely unfolded, maximizing the hydrophobic residues exposed to solvent. The temperature gradient is created and the change in fluorescence monitored by a RT-PCR instrument. The data is plotted as fluorescence vs. temperature to define a curve for the thermal unfolding transition, with the mid-point of the unfolding transition defined as a protein's melting temperature (T_m). DSF is useful for rapidly screening molecules for those that cause a positive shift in the melting point, indicating a stabilizing interaction with the protein. This stabilization may be due to a general, non-specific enhancement of a proteins globular fold, or it may be due to a specific binding interaction at a defined site. Both results are useful. Conditions that provide overall protein stabilization promote crystallization, while the identification of small molecules that bind specifically to a protein may serve as initial hits for drug discovery programs.

Thus far, we have screened 500 different compounds and have found 10 compounds that significantly positively shift the melting temp of SK. Analysis of the individual compound structures yielded a compound, pipicolinic acid, with characteristics similar to the native shikimic acid substrate. Both molecules contain a carboxyl substituted ring structure. It is easy to see how pipicolinic acid might be derivatized to create a shikimic acid mimic by adding hydroxyl groups to the ring.

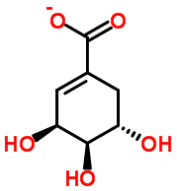

Shikimic acid

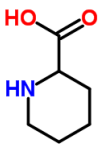

Pipicolinic acid

We have examined the fragments that stabilize and destabilize SK (Table 1). A recent paper indicates that destabilizing fragments are also good starting points for identifying ligands (*7*). Each of these compounds represents a potential starting point for structure based drug design.

Table 1. Chemical Fragments affecting the Tm of Shikimate kinase

Maybridge Library Compound Number	Chemical Name
31	2-piperazin-1-ylaniline
71	(4-methoxyphenyl)(4-piperidyl)methanone hydrochloride
79	2-(1,4-diazepan-1-yl)ethan-1-ol
88	2-Amino-5-hydroxypyrimidine
107	(4-thien-2-yltetrahydropyran-4-yl)methylamine
111	1-(4-acetylpiperidino)ethan-1-one
114	4-(3-chloro-2-pyridinyl)morpholine
123	2-methoxy-6-(2,2,2-trifluoroethoxy)benzonitrile
130	N-pyridin-3-ylacetamide
140	2-(methoxymethyl)-1-methyl-1H-benzimidazole
144	3-hydroxy-1,2-dimethyl-1,4-dihydropyridin-4-one
150	2-phenoxyacetamide
153	5-Methoxybenzimidazole
157	1-Ethyl-2-pyrrolidinone
169	2-chloro-6-methylnicotinamide
180	5-chloro-1,3-dimethyl-1H-pyrazole
185	(2,4-dimethyl-1,3-thiazol-5-yl)methanol
192	3-Cyanopyridine
203	DL-Pipecolinic acid
208	Benzenesulfonamide

Kinetics of shikimate kinase.

The SK shikimate-binding site has been proposed as a more promising target for drug design than its ATP-binding site due to the diminished likelihood of activity towards off-targets. Moreover, the two SK paralogues expressed by *E. coli*, ecSK I (*aroK*-encoded) and ecSK II (*aroL*-encoded), exhibit strikingly different K_m values for shikimate, 20 mM and 200 µM, respectively. Thus, enzyme kinetic parameters for *A. baumannii* SK and its shikimate substrate were determined in an excess of ATP (Fig. 6). Non-linear regression analysis of initial velocity measurements versus shikimate concentration indicated the presence of modest substrate inhibition at high levels of shikimate, with V_{max}=1.07±0.05 µmol s^{-1}, k_{cat}=21.4 s^{-1}, K_m= 147±15 µM, and K_i=4950±925 µM (K_i is the dissociation constant for the substrate inhibited complex), with R^2=0.99. By contrast, non-linear regression analysis assuming conventional Michaelis-Menten kinetics yielded a poor fit to the data (R^2=0.81). The *A. baumannii* SK kinetic parameters are generally comparable to published values for other bacterial SKs, including the *aroL*-encoded dcSK. The key exception is comparison to ecSK I, which exhibits a shikimate K_m that is >100-fold larger, as noted above, and thus may be an atypical member of the family. These kinetic parameters will be valuable to the design and interpretation of fragment library screening assays.

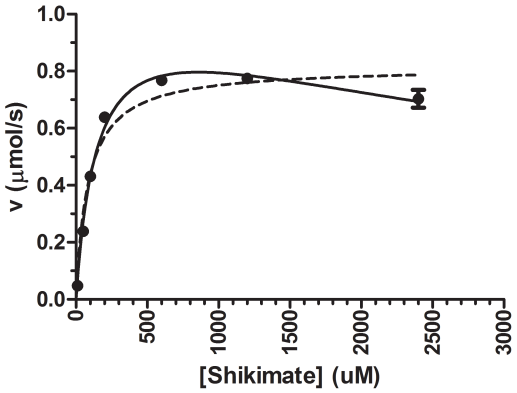

Figure 6. *A. baumannii* SK shikimate kinetics data analysis. Non-linear regression analyses of initial velocity versus shikimate concentration in an excess of ATP using a substrate inhibition model (solid line, R^2=0.99), and assuming conventional Michaelis-Menten kinetics (dashed line, R^2=0.81). The assay was conducted in triplicate.

Shikimate kinase-shikimate-SO_4^{2-} ternary complex crystal structure.

The crystal structure of the *A. baumannii* shikimate kinase-shikimate-SO_4^{2-} ternary complex was determined to 1.91 Å resolution (Fig. 7; R=0.192 and R_{free}=0.235; PDB: 4Y0A). Shikimate is bound to SK in what is expected to be an enzymatically productive pose, and the SO_4^{2-} ion is bound to SK's Walker A (or P-loop) motif, mimicking the interactions typically observed between SK and the β-phosphate of ATP (substrate) or ADP (product). Importantly, this ternary complex displays extensive conformational changes triggered by ligand binding, and which presumably results in *A. baumannii* SK converting to the enzymatically active structure. Specifically, the determined crystal structure is in what is termed the *closed* conformation. This change involves a large movement of the LID domain, estimated to be > 20 Å compared to SK structures in the *open* LID conformation.

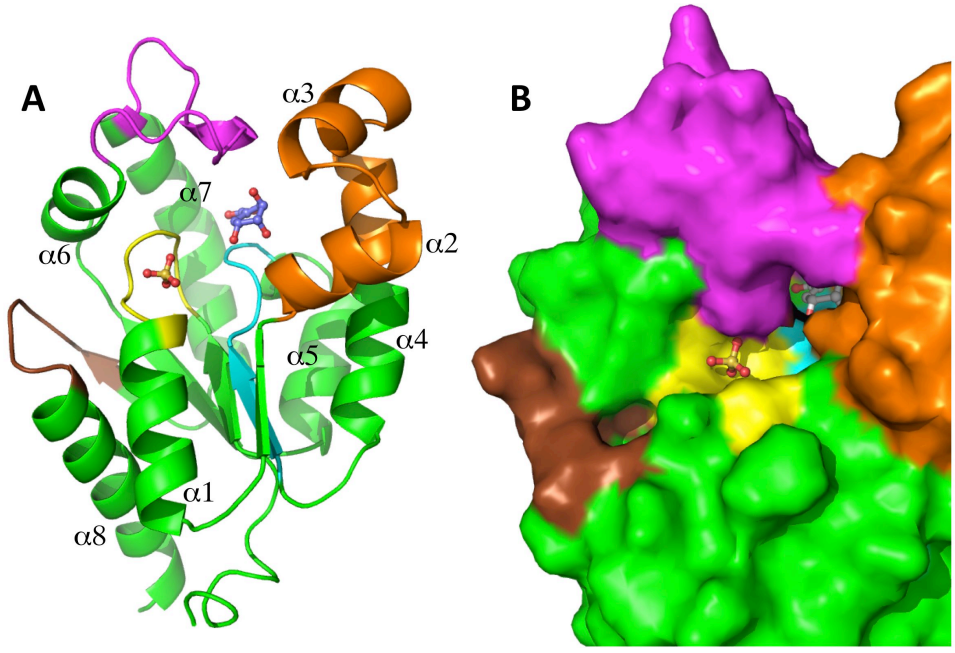

Figure 7. Crystal structure of the *A. baumannii* SK-shikimate-SO_4^{2-} complex. (A) *A. baumannii* SK displayed as a ribbons cartoon, with bound shikimate and the SO_4^{2-} interacting with the P-loop displayed as ball-and-stick models. (B) A surface representation of *A. baumannii* SK zoomed in on the bound ligands. Shikimate is almost completely buried by the closed LID conformation. Important functional motifs are color-coded: Core domain, green; Walker A motif (P-loop), yellow; Walker B motif, cyan; shikimate-binding domain, orange; adenine-binding loop, brown; LID, magenta.

A. baumannii SK exhibits significant sequence diversity compared to the SK crystal structures currently deposited in the PDB, representing a total of nine homologues (eight from prokaryotes and one from plantae). *E. coli* SK I is the closest neighbor at 54% sequence identity over 88% coverage. The remaining SK PDB entries range from 30% to 45% sequence identity to *A. baumannii* SK. Comparison of *A. baumannii* SK with these nine SK homologues reveals only 16 fully conserved residues and 19 additional highly conserved residues (8.5% and 10% of *A. baumannii* SK's 189 residues, respectively). While *A. baumannii* SK exhibits the fold characteristic of SKs, even modest sequence and resulting conformational differences may have significant consequences for antibiotic drug development against bacterial pathogen SKs, especially in the context of the induced-fit conformational changes typical within the SK family. For example, there appears to be no canonical open or closed LID conformation, but rather general structural trends (Fig. 8). In part, this may be due to significant sequence variability in the LID region across SK homologues. The distinctly different observed open LID conformations plus the occurrence of partially or fully disordered LIDs indicate high mobility of this region in the absence of both shikimate and ATP/ADP. It is not surprising that there may not be a consensus open LID conformation across the SK family, as the purpose of the open LID is to allow ingress or egress from the ligand binding sites. LIDs in the closed form display less severe structural differences due to the functional requirement of shielding the shikimate-binding site plus participating in forming the ATP-binding cleft. The most conserved structural element of the closed LID is the arginine (R134 in *A. baumannii* SK) positioned such that its guanidino group interacts with both the β-phosphate of ATP or ADP (or SO_4^{2-} mimicking phosphate) and shikimate. Similar LID conformations (e.g., *A. baumannii* SK and *M. tuberculosis* SK, PDB: 2IYQ) still display structural diversity, with corresponding C^{α} atoms of superimposed LIDs differing by up to 3.5 Å (*A. baumannii* SK V139 and *M. tuberculosis* SK G122) while being most similar (0.32 Å) at the conserved and catalytically important arginine (*A. baumannii* SK R134 and *M. tuberculosis* SK R117). By comparison, the distance between theses same two arginine C^{α} is 24.5 Å for *A. baumannii* SK superimposed upon *M. tuberculosis* SK with an open LID (PDB: 2IYU). Thus, the determination of the *A. baumannii* SK crystal structure in a mechanistically important conformation provides a platform for structure-based development of (a) *A. baumannii*-specific SK inhibitors or antibiotics, and (b) broad-spectrum SK inhibitors or antibiotics, for which binding-site differences across SK homologues must be accommodated.

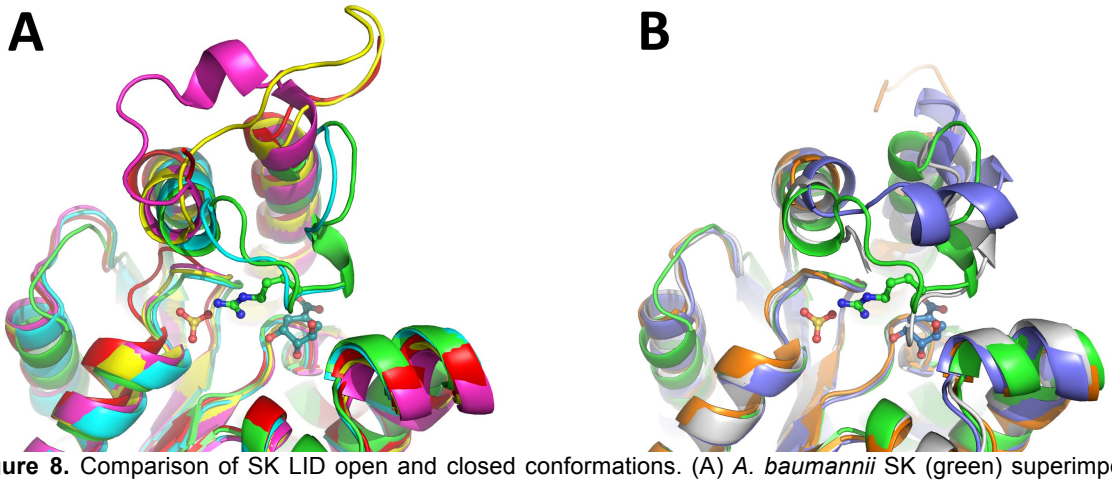

Figure 8. Comparison of SK LID open and closed conformations. (A) *A. baumannii* SK (green) superimposed with selected *M. tuberculosis* SK structures, illustrating induced-fit conformation differences: 2IYQ, cyan (closed); 2IYU, magenta (open); 2IYW, yellow (open); 2G1J, red (open, disordered LID). (B) *A. baumannii* SK (green) superimposed with selected *H. pylori* SK structures: 1ZUI, light grey (closed with partially disordered LID); 3N2E, blue (partially closed); 3HR7, orange (open, disordered LID). abSK R134 plus the abSK ligands (shikimate and SO_4^{2-} interacting with the P-loop) are displayed as balls-and-sticks.

PSCVT stability and substrate binding assays.

In preparation for screening *A. baumannii* PSCVT with a drug fragment library, we examined the stability of PSCVT by differential scanning fluorimetry (DSF), which allows for the rapid screening of individual compounds and detects interactions with the target protein by monitoring changes in the protein melting temperature.

Condition	Run 1	Run 2
PSCVT+buffer	53.876	53.848
PSCVT+H2O	53.102	52.242
PSCVT+0.5mM S3P	59.313	59.271
PSCVT+2.5mM S3P	61.728	61.829
PSCVT+0.5mM SA	53.724	53.739
PSCVT+2.5mM SA	52.913	53.236
PSCVT+0.5mM S3P+0.1mM GLP	59.913	59.806
PSCVT+0.5mM S3P+1mM GLP	60.848	60.807
PSCVT+2.5mM S3P+0.1mM GLP	63.325	62.131
PSCVT+2.5mM S3P+1mM GLP	63.201	62.701
PSCVT+5%DMSO	53.778	54.062
PSCVT+10%DMSO	52.850	52.771

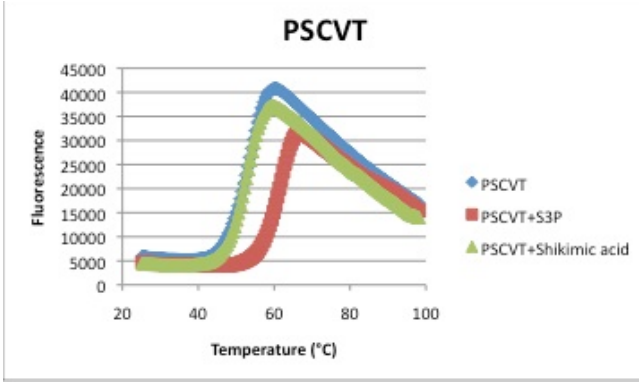

Figure 9. Table of T_m values for the DSF of PSCVT and graph showing the shift in T_m of PSCVT (blue) when the substrate shikimate 3-phosphate is added (red) versus the minimal T_m shift in the presence of shikimic acid control (green), demonstrating the ability of the assay to distinguish ligand binding events.

A conformational change from an open form of PSCVT to a closed form occurs during substrate binding. We hypothesized that in the closed, substrate-bound state, PSCVT will be more thermostable. Using DSF (Figure 9), the midpoint of the thermal melting curve (T_m) of the unliganded PSCVT was determined to be 53ºC and the addition of the substrate, shikimate 3-phosphate (S3P), shifts the T_m up to 61.7ºC. This shift of almost 8ºC indicates that in the presence of substrate, PSCVT is more thermostable. As a control, addition of shikimate did not result in a shift of the T_m indicating very weak or no binding. According to the kinetics assay of PSCVT, *A. baumannii* PSCVT is insensitive to the inhibitor glyphosate (GLP). When examined by DSF, the addition of GLP results in a minimal shift in T_m supporting that GLP does not bind to PSCVT in the presence of S3P. In addition, the stability of PSCVT was unchanged in the presence of 5% or 10% DMSO, a solute for the fragment library. With the significant change in T_m occurring with the addition of substrate, we were able to easily detect the binding of drug fragments to the active site of PSCVT.

Fragment-based screening of PSCVT.

Analysis and screening of PSCVT with the 500 compound fragment library by differential scanning fluorimetry (DSF) was completed. Several fragments were identified that stabilized or destabilized PSCVT. Interestingly, a single hit, compound #173 was found that stabilized both SK and PSCVT (Figure 10). Our goal has been to identify fragments that will bind to multiple enzymes in the same pathway. By targeting multiple enzymes in the same pathway with a single drug, we hope to reduce development of resistance. Future studies may include determining crystal structures of SK and PSCVT in complex with #173 to identify the important interactions to be exploited in the future hit-to-lead optimization cycle of a multi-target agent.

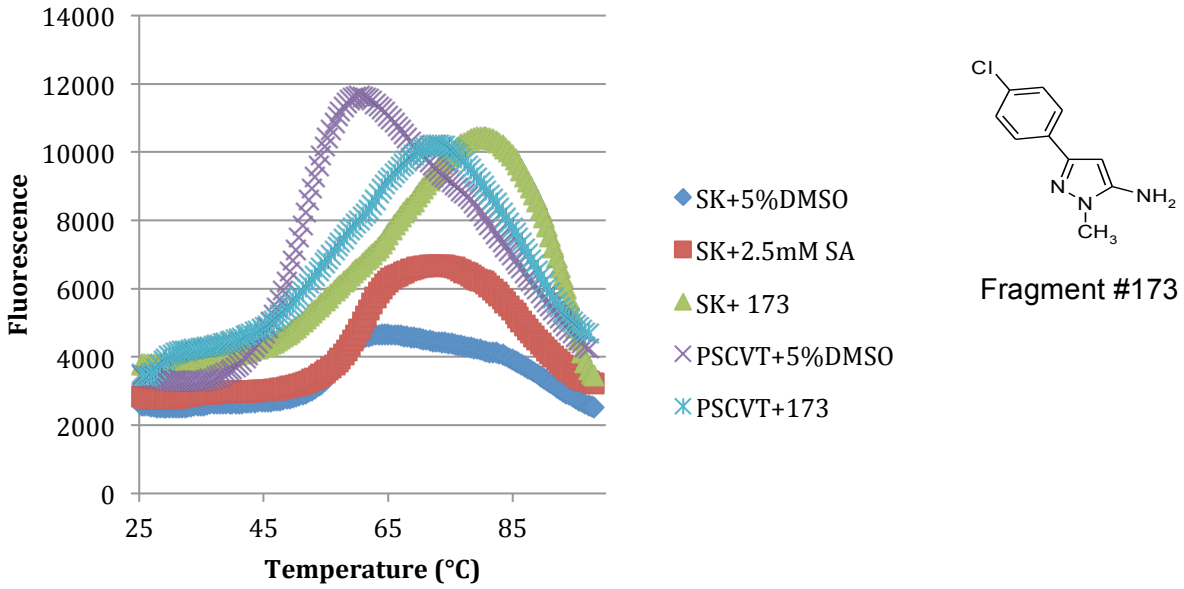

Figure 10. DSF experiments using Fragment 173 show stabilization of both *A. baumannii* SK and PSCVT. Addition of Fragment 173 to SK results in a 10.8°C shift in the Tm (dark blue to green curve). Addition of Fragment 173 to PSCVT also results in a 14.1°C shift in the Tm (purple to cyan curve). Fragment 173 stabilizes both proteins likely indicating that it is mimicking the same structure interactions in each enzyme active site.

The following compounds were discovered to increase the Tm of PSCVT and represent additional starting points for structure based drug design (Table 2).

Table 2. Compounds that impact PSCVT melting temperature

Compound	Δ Tm (°C)
Indole-5-carboxylic acid	4.03
2-Spiro(6-oxopiperidin-2-yl)-1,3,3,5-tetramethylindoline	3.11
Imidazo[1,2-a]pyridine-2-carboxylic acid hydrate	1.5
'3-[(1,1-diethylprop-2-ynyl)amino]thiophene-2-carboxylic acid	1.3

PSCVT crystal structure.

The crystal structure of *A. baumannii* PSCVT residues 301-756 ($PSCVT^{301-756}$) has been determined to 2.37 Å resolution (R=0.183 and R_{free}=0.229). We pursued the crystallization of the individual PSCVT domain from the PD-PSCVT protein as a solution to the poor crystals formed by the full-length wild-type fusion protein. PSCVT has been shown to occupy an open conformation in the absence of substrate (Agrobacterium sp. CP4 PSCVT; PDB 2GG4) and a closed conformation when a substrate-mimic (shikimate) and inhibitor (glyphosate) are bound (*E. coli* PSCVT; PDB 2AAY). The open to closed conformation transition occurs through a hinge between the N- and C-terminal domains. The catalytic active site is positioned between the two domains, with residues from both contributing to form the substrate binding sites. Our *A. baumannii* PSCVT structure exhibits an open conformation (Fig. 11). For the purpose of drug screening, the open conformation is ideal because the active site available to bind candidate ligands. Additionally, an inhibitor that locks PSCVT into the open conformation will prevent formation of the catalytically active form of the enzyme.

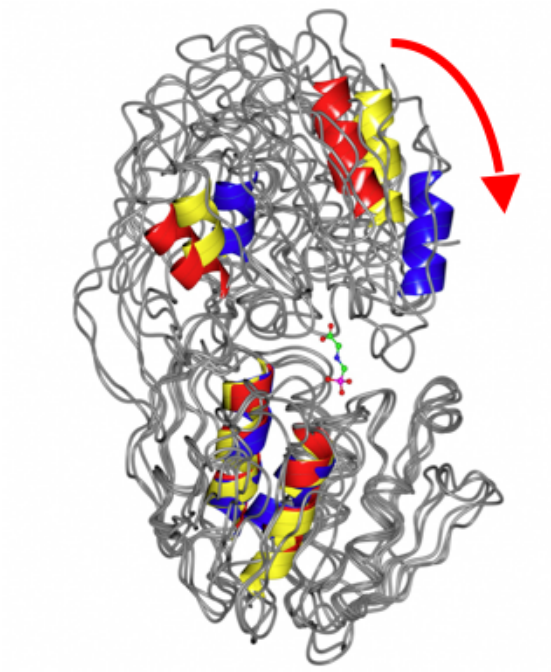

Figure 11.The structure of the individual domain of PSCVT is in the open conformation. Superposition of the N-terminal domain (residues 314-500) of *A. baumannii* PSCVT (yellow helices) with Agrobacterium sp. CP4 PSCVT in the open conformation (red helices; PDB 2GG4) and *E. coli* PSCVT in the closed ligand bound conformation (blue helices; PDB 2AAY). The red arrow indicates the motion of the C-terminal domain relative to the N-terminal domain (residues 501-756 in *A. baumannii* PSCVT) upon transition to the closed conformation.

CS stability and substrate binding assays.

Analogous to PSCVT, we implemented DSF to characterize the effect different buffer components have on the thermostability of *A. baumannii* CS. In particular, *A. baumannii* CS proved recalcitrant to the formation of crystals that diffracted X-rays to high resolution. While large (>0.2 mm per side), visually well-formed CS crystals were repeatedly obtained, none were identified that diffracted X-rays to greater than ~4 Å resolution. The presence of large but poorly diffracting crystals suggested micro-heterogeneity within the crystal lattice, possibly caused by regions within CS capable of adopting several different conformations. Small molecule(s) that increase CS thermostability may result in a reduction of such conformational micro-heterogeneity. DSF on baseline conditions (CS at 1.0 mg/ml in 20 mM Hepes, 100 mM NaCl, pH 7.5) was conducted. A well-formed and highly reproducible melting curve was obtained for CS under these conditions, with a T_m of 56.4 C (average of three measurements) (Figure 12). Thus, CS is an excellent candidate for both identifying chemical additives and buffer conditions that further stabilize the enzyme's structure, and for screening libraries of small molecules for potential inhibitors.

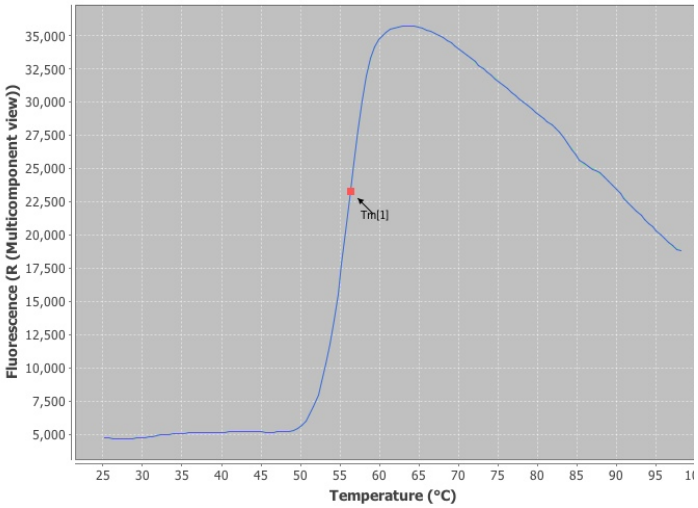

Figure 12. DSF on CS sample at baseline buffer conditions. Melting curve derived from DSF on CS at 1 mg/ml in 20 mM Hepes, 100 mM NaCl, pH 7.5. The melting temperature (T_m; red dot) is 56.4 °C (average of three runs).

A screen was conducted over 96 different buffer additives, and determined three additives resulted in a significant increase of CS's thermal T_m, indicating stabilization. Interestingly, one of the stabilizing additives is phosphate. CS catalyzes the conversion of 5-enolpyruvylshikimate-3-phosphate to chorismate, with the release of phosphate. A possibility is that phosphate stabilizes CS by binding to the portion of the substrate-binding pocket that interacts with the substrate's phosphate moiety.

Table 3. Stabilizing compounds for Chorismate Synthase.

Additive (50 mM)	**Tm (°C)**
None (baseline)	56.4
Betaine	58.3
Sodium phosphate	60.8
Trimethylamine N-oxide	62.4

We then investigated if phosphate specifically binds CS using the DSF assay and varying phosphate concentrations. If CS stabilization was due to a tight, specific binding interaction with phosphate, then the stabilization effect should plateau at relatively low phosphate concentrations (i.e., saturation of the binding site). However, our DSF assay indicates that CS undergoes increasing thermal stabilization as the phosphate concentration increases to high levels, with an increase in Tm of ~1.5 °C per 100 mM phosphate added (max. concentration tested: 400 mM). Thus, CS stabilization by phosphate is likely due primarily to a non-specific interaction or multiple low affinity binding sites rather than due to a single (or relatively few) high affinity binding event(s). We predicted that both betaine and trimethylamine N-oxide stabilized CS through non-specific interactions, as both of these chemicals are known to exhibit protein stabilization effects. We confirmed this prediction using DSF and varied concentrations of each additive, similar to above. These results will be useful for modifying CS storage buffer conditions in order to stabilize the enzyme for both structural and enzyme activity studies.

Future studies may include screening *A. baumannii* CS with a library of small molecules that possess drug-like aspects using DSF to identify potential lead molecules for the development of CS inhibitors.

CS druggability assessment.

A. baumannii CS was assessed for its *druggability* potential. This assessment is important as many promising therapeutic targets lack surface features (e.g., a sufficiently deep binding cleft

lined with a mixture of hydrophobic and hydrophilic amino acid residues) necessary for conferring high affinity, high specificity binding interactions with small molecule drug-like compounds. We took a computational approach for a predictive assessment of *A. baumannii* CS. Specifically, a 3-D structure of *A. baumannii* CS was created through homology modeling using the crystal structure of *Helicobacter pylori* CS as a template (PDB 1UM0; 1.95 Å resolution; 44% amino acid sequence identity). The core fold of CS, including the region around the active and the FMN cofactor binding sites, is highly conserved across prokaryotic orthologues, and so the confidence level for the modeling of the core structure is high (Figure 13).

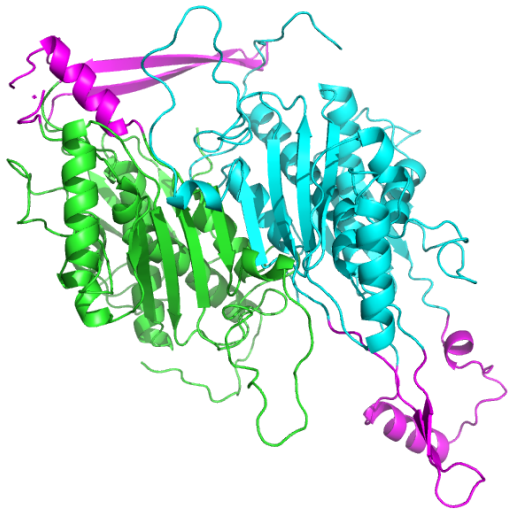

Figure 13. The 3-D structure of *A. baumannii* CS based upon homology modeling. A homodimer is displayed, with green and cyan representing the individual chains. The magenta colored regions indicate extended loops that are modeled with low confidence, as these regions were absent from the *H. pylori* CS template structure. The lower confidence model regions lie outside of the active and cofactor sites.

Next, the *A. baumannii* CS homology model was subjected to a small molecule *in silico* fragment probe docking analysis, as implemented in FTMAP (*8*). The purpose was to identify small molecule ligand *hotspots* that may serve as putative drug binding sites. Specifically, fragment probes are very small (typically ≤ 150 Da) and chemically simple organic compounds. The rationale for the docking exercise is to perform quickly and efficiently a whole protein analysis for likely druggable sites rather than to predict a specific drug-protein target interaction. For the former case a model will typically yield acceptable results, while in the later case the use of a homology model will likely provide unreliable results. A small set of fragment probes is used to scan the entire protein target surface to identify regions predicted form energetically favorable interactions with each fragment in the test set. Predicted binding interactions are then clustered and then ranked based on the average interaction energy. Protein surface regions predicted to bind several probe clusters are then predicted to be binding hotspots that should be further explore for drug discovery. Importantly, since the entire target protein's surface is analyzed, there is not an a priori bias towards a specific target surface region to be druggable. The results for the *A. baumannii* CS target indicated four clusters of probe molecules binding at the neighboring cofactor and active sites (Figure 14). These results strongly suggest that this region of *A. baumannii* CS is capable of binding drug-like molecules.

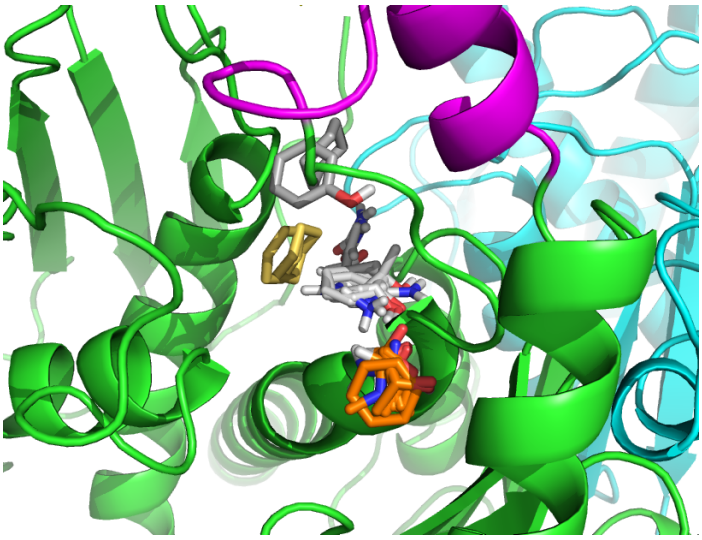

Figure 14. Results of fragment probes computationally docked to *A. baumannii* CS. In total, four probe clusters represented as stick molecules) were identified adjacent to one another in the target's cofactor and active sites. These four probe clusters are ranked in the top ten energetically. The binding pocket is in the core of the model (green), and does not contain portions of the protein modeled with a lower confidence level (magenta).

Goal 2. Characterization of a Novel NRPS Biosynthetic Cluster

The nonribosomal peptide synthetases (NRPSs) are a family of large, modular enzymes that produce peptides with important activities (*9, 10*). NRPS products are diverse, incorporating as many as 100 different substrate amino acids and exhibiting additional chemical modifications including glycosylations, cyclizations, and halogenations. The products play important roles in microbial pathogenesis, including nutrient acquisition, intercellular communication, and exhibiting antibiotic activity. While novel NRPS natural products have been identified in soil and marine bacterial species, there has been limited effort to characterize the small NRPS clusters that are present in many human pathogens.

We identified an operon in *A. baumannii* to expand our investigation into NRPS synthesis of natural products in pathogenic bacteria. The operon encompasses eight genes that are co-transcribed (Table 4, blue). Upstream of the synthetic operon is an acyl-HSL synthase, an enzyme involved in synthesis of quorum signaling homoserine lactones. Immediately upstream of these genes encoding the synthetic operon is a homolog of the *P. aeruginosa* PhzR/LasR protein that is involved in transcriptional regulation in response to quorum signaling (*11*). The ABBFA_003407 regulator likely is responsible for the quorum signal-dependent regulation of this operon (*12*).

Within this NRPS operon are eight proteins encoded by the genes ABBFA_003406 through ABBFA_003399. In the related *A. baumannii* strains, the genes of this NRPS cluster are annotated as A1S_0112 through A1S_0119. ABBFA_003402, is a RND transporter that is likely involved in efflux of the natural product. ABBFA_003399, is a phosphopantetheinyl transferase (*13*), an enzyme that post-translationally modifies the acyl carrier protein domains of two of the NRPS proteins to convert from their inactive *apo* to the active *holo* state. The remaining six proteins therefore form the synthetic operon and are the focus of our studies.

Table 4. The targeted ABBFA_003406 NRPS operon of *A. baumannii*.

	Function	AB307-0294	Status
1	Acyl-HSL Synthase (*abaI* or *cepI*)	ABBFA_003409	
2	Hypothetical	ABBFA_003408	
3	PhzR-type Regulator	ABBFA_003407	
4	NRPS (Free-standing Adenylation Domain)	ABBFA_003406	Cloned, Purified, Biochemically analyzed
5	Acyl-CoA dehydrogenase	ABBFA_003405	Cloned, expressed
6	NRPS (Free-standing Carrier Protein)	ABBFA_003404	Structure Determined and Published
7	NRPS (Condensation-Adenylation-PCP-Thioesterase)	ABBFA_003403	Cloned, Purified, Biochemically Analyzed, Crystals, Dataset to 3.0Å
8	RND Transporter	ABBFA_003402	Cloned
9	Hypothetical	ABBFA_003401	Cloned
10	Bifunctional Dehydratase / esterase	ABBFA_003400	Cloned, Expressed
11	Phosphopantetheinyl transferase (PPTase)	ABBFA_003399	Not targeted at this time

Genes are numbered consecutively. The proteins of the operon of interest are listed in blue. The upstream genes that are likely to be involved in regulation are included in black. The presumed function is listed based on sequence homology. Gene and Protein names from two strains are reported. In the ATCC17978 strain, the gene names are A1S_0109 through A1S_0119.

The specific objectives of this goal of the project are to a) identify the natural product of this biosynthetic cluster through a combination of metabolic labeling experiments, *in vitro* reconstitution with specific enzymes and known substrates, and examination of culture supernatents from genetic deletion strains of *A. baumannii*, b) examine the substrate specificity of the two adenylating enzymes that serve to incorporate the building blocks into the natural product, and c) examine the contribution of this product to growth and virulence properties of *A. baumannii* through the generation of mutant strains and analysis in multiple growth environments.

To better organize the results, these three objectives are presented out of order, starting with objective b, the identification of the substrate building blocks. We will then describe the analysis of the genetic knockout strains, objective c. Finally, we will present our structural and functional results directed toward the characterization fo the enzymes involved in this uncharacterized NRPS pathway.

Objective 2B. Functional Studies of the NRPS Proteins ABBFA_003403, ABBFA_003404, and ABBFA_03406 and identification of the substrate building blocks.

NRPS proteins are multi-domain enzymes that use a modular strategy to catalyze synthesis of important peptide molecules. These enzymes use a peptidyl carrier protein (PCP) that is covalently loaded with the substrate amino acid through the activity of an adenylation domain. The ABBFA_03406-ABBFA_003399 operon contains two carrier protein domains and two adenylation domains. We hypothesized that the free-standing carrier ABBFA_003404 would be covalently loaded by the ABBFA_003406 adenylation domain. The structure of the ABBFA_003404 carrier protein was determined.

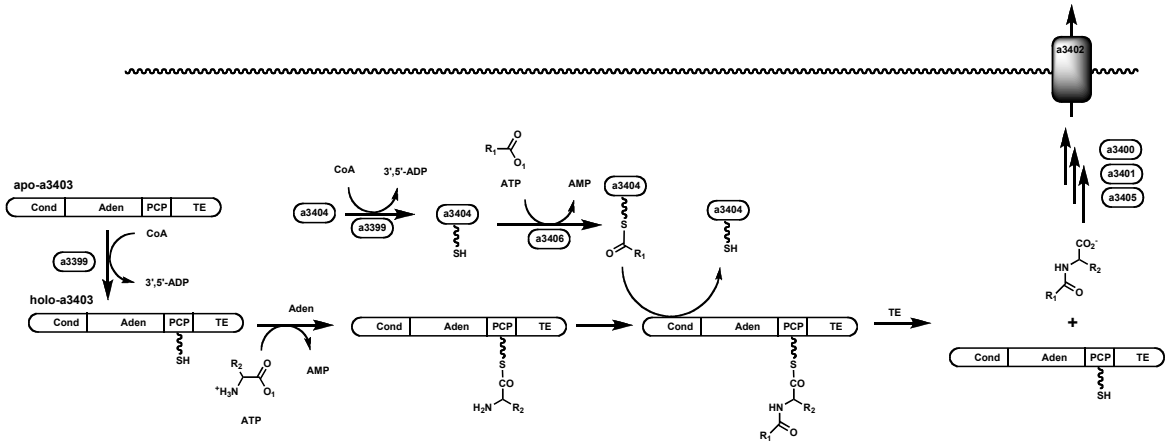

Figure 15. Biosynthetic steps of the NRPS cluster. The activities of ABBFA_003399, ABBFA_003402, ABBFA_003403, ABBFA_003404, and ABBFA_003406 can be confidently assigned on the basis of sequence homology to well-characterized NRPS clusters.

As an initial step toward characterizing this pathway, we identified the amino acids that were activated by the two adenylation domains. A standard assay that we have performed many times in the lab detects the reversible incorporation of radiolabeled pyrophosphate into ATP. We probed each protein with all 20 proteinogenic amino acids, as well as several other representative substrates to examine if a preferred non-amino acid might be used. We demonstrated that glycine is the preferred substrate of the ABBFA_003403 adenylation domain. As shown in the proposed biosynthetic pathway (Figure 15), this identifies the substrate for the second NRPS module suggesting R_2 is a hydrogen atom. The results of the pyrophosphate exchanges assay with ABBFA_003406, the freestanding adenylation domain, were not as conclusive. Activity was observed with threonine; however the enzyme showed marginal activity with a number of other substrates, including valine and lysine. Additional non-proteinogenic and fatty acids were also included in the assay.

Objective 2C. Analysis of mutant *A. baumannii* strains.

Rather and colleagues (*12*) identified that this NRPS pathway is involved in motility in *A. baumannii* strains when grown on low percentage agar. The exact morphology of the colony was dependent on both the *A. baumannii* strain as well as the source of the agar, with observations of outward growth of concentric rings, often containing small projections or “a manner that resembled branching tentacles”. A directed assessment of the involvement of the *pilT* and *abaI* genes demonstrated the involvement of pilus formation and quorum signaling as playing a role in this *A. baumannii* motility. Random mutants for other genes that played a role in motility identified seven genes that, upon disruption, resulted in decreases in motility to values that were 20-70% of the wild-type (as measured by the radius of colony growth). Among the seven genes were the homologs of ABBFA_003405 and ABBFA_003403, two genes of the NRPS operon that we are studying. The authors also noted that this operon was transcriptionally activated by the *A. baumannii* quorum signal, 3-hydroxy-dodecanoyl-homoserine lactone (3OH-C_{12}-HSL).

A second report demonstrates a potential role of this NRPS pathway in *A. baumannii* biofilms (*14*). In this study, it was shown through whole transcriptome analysis that this NRPS operon is among the most highly differentially regulated, with very low–and in one case, no–expression in planktonic or stationary phase cells compared with cells from a biofilm. Additionally, a mutation in the ABBFA_003404 gene, encoding the peptidyl carrier protein that we have structurally characterized, resulted in compromised biofilm formation in a quantitative assay.

Five independent studies support a connection between this operon and motility. First, a directed search for genes associated with surface-associated motility showed *pilT*, encoding an ATPase involved in pilus retraction, and *abaI*, an acyl-HSL synthase, are both involved in motility (*12*). A transposon mutagenesis screen was then performed to find additional genes that contribute to motility and identified the NRPS operon (*12*). Second, five hyper-motile strains were identified and sequenced to identify the cause of this increased surface-motility (*15*). These strains contained a disruption of the histone-like nucleoid structuring (H-NS) global regulator. Transcriptome analysis of these *hns* strains identified several operons that were up-regulated by 5- to 20-fold, including those encoding a Type IV secretion system and type I pili. The most highly up-regulated genes, however, were the NRPS cluster that is the focus of our work, which exhibit at 50- to 700-fold increase in transcriptional level (*15*). Third, streptomycin has been shown to inhibit motility but not planktonic growth and to down-regulate the a3406 operon via inhibition of the quorum signaling pathway (*16*). Fourth, transcriptome analysis compared *A. baumannii* grown in a biofilm to planktonic cells in either exponential or stationary phase of growth. Once again, the most highly over-expressed genes in the biofilm cultures were the genes that encode this NRPS cluster. Finally, the a3406 operon is positively regulated by acyl-HSLs (*12*) and acyl-HSL agonists likewise inhibit surface-associated motility (*17*).

These results tied the natural product from the ABBFA_003406 NRPS cluster to motility and biofilm formation, two phenotypes that are associated with virulence in gram negative bacteria (*18, 19*). Additionally, it allows us to develop a bioassay to use to isolate the active molecule that is produced by the ABBFA_003406 NRPS cluster. We obtained the M2 (wild-type), M2-2, and M2-11 strains from Dr. Rather and have used them to develop this assay. The M2-2 and M2-11 strains harbor disruptions in ABBFA_003405 and ABBFA_003403, respectively. (Note that the homologs of these genes in the ATCC 17978 strain used by both Clemmer (*12*) and Rumbo-Feal (*14*) are A1S_0113 and A1S_0115, respectively).

We also obtained from the *A. baumannii* transposon mutagenesis collection that Dr. Russo had constructed a mutant in the H-NS gene in the strain AB307-0294 background. This mutant strain overexpresses the NRPS cluster by 50- to 700-fold (*15*).

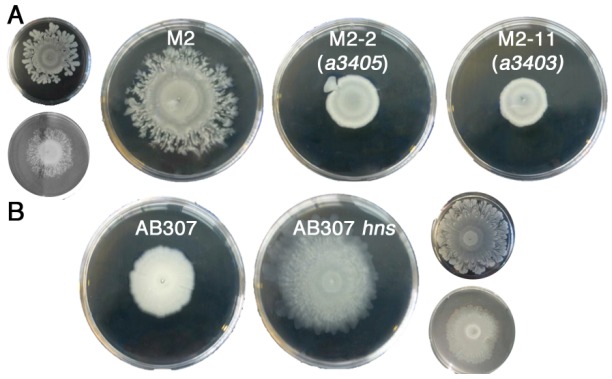

Figure 16. Surface-associated motility of *A. baumannii* mutants. A. Wild-type M2 strain shows branched motility, while M2-2 and M2-11 mutants show dramatically reduced motility. B. Wild-type AB307 strain shows less branching than M2, while the *hns* mutant shows increased surface-associated motility. Small images demonstrate alternate phenotypes of the closest plate (M2 top and *hns* bottom).

Acquisition of these mutant strains enabled confirmation and the development of tools to assay for the presence of this potential signaling molecule. We present below our results with two series of cell lines. First, analysis of the M2, M2-2, and M2-11 cell lines demonstrates that surface-associated motility is dramatically reduced in the strains that are disrupted in the NRPS operon. We additionally investigated the motility of the *hns* mutant, albeit in a different parental

background, the *A. baumannii* AB307-0294 (*20*). The AB307 parental strain exhibits less surface-associated motility than the wild-type M2 strain (Figure 16). The motility, however, is greatly increased in the *hns* mutant. Growth rates of all strains in liquid culture are similar, although both wild-type strains reach a slightly higher saturation density.

Our working hypothesis is that the *hns* mutant strain would overproduce the NRPS peptide product that could induce motility in the M2-2 and M2-11 mutant strains. Therefore, a series of experiments was performed to isolate media from liquid and agar cultures of the *hns* strain and use that to supplement the NRPS defective mutants. We used media as isolated and additionally attempted organic extractions or other limited fractionation steps. To date, we have been unable to identify conditions that allowed us to isolate an active fraction that could chemically complement to induce motility in the M2-2 or M2-11 strains.

Possible explanations for this include the low concentration of the product in culture media. We have attempted to circumvent this by concentrating the culture media via evaporation and resuspending the dried material in a low volume. Alternately, the product may simply not be very stable or may not be exported out of the cell at all. We continue to investigate the possible explanation for this and plans are in place to make the NRPS disruption mutants in the same AB307-0294 parental strain so that we can compare the different cell lines in the same parental background.

Objective 2A. Identification of the natural product through biochemical reconstitution.

As described in the prior section, we have been as yet unable to identify conditions that suggest the production of the natural product to enable isolation and characterization from culture supernatents. We therefore turned to biochemical reconstitution with the available enzymes. Based on other NRPS pathways, the proposed biochemical pathway (Figure 15) would involve activation of the substrate building blocks by the adenylation domains of ABBFA_003403 and ABBFA_003406. As determined in objective 2B, the enzymes each load threonine (ABBFA_003406) and glycine (ABBFA_003403). We therefore anticipate a two step reaction to be catalyzed by the freestanding ABBFA_003406. In the first step, the threonine would be adenylated through a reaction with ATP. The threonyl-AMP acid anhydride would then serve as a substrate for a second reaction in which the threonine would be transferred to the pantetheine cofactor of the freestanding ABBFA_003404.

We therefore used mass spectrometry to test if threonine once activated by the adenylating activity of ABBFA_003406 becomes covalently loaded onto the pantetheine cofactor of ABBFFA_003404. Unfortunately, we were unable to detect the transfer of threonine onto the carrier protein cofactor.

NRPS carrier proteins are produced as *apo* proteins that are converted post-translationally to a *holo* form via the covalent addition of the phosphopantetheine cofactor, derived from CoA. The thiol from this cofactor is expected to be loaded with threonine, forming a thioester linkage. The ABBFA_003404 carrier protein is produced with a histidine-tag, used for purification, that is removed via cleavage with the TEV protease. During tag cleavage, the protein is simultaneously converted to the *holo* form using a promiscuous phosphopantetheinyl transferase.

The molecular weight of the untagged protein is 9843.15 Da. Addition of the pantetheine cofactor from CoA results in an increase in mass of 341 Da. Further addition of the threonine moiety results in an increase in mass of an additional 73 Da.

Mass spectrometry (Figure 17) showed two peaks that were present in our sample of ABBFA_003404 that was pantetheinylated and subsequently reacted with the adenylation domain ABBFA_003406, along with ATP and threonine. Deconvoluted mass patterns were observed for protein peaks at 10184 Da and 10949 Da. The smaller mass accurately represents

the mass of the *holo*-carrier protein domain. The larger mass represents an increase in 765 Da. Coenzyme A has a molecular weight of 764.5 Da, so this likely represents a covalent or non-covalent adduct from the pantetheinylation step.

MW of Tagged protein, lacking the N-terminal methionine is:

```
         10         20         30         40         50         60
GSSHHHHHSS GENLYFQGHM NKDKAYWSAI IRTLVAKEMR VEPETIDPDQ KFTSYGLDSI
         70         80         90        100
VALSVSGDLE DLTKLELEPT LLWDYPTINA LAEYLVSELQ QGVAS
```

Theoretical pI/Mw: 4.87 / 11786.13

MW of the Protein left after cleavage with TEV protease is:

Theoretical pI/Mw (average) for the user-entered sequence:

```
         10         20         30         40         50         60
GHMNKDKAYW SAIIRTLVAK EMRVEPETID PDQKFTSYGL DSIVALSVSG DLEDLTKLEL
         70         80
EPTLLWDYPT INALAEYLVS ELQQGVAS
```

Theoretical pI/Mw: 4.34 / 9843.15

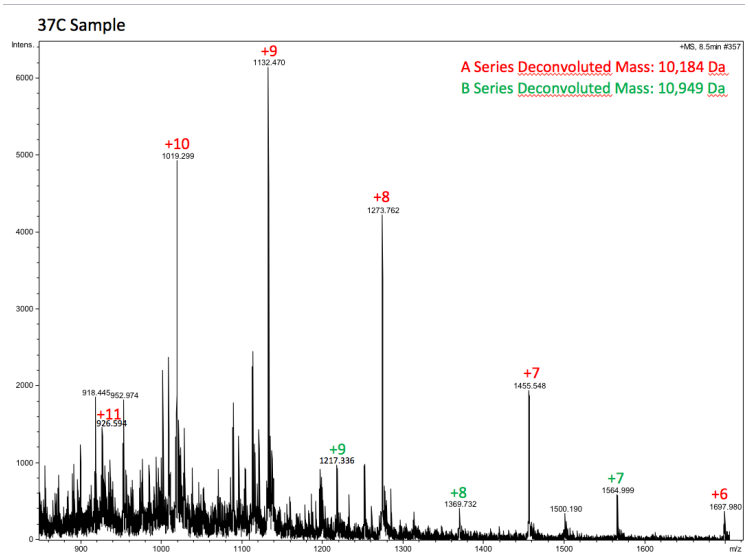

Figure 17. Mass spectrometric analysis of the ABBFA_003404 carrier protein upon incubation with the adenylating enzyme ABBFA_003406 and substrates ATP and threonine.

We did not see a mass increase that represents loading with threonine, demonstrating that the ABBFA_003406 adenylation domain is not loading ABBFA_003404. Possible explanations for this observation could be that we have not correctly identified the true substrate for the adenylation domain or that the protein as produced is not active to carry out the second thioester-forming reaction.

Conclusive demonstration of a failure to load the carrier protein led to a more complete analysis of the structure of ABBFA_003404. Portions of the following text result from our publication (*21*), which is also included in the appendix. This analysis focused on the features of carrier proteins that distinguish the carrier proteins of natural product biosynthesis (from NRPS or Polyketide Synthase (PKS) pathways) from the fatty acyl carrier proteins (ACPs) of fatty acid synthesis and transport.

We examined the protein structures that were most closely related to ABBFA_003404 as predicted by the DALI structural homology server (*22*). Interestingly, the 14 proteins contain seven ACPs from fatty acid synthesis and transport and seven protein from natural product

(NRPS or PKS) pathways. The top five proteins as scored by DALI–and six of the top seven–are all from natural product systems (Figure 18).

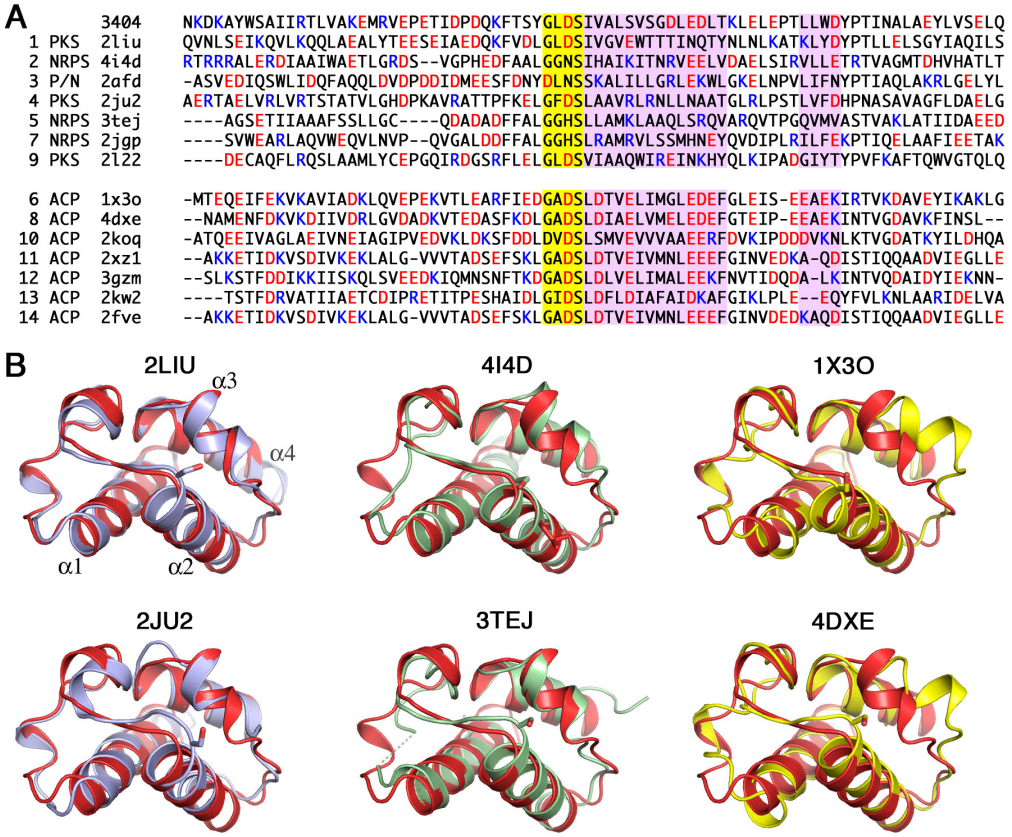

Figure 18. Sequence and structural comparison of A3404 to related carrier protein structures. The 14 structures of closest homologs as identified by the DALI server were compared to A3404. A. Sequence alignment of the homologous proteins. The first three columns represent the rank in the DALI scoring, the type of protein, and the PDB code. Proteins in the top half of the alignment are from NPRS or PKS clusters, while proteins in the bottom half are ACPs from fatty acid synthesis and transport. The pantetheinylation motif is highlighted in yellow; helices α2 and α3 are shaded in pink. In the alignment, acidic amino acids are red, while basic residues are blue. B. A ribbon diagram of A3404 (red) is superimposed on the top two closest homologs of each of the three carrier protein types. The same orientation is used in all panels and the helix designations are shown in the top left panel. The two PKS acyl carrier proteins 2LIU and 2JU2 are shown in light blue. Two NRPS PCP domains, the type II 4I4D and the type I 3TEJ are shown in green. Two acyl carrier proteins (1X3O and 4DXE) are shown in yellow. In all structures the serine residue at the start of helix α2 is shown as a stick representation.

The regions of the carrier protein that are most important for distinguishing among they different types are the loop between helix α1 and α2, the α2 helix itself, and the α3 helix (*23-26*). Not surprisingly, these are the regions of the proteins that interact with partner proteins, largely due to the proximity to the site of loading at the start of the α2 helix. We examined the multiple sequence alignment generated from DALI, and additionally examined the structures of each protein compared to ABBFA_003404. This limited alignment of closely related structures provides insight into the comparison between the three types of carrier protein. First, we examined the sequence of the pantetheine binding motif. Of interest, all ACPs, whether from FAS or PKS systems contained an aspartic acid immediately preceding the serine residue. The acidic nature of the hydrophilic face of helix α2 is also quite striking. All FAS ACPs except 2KOQ contain acidic residues at the second and fifth residues following the pantetheinylated serine, and are much more highly acidic at the C-terminal end of the helix. Similarly, the amino

acids that immediately precede helix α3 also are much more highly acidic in the FAS ACP sequences.

The structure of ABBFA_003404 was compared to all fourteen of the most closely related ACP structures and structural alignments for the two most similar structures of each class are shown (Figure 18B). The structure of the ACP from the curamicin PKS (2LIU) illustrates the best alignment with ABBFA_003404. In particular, the path traced by the main chain in the divergent loop between helices α1 and α2 as well as the α3 helix are very similar. The positional conservation with a second PKS ACP is also quite good, although differences in the position of the second 3_{10} helix of the loop that precedes helix α2 is more pronounced. The comparison with the two NRPS PCP structures, BlmI and EntF, show comparable overall similarities. A noteworthy difference is the lack of the first 3_{10} helix in the two PCP structures. Finally, comparison of the structure to the FAS ACP structures shows larger differences in the loop between helices α1 and α2, and, most strikingly, the orientation of the α3 helix. This potentially reflects the predominant acid nature of the loop immediately before this helix.

The figure presents the structures of carrier protein domains from the perspective of the partner protein. The right half of the molecules represent helices α2 and α3, and the loop that joins them. What is striking from the sequence alignment is the number of negatively charged residues in this region of the ACPs of FAS systems. Of the seven sequences shown, there are an average of more than seven aspartic or glutamic acid residues within this 25-residue stretch. In contrast, the carrier proteins from PKS or NRPS systems show only an average of less than two anionic residues. The ABBFA_003404 protein has six glutamic acid residues. It seems, however, that this does not represent that ABBFA_003404 is an ACP from fatty acid metabolism. Rather this appears to be a function of the type II nature of this protein. BlmI, the recently characterized type II PCP (*25*) has five acidic residues, as do SgcC2 and MdpC2, two additional type II PCPs from hybrid NRPS/PKS systems (*27, 28*). It is possible, then, that the highly acidic nature of this region of the protein reflects not the specific function of the protein as an ACP or PCP but rather is a requirement of the type II carrier proteins.

Key Research Accomplishments

We have accomplished the following tasks that contribute towards goals of the project.

Goal 1. Preliminary data have established that chorismate synthase and prephenate dehydrogenase/3-phosphoshikimate-1-carboxyvinyl transferase are essential proteins for *A. baumannii* infection. Therefore our hypothesis is that these proteins are potential therapeutic targets. The object of this goal is to validate these proteins in the chorismate biosynthesis pathway as therapeutic targets.

- Two different methodologies were developed to generate site-specific mutants in clinical isolates of *A. baumannii*
- Site specific disruptions were created in the *aroA* gene in three independent strains, AB307, AB714, and AB764.
- The *aroA* mutants show growth defects in minimal media, when compared to wild-type parental strains.
- Because the AB714 and AB764 strains are less virulent in rat models, a higher inoculation density is needed in rat abscess infection models. The *aroA* mutant strains survive less well in this model; however, the effect is not as dramatic as with the more virulent AB307 strain wild-type and *aroA* mutant.
- The AB307 Δ*aroK* mutant, lacking SK activity, shows defective growth in minimal media and the rat soft-tissue infection model, supporting *in vivo* essentiality of *aroK* similar to that previously observed for the downstream *aroA* and *aroC* genes (encoding PSCVT and CS, respectively) within the chorismate pathway.
- Differential scanning fluorimetry (DSF) has been successfully used to identify small molecules that increased the thermostability of SK, PSCVT, and CS. These results provided both proof of principle that these enzymes were appropriate for use with the DSF binding assay, and provided suggestive modified storage buffers to enhance protein stability.
- DSF was successfully used to screen a library of 500 chemical fragments, which may serve as the basis for fragment-based lead discovery (FBLD), against both SK and PSCVT. A number of fragments were identified that interacted with each of these enzymes. One (Fragment 173) interacted with both, suggesting the possibility small molecules do exist that bind to multiple enzymes in the chorismate pathway, and which may be further developed as multi-target inhibitors and possibly ultimately antibiotics.
- An *in silico* assessment of fragment-binding that is predictive for protein surface regions amenable for binding drug-like molecules was conducted for CS. This analysis found that four of the ten top ranked fragment-binding clusters were located at or near the catalytic active site and the substrate-binding pocket. This result is indicative that *A. baumannii* CS likely is capable of binding drug-like molecules in a manner that will inhibit CS enzymatic activity that is *in vivo* essential for this pathogen.
- The crystal structure of a ternary complex of *A. baumannii* SK – shikimate – SO_4^{2-} was determined at 1.91 Å resolution, and has been deposited in the PDB (4Y0A).
- Two crystal structures of *A. baumannii* PSCVT have been determined at 2.49 Å and 2.37 Å resolution, respectively, and deposited in the PDB (5BS5 and 5BUF).
- In summary, the final three enzymes of the chorismate pathway (i.e., SK, PSCVT, and CS) are essential for *in vivo* growth and survival of *A. baumannii*. Data suggest that each of these enzymes is capable of binding drug-like molecules, which encourages further investigated as antibiotic targets in *A. baumannii* and other multi- and extreme drug resistant GNB. Importantly, the respective substrates for each of these enzymes share a

similar scaffold, suggesting the possibility of the development of a small molecule inhibitor / antibiotic that targets two or all three of these enzymes. Such a multi-target antibiotic promises to increase durability, as multiple mutations would be required to render it ineffective.

Goal 2. Characterize a novel natural product synthetic pathway encoded by an *A. baumannii* nonribosomal peptide synthetases pathway. Our hypothesis is that this cluster is responsible for the production of a novel compound that may impact growth or virulence of *A. baumannii*.

- The amino acid building blocks of the natural product pathway have been identified as glycine and threonine. Covalent loading of the threonine substrate by the freestanding adenylation domain ABBFA_003406 onto the presumed carrier protein has not been observed.
- Colony morphology of *A. baumannii* M2-2 and M2-11, two transposon mutants with disruptions in the ABBFA_003406-ABBFA_003399 operon, is dramatically different than wild-type cells and shows reduced surface-associated, the flagella-independent spread of cell colonies across semi-soft agar plates.
- Strain AB307.193, containing a transposon mutation in the global transcriptional regulator histone-like nucleoid structuring factor (*hns*) gene, dramatically over-expresses the ABBFA_003406-ABBFA_003399 operon and exhibits a hyper-motile phenotype.
- The self-standing amino acyl carrier protein ABBFA_003404 has been successfully cloned, expressed, purified, and crystallized. The protein structure has been solved at 1.4Å resolution. The structure factors and atomic coordinates have been deposited at the Protein Data Bank under accession code **4HKQ**.
- Analysis of the structure of ABBFA_003404 has identified common sequence motifs that distinguish among the different types of peptidyl and acyl carrier proteins from NRPS, polyketide synthase, and fatty acid synthase systems. Acyl carrier proteins uniformly contain an aspartic acid residue that precedes the pantetheinylation site. The highly acidic nature of the helix two and helix three regions of the free-standing (type II) carrier proteins was also noted.

Reportable Outcomes

The following publications were supported by this award.

Manuscripts

Umland, T. C., Schultz, L. W., MacDonald, U., Beanan J. M., Olson, R., and Russo, T. A. (2012) *In vivo*-Validated Essential Genes Identified in *Acinetobacter baumannii* by Using Human Ascites Overlap Poorly with Essential Genes Detected on Laboratory Media. mBio **3**, e00113-12. doi:10.1128/Bio.00113-12.

Russo, T. A., Beanan, J. M., Olson, R., MacDonald, U., Cox, A. D., St. Michael, F., Vinogradov, E. V., Spellberg, B., Luke-Marshall, N. R., and Campagnari, A. A. (2013) Te K1 Capsular Polysaccharide from *Acinetobacter bauamannii* is a Potential Therapeutic Target via Passive Immunization. *Infection and Immunity* 81, 915-922.

Russo, T. A., Olson, R., MacDonald, U., Metzger, D., Maltese, L., Drake, E. J., and Gulick, A. M. (2014) Aerobactin mediates virulence and accounts for the increased siderophore production under iron limiting conditions by hypervirulent (hypermucoviscous) Klebsiella pneumoniae. *Infection and Immunity* **82**, 2356-2367.

Allen, C. L. and Gulick, A. M. (2014) Structural and bioinformatic characterization of an Acinetobacter baumannii type II carrier protein. *Acta Crystallographica* **D70**: 1718-1725.

Wurst, J. M., Drake, E. J., Theriault, J. R., Jewett, I. T., VerPlank, L., Perez, J. R., Dandapani, S., Palmer, M., Moskowitz, S. M., Schreiber, S. L., Munoz, B., and Gulick, A. M. (2014) Identification of Inhibitors of PvdQ, an enzyme involved in the synthesis of the siderophore pyoverdine. *ACS Chemical Biology* **9**, 1536-1544.

Umland, T. C., Schultz, L. W., and Russo, T. A., (2014). Reevaluating the approach to drug target discovery in multi-drug resistant gram negative bacilli. *Future Microbiology* **9**, 1113-1116.

Sutton, K.A., Breen, J., MacDonald, U., Beanan, J., Olson, J., Russo, T. A., Schultz, L. A. and Umland, T. C., (2015). Crystal structure of shikimate kinase in complex with shikimate, an *in vivo* essential metabolic enzyme in the nosocomial pathogen *Acinetobacter baumannii*. *Acta Crystallographica* **D**, Accepted pending revision.

Posters

Timothy C. Umland, Joseph R. Luft, Eleanor Cook, George T. DeTitta, Angela M. Lauricella, Raymond M. Nagel, Edward H. Snell, Jennifer R. Wolfley, “High-throughput crystallization of cytosolic and membrane proteins to structurally enable drug discovery,” The 7th Drug Design and Medicinal Chemistry Conference. Boston, MA, May 8-10, 2013.

L. Wayne Schultz, Joseph R. Luft, Eleanor Cook, George T. DeTitta, Angela M. Lauricella, Raymond M. Nagel, Edward H. Snell, Jennifer R. Wolfley, “High-throughput crystallization of cytosolic and membrane bound proteins” Cambridge Healthtech Institute 8th Annual Drug Discovery Chemistry Conference. San Diego, CA, April 16-18, 2013. Abstract #212.

L. Wayne Schultz, Thomas Russo, Jennifer Breen, Jessica Kocsis, Timothy C. Umland "Structural Biology of the Shikimate Pathway in Multi-drug Resistant Gram Negative Bacteria", Annual Meeting of the American Crystallographic Association. Honolulu, HI, July 22, 2013. Abstract #1578.

Nathan Roach, Jesica Kocsis, and Timothy Umland, "The Purification and Crystallization of *Acinetobacter baumannii* Chorismate Synthase," University at Buffalo Biomedical Research Day. Buffalo, NY August 2, 2013.

Kristin Sutton, Thomas Russo, Jennifer Breen, Jessica Kocsis, Timothy C. Umland, L. Wayne Schultz "Structural Biology of the Shikimate Pathway in Multi-drug Resistant Gram Negative Bacteria" The 74th Annual Pittsburgh Diffraction Conference. Buffalo, NY, September 19, 2013. Abstract #P21.

C.L. Allen and A.M. Gulick. "Investigation of nonribosomal peptide synthetase-related genes from an uncharacterized operon implicated in *Acinetobacter baumannii* motility" 23rd Enzyme Mechanisms Conference, Coronado CA. January 2013.

K.M. Armbruster, C.L. Allen, and A.M. Gulick. 26th Annual Witebsky Center Conference on Microbial Pathogenesis, Buffalo, NY. "Exploring the role of a nonribosomal peptide synthetase cluster in *Acinetobacter baumannii* motility." April 2014.

L.W. Schultz, K. Sutton, J. Breen, T.A. Russo, and T.C. Umland. American Crystallographic Association Annual Meeting. Albuquerque, NM. "Fragment screening of the shikimate pathway in multi-drug resistant gram negative bacteria. May 2014.

The following protein structure datasets, including atomic coordinates and structure factors, were deposited with the Protein Data Base (http://www.pdb.org) using funds from this award.

4HKQ, *Crystal Structure of Free-Standing Peptidyl Carrier Protein from Uncharacterized Acinetobacter baumannii Secondary Metabolic Pathway*. Released Oct 2013.

4Y0A, *Crystal structure of shikimate kinase in complex with shikimate, an in vivo essential metabolic enzyme in the nosocomial pathogen Acinetobacter baumannii*. Pending release upon acceptance of revised manuscript by *Acta Crystallographica* **D.**

4ZXH and **4ZXI**. Two additional PDB datasets have been deposited and will be released upon publication of the manuscript.

5BS5 and **5BUF**. Two additional PDB datasets for PSCVT have been deposited and will be released upon publication of the manuscript.

Funding Awarded based on work supported by this award as preliminary results.

A grant from the McCauley foundation was awarded ($18,700) to support the cloning and expression of shikimate kinase necessary for the biosynthesis of a substrate needed to develop assays to study the activity and inhibition of PSCVT.

Employment and Research Opportunities Received based on training supported by this award.

Ms. Krista Armbruster, supported on this award in 2014, was admitted to the graduate program in Biochemistry and Molecular Biology in September 2014.

Dr. C. Leigh Allen, supported as a post-doctoral scientist in 2012-2014, is working as a Post-Doctoral Research Scholar at North Carolina State University.

Conclusions

A. baumannii remains a significant biomedical problem that is increasingly being recognized as a cause of nosocomial infections in a wide variety of health care settings (*29*). The prevalence of resistant strains of *A. baumannii (30, 31)* and the current lack of effective treatments suggests a pressing need for novel approaches to identify and validate new targets for antibiotic treatments. We continue to pursue two complementary approaches to address this problem that comprise the aims of this research project and together will identify, characterize, and validate novel antibiotic targets in *A. baumannii*.

We have implemented the strategy of investigating *in vivo* essential genes (i.e., essential for growth and survival during infection of a host) to advance the traditional antibacterial drug development pipeline in order to achieve the first goal of this project. Our methodology for screening and validating *in vivo* essential genes identified *A. baumannii* targets that previously were largely overlooked as antibacterial targets (*2*), including CS and PD-PSCVT. In the second goal, we are making an investment in the understanding of the fundamental microbial physiology of this pathogen. Towards this end, we have initiated the investigation of a novel natural product biosynthetic pathway that has been implicated in bacterial motility. These genes encoding this pathway are upregulated in response to a bacterial quorum signal.

We have now obtained *aroA* mutants in three parental background strains. The *in vitro* and *in vivo* data from all three lines support the essentiality of the *aroA* gene product despite minor differences in the overall virulence levels of the different parental strains. This validates the pursuit of specific inhibitors of PD-PSCVT and, by extension, other enzymes of the shikimate pathway.

We determined the crystal structure of PD-PSCVT at a resolution sufficient for use in fragment-based lead discovery methods. Additionally, we have determined the crystal structure of SK, the enzyme preceding the PSCVT in the shikimate pathway, and which may also serve as antibacterial target. Fragment-based methods were used to identify small molecules that may serve as antibacterial leads against these targets. We will place particular emphasis on any fragments that exhibit binding to multiple targets, as these compounds have the potential to be developed into multi-target inhibitors, thereby reducing the likelihood of the development of resistant mutants.

We have made important progress in understanding the natural product produced by the identified nonribosomal peptide synthetase cluster, having cloned and produced the synthetic enzymes and identified the molecular building blocks. We have demonstrated that the free-standing adenylation and carrier protein domains do not functionally interact, which has led to a revision to the working model for the complete biosynthetic pathway.

The acquisition this year of the mutant strains harboring disruptions in the NRPS biosynthetic operon has allowed us to examine the phenotype of bacterial motility. All lines of evidence point to a role for the natural product of the ABBFA_003406 through ABBFA_003399 biosynthetic operon as playing a role in increased surface-associated motility with *A. baumannii*. Efforts to isolate a fraction containing the active component have not yet led to the ability to chemically complement the knockout strains. On-going experiments will continue to identify conditions enable the isolation and chemical characterization of the NRPS product.

References

1. Russo, T. A., MacDonald, U., Beanan, J. M., Olson, R., MacDonald, I. J., Sauberan, S. L., Luke, N. R., Schultz, L. W., and Umland, T. C. (2009) Penicillin-binding protein 7/8 contributes to the survival of Acinetobacter baumannii in vitro and in vivo, *J Infect Dis 199*, 513-521.
2. Umland, T. C., Schultz, L. W., Macdonald, U., Beanan, J. M., Olson, R., and Russo, T. A. (2012) In Vivo-Validated Essential Genes Identified in Acinetobacter baumannii by Using Human Ascites Overlap Poorly with Essential Genes Detected on Laboratory Media, *mBio 3*.
3. Roberts, C. W., Roberts, F., Lyons, R. E., Kirisits, M. J., Mui, E. J., Finnerty, J., Johnson, J. J., Ferguson, D. J., Coggins, J. R., Krell, T., Coombs, G. H., Milhous, W. K., Kyle, D. E., Tzipori, S., Barnwell, J., Dame, J. B., Carlton, J., and McLeod, R. (2002) The shikimate pathway and its branches in apicomplexan parasites, *J Infect Dis 185 Suppl 1*, S25-36.
4. Tucker, A. T., Nowicki, E. M., Boll, J. M., Knauf, G. A., Burdis, N. C., Trent, M. S., and Davies, B. W. (2014) Defining gene-phenotype relationships in Acinetobacter baumannii through one-step chromosomal gene inactivation, *mBio 5*, e01313-01314.
5. Cummings, M. D., Farnum, M. A., and Nelen, M. I. (2006) Universal screening methods and applications of ThermoFluor, *J Biomol Screen 11*, 854-863.
6. Matulis, D., Kranz, J. K., Salemme, F. R., and Todd, M. J. (2005) Thermodynamic stability of carbonic anhydrase: measurements of binding affinity and stoichiometry using ThermoFluor, *Biochemistry 44*, 5258-5266.
7. Dai, R., Wilson, D. J., Geders, T. W., Aldrich, C. C., and Finzel, B. C. (2014) Inhibition of Mycobacterium tuberculosis transaminase BioA by aryl hydrazines and hydrazides, *Chembiochem 15*, 575-586.
8. Brenke, R., Kozakov, D., Chuang, G. Y., Beglov, D., Hall, D., Landon, M. R., Mattos, C., and Vajda, S. (2009) Fragment-based identification of druggable 'hot spots' of proteins using Fourier domain correlation techniques, *Bioinformatics 25*, 621-627.
9. Giessen, T. W., and Marahiel, M. A. (2012) Ribosome-independent biosynthesis of biologically active peptides: Application of synthetic biology to generate structural diversity, *FEBS Lett 586*, 2065-2075.
10. Strieker, M., Tanovic, A., and Marahiel, M. A. (2010) Nonribosomal peptide synthetases: structures and dynamics, *Curr Opin Struct Biol 20*, 234-240.
11. Khan, S. R., Herman, J., Krank, J., Serkova, N. J., Churchill, M. E., Suga, H., and Farrand, S. K. (2007) N-(3-hydroxyhexanoyl)-l-homoserine lactone is the biologically relevant quormone that regulates the phz operon of Pseudomonas chlororaphis strain 30-84, *Appl Environ Microbiol 73*, 7443-7455.
12. Clemmer, K. M., Bonomo, R. A., and Rather, P. N. (2011) Genetic analysis of surface motility in Acinetobacter baumannii, *Microbiology 157*, 2534-2544.
13. Lambalot, R. H., Gehring, A. M., Flugel, R. S., Zuber, P., LaCelle, M., Marahiel, M. A., Reid, R., Khosla, C., and Walsh, C. T. (1996) A new enzyme superfamily - the phosphopantetheinyl transferases, *Chem Biol 3*, 923-936.
14. Rumbo-Feal, S., Gomez, M. J., Gayoso, C., Alvarez-Fraga, L., Cabral, M. P., Aransay, A. M., Rodriguez-Ezpeleta, N., Fullaondo, A., Valle, J., Tomas, M., Bou, G., and Poza, M. (2013) Whole Transcriptome Analysis of Acinetobacter baumannii Assessed by RNA-Sequencing Reveals Different mRNA Expression Profiles in Biofilm Compared to Planktonic Cells, *PLoS One 8*, e72968.
15. Eijkelkamp, B. A., Stroeher, U. H., Hassan, K. A., Elbourne, L. D., Paulsen, I. T., and Brown, M. H. (2013) H-NS plays a role in expression of Acinetobacter baumannii virulence features, *Infect Immun 81*, 2574-2583.

16. Saroj, S. D., and Rather, P. N. (2013) Streptomycin inhibits quorum sensing in Acinetobacter baumannii, *Antimicrob Agents Chemother 57*, 1926-1929.
17. Stacy, D. M., Welsh, M. A., Rather, P. N., and Blackwell, H. E. (2012) Attenuation of quorum sensing in the pathogen Acinetobacter baumannii using non-native N-Acyl homoserine lactones, *ACS Chem Biol 7*, 1719-1728.
18. Burrows, L. L. (2012) Pseudomonas aeruginosa Twitching Motility: Type IV Pili in Action, *Annu Rev Microbiol 66*, 493-520.
19. McConnell, M. J., Actis, L., and Pachon, J. (2013) Acinetobacter baumannii: human infections, factors contributing to pathogenesis and animal models, *FEMS Microbiol Rev 37*, 130-155.
20. Adams, M. D., Goglin, K., Molyneaux, N., Hujer, K. M., Lavender, H., Jamison, J. J., MacDonald, I. J., Martin, K. M., Russo, T., Campagnari, A. A., Hujer, A. M., Bonomo, R. A., and Gill, S. R. (2008) Comparative genome sequence analysis of multidrug-resistant Acinetobacter baumannii, *J Bacteriol 190*, 8053-8064.
21. Allen, C. L., and Gulick, A. M. (2014) Structural and bioinformatic characterization of an Acinetobacter baumannii type II carrier protein, *Acta Crystallogr D Biol Crystallogr 70*, 1718-1725.
22. Holm, L., and Rosenstrom, P. (2010) Dali server: conservation mapping in 3D, *Nucleic Acids Res 38*, W545-549.
23. Crosby, J., and Crump, M. P. (2012) The structural role of the carrier protein--active controller or passive carrier, *Nat Prod Rep 29*, 1111-1137.
24. Lai, J. R., Koglin, A., and Walsh, C. T. (2006) Carrier protein structure and recognition in polyketide and nonribosomal peptide biosynthesis, *Biochemistry 45*, 14869-14879.
25. Lohman, J. R., Ma, M., Cuff, M. E., Bigelow, L., Bearden, J., Babnigg, G., Joachimiak, A., Phillips, G. N., Jr, and Shen, B. (2014) The crystal structure of BlmI as a model for nonribosomal peptide synthetase peptidyl carrier proteins, *Proteins: Structure, Function, and Bioinformatics*.
26. Mercer, A. C., and Burkart, M. D. (2007) The ubiquitous carrier protein--a window to metabolite biosynthesis, *Nat Prod Rep 24*, 750-773.
27. Van Lanen, S. G., Lin, S., Dorrestein, P. C., Kelleher, N. L., and Shen, B. (2006) Substrate specificity of the adenylation enzyme SgcC1 involved in the biosynthesis of the enediyne antitumor antibiotic C-1027, *J Biol Chem 281*, 29633-29640.
28. Van Lanen, S. G., Oh, T. J., Liu, W., Wendt-Pienkowski, E., and Shen, B. (2007) Characterization of the maduropeptin biosynthetic gene cluster from Actinomadura madurae ATCC 39144 supporting a unifying paradigm for enediyne biosynthesis, *J Am Chem Soc 129*, 13082-13094.
29. Visca, P., Seifert, H., and Towner, K. J. (2011) Acinetobacter infection--an emerging threat to human health, *IUBMB life 63*, 1048-1054.
30. Cerqueira, G. M., and Peleg, A. Y. (2011) Insights into Acinetobacter baumannii pathogenicity, *IUBMB life 63*, 1055-1060.
31. Peleg, A. Y., Seifert, H., and Paterson, D. L. (2008) Acinetobacter baumannii: emergence of a successful pathogen, *Clin Microbiol Rev 21*, 538-582.

Appendices

We have attached the following publication that resulted from research supported by this award.

Umland, T. C., Schultz, L. W., MacDonald, U., Beanan J. M., Olson, R., and Russo, T. A. (2012) *In vivo*-Validated Essential Genes Identified in *Acinetobacter baumannii* by Using Human Ascites Overlap Poorly with Essential Genes Detected on Laboratory Media. mBio **3**, e00113-12. doi:10.1128/Bio.00113-12.

Russo, T. A., Beanan, J. M., Olson, R., MacDonald, U., Cox, A. D., St. Michael, F., Vinogradov, E. V., Spellberg, B., Luke-Marshall, N. R., and Campagnari, A. A. (2013) The K1 Capsular Polysaccharide from *Acinetobacter bauamannii* is a Potential Therapeutic Target via Passive Immunization. *Infection and Immunity* 81, 915-922.

Russo, T. A., Olson, R., MacDonald, U., Metzger, D., Maltese, L., Drake, E. J., and Gulick, A. M. (2014) Aerobactin mediates virulence and accounts for the increased siderophore production under iron limiting conditions by hypervirulent (hypermucoviscous) Klebsiella pneumoniae. *Infection and Immunity* **82**, 2356-2367.

Allen, C. L. and Gulick, A. M. (2014) Structural and bioinformatic characterization of an Acinetobacter baumannii type II carrier protein. *Acta Crystallographica* **D70**: 1718-1725.

Wurst, J. M., Drake, E. J., Theriault, J. R., Jewett, I. T., VerPlank, L., Perez, J. R., Dandapani, S., Palmer, M., Moskowitz, S. M., Schreiber, S. L., Munoz, B., and Gulick, A. M. (2014) Identification of Inhibitors of PvdQ, an enzyme involved in the synthesis of the siderophore pyoverdine. *ACS Chemical Biology* **9**, 1536-1544.

Umland, T. C., Schultz, L. W., and Russo, T. A., (2014). Re-evaluating the approach to drug target discovery in multi-drug resistant gram negative bacilli. *Future Microbiology* **9**, 1113-1116.

The following manuscript is under revision and is not attached.

Sutton, K.A., Breen, J., MacDonald, U., Beanan, J., Olson, J., Russo, T. A., Schultz, L. A. and Umland, T. C., (2015). Crystal structure of shikimate kinase in complex with shikimate, an *in vivo* essential metabolic enzyme in the nosocomial pathogen *Acinetobacter baumannii*. *Acta Crystallographica* **D**, Accepted pending revision.

Acta Crystallographica Section D
Biological Crystallography
ISSN 1399-0047

Structural and bioinformatic characterization of an *Acinetobacter baumannii* type II carrier protein

C. Leigh Allen and Andrew M. Gulick*

Hauptman–Woodward Medical Research Institute and Department of Structural Biology, University at Buffalo, Buffalo, NY 14203, USA

Correspondence e-mail: gulick@hwi.buffalo.edu

Received 23 December 2013
Accepted 12 April 2014

PDB reference: NRPS PCP domain, 4hkg

Microorganisms produce a variety of natural products *via* secondary metabolic biosynthetic pathways. Two of these types of synthetic systems, the nonribosomal peptide synthetases (NRPSs) and polyketide synthases (PKSs), use large modular enzymes containing multiple catalytic domains in a single protein. These multidomain enzymes use an integrated carrier protein domain to transport the growing, covalently bound natural product to the neighboring catalytic domains for each step in the synthesis. Interestingly, some PKS and NRPS clusters contain free-standing domains that interact intermolecularly with other proteins. Being expressed outside the architecture of a multi-domain protein, these so-called type II proteins present challenges to understand the precise role they play. Additional structures of individual and multi-domain components of the NRPS enzymes will therefore provide a better understanding of the features that govern the domain interactions in these interesting enzyme systems. The high-resolution crystal structure of a free-standing carrier protein from *Acinetobacter baumannii* that belongs to a larger NRPS-containing operon, encoded by the ABBFA_003406–ABBFA_003399 genes of *A. baumannii* strain AB307-0294, that has been implicated in *A. baumannii* motility, quorum sensing and biofilm formation, is presented here. Comparison with the closest structural homologs of other carrier proteins identifies the requirements for a conserved glycine residue and additional important sequence and structural requirements within the regions that interact with partner proteins.

1. Introduction

Many microorganisms produce peptide natural products *via* novel secondary metabolic biosynthetic pathways (Gross & Loper, 2009; Li & Vederas, 2009; Meinwald, 2011). These products include the siderophore enterobactin, the biosurfactant surfactin, and antibiotics and cytostatic agents such as vancomycin and bleomycin, respectively, that have given rise to commercial therapeutics. These substances are all produced by nonribosomal peptide synthetases (NRPSs; Fischbach & Walsh, 2006). These molecular machines use a wide range of substrate amino acids to catalyze peptide synthesis independently of the ribosome.

The NRPSs use a modular catalytic strategy in which multiple protein activities that are required for the incorporation of a single amino acid into the final peptide define a single module. Typically, one module is present for each amino acid incorporated into the polypeptide. Most commonly, these multiple domains are joined in a single polypeptide, and large NRPSs that contain multiple modules and thousands of amino acids are not uncommon. During NRPS biosynthesis, the

peptide intermediates are covalently attached to a peptidyl carrier protein (PCP) domain (Mercer & Burkart, 2007), which delivers the substrate to neighboring catalytic domains. The PCP domains are small ~75-residue units that are post-translationally modified with a phosphopantetheine cofactor that binds the amino acid and peptide intermediates as a thioester (Beld *et al.*, 2013). Unlike the more common multi-domain architecture, some NRPS systems contain catalytic and carrier domains expressed as single free-standing proteins. These so-called type II systems provide additional challenges that arise from the need for specific protein–protein interactions to govern proper biosynthesis.

A similar modular architecture is used by the polyketide synthase (PKS) machinery to incorporate malonate starter units into polyketide natural products. PKS enzymes also utilize integrated carrier proteins, described as ACPs to reflect the acyl substrates, that shuttle the polyketide intermediates between catalytic domains (Keatinge-Clay, 2012; Strieker *et al.*, 2010). Finally, fatty-acid synthase (FAS) enzymes use ACP domains to deliver the acyl groups to catalytic domains during the iterative elongation of fatty acids.

These three types of carrier proteins have been studied functionally, and structures of carrier domains have been determined by both crystallography and NMR. These structures illustrate that the carrier proteins adopt a common fold containing four helices (Crosby & Crump, 2012; Mercer & Burkart, 2007). Helices $\alpha1$, $\alpha2$ and $\alpha4$ are longer and are mostly parallel, while the shorter helix $\alpha3$ lies nearly perpendicular to the other three. The conserved serine residue that receives the phosphopantetheine cofactor lies at the start of helix $\alpha2$. The structural characterization of the holo and apo forms of the TycC3 PCP (Koglin *et al.*, 2006) illustrates multiple states of the protein in solution that are dynamically interconverting (designated the A and H states for the unique apo and holo states, respectively, as well as a third state that is shared by both apo and holo forms of the protein and is designated the A/H state). The authors of the recent crystal structure of BlmI (Lohman *et al.*, 2014), a type II PCP, note that carrier protein domains from X-ray crystal structures are predominantly in the A/H state and suggest that the alternate conformations observed for TycC3 may result from excising this carrier protein from the larger type I architecture.

Many human pathogens contain small NRPS clusters that are involved in the production of novel uncharacterized peptides. *Acinetobacter baumannii*, a Gram-negative bacterium that causes infectious outbreaks in multiple healthcare settings (Howard *et al.*, 2012), contains a small NRPS cluster derived from eight genes. Based on the presence of two adenylation domains (within a four-domain NPRS protein and the free-standing adenylation domain), this pathway is likely to form two separate acyl adenylates and is expected to produce a dipeptide or a derivative thereof.

This operon has been implicated in bacterial motility and quorum sensing (Clemmer *et al.*, 2011), two phenotypes that are dependent on the production of acyl-homoserine lactone signaling molecules. A random screen for mutants of the M-2 strain of *A. baumannii* that exhibit reduced motility identified transposon insertions into two genes within this operon (Clemmer *et al.*, 2011). These genes were additionally noted to be upregulated in response to quorum signals. Subsequently, transcriptome analysis of strain ATCC17978 demonstrated that mRNA encoding the type II carrier protein, annotated as gene A1S_0114, was exclusively expressed in biofilms and was not detected in planktonic cells (Rumbo-Feal *et al.*, 2013). Furthermore, the genes of this operon were overexpressed in biofilms by tenfold to 150-fold when compared with either exponential or stationary phase planktonic cell cultures. When the A1S_0114 gene was disrupted, there was an eightfold reduction in biofilm formation compared with the wild-type strain. Taken together, this evidence suggests that the carrier protein and this natural product operon are important in motility, quorum sensing and biofilm formation, phenotypes that are closely associated with bacterial virulence.

As an initial step towards understanding this uncharacterized NRPS pathway, we have subjected the core domains to structural investigation. Here, we report the structure of the free-standing carrier protein domain from this operon from *A. baumannii* strain AB307-0294 (Adams *et al.*, 2008). The biological function of this carrier protein is currently unknown; however, the co-translational expression of the operon suggests that this carrier domain may contribute a substrate to the NRPS system. Within the NRPS machinery, a type II PCP is a relatively rare occurrence. Du & Shen (1999) identified and characterized BlmI from the NRPS pathway involved in the synthesis of bleomycin, a protein that has recently been structurally characterized (Lohman *et al.*, 2014). Here, we present the crystal structure of this carrier protein and compare it with other carrier protein domains. Using features that have been described to distinguish the three types of carrier protein domains, we note that the *A. baumannii* carrier protein is more similar to the carrier proteins of natural product biosynthetic operons than to the ACPs of fatty-acid biosynthesis. We further characterize several conserved sequence motifs and compare the regions of the proteins that interact with biochemical partners.

2. Materials and methods

2.1. Cloning, expression and purification of A3404

For the overexpression of A3404[1] in *Escherichia coli*, we PCR-amplified the gene encoding A3404 (NCBI accession YP_002327276) from AB307-0294 genomic DNA and ligated the gene into the pET-15b-TEV expression vector (Kapust *et al.*, 2001). This yielded a construct that produced A3404 with a pentahistidine tag at the N-terminus that was cleaved by *Tobacco etch virus* (TEV) protease. The a3404 gene was cloned from *A. baumannii* strain AB307 genomic DNA (a gift from Dr Thomas Russo, University at Buffalo) by PCR. The

[1] The genes from strain AB307-0294 are annotated ABBFA_00####. For simplification, we will describe the genes as a####; the encoded proteins will be designated A####. Within the ATCC17978 and M-2 strains used in the genetic studies described in §1, the genes are annotated A1S_####. Both naming conventions are included in Fig. 1.

Table 1
Crystallographic and refinement data.

Values in parentheses are for the highest resolution shell. Because of the high noncrystallographic symmetry, the R_{free} reflections were generated in thin shells. The high-resolution R_{free} value is reported for data from 1.32 to 1.30 Å resolution.

Data collection	
Source	BL9-2, SSRL
Resolution (Å)	31.22–1.30
Space group	$P6_5$
Unit-cell parameters (Å, °)	$a = b = 61.81$, $c = 76.85$, $\alpha = \beta = 90$, $\gamma = 120$
R_{merge} (%)	6.0 (52.6)
Completeness (%)	99.1 (97.2)
$\langle I/\sigma(I)\rangle$	19.3 (5.7)
Multiplicity	10.3 (8.0)
Total reflections	415971
Unique reflections	40546
Refinement	
R_{cryst} (%)	14.9 (16.1)
R_{free} (%)	16.8 (16.6)
Wilson B factor (Å^2)	11.90
Average B factors (Å^2)	
Overall	16.7
Macromolecules	11.7
Solvent	27.0
R.m.s.d., bond lengths (Å)	0.005
R.m.s.d., angles (°)	1.00
No. of atoms	
Total	1624
Macromolecules	1294
Ligands	16
Water	311
Ramachandran favored (%)	98
Ramachandran outliers (%)	0
Clashscore†	2.24
PDB code	4hkg

† The *MolProbity* clashscore placed this structure in the 99th percentile.

primers used were 5′-ATT TTC AGG GC**C ATA TG**A ATA AAG ATA AAG CTT ACT GGA G-3′ and 5′-GTT AGC AGC C**GG ATC C**TC CTC ATG AAG CAA CTC CCT GC-3′. The 261-nucleotide gene was cloned using *Nde*I and *Bam*HI restriction sites (bold) into a modified pET-15b plasmid that contained a TEV protease site, and the sequence was confirmed by DNA sequencing. The resultant plasmid was used for expression in *E. coli* BL21(DE3) cells. Following inoculation with a small-scale overnight culture, a 1 l culture of cells was grown to an OD_{600} of ∼0.6 at 37°C and induced with 0.5 m*M* IPTG for 3 h. The cells were then pelleted by centrifugation and were either used immediately for protein purification or were flash-frozen in liquid nitrogen and stored at −80°C.

Cells were lysed by sonication in a buffer consisting of 50 m*M* HEPES (pH 7.5 at 4°C), 150 m*M* NaCl, 10 m*M* imidazole. The protein was purified by nickel ion-immobilized metal-affinity chromatography (IMAC). Following protein adsorption, the column was washed with 40 m*M* imidazole followed by elution of tagged A3404 with lysis buffer containing 300 m*M* imidazole. The purified protein was dialyzed overnight at 4°C against 1 l cleavage buffer consisting of 50 m*M* HEPES (pH 8.0 at 4°C), 150 m*M* NaCl, 0.5 m*M* EDTA with TEV protease included in the dialysis bag with the His_5-tagged protein and allowed to react overnight at 4°C during the dialysis step. The cleaved protein was passed over the same IMAC column and the untagged protein was collected in the flowthrough. The final protein, containing an N-terminal Gly-His sequence remaining after TEV cleavage, was dialyzed against 10 m*M* HEPES (pH 7.5 at 4°C), 50 m*M* NaCl. From 1 l of cells, ∼10 mg protein was obtained. The protein stock was frozen by pipetting directly into liquid nitrogen for storage at −80°C (Deng *et al.*, 2004).

2.2. Crystallization of A3404 and structure determination

Crystallization of apo A3404 was achieved *via* an initial screen with sparse-matrix conditions that utilized a broad array of PEG-based and salt-based precipitants (Carter & Carter, 1979; Jancarik & Kim, 1991). The final crystals of A3404 were grown at 4°C by hanging-drop vapor diffusion with a precipitant consisting of 25%(*v*/*v*) PEG 400, 5%(*v*/*v*) MPD, 0.2 m*M* TCEP, 50 m*M* CHES pH 9.0. Despite numerous attempts, we could not obtain crystals of the holo protein. Two sets of diffraction data were collected, with the first being collected at 100 K using a Rigaku MicroMax-007 microfocus X-ray generator, Osmic Max-Flux confocal focusing mirrors and a Saturn 944+ CCD detector. A higher resolution data set was subsequently collected using a wavelength of 0.9795 Å on SSRL beamline 9-2 equipped with a Si(111) double-crystal monochromator and a 325 mm MAR Mosaic CCD detector. Diffraction images were processed and scaled with the *HKL*-2000 suite (Otwinowski & Minor, 1997) and were converted to structure factors with *TRUNCATE* from the *CCP*4 software suite (Winn *et al.*, 2011).

The A3404 structure was initially determined by molecular replacement by using the first model (converted to poly-alanine) of the Asl1650 protein ensemble (Johnson *et al.*, 2006; PDB entry 2afd) as a search model against a data set collected on the home source. *EPMR* (Kissinger *et al.*, 2001) was used to identify the locations of the two molecules in the asymmetric unit. More than 20 models of ACP and PCP proteins were probed using multiple molecular-replacement programs before the successful search model was found using a poly-alanine chain derived from model 1 of PDB entry 2afd, an NMR structure with 29% identical (45% similar) residues to A3404. Following data collection to higher resolution, the low-resolution model was used with *Phaser* as utilized by the *PHENIX* (Adams *et al.*, 2010) molecular-replacement GUI. Refinement of the initial solution with *PHENIX* resulted in a model with an R_{cryst} of 14.9% (R_{free} of 16.8%).

The final model contains 1294 protein atoms and 311 solvent molecules. Additionally, there were two molecules of MPD bound near the pantetheine-binding motif in both subunits, a single molecule of ethylene glycol and a partial molecule of polyethylene glycol. Statistics for the data collection and refinement are presented in Table 1. The structure-based sequence alignment was generated with the *DALI* server (Holm & Rosenström, 2010); the structures were aligned with *CHIMERA* (Pettersen *et al.*, 2004).

3. Results and discussion

3.1. Sequence analysis of the *A. baumannii* NRPS cluster

The novel synthetic pathway encoded by *A. baumannii* under investigation in this work is approximately 15 kb of DNA in length and contains eight open reading frames (Fig. 1). This cluster has been identified in all available genomic sequences of *A. baumannii* (Adams *et al.*, 2008; Smith *et al.*, 2007; Vallenet *et al.*, 2008) and is not present in the nonpathogenic SDF strain or the related species *A. baylyi*. This predicted operon lies downstream of a transcriptional regulatory protein, ABBFA_003407, with homology to the PhzR and LuxR regulators as well as the acyl-homoserine lactone synthase CepI at ABBFA_003409.

The operon has all of the hallmarks of a pathway that produces a novel natural product. Gene a3399 encodes a phosphopantetheinyl transferase, or holo ACP synthase, that converts the carrier proteins from the apo to the holo state (Beld *et al.*, 2013). The operon encodes three NRPS proteins, an adenylation domain at a3406, a free-standing (type II) carrier protein at a3404 and a four-domain NRPS at a3403, which is composed of condensation, adenylation, carrier protein and thioesterase domains. A3404 is a free-standing carrier protein that could deliver a substrate to the NRPS system. Also encoded by the operon are two proteins, at a3400 and a3405, that show homology to NAD-dependent enzymes, as well as a hypothetical protein at a3401 that has no homology to characterized proteins but could function upstream or downstream to either generate alternate substrates or to modify the released product. Finally, the operon also encodes A3402, an efflux transporter that would be available to transport the final product outside of the cell.

The a3404 gene encodes a protein of 88 amino acids with a calculated pI of 4.22 and a molecular weight of 9643 Da. Similar to the carrier protein domains of NRPSs and the ACP domains of PKSs and FASs, A3404 has the highly conserved 4′-phosphopantetheinylation signature motif of GLDS. We examined this motif in the sequences of the more than 40 000 members of the Pfam family of carrier proteins, designated as PF00550, phosphopantetheine-attachment site. In this motif, the initial glycine three residues in front of the modified serine is observed in 91% of the family members. Two residues in front of the serine is a glycine (40%), leucine (19%), alanine (14%) or another hydrophobic residue such as valine or isoleucine (24% in total). The residue immediately in front of the serine is most commonly an aspartic acid (67%), histidine (17%) or asparagine (6%). This motif is thus best described as G-(G/L/A)-(D/H/N)-S.

3.2. Structure determination of A3404

The single-domain A3404 protein structure was initially determined using a data set collected on a home-source X-ray generator by molecular replacement with PDB entry 2afd as a

#	AB 307 orf	M2 orf	AAs	Proposed function
1	ABBFA_003406	A1S_0112	629	Adenylation (A) domain
2	ABBFA_003405	A1S_0113	597	Acyl-CoA dehydrogenase
3	ABBFA_003404	A1S_0114	86	Peptidyl carrier protein (PCP) domain
4	ABBFA_003403	A1S_0115	1319	Multi-domain NRPS protein containing condensation, A, PCP and thioesterase domains
5	ABBFA_003402	A1S_0116	1216	RND efflux transporter
6	ABBFA_003401	A1S_0117	423	Hypothetical
7	ABBFA_003400	A1S_0118	621	Homology to NAD-dependent epimerase/ dehydratase enzymes and esterases
8	ABBFA_003399	A1S_0119	256	4′-Phosphopantethienyl transferase

(*a*)

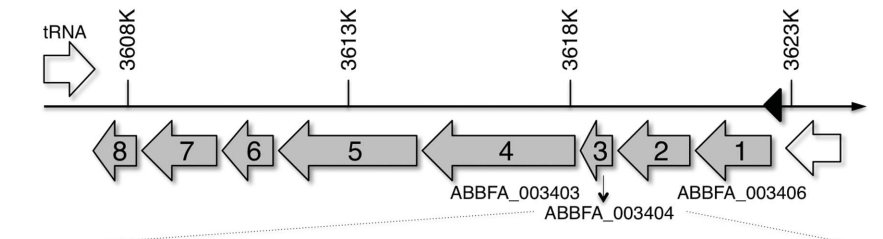


```
ATGAATAAAGATAAAGCTTACTGGAGCGCAATCATTCGTACGCTAGTCGCTAAAGAGATGCGCGTAGAGCCTGAGACG  78
M  N  K  D  K  A  Y  W  S  A  I  I  R  T  L  V  A  K  E  M  R  V  E  P  E  T
ATTGATCCAGATCAAAAATTTACCAGTTATGGTCTTGATTCGATTGTTGCTTTGTCTGTGTCTGGGGATTTAGAAGAT 156
I  D  P  D  Q  K  F  T  S  Y  G  L  D  S  I  V  A  L  S  V  S  G  D  L  E  D
CTGACGAAATTAGAACTTGAGCCGACACTATTATGGGATTACCCAACAATCAATGCGTTGGCCGAATATCTTGTTTCT 234
L  T  K  L  E  L  E  P  T  L  L  W  D  Y  P  T  I  N  A  L  A  E  Y  L  V  S
GAGCTGCAGCAGGGAGTTGCTTCATGA
E  L  Q  Q  G  V  A  S  *
```

(*b*)

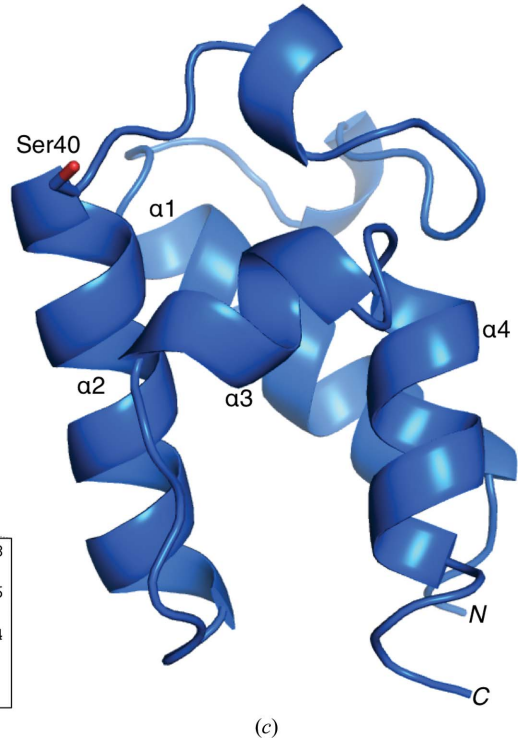

(*c*)

Figure 1
(*a*) The NRPS cluster from *A. baumannii* (with the gene nomenclature from both the AB307-0294 and ATCC17978/M2 strains). Protein sizes and proposed functions are included. (*b*) The genes are organized in a polycistronic operon containing eight genes (grey) preceded by a transcriptional regulatory protein (white). The sequences of the a3404 gene and protein are shown, with the carrier protein phosphopantetheinylation motif in red. (*c*) A ribbon diagram of A3404 highlights the four primary helices, α1–α4, and the long turn between the first two helices that contains two single-turn 3_{10}-helices. Ser40, the site of phosphopantetheinylation, is shown in a stick representation.

Table 2
Top unique homologs of A3404 from the *DALI* server (Z score > 10).

Molecule	PDB code	Type	Z†	R.m.s.d. (Å)	Res.‡	Align.§	Identity (%)	Method	Reference
CurA ACP_I	2liu	PKS ACP	14.0	1.0	99	80	30	NMR	Busche *et al.* (2011)
BlmI	4i4d	Type II NRPS PCP	13.9	1.6	83	78	19	X-ray	Lohman *et al.* (2014)
Protein ASL1650	2afd	PKS/NRPS carrier protein	13.0	1.4	88	79	32	NMR	Johnson *et al.* (2006)
Erythronolide synthase	2ju2	PKS ACP	12.0	1.6	95	79	29	NMR	Alekseyev *et al.* (2007)
EntF	3tej	NRPS PCP	11.5	2.0	320	72	19	X-ray	Liu *et al.* (2011)
TtACP	1x3o	*Thermus thermophilus* ACP	11.2	1.8	78	80	23	X-ray	RIKEN Structural Genomics/Proteomics Initiative (unpublished work)
Tyrocidine synthetase 3	2jgp	Type II NRPS PCP	11.0	1.9	520	74	19	X-ray	Samel *et al.* (2007)
SaACP	4dxe	*Staphylococcus aureus* ACP	10.7	1.8	75	77	16	X-ray	Center for Structural Genomics of Infectious Diseases (unpublished work)
Mupircin ACP	2l22	Tandem PKS ACP	10.6	1.8	76	183	22	NMR	Haines *et al.* (2013)
ScACP	2koq	*Streptomyces coelicolor* ACP	10.4	2.1	79	81	14	NMR	Płoskoń *et al.* (2010)
RcACP	2xz1	Rice ACP	10.4	2.2	76	82	18	X-ray	Guy *et al.* (2011)
PfACP	3gzm	*Plasmodium falciparum* ACP	10.2	2.0	77	81	18	X-ray	Gallagher & Prigge (2010)
RpACP	2kw2	*Rhodopseudomonas palustris* ACP	10.1	1.9	74	101	19	NMR	Ramelot *et al.* (2012)
SoACP	2fve	Spinach ACP	10.0	2.1	77	82	18	NMR	Zornetzer *et al.* (2006)

† The Z-score is a pairwise comparison score to allow ranking of the results. ‡ The number of total residues in a given structure. § The number of residues that were aligned with the query sequence (A3404).

search model. Following higher resolution data collection, the structure in progress was used as a model for molecular replacement. The asymmetric unit contains two A3404 monomers. The final model of A3404 contains 81 residues for each chain; both monomers are missing Gly−1 and His0, remnants from the N-terminal purification tag that remain after TEV cleavage, and Met1, as well as five C-terminal residues (Gln82–Ser86). Crystallographic and refinement data statistics are shown in Table 1.

The domain structure of A3404 is the archetypal carrier protein consisting of four α-helices. The conserved serine that is the site of the 4′-phosphopantetheinylation modification, Ser40, is positioned at the N-terminal end of the second helix (Fig. 1). Multiple carrier protein structures from NRPS clusters and ACPs from PKS and FAS systems have been determined by X-ray crystallography and NMR (Crosby & Crump, 2012; Mercer & Burkart, 2007). Although there is significant structural variation among the previous structures, nearly all structures retain the four main helices. An extended loop joins helices α1 and α2. In the case of A3404, this loop contains two single-turn 3_{10}-helices. While helices α1, α2 and α4 are of similar lengths and are roughly parallel, helix α3 is shorter and is nearly perpendicular to helices α2 and α4. Using the *DALI* alignment server (Holm & Rosenström, 2010), the 14 closest structural homologs to A3404 were determined (all resulting in Z-scores greater than 10; Table 2). Within these structures, the sequence similarity ranged from 13% for an inhibitor-bound adenylation-PCP domain module from *Pseudomonas aeruginosa* (Mitchell *et al.*, 2012) to 32% for the 2afd structure (Johnson *et al.*, 2006) that was used as a model for molecular replacement. This sampling of structures, which included a wide array of representative carrier proteins, all had less than 2.5 Å root-mean-square displacement of C^{α} positions. Interestingly, the list of the proteins that are the closest homologs contains equal numbers of structures determined by X-ray crystallography and by NMR spectroscopy.

3.3. Comparison of the structure of A3404 to other carrier proteins

The classification of carrier proteins into one of the three classes based on sequence or structure alone can be difficult and, indeed, genomic context is another important tool that should be considered. The co-expression of A3404 with the adenylation domain of A3406 and the four-domain NRPS protein at A3403 suggests that this protein will serve in a natural product pathway. We therefore examined the 14 protein structures that were most closely related as predicted by the *DALI* server more closely. Interestingly, the 14 proteins contain seven ACPs from fatty-acid synthesis and transport and seven proteins from natural product (NRPS or PKS) pathways. The top five proteins as scored by *DALI*, and six of the top seven, are all from natural product systems. One protein, a carrier protein from *Anabaena*, is of unclear function; however, the authors considered it to be a carrier protein for either an NRPS or PKS (or hybrid) cluster (Johnson *et al.*, 2006).

The regions of the carrier protein that are most important for distinguishing among the different types are the loop between helix α1 and α2, the α2 helix itself and the α3 helix (Crosby & Crump, 2012; Lai *et al.*, 2006; Lohman *et al.*, 2014; Mercer & Burkart, 2007). Not surprisingly, these are the regions of the proteins that interact with partner proteins, largely owing to the proximity to the site of loading at the start of the α2 helix. We examined the multiple sequence alignment generated from *DALI* and additionally examined the structures of each protein compared with A3404 (Fig. 2). This limited alignment of closely related structures provides some insight into the comparison between the three types of carrier protein. Firstly, we examined the sequence of the pantetheine-binding motif. Of interest, all ACPs, whether from FAS or PKS systems, contained an aspartic acid immediately preceding the serine residue. This trend is consistent with larger alignments presented by others (Crosby & Crump, 2012; Lohman *et al.*,

2014); however, exceptions are clearly present. The acidic nature of the hydrophilic face of helix $\alpha2$ is also quite striking. All FAS ACPs except for PDB entry 2koq contain acidic residues at the second and fifth residues following the pantetheinylated serine and are much more highly acidic at the C-terminal end of the helix. Similarly, the amino acids that immediately precede helix $\alpha3$ also are much more highly acidic in the FAS ACP sequences. These two features are also similar to the observations used to characterize the Asl1650 carrier protein (Johnson *et al.*, 2006).

The structure of A3404 was compared with all 14 of the most closely related ACP structures, and structural alignments for the two most similar structures of each class are shown in Fig. 2(*b*). The structure of the ACP from the curamicin PKS (PDB entry 2liu) illustrates the best alignment with A3404, which is also reflected by the lowest r.m.s. displacement of C^{α} positions (Table 2). In particular, the path traced by the main chain in the divergent loop between helices $\alpha1$ and $\alpha2$ and the $\alpha3$ helix are very similar. The positional conservation with a second PKS ACP is also quite good, although differences in the position of the second 3_{10}-helix of the loop that precedes helix $\alpha2$ are more pronounced. The comparison with the two NRPS PCP structures, BlmI and EntF, show comparable overall similarities. A noteworthy difference is the lack of the first 3_{10}-helix in the two PCP structures. Finally, comparison of the A3404 structure with the FAS ACP structures shows larger

```
        3404    NKDKAYWSAIIRTLVAKEMRVEPETIDPDQKFTSYGLDSIVALSVSGDLEDLTKLELEPTLLWDYPTINALAEYLVSELQ
 1 PKS  2liu    QVNLSEIKQVLKQQLAEALYTEESEIAEDQKFVDLGLDSIVGVEWTTTINQTYNLNLKATKLYDYPTLLELSGYIAQILS
 2 NRPS 4i4d    RTRRRALERDIAAIWAETLGRDS--VGPHEDFAALGGNSIHAIKITNRVEELVDAELSIRVLLETRTVAGMTDHVHATLT
 3 P/N  2afd    -ASVEDIQSWLIDQFAQQLDVDPDDIDMEESFDNYDLNSSKALILLGRLEKWLGKELNPVLIFNYPTIAQLAKRLGELYL
 4 PKS  2ju2    AERTAELVRLVRTSTATVLGHDPKAVRATTPFKELGFDSLAAVRLRNLLNAATGLRLPSTLVFDHPNASAVAGFLDAELG
 5 NRPS 3tej    ----AGSETIIAAAFSSLLGC----QDADADFFALGGHSLLAMKLAAQLSRQVARQVTPGQVMVASTVAKLATIIDAEED
 7 NRPS 2jgp    ----SVWEARLAQVWEQVLNVP--QVGALDDFFALGGHSLRAMRVLSSMHNEYQVDIPLRILFEKPTIQELAAFIEETAK
 9 PKS  2l22    ----DECAQFLRQSLAAMLYCEPGQIRDGSRFLELGLDSVIAAQWIREINKHYQLKIPADGIYTYPVFKAFTQWVGTQLQ

 6 ACP  1x3o    -MTEQEIFEKVKAVIADKLQVEPEKVTLEARFIEDGADSLDTVELIMGLEDEFGLEIS-EEAEKIRTVKDAVEYIKAKLG
 8 ACP  4dxe    --NAMENFDKVKDIIVDRLGVDADKVTEDASFKDLGADSLDIAELVMELEDEFGTEIP-EEAEKINTVGDAVKFINSL--
10 ACP  2koq    -ATQEEIVAGLAEIVNEIAGIPVEDVKLDKSFDDLDVDSLSMVEVVVAAEERFDVKIPDDDVKNLKTVGDATKYILDHQA
11 ACP  2xz1    --AKKETIDKVSDIVKEKLALG-VVVTADSEFSKLGADSLDTVEIVMNLEEEFGINVEDKA-QDISTIQQAADVIEGLLE
12 ACP  3gzm    --SLKSTFDDIKKIISKQLSVEEDKIQMNSNFTKDGADSLDLVELIMALEEKFNVTIDQDA-LKINTVQDAIDYIEKNN-
13 ACP  2kw2    ----TSTFDRVATIIAETCDIPRETITPESHAIDLGIDSLDFLDIAFAIDKAFGIKLPLE--EQYFVLKNLAARIDELVA
14 ACP  2fve    --AKKETIDKVSDIVKEKLALG-VVVTADSEFSKLGADSLDTVEIVMNLEEEFGINVEDEKAQDISTIQQAADVIEGLLE
```

(*a*)

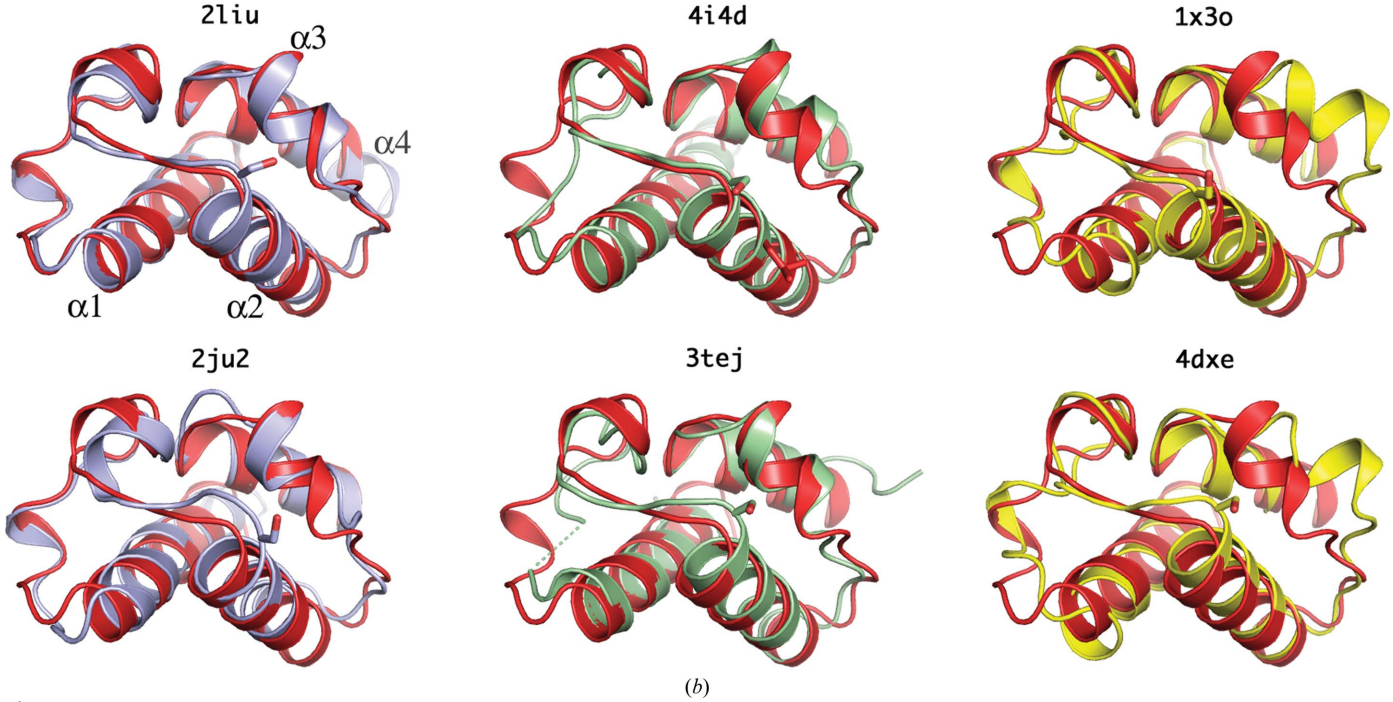

(*b*)

Figure 2
The 14 structures of closest homologs as identified by the *DALI* server were compared with A3404. (*a*) Sequence alignment of the homologous proteins. The first three columns represent the rank in the *DALI* scoring, the type of protein and the PDB code. Proteins in the top half of the alignment are from NPRS or PKS clusters, while proteins in the bottom half are ACPs from fatty-acid synthesis and transport. The pantetheinylation motif is highlighted in yellow; helices $\alpha2$ and $\alpha3$ are shaded in pink. In the alignment, acidic amino acids are red, while basic residues are blue. (*b*) A ribbon diagram of A3404 (red) is superimposed on the top two closest homologs of each of the three carrier protein types. The same orientation is used in all panels and the helix designations are shown in the top left panel. The two PKS acyl carrier proteins 2liu and 2ju2 are shown in light blue. Two NRPS PCP domains, the type II 4i4d and the type I 3tej, are shown in green. Two acyl carrier proteins (1x3o and 4dxe) are shown in yellow. In all structures, the serine residue at the start of helix $\alpha2$ is shown in a stick representation.

differences in the loop between helices $\alpha1$ and $\alpha2$, and, most strikingly, the orientation of the $\alpha3$ helix. This potentially reflects the predominantly acidic nature of the loop immediately before this helix.

Fig. 2(*b*) presents the structures of carrier protein domains from the perspective of the partner protein. The right half of the molecules represents helices $\alpha2$ and $\alpha3$ and the loop that joins them. What is striking from the sequence alignment is the number of negatively charged residues in this region of the ACPs of FAS systems. Of the seven sequences shown, there are an average of more than seven aspartic or glutamic acid residues within this 25-residue stretch. In contrast, the carrier proteins from PKS or NRPS systems show only an average of less than two anionic residues. The A3404 protein has six glutamic acid residues. It seems, however, that this does not imply that A3404 is an ACP from fatty acid metabolism. Rather, this appears to be a function of the type II nature of this protein. BlmI, the recently characterized type II PCP (Lohman *et al.*, 2014), has five acidic residues, as do SgcC2 and MdpC2, two additional type II PCPs from hybrid NRPS/PKS systems (Van Lanen *et al.*, 2006, 2007). It is possible, then, that the highly acidic nature of this region of the protein does not reflect the specific function of the protein as an ACP or PCP but is rather a requirement of the type II carrier proteins. These three proteins, along with A3404, contain the cluster of negatively charged residues at the C-terminal end of helix $\alpha2$; however, none of them contains the anionic residues at the N-terminal portion of this helix.

The first glycine of the pantetheine attachment motif is the most highly conserved residue of the PF00550 family, not including the serine that serves as the necessary pantetheine attachment site. The φ and ψ angles of this residue in A3404 are 94.7 and 2.6°, respectively, in chain *A*, and 97.8 and 0.7°, respectively, in chain *B*. These angles place this residue in a region of the Ramachandran plot that is not allowed for all side-chain-bearing residues. These angles are highly conserved in the closest homologous carrier proteins, including BlmI (85.4 and 12.3°), CurA (142.6 and 5.5°) and the DEBS synthase (112.0 and 56°). This glycine residue is positioned at the end of the 3_{10}-helix and allows the chain to adopt a uniform path to the start of the $\alpha2$ helix. In the 12 structures in Table 2 that contain a glycine at this position, the φ angles range from 63 to 142° and the ψ angles range from −6 to 88°. It appears that this is a structurally conserved configuration that is consistent in a wide variety of carrier protein structures either in isolation or interacting with catalytic domains. The two proteins structures that do not contain a glycine here show main-chain torsion angles φ, ψ of −50, −26° (PDB entry 2afd, residue Asp44) and 74, 85° (PDB entry 2koq, residue Asp37). This highly strained position in the *Streptomyces coelicolor* ACP structure lies just outside the allowable region of the Ramachandran plot for a nonglycine residue.

4. Conclusion

Our laboratory is interested in the production of novel natural products, and in particular we have focused our attention on the NRPS enzymes that are responsible for the production of peptide siderophores. Using the enterobactin and pyoverdine systems of *E. coli* and *P. aeruginosa*, respectively, we have determined the structures of several NRPS domains and associated enzymes. To expand these efforts, we have begun to pursue a novel cluster from the human pathogen *A. baumannii*. The A3404 protein is part of an operon derived from the ABBFA_003406–ABBFA_003399 genes of *A. baumannii* strain AB307-0294 (Adams *et al.*, 2008). Recent studies have demonstrated that genetic disruptions of this operon result in reductions in bacterial motility (Clemmer *et al.*, 2011) and biofilm formation (Rumbo-Feal *et al.*, 2013). This report represents our initial structural characterization of a protein within this pathway. Structural, biochemical and biological experiments are under way to isolate and identify the product of this novel pathway.

The current study presents the structure of a novel carrier protein that is encoded within this biosynthetic operon. Here, we have presented the three-dimensional structure of this protein and compared the sequence and structural features with those of related carrier protein domains from both primary (fatty-acid biosynthesis) and secondary (polyketide and nonribosomal peptide) pathways. The proteins of these processes share many structural features, owing to their shared function, namely the delivery of covalently attached substrates to a variety of interacting catalytic domains. The expression of type II carrier proteins as isolated proteins may pose different demands on their sequence and structure. For example, the free-standing proteins need to bind to their partners intermolecularly in the crowded cellular environment and may therefore require a higher affinity for their partners. Additionally, the solubility requirements for a small isolated protein may result in different global properties than for a domain that is integrated into a larger type I system.

From the structure of A3404, we have identified the features that it shares with carrier proteins of other natural product (NRPS and PKS) systems. The low pI of carrier proteins has been noted previously (Crosby & Crump, 2012; Mercer & Burkart, 2007); however, we have identified potential regions that may be required by free-standing carrier proteins from these different systems. Understanding the structural features of carrier proteins and the interfaces that they form with partner catalytic domains is a valuable step toward characterizing the potential interactions between different proteins of the NRPS and PKS pathways. Similarly, the modular nature of NRPS clusters has raised the potential for engineering these pathways to produce novel peptide products. Clearly, an improved understanding of the key elements that allow functional interactions between the carrier and catalytic domains is necessary for these efforts to succeed.

This work was funded in part by NIH Grant GM-068440 and a grant awarded from and administered by the Telemedicine and Advanced Technology Research Center (TATRC) of the US Army Medical Research and Materiel Command (USAMRMC), Award No. W81XWH-11-2-0218.

Diffraction data were collected at the Stanford Synchrotron Radiation Laboratory, a national user facility operated by Stanford University on behalf of the US Department of Energy, Office of Basic Energy Sciences. The SSRL Structural Molecular Biology Program is supported by the Department of Energy, Office of Biological and Environmental Research, and by the National Institutes of Health National Center for Research Resources, Biomedical Technology Program and the National Institute of General Medical Sciences. We also thank Anyango Kamina for assistance with protein production and crystallization.

References

Adams, M. D., Goglin, K., Molyneaux, N., Hujer, K. M., Lavender, H., Jamison, J. J., MacDonald, I. J., Martin, K. M., Russo, T., Campagnari, A. A., Hujer, A. M., Bonomo, R. A. & Gill, S. R. (2008). *J. Bacteriol.* **190**, 8053–8064.
Adams, P. D. *et al.* (2010). *Acta Cryst.* D**66**, 213–221.
Alekseyev, V. Y., Liu, C. W., Cane, D. E., Puglisi, J. D. & Khosla, C. (2007). *Protein Sci.* **16**, 2093–2107.
Beld, J., Sonnenschein, E. C., Vickery, C. R., Noel, J. P. & Burkart, M. D. (2014). *Nat. Prod. Rep.* **31**, 61–108.
Busche, A., Gottstein, D., Hein, C., Ripin, N., Pader, I., Tufar, P., Eisman, E. B., Gu, L., Walsh, C. T., Sherman, D. H., Löhr, F., Güntert, P. & Dötsch, V. (2011). *ACS Chem. Biol.* **7**, 378–386.
Carter, C. W. Jr & Carter, C. W. (1979). *J. Biol. Chem.* **254**, 12219–12223.
Clemmer, K. M., Bonomo, R. A. & Rather, P. N. (2011). *Microbiology*, **157**, 2534–2544.
Crosby, J. & Crump, M. P. (2012). *Nat. Prod. Rep.* **29**, 1111–1137.
Deng, J., Davies, D. R., Wisedchaisri, G., Wu, M., Hol, W. G. J. & Mehlin, C. (2004). *Acta Cryst.* D**60**, 203–204.
Du, L. & Shen, B. (1999). *Chem. Biol.* **6**, 507–517.
Fischbach, M. A. & Walsh, C. T. (2006). *Chem. Rev.* **106**, 3468–3496.
Gallagher, J. R. & Prigge, S. T. (2010). *Proteins*, **78**, 575–588.
Gross, H. & Loper, J. E. (2009). *Nat. Prod. Rep.* **26**, 1408–1446.
Guy, J. E., Whittle, E., Moche, M., Lengqvist, J., Lindqvist, Y. & Shanklin, J. (2011). *Proc. Natl Acad. Sci. USA*, **108**, 16594–16599.
Haines, A. S. *et al.* (2013). *Nature Chem. Biol.* **9**, 685–692.
Holm, L. & Rosenström, P. (2010). *Nucleic Acids Res.* **38**, W545–W549.
Howard, A., O'Donoghue, M., Feeney, A. & Sleator, R. D. (2012). *Virulence*, **3**, 243–250.
Jancarik, J. & Kim, S.-H. (1991). *J. Appl. Cryst.* **24**, 409–411.
Johnson, M. A., Peti, W., Herrmann, T., Wilson, I. A. & Wüthrich, K. (2006). *Protein Sci.* **15**, 1030–1041.
Kapust, R. B., Tözsér, J., Fox, J. D., Anderson, D. E., Cherry, S., Copeland, T. D. & Waugh, D. S. (2001). *Protein Eng.* **14**, 993–1000.
Keatinge-Clay, A. T. (2012). *Nat. Prod. Rep.* **29**, 1050–1073.
Kissinger, C. R., Gehlhaar, D. K., Smith, B. A. & Bouzida, D. (2001). *Acta Cryst.* D**57**, 1474–1479.
Koglin, A., Mofid, M. R., Löhr, F., Schäfer, B., Rogov, V. V., Blum, M. M., Mittag, T., Marahiel, M. A., Bernhard, F. & Dötsch, V. (2006). *Science*, **312**, 273–276.
Lai, J. R., Koglin, A. & Walsh, C. T. (2006). *Biochemistry*, **45**, 14869–14879.
Li, J. W.-H. & Vederas, J. C. (2009). *Science*, **325**, 161–165.
Liu, Y., Zheng, T. & Bruner, S. D. (2011). *Chem. Biol.* **18**, 1482–1488.
Lohman, J. R., Ma, M., Cuff, M. E., Bigelow, L., Bearden, J., Babnigg, G., Joachimiak, A., Phillips, G. N. Jr & Shen, B. (2014). *Proteins*, doi:10.1002/prot.24485.
Meinwald, J. (2011). *J. Nat. Prod.* **74**, 305–309.
Mercer, A. C. & Burkart, M. D. (2007). *Nat. Prod. Rep.* **24**, 750–773.
Mitchell, C. A., Shi, C., Aldrich, C. C. & Gulick, A. M. (2012). *Biochemistry*, **51**, 3252–3263.
Otwinowski, Z. & Minor, W. (1997). *Methods Enzymol.* **276**, 307–326.
Pettersen, E. F., Goddard, T. D., Huang, C. C., Couch, G. S., Greenblatt, D. M., Meng, E. C. & Ferrin, T. E. (2004). *J. Comput. Chem.* **25**, 1605–1612.
Płoskoń, E., Arthur, C. J., Kanari, A. L., Wattana-amorn, P., Williams, C., Crosby, J., Simpson, T. J., Willis, C. L. & Crump, M. P. (2010). *Chem. Biol.* **17**, 776–785.
Ramelot, T. A. *et al.* (2012). *Biochemistry*, **51**, 7239–7249.
Rumbo-Feal, S., Gómez, M. J., Gayoso, C., Álvarez-Fraga, L., Cabral, M. P., Aransay, A. M., Rodríguez-Ezpeleta, N., Fullaondo, A., Valle, J., Tomás, M., Bou, G. & Poza, M. (2013). *PLoS One*, **8**, e72968.
Samel, S. A., Schoenafinger, G., Knappe, T. A., Marahiel, M. A. & Essen, L. O. (2007). *Structure*, **15**, 781–792.
Smith, M. G., Gianoulis, T. A., Pukatzki, S., Mekalanos, J. J., Ornston, L. N., Gerstein, M. & Snyder, M. (2007). *Genes Dev.* **21**, 601–614.
Strieker, M., Tanović, A. & Marahiel, M. A. (2010). *Curr. Opin. Struct. Biol.* **20**, 234–240.
Vallenet, D. *et al.* (2008). *PLoS One*, **3**, e1805.
Van Lanen, S. G., Lin, S., Dorrestein, P. C., Kelleher, N. L. & Shen, B. (2006). *J. Biol. Chem.* **281**, 29633–29640.
Van Lanen, S. G., Oh, T.-J., Liu, W., Wendt-Pienkowski, E. & Shen, B. (2007). *J. Am. Chem. Soc.* **129**, 13082–13094.
Winn, M. D. *et al.* (2011). *Acta Cryst.* D**67**, 235–242.
Zornetzer, G. A., Fox, B. G. & Markley, J. L. (2006). *Biochemistry*, **45**, 5217–5227.

Future MICROBIOLOGY

EDITORIAL

Re-evaluating the approach to drug target discovery in multidrug-resistant Gram-negative bacilli



Timothy C Umland[1,2], L Wayne Schultz[1,2] & Thomas A Russo*[,3,4,5,6]

KEYWORDS
• *Acinetobacter baumannii* • antibiotic target • bacterial drug target • essential genes • Gram-negative bacilli • multidrug resistant

The incidence of infections due to multi-, extreme- and pan-drug resistant (MDR, XDR and PDR) bacteria is increasing. The term ESKAPE pathogens was coined by the Infectious Disease Society of America to designate bacterial pathogens that cause life-threatening infections and exhibit a high incidence of drug resistant strains [1]. ESKAPE represents *Enterococcus faecium*, *Staphylococcus aureus*, *Klebsiella pneumoniae*, *Acinetobacter baumannii*, *Pseudomonas aeruginosa* and *Enterobacter* spp. *Escherichia coli* has joined the line-up with its ability to acquire and express extended-spectrum beta-lactamases and carbapenemases. *A. baumannii* is one of the most problematic species and has been termed a poster child for XDR and PDR Gram-negative bacilli (GNB) [1]. Treatment of drug-resistant infections is challenging, with resultant increased morbidity, mortality and healthcare costs. The mortality rate is up to 50% for infections caused by XDR *K. pneumoniae* or XDR *A. baumannii* and clinicians often must resort to therapeutics possessing significant toxicity or side effects, such as colistin. Strains of *A. baumannii* resistant to colistin have recently been reported, with concomitant development of cross-resistance to host antimicrobial peptides [2]. The fear of a postantibiotic era was initially predicted to be due to methicillin-resistant *S. aureus* (MRSA) or vancomycin-resistant *Enterococcus* (VRE) but never realized. It is now on the cusp of being

[1]Hauptman-Woodward Medical Research Institute, 700 Ellicott St., Buffalo, NY 14203, USA
[2]Department of Structural Biology, University at Buffalo, State University of New York, 700 Ellicott St., Buffalo, NY 14203, USA
[3]Department of Medicine, University at Buffalo, State University of New York, 3435 Main Street, Buffalo, NY 14214, USA
[4]Department of Microbiology & Immunology, University at Buffalo, State University of New York, 3435 Main Street, Buffalo, NY 14214, USA
[5]The Witebsky Center for Microbial Pathogenesis, University at Buffalo, State University of New York, 3435 Main Street, Buffalo, NY 14214, USA
[6]Veterans Administration Western New York Healthcare System, 3495 Bailey Avenue Buffalo, NY 14215, USA
*Author for correspondence: Tel.: +1 716 829 2674; Fax: +1 716 829 3889; trusso@buffalo.edu

Future Medicine part of fsg

fulfilled by GNB such as *A. baumannii*. Over 2 million people acquire serious drug-resistant bacterial infections annually in the USA, resulting in more than 23,000 deaths. Many more deaths are attributed to medical conditions complicated by antibiotic-resistant infections [3]. The annual cost to the US economy of treating drug-resistant infections is estimated to be $20–$35 billion.

New classes of antibiotics against all types of bacterial pathogens are required, but the situation is particularly urgent with respect to GNB. Unfortunately, a 2013 review revealed that there were virtually no new antimicrobial agents active against GNB in the pharmaceutical pipeline [4]. In fact, avibactam, a non-β-lactam β-lactamase inhibitor, delivered in combination with ceftazadime was the only novel anti-GNB in clinical trials. Development of new antimicrobials is a long, arduous and expensive process. As a result, many major pharmaceutical companies have exited antimicrobial R&D. In order to address the dearth of antibiotic development, in 2012 the Generating Antibiotic Incentives Now Act was enacted in the USA to provide incentives for the development of new antibiotics, including priority review by the US FDA and a 5-year extension of exclusivity. Even with new incentives, there has been little advancement in the treatment of GNB infections.

"In order to address the dearth of antibiotic development, in 2012 the Generating Antibiotic Incentives Now Act was enacted in the USA to provide incentives for the development of new antibiotics…"

A variety of approaches are being used to fill this need. Examples include analogs of currently approved antibiotics, repurposing of approved or candidate drugs, development of efflux pump and β-lactamase inhibitors and discovery of new chemical entities. Screening campaigns to identify new small molecule compounds follow two general strategies: whole-cell phenotype or target based. Phenotype screens offer the advantage of directly identifying compounds possessing bactericidal or bacteriostatic activity. However, this strategy often does not connect activity to a specific target(s), adding significant difficulty during the hit-to-lead optimization process. Target-based screens offer the promise of a theoretically elegant approach, but have yet to result in a bountiful yield of new antibiotics. The limiting factor of this approach is that compounds active against purified targets may not display activity against live bacteria, most often due to permeability and/or efflux issues. Target-based methods gained favor in the mid 1990s when whole-genome sequencing data became available. However, the increased focus on target-based screening occurred while FDA approvals of new antibiotics were decreasing, particularly those representing novel classes. Therefore, this inverse relationship has given target-based antibiotic discovery a poor reputation. The trend of decreased antibiotic discovery began well before target-based methods came into vogue (only a single new class, mupirocin, was launched between the early 1970s and 1999), due to a variety of economic, regulatory and scientific factors [4]. In natural product screens, the low-hanging fruit were picked (and repicked) over the past decades and now methods are required to avoid rediscovering these known natural products while identifying new natural products with antibacterial activity [5]. Many target-based screens suffered from nonoptimal selections of chemical libraries [6]. For pragmatic reasons, large chemical libraries are often biased toward chemical space favorable for identifying drug-like molecules against eukaryotic therapeutic targets (e.g., oncology and cardiovascular, among others). Chemoinformatic studies have demonstrated that drugs acting upon eukaryotic versus prokaryotic targets possess significantly different chemical properties [7]. The lack of positive results may be partially due to looking in the wrong place rather than due to the target-based strategy itself. Lessons learned from past antibiotic discovery efforts will inform the newly re-emerging and urgently needed efforts.

Target-based antibiotic discovery strategies place great weight on gene essentiality. However, selection and prioritization of putative antibacterial targets have largely relied on inferred essentiality annotations due to the relatively small number of genome-wide essentiality screens, with the majority conducted on rich lab media [8,9]. Unfortunately, inferred essentiality often neglects the significant disparity in annotation for a given orthologous family across experimental essentiality screens. Pairwise comparison of genome-wide prokaryotic essential gene sets typically have 50–70% overlap, but this rapidly decreases as the number of species being compared increases [10]. This disparity reflects real genetic and phenotypic differences between species and even strains, but also reflects experimental approaches and data analysis. Confidence levels vary greatly

for gene essentiality predictions and in the past (and present) have resulted in the selection of nonoptimal targets to pursue for antibiotic drug discovery or the exclusion of targets perhaps worthy of consideration.

Further, gene essentiality has been traditionally defined as the minimal gene set required for growth of a specific organism under optimal growth conditions. However, gene essentiality is increasingly being viewed as contextual [11]. Altered nutrient levels, changes in carbon sources and environmental stressors have been demonstrated to change the set of genes required for growth or survival [12,13]. Microorganisms infrequently encounter ideal growth conditions, except for in the lab and so they have evolved to grow and survive in multiple and changing environments. For example, bacterial pathogens have coevolved with their host(s) and will typically encounter a very different environment during infection of a host (nutrient poor, host defenses) versus during growth on lab media (nutrient rich). Inclusion of genes required to grow and survive under nonoptimal conditions (contextual essential genes) may expand the set of potential antibacterial targets. Conversely, genes experimentally determined as essential under optimal *in vitro* growth conditions have been later discovered to be dispensable during infection of a host, resulting in reconsideration of drugs under development [14,15].

Our group has recently published a unique methodology that employed screening of *A. baumannii* mutants in ascites, a clinically relevant human body fluid and subsequent *in vivo* validation to specifically and efficiently select for and identify what we termed *in vivo* essential genes [16–18]. These *in vivo* essential genes are not essential for growth and survival under standard rich lab media growth conditions, but are essential for growth and survival during infection of a host. Comparison of these *A. baumannii in vivo* essential genes against the Database of Essential Genes (DEG) demonstrated that 89% of these genes could not be readily predicted as being essential *in vivo*. This figure is even more profound considering that essentiality data for a related species, *Acinetobacter baylyi* is present within DEG. Likely, this observation was due to most genome-wide screens cataloged in DEG being performed *in vitro* using rich laboratory media and none used a clinically relevant medium. The *A. baylyi* essentiality screen used a defined minimal medium, but that failed to fully represent *in vivo* conditions. These results emphasize that when prioritizing antibacterial targets, caution is required when trying to predict essential genes either for a single species under different growth environments or across species. Neglecting these important caveats may result in unnecessarily excluding potential targets or assigning falsely high rankings to targets. In other words, there is no replacement for experimental data conducted under conditions that best represent those of an actual infection. Our method is efficient and can be extended for use with any pathogens that grow in a relevant human body fluid. This philosophy has been implemented at Pfizer in screen mimicking carbon source conditions encountered during infection that identified antimicrobial lead compounds acting upon the two glyoxylate shunt enzymes in *P. aeruginosa* [19].

There is no silver bullet for antimicrobial drug development and especially for agents effective against drug-resistant GNB. At the target identification stage, it would seem prudent to design a screening strategy that identifies essential genes under clinically relevant conditions. Likewise, if a previously identified putative target is chosen for further study, it is critical to confirm essentially under conditions similar to those the pathogen will experience during human infection. In this manner, the chances of discovering that a target is dispensable during human infection after significant resource investment will be minimized [14,20]. We are faced with an extremely difficult challenge in an era of decreasing resources for antimicrobial development. It is imperative that logical drug design is based on logical target identification.

"We are faced with an extremely difficult challenge in an era of decreasing resources for antimicrobial development. It is imperative that logical drug design is based on logical target identification."

Financial & competing interests disclosure

This work was supported in part by a Telemedicine and Advance Technical Research Center (TATRC) cooperative agreement W81XWH-11-2-0218 (TA Russo, LW Schultz and TC Umland) and a VA Merit Review from the Department of Veterans Affairs (TA Russo). The authors have no other relevant affiliations or financial involvement with any organization or entity with a financial interest in or financial conflict with the subject matter or materials discussed in the manuscript apart from those disclosed.

No writing assistance was utilized in the production of this manuscript.

References

1 Boucher HW, Talbot GH, Bradley JS *et al.* Bad bugs, no drugs: no ESKAPE! An update from the Infectious Diseases Society of America. *Clin. Infect. Dis.* 48(1), 1–12 (2009).

2 Napier BA, Burd EM, Satola SW *et al.* Clinical use of colistin induces cross-resistance to host antimicrobials in *Acinetobacter baumannii*. *MBio* 4(3), e00021–e00013 (2013).

3 *Antibiotic Resistance Threats in the United States, 2013.* U.S. Centers for Disease Control and Prevention (CDC), Atlanta, GA, USA (2013).

4 Butler MS, Blaskovich MA, Cooper MA. Antibiotics in the clinical pipeline in 2013. *J. Antibiot.* 66(10), 571–591 (2013).

5 Kirst HA. Developing new antibacterials through natural product research. *Expert Opin. Drug Discov.* 8(5), 479–493 (2013).

6 Gwynn MN, Portnoy A, Rittenhouse SF, Payne DJ. Challenges of antibacterial discovery revisited. *Ann. NY Acad. Sci.* 1213, 5–19 (2010).

7 Macielag MJ. Chemical properties of antimicrobials and their uniqueness. In: *Antibiotic Discovery and Development*. Dougherty TJ, Pucci MJ (Eds). Springer, New York, NY, USA 793–820 (2012).

8 Luo H, Lin Y, Gao F, Zhang CT, Zhang R. DEG 10, an update of the database of essential genes that includes both protein-coding genes and noncoding genomic elements. *Nucleic Acids Res.* 42, D574–D580 (2014).

9 Panjkovich A, Gibert I, Daura X. antibacTR: dynamic antibacterial-drug-target ranking integrating comparative genomics, structural analysis and experimental annotation. *BMC Genomics* 15, 36 (2014).

10 Salama NR, Shepherd B, Falkow S. Global transposon mutagenesis and essential gene analysis of *Helicobacter pylori*. *J. Bacteriol.* 186(23), 7926–7935 (2004).

11 D'elia MA, Pereira MP, Brown ED. Are essential genes really essential? *Trends Microbiol.* 17(10), 433–438 (2009).

12 Joyce AR, Reed JL, White A *et al.* Experimental and computational assessment of conditionally essential genes in *Escherichia coli*. *J. Bacteriol.* 188(23), 8259–8271 (2006).

13 Van Opijnen T, Camilli A. A fine scale phenotype-genotype virulence map of a bacterial pathogen. *Genome Res.* 22(12), 2541–2551 (2012).

14 Brinster S, Lamberet G, Staels B, Trieu-Cuot P, Gruss A, Poyart C. Type II fatty acid synthesis is not a suitable antibiotic target for Gram-positive pathogens. *Nature* 458(7234), 83–86 (2009).

15 Parsons JB, Frank MW, Subramanian C, Saenkham P, Rock CO. Metabolic basis for the differential susceptibility of Gram-positive pathogens to fatty acid synthesis inhibitors. *Proc. Natl Acad. Sci. USA* 108(37), 15378–15383 (2011).

16 Russo TA, Luke NR, Beanan JM *et al.* The K1 capsular polysaccharide of *Acinetobacter baumannii* strain 307–0294 is a major virulence factor. *Infect. Immun.* 78(9), 3993–4000 (2010).

17 Russo TA, Macdonald U, Beanan JM *et al.* Penicillin-binding protein 7/8 contributes to the survival of *Acinetobacter baumannii in vitro* and *in vivo*. *J. Infect. Dis.* 199(4), 513–521 (2009).

18 Umland TC, Schultz LW, MacDonald U, Beanan JM, Olson R, Russo TA. *In vivo*-validated essential genes identified in *Acinetobacter baumannii* by using human ascites overlap poorly with essential genes detected on laboratory media. *MBio* 3(4), pii: e00113–12 (2012).

19 Fahnoe KC, Flanagan ME, Gibson G, Shanmugasundaram V, Che Y, Tomaras AP. Non-traditional antibacterial screening approaches for the identification of novel inhibitors of the glyoxylate shunt in Gram-negative pathogens. *PLoS ONE* 7(12), e51732 (2012).

20 Silver LL. Challenges of antibacterial discovery. *Clin. Microbiol. Rev.* 24(1), 71–109 (2011).

IAI Journals.ASM.org

Aerobactin Mediates Virulence and Accounts for Increased Siderophore Production under Iron-Limiting Conditions by Hypervirulent (Hypermucoviscous) *Klebsiella pneumoniae*

Thomas A. Russo,[a,b,c,e] Ruth Olson,[a,b] Ulrike MacDonald,[a,b] Daniel Metzger,[a,b] Lauren M. Maltese,[b] Eric J. Drake,[d,f] Andrew M. Gulick[d,f]

Veterans Administration Western New York Healthcare System, Buffalo, New York, USA[a]; Department of Medicine,[b] Department of Microbiology and Immunology,[c] Department of Structural Biology,[d] and The Witebsky Center for Microbial Pathogenesis,[e] University at Buffalo-State University of New York, Buffalo, New York, USA; Hauptman-Woodward Medical Research Institute, Buffalo, New York, USA[f]

Hypervirulent (hypermucoviscous) *Klebsiella pneumoniae* (hvKP) strains are an emerging variant of "classical" *K. pneumoniae* (cKP) that cause organ and life-threatening infection in healthy individuals. An understanding of hvKP-specific virulence mechanisms that enabled evolution from cKP is limited. Observations by our group and previously published molecular epidemiologic data led us to hypothesize that hvKP strains produced more siderophores than cKP strains and that this trait enhanced hvKP virulence. Quantitative analysis of 12 hvKP strains in iron-poor minimal medium or human ascites fluid showed a significant and distinguishing 6- to 10-fold increase in siderophore production compared to that for 14 cKP strains. Surprisingly, high-pressure liquid chromatography (HPLC)-mass spectrometry and characterization of the hvKP strains hvKP1, A1142, and A1365 and their isogenic aerobactin-deficient (Δ*iucA*) derivatives established that aerobactin accounted for the overwhelming majority of increased siderophore production and that this was not due to gene copy number. Further, aerobactin was the primary factor in conditioned medium that enhanced the growth/survival of hvKP1 in human ascites fluid. Importantly the *ex vivo* growth/survival of hvKP1 Δ*iucA* was significantly less than that of hvKP1 in human ascites fluid, and the survival of outbred CD1 mice challenged subcutaneously or intraperitoneally with hvKP1 was significantly less than that of mice challenged with hvKP1 Δ*iucA*. The lowest subcutaneous and intraperitoneal challenge inocula of 3×10^2 and 3.2×10^1 CFU, respectively, resulted in 100% mortality, demonstrating the virulence of hvKP1 and its ability to cause infection at a low dose. These data strongly support that aerobactin accounts for increased siderophore production in hvKP compared to cKP (a potential defining trait) and is an important virulence factor.

The emergence of a "hypervirulent" (hypermucoviscous) variant of *Klebsiella pneumoniae* (hvKP) is a major challenge that needs to be confronted (1, 2). This pathogen is undergoing global dissemination from the Asian Pacific Rim, where it was first recognized in 1986 (3). In contrast to the usual health care-associated venue for "classical" *K. pneumoniae* (cKP) infections in the West, which have received increased notoriety due to their propensity for acquiring antimicrobial resistance determinants (4, 5), hvKP causes serious, life-threatening infections in younger, healthy individuals in the community setting (6–8). Due to a lack of awareness and of an objective diagnostic test to differentiate hvKP from cKP, the incidence and full spectrum of disease are still being defined. Nonetheless, it is clear that the initially described community-acquired pyogenic liver abscess (CA-PLA) in the absence of biliary tract disease represents just one of many possible primary infections (9), which also include endophthalmitis, meningitis, and necrotizing fasciitis (10–12). Another clinically defining feature is the ability to metastatically spread from primary sites of infection in noncompromised hosts, which further distinguishes hvKP from cKP and enteric Gram-negative bacilli (GNB) in general (3, 13, 14). Both clinically (2) and experimentally (7, 15), hvKP is more virulent than cKP. One of many knowledge gaps regarding hvKP is an understanding of hvKP-specific virulence mechanisms that distinguish these strains from cKP, from which they evolved.

The ability of bacterial pathogens to modify their inherent virulence most commonly occurs by horizontal gene transfer. Virulence plasmid acquisition may be an important mechanism for the increased virulence of hvKP. Genes that encode a number of virulence factors, including those that are responsible for the hypermucoviscous phenotype (RmpA) and the siderophores (SP) aerobactin and salmochelin, are located on a large, 200- to 220-kb virulence plasmid that is not present in most cKP strains (16–18). Since the hypermucoviscous phenotype (which is probably due to increased capsule production) (reviewed in reference 2) was the initial defining trait of hvKP strains, it has received significant attention as a virulence factor and, despite conflicting data (2, 19–21), likely contributes to the increased pathogenicity. Other studies have identified factors that contribute to the virulence of hvKP, but these factors or properties are often present in cKP strains. More experiments are needed to establish whether a virulence factor or property present in both cKP and hvKP is equally important for their pathogenesis or whether it accounts for the increased virulence of hvKP strains compared to cKP strains (22).

Received 27 December 2013 **Returned for modification** 3 February 2014
Accepted 17 March 2014
Published ahead of print 24 March 2014
Editor: A. Camilli
Address correspondence to Thomas A. Russo, trusso@acsu.buffalo.edu.

doi:10.1128/IAI.01667-13

TABLE 1 Bacterial strains used in this study

Strain	Siderophore genotype	Phenotype[a]	Site(s) of isolation/clinical syndrome(s)	Location (reference)
hvKP1	*entB*$^+$ *iroB*$^+$ *irp2*$^+$ *iucA*$^+$	ST$^+$, K2	Liver aspirate, blood/PLA	Buffalo, NY (7)
hvKP2	*entB*$^+$ *iroB*$^+$ *irp2*$^+$ *iucA*$^+$	ST$^+$, K1	Blood/endophthalmitis	Buffalo, NY (this study)
hvKP3	*entB*$^+$ *iroB*$^+$ *irp2*$^+$ *iucA*$^+$	ST$^+$, K1	Stool/colonization	Buffalo, NY (this study)
hvKP4	*entB*$^+$ *iroB*$^+$ *irp2 iucA*$^+$	ST$^+$	Blood/PLA	Minneapolis, MN (this study)
NTUH-K2044	*entB*$^+$ *iroB*$^+$ *irp2*$^+$ *iucA*	ST$^+$, K1	Blood/PLA, meningitis	Taipei, Taiwan (31)
A1142	*entB*$^+$ *iroB*$^+$ *irp2 iucA*$^+$	ST$^+$, K57	Blood/PLA	Taipei, Taiwan
A1365	*entB*$^+$ *iroB*$^+$ *irp2*$^+$ *iucA*$^+$	ST$^+$, K54	Blood/PLA	Taipei, Taiwan
A4528	*entB*$^+$ *iroB*$^+$ *irp2 iucA*$^+$	ST$^+$, K2	Blood/PLA	Taipei, Taiwan
A9534	*entB*$^+$ *iroB*$^+$ *irp2 iucA*$^+$	ST$^+$, K5	Blood/PLA	Taipei, Taiwan
N4252	*entB*$^+$ *iroB*$^+$ *irp2 iucA*$^+$	ST$^+$, K57	Blood/cholangitis	Taipei, Taiwan
N6319	*entB*$^+$ *iroB*$^+$ *irp2*$^+$ *iucA*$^+$	ST$^+$, K2	Blood/sepsis	Taipei, Taiwan
N7205	*entB*$^+$ *iroB*$^+$ *irp2*$^+$ *iucA*$^+$	ST$^+$, K1	Blood/cholecystitis	Taipei, Taiwan
cKP1	*entB*$^+$ *iroB irp2 iucA*	ST$^-$	Blood/unknown	Buffalo, NY (7)
cKP2	*entB*$^+$ *iroB irp2 iucA*	ST$^-$	Blood/unknown	Buffalo, NY (7)
cKP3	*entB*$^+$ *iroB irp2 iucA*	ST$^-$	Blood/unknown	Buffalo, NY (7)
cKP4	*entB*$^+$ *iroB irp2 iucA*	ST$^-$	Blood/unknown	Buffalo, NY (7)
KP1	*entB*$^+$ *iroB irp2 iucA*	ST$^-$	Blood/unknown	Buffalo, NY (this study)
KP2	*entB*$^+$ *iroB irp2 iucA*	ST$^-$	Blood/unknown	Buffalo, NY (this study)
KP3	*entB*$^+$ *iroB irp2 iucA*	ST$^-$	Blood/unknown	Buffalo, NY (this study)
KP4	*entB*$^+$ *iroB irp2 iucA*	ST$^-$	Blood/unknown	Buffalo, NY (this study)
KP5	*entB*$^+$ *iroB irp2 iucA*	ST$^-$	Blood/unknown	Buffalo, NY (this study)
KP6	*entB*$^+$ *iroB irp2*$^+$ *iucA*	ST$^-$	Blood/unknown	Buffalo, NY (this study)
KP7	*entB*$^+$ *iroB irp2 iucA*	ST$^-$	Blood/unknown	Buffalo, NY (this study)
KP8	*entB*$^+$ *iroB irp2 iucA*	ST$^-$	Blood/unknown	Buffalo, NY (this study)
KP9	*entB*$^+$ *iroB irp2 iucA*	ST$^-$	Blood/unknown	Buffalo, NY (this study)
KP24	*entB*$^+$ *iroB irp2 iucA*	ST$^-$	Blood/unknown	Buffalo, NY (this study)

[a] ST, string test; K, capsular serotype.

The ability to acquire iron (Fe) is essential for bacterial growth and replication. This trait has been shown to play a crucial role in the progression of infection, including cKP infection (23). The host has a number of Fe binding proteins (e.g., transferrin) that serve to withhold Fe from the invading pathogen. *K. pneumoniae*, like other *Enterobacteriaceae*, produces and secretes SP that acquire Fe from host binding proteins and then reenter the bacterial cell by SP-specific receptors (24). Aerobactin, enterobactin, salmochelin, and yersiniabactin are SP that have been described in *K. pneumoniae* (25). Gene clusters for the *Yersinia* high-pathogenicity island (encodes yersiniabactin) and *iucABCD-iutA* (encodes aerobactin and its cognate receptor) were more prevalent in hvKP (38/42 and 39/42 strains, respectively) than in cKP (7/32 and 6/32, respectively) (25). In addition, aerobactin genes and aerobactin production, as demonstrated by a cross-feeding assay, were more common in hvKP strains than in cKP strains (8, 15).

These bioinformatic-molecular epidemiologic analyses suggested that hvKP strains might have the capability to acquire Fe more readily than cKP strains. Hsieh et al. began to address this possibility by assessing the virulence of mutant derivatives of the hvKP strain NTUH-K2044 (25). However, a decrease in virulence after intraperitoneal (i.p.) challenge was seen only when the production of yersiniabactin, aerobactin, and salmochelin was disrupted together. Recent data from our group, however, have established that the hvKP strain hvKP1 produced more Fe acquisition factors than four cKP bacteremic isolates (22). Further, it was shown that this property enhanced the growth/survival of hvKP1 in human ascites fluid *ex vivo*. Although this study established that hvKP1 produced more Fe acquisition factors, it was not formally established whether SP were responsible or whether this observation was generally applicable for hvKP strains.

In this study, we tested the hypotheses that hvKP strains produce more SP than do cKP strains and that this trait is an important mechanism contributing to the hypervirulence of hvKP. We demonstrate that increased SP production in hvKP compared to cKP strains was a distinguishing trait that enhanced the growth of hvKP strains in human ascites fluid. Surprisingly, physical and genetic evidence illustrated that nearly all of the increased SP production by hvKP strains was due to increased aerobactin production and that this increased production appears to be mediated by a novel mechanism. Lastly, aerobactin was shown to increase growth/survival *ex vivo* in human ascites fluid and in mice challenged subcutaneously (s.c.) or intraperitoneally, enabling infection to occur at a low challenge inoculum, a critical feature for a pathogen. These data establish aerobactin as an important virulence factor for hvKP.

MATERIALS AND METHODS

Strain description. hvKP1 (ST86, K2 serotype, ampicillin resistant) was isolated from blood and liver abscess aspirate from a previously healthy 24-year-old male from Buffalo, NY, USA, with CA-PLA and metastatic spread to the spleen (7). Additional wild-type hvKP and cKP clinical isolates used in this study are described in Table 1. Although the definition is imperfect, since an unequivocal test that distinguishes between hvKP and cKP strains is presently lacking, hvKP strains were defined as having a positive string test and/or being associated with community-acquired *K. pneumoniae* infections with clinical features characteristic of hvKP, such as metastatic spread (2). Genotypes for SP biosynthetic genes were designated by the presence or absence of PCR-generated amplicons: en-

terobactin (*entB* plus, 5′-GATGAAGACGATACCGTGC-3′; *entB* minus, 5′-ACCGAATCCAGACCGTAGTC-3′), salmochelin (*iroB* plus, 5′-ATCTCATCATCTACCCTCCGCTC-3′; *iroB* minus, 5′-GGTTCG CCGTCGTTTTCAA-3′), yersiniabactin (*irp2* plus, 5′-GCTACAATG GGACAGCAACGAC-3′; *irp2* minus, 5′-GCAGAGCGATACGGAAA ATGC-3′), and aerobactin (*iucA* plus, 5′-AATCAATGGCTATTCCC GCTG-3′; *iucA* minus, 5′-CGCTTCACTTCTTTCACTGACAGG-3′). Aerobactin-deficient derivatives of hvKP1 (hvKP1 Δ*iucA*), A1142 (A1142 Δ*iucA*), and A1365 (A1365 Δ*iucA*) were generated by allelic exchange as described previously (26). Constructs were confirmed by sequence analysis of PCR-generated amplicons using primers outside *iucA* (plus, 5′-ATAAGGCAGGCAATCCAG-3′; minus, 5′-TAACGGC GATAAACCTCG-3′). Polar effects were excluded by reverse transcription-PCR (RT-PCR) identification of the expected transcript for *iucB* (plus, 5′-GCAGTTACCGCTATGGCTGAGTTC-3′; minus, 5′-C CGCTTTGCTCCCAGAAATACTC-3′), which is immediately downstream from *iucA* (data not shown). Further, the Δ*iucA* derivatives remained *rmpA*, *iroN*, and string test positive. For *trans* complementation of hvKP1 Δ*iucA*, the plasmid pFUS2[*iucA-D*] was constructed by ligating the *iucA-D* PCR-generated amplicon (plus, 5′-ATGGATC CGAACAGCATTGAGCCAAGC-3′ [261bp 5′ to the *iucA* open reading frame {ORF}); minus, 5′-GTAGGTACCAGAAGCAGTGGGTTG AGAG-3′ [131bp 3′ to the *iucD* ORF]), which contains its native promoter and upstream regulatory sequence, into pFUS2 (confers gentamicin resistance) (27). pFUS2[*iucA-D*] was introduced by electroporation into hvKP1 Δ*iucA*, resulting in hvKP1 Δ*iucA*/pFUS2[*iucA-D*]. A quantitative SP assay performed on conditioned medium, generated by the growth of hvKP1 Δ*iucA*/pFUS2[*iucA-D*] grown in Fe-poor minimal medium (MM) plus gentamicin, demonstrated that SP production was 81% of that observed for its parent hvKP1. pFUS2[*iucA-D*] was poorly retained by hvKP1 Δ*iucA* in the absence of positive selection by the addition of gentamicin (2.5 μg/ml). Initially, a plasmid construct that contained only *iucA* (pFUS2[*iucA*]) was generated, but it did not result in SP production when used for *trans* complementation of hvKP1 Δ*iucA*. In addition, pFUS2 was introduced into hvKP1 (resulting in hvKP1/pFUS2) and hvKP1 Δ*iucA* (resulting in hvKP1 Δ*iucA*/pFUS2) for use in complementation experiments. All strains were maintained at −80°C in 50% Luria-Bertani (LB) broth and 50% glycerol prior to use.

Media. The procedures for obtaining human ascites fluid were reviewed and approved by the Western New York Veterans Administration Institutional Review Board. The Western New York Veterans Administration Institutional Review Board waived the need for informed consent for the process of obtaining ascites fluid. An expedited review was performed because the ascites fluid was collected from deidentified patients who were undergoing therapeutic paracentesis for symptoms due to abdominal distension. These individuals were not being treated with antimicrobials and were not infected with human immunodeficiency, hepatitis B, or hepatitis C virus. The ascites fluid was cultured to confirm sterility, divided into aliquots, and stored at −80°C. Each batch was obtained from a different patient and was designated by the date of removal. Ascites fluid batch 8/27/2009 was used for the growth studies reported in Fig. 1, and batch 10/18/2012 was used for all other studies in this report. For various *in vitro* growth studies, 100% ascites fluid, LB medium, or M9 MM was used.

Development of conditioned medium. Conditioned medium was generated as described previously (22).

***In vitro* growth in ascites fluid, LB, and M9 MM.** Growth in ascites fluid, LB, and M9 MM was determined as described previously with aliquots removed for bacterial enumeration at various times (28). The growth rates and plateau densities achieved by wild-type cKP and hvKP strains were similar in ascites fluid treated at 56°C for 30 min to inactivate complement activity, LB, and M9 MM. In some experiments, conditioned medium generated from various strains or high-pressure liquid chromatography (HPLC)-generated fractions of conditioned medium were added.

Quantitative SP assay. The quantitative SP concentration in conditioned medium and in HPLC fractions of conditioned medium generated by cKP and hvKP strains was determined using a modified chrome azurol S (CAS) assay (29). In brief, standards containing 0, 1.5, 3.1, 6.25, 12.5, 25, 50, and 100 μg/ml of SP were prepared. The SP assay solution consisted of 50 ml of 1.2 mM hexadecyltrimethylammonium bromide, 7.5 ml of 2 mM CAS, 1.5 ml of 1 mM $FeCl_3 \cdot 6H_2O$ in 10 mM HCl, and 1.37 M piperazine (the pH was adjusted to 5.6 with HCl). In a flat-bottom 96-well plate, 100 μl of each standard or sample was added to wells, followed by the addition of 100 μl of 98% SP assay solution and 2% 0.2 M 5-sulfosalicyclic acid solution in duplicate. The reaction mixture was incubated for 30 min, and results were read at 630 nm. For quantitative interpretation, a reference curve was calculated as follows: (optical density [OD] standard/OD zero standard) × 100. A curve was generated using cubic spline analysis in Prism software. The SP concentration in each sample was extrapolated from the linear portion of the reference curve. SP concentrations were reported in μg/ml/1×10^9 bacterial CFU. SP assays performed on HPLC-generated fractions of unconditioned MM and human ascites fluid demonstrated background detection levels of 10.8 μg/ml and 2.4 μg/ml, respectively, in fraction 1. These amounts were subtracted from the appropriate conditioned-medium SP values.

Analysis of conditioned medium via HPLC. Conditioned medium was subjected to fractionation utilizing HPLC on an Agilent 1260 system in line with a C_{18} column (Eclipse; 4.6 by 100 mm, 3.5 μm) running an aqueous mobile phase containing 0.1% (vol/vol) formic acid at a flow rate of 1 ml/min. All runs were monitored at 230 nm with the samples reconstituted in the initial HPLC gradient buffer. Exploratory runs were conducted with an initial linear gradient from 5% methanol (MeOH) to 40% MeOH over 40 min at a column temperature of 40°C. The 20 largest peaks were collected, spotted on chrome azurol agar, and monitored qualitatively for SP activity. Of the 20 peaks, only one peak, subsequently designated fraction 5 (see Fig. 3A), displayed substantial Fe acquisition capability (data not shown). The HPLC gradient profile was subsequently modified to a 5% to 23% linear MeOH gradient over 20 min, and 5 fractions from the conditioned-medium sample, designated fractions 1 to 5, were collected.

Further purification of fraction 5 was undertaken by evaporating the fraction to dryness and reconstituting in 5% acetonitrile (ACN). This sample was run using a linear gradient from 5 to 40% ACN over 20 min at a column temperature of 40°C. Fractions collected from this run were designated 5a to 5e.

Analysis of HPLC fraction by MS. Mass spectrometry (MS) analysis was carried out by injecting 250 ng of purified fraction 5c onto a ThermoFinnigan LCQ Advantage equipped with an electrospray ionization source. Conditions were evaluated in 60% MeOH with a source voltage of 4.5 kV, a capillary voltage of 23.5 V, and a transfer tube temperature of 250°C. Spectra were scanned in negative-ion mode over the range of *m/z* 150 to 1000.

Mouse s.c. challenge infection model. The mouse s.c. challenge infection models have been previously described (22, 30). These animal studies were reviewed and approved by the University at Buffalo-SUNY and Veterans Administration Institutional Animal Care Committee. This study was carried out in strict accordance with the recommendations in the Guide for the Care and Use of Laboratory Animals of the National Institutes of Health, and all efforts were made to minimize suffering. In brief, outbred male CD1 mice (18 to 22 g) were challenged subcutaneously (s.c.) with either 3.0×10^2 ($n = 5$), 3.5×10^3 ($n = 10$), 3.5×10^4 ($n = 10$), or 3.5×10^5 ($n = 10$) CFU of hvKP1 or 2.8×10^2 ($n = 5$), 3.6×10^3 ($n = 10$), 3.6×10^4 ($n = 10$), or 3.6×10^5 ($n = 10$) CFU of hvKP1 Δ*iucA* (results for groups with $n = 10$ represent average titers from 2 experiments). In another experiment, CD1 mice were challenged i.p. with either 3.2×10^1 ($n = 5$), 3.2×10^2 ($n = 5$), 3.2×10^3 ($n = 5$), or 3.2×10^4 ($n = 5$) CFU of hvKP1 or 2.4×10^1 ($n = 5$), 2.4×10^2 ($n = 5$), 2.4×10^3 ($n = 5$), or

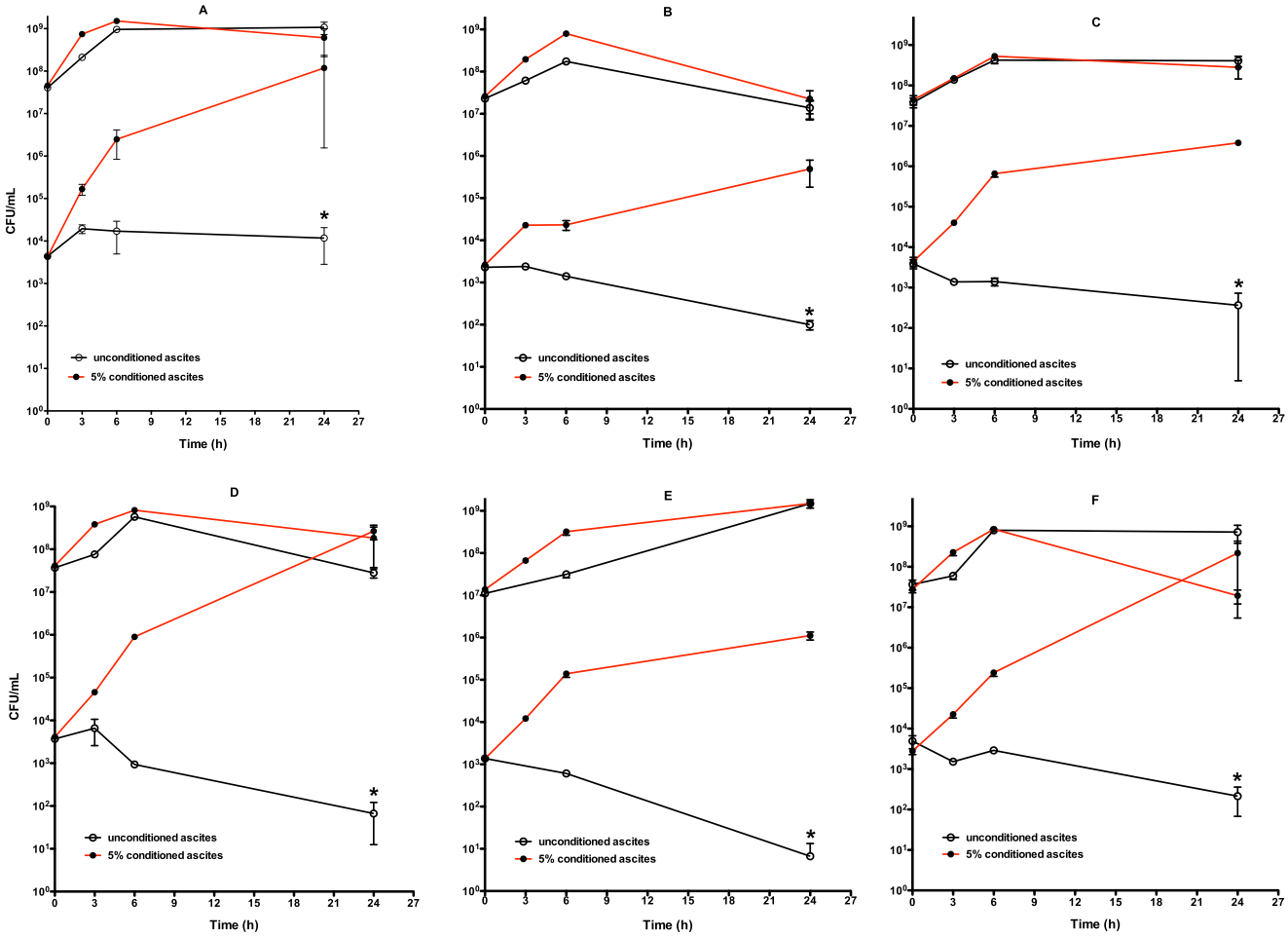

FIG 1 Growth/survival of hypervirulent *Klebsiella pneumoniae* (hvKP) strains grown in human ascites fluid supplemented with 0% and 5% homologous, conditioned ascites fluid. The growth/survival of six hvKP strains was assessed at 0, 3, 6, and 24 h in 100% human ascites fluid supplemented with 0% or 5% homologous conditioned ascites fluid. Both low (between 10^3 and 10^4 CFU) and high (between 10^7 and 10^8 CFU) starting titers were evaluated. (A) NTUH-K2044. (B) N7205. (C) A4528. (D) A1365. (E) A9534. (F) A1142. Supplementation with conditioned, homologous ascites fluid (5% final concentration) resulted in a significant increase in growth/survival for all strains at the low starting titer compared to 0% supplementation (*, $P < 0.05/2$). Data are means ± SEM; n = 3 or 4.

2.4×10^4 ($n = 5$) CFU of hvKP1 Δ*iucA*. Animals were followed for 14 days, with an *in extremis* state or death used as the study endpoint.

Statistical analyses. Data are presented as means ± standard errors of the means (SEM). *P* values of $0.05/n$ (n = the number of comparisons) are considered statistically significant based on the Bonferroni correction for multiple comparisons, and *P* values of $>0.05/n$ but <0.05 are considered as representing a trend. To normalize *in vitro* and *ex vivo* growth/survival data (see Fig. 1, 6, and 7), $\log_{10}$-transformed values were utilized, the area under each curve was calculated, and these areas were compared using two-tailed unpaired *t* tests (Prism 4 for MacIntosh; GraphPad Software Inc.). Two-tailed unpaired *t* tests were used for comparison of quantitative SP data (see Fig. 2 and 4). A log rank (Mantel-Cox) test was used for the analysis of the Kaplan-Meier plot (see Fig. 8) (Prism 4 for MacIntosh; GraphPad Software Inc.).

RESULTS

The growth/survival of hvKP strains in human ascites fluid is enhanced by the addition of conditioned medium. It was initially observed that the addition of conditioned medium enhanced the growth/survival of the hvKP strain hvKP1 in human ascites fluid at a low ($<10^5$ CFU/ml), but not at a high ($>10^7$CFU/ml), starting titer. An Fe acquisition factor(s) was established to be responsible (22). To extend these observations for additional hvKP strains, 6 hvKP clinical isolates were assessed for growth in human ascites fluid with and without the addition of 5% homologous conditioned medium. The addition of conditioned medium significantly increased the growth of all hvKP strains tested for low, but not high, starting inocula (Fig. 1).

hvKP strains secrete 6- to 9.6-fold more SP than cKP strains when grown under Fe-poor conditions. Our collection of 12 hvKP strains and 14 cKP strains were grown overnight in human ascites fluid (with complement inactivated to enable comparable growth of all strains) or Fe-poor minimal medium (MM) (Table 1). Total SP were measured in the supernatants using a quantitative chrome azurol S (CAS) assay and normalized to 1×10^9 CFU (Fig. 2A and B). The median SP concentration in ascites fluid was 6-fold greater for hvKP strains than for cKP strains ($P < 0.0001$) (median [range] of 138 [33.2 to 186] versus 23.1 [9.7 to 39.6] μg/ml) and 9.6-fold greater for hvKP strains grown in MM than for cKP strains (190 [55.6 to 624] versus 19.8 [13 to 74.7] μg/ml)

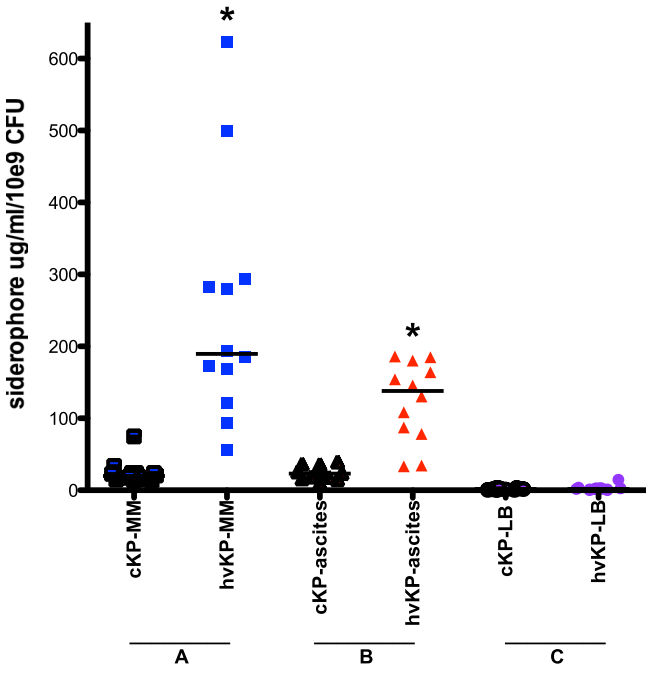

FIG 2 Quantitative measurement of siderophores (SP) in 12 hvKP and 14 cKP strains grown in iron-poor minimal medium (MM), human ascites fluid, and Luria-Bertani broth (LB). Quantitative SP measurements were performed on bacterium-free supernatants harvested after overnight growth. A, MM. B, human ascites fluid. C, LB. The median SP concentration for hvKP strains grown in MM and human ascites fluid, but not LB, was significantly greater than that for cKP strains (*, $P < 0.05/3$). Each symbol represents the mean concentration from 3 independent conditioned media measured in duplicate for a single strain.

($P < 0.0001$). These data extended our published observations and strongly supported the hypothesis that increased SP production was a defining trait for hvKP strains.

SP production is appropriately low when hvKP and cKP strains are grown under Fe-replete conditions. The same hvKP and cKP strains were grown overnight in Luria-Bertani (LB) medium (Fe replete), and SP production was measured as described above. Both hvKP and cKP strains produced similarly low levels of SP ($P = 0.3$) (median [range] of 1.9 [0.08 to 14.7] versus 1.8 [0.92 to 3.1] μg/ml, respectively) (Fig. 2C). SP production normally is low when *Klebsiella* is grown under Fe-replete conditions. Therefore, these data indicated that Fe concentration-mediated regulation of SP production was appropriate in these strains.

HPLC-MS analysis of conditioned medium from hvKP1 demonstrates that aerobactin is the major SP secreted into human ascites fluid and MM. High-pressure liquid chromatography (HPLC) was performed on conditioned media generated from the growth of hvKP1 in human ascites fluid and Fe-poor MM. The observed HPLC profiles were similar, demonstrating 5 major peaks, which were separated and collected as five fractions (1 to 5) (Fig. 3A). Quantitative SP analyses performed on these fractions established that 74.8% and 96.4% of SP from growth in MM and ascites fluid, respectively, were located in fraction 5 (Table 2). Next, fraction 5 was separated into an additional 5 fractions (5a to 5e) (Fig. 3B). One hundred percent of the SP were present in fraction 5c and 5d, with nearly 90% present in 5c. To confirm these quantitative assays, biologic growth/survival assays were performed in which human ascites fluid was supplemented with fractions 5a to 5e. As expected, growth/survival of hvKP1 was optimized by supplementation with fractions 5c and 5d (Fig. 3D). As 5c and 5d elute in neighboring fractions, the activity in fraction 5d probably represents carryover from fraction 5c. Fraction 5c underwent mass spectrometric (MS) analysis, which revealed that fraction 5c contained the SP aerobactin (Fig. 3C). These data demonstrated that for hvKP1, aerobactin was the dominant SP produced, a surprising result considering that all SP are believed to be regulated in a similar manner.

Quantitation of SP from hvKP1 and hvKP1 Δ*iucA* further substantiates that aerobactin is the major SP secreted into human ascites fluid and MM. To further substantiate that aerobactin was the major SP produced by hvKP1 in Fe-poor MM and human ascites fluid, an isogenic derivative of hvKP1 with a disruption in the aerobactin biosynthetic gene *iucA* was generated (hvKP1 Δ*iucA*). hvKP1 and hvKP1 Δ*iucA* were grown overnight in Fe-poor MM, human ascites fluid, or LB medium, and total SP were measured in the supernatants and normalized to 1×10^9 CFU (Fig. 4A). hvKP1 produced a median (range) of 581 (318 to 676) μg/ml in MM, 183 (73 to 214) μg/ml in ascites fluid, and 2.0 (1.1 to 7.8) μg/ml in LB. In contrast, hvKP1 Δ*iucA* produced 21.9 (8.3 to 53.9) μg/ml in MM, 14.8 (8.8 to 17.5) μg/ml in ascites fluid, and no detectable SP in LB, which represent 96.2% and 92% decreases, respectively, in SP production in MM and ascites fluid. These data further demonstrated that aerobactin was the dominant SP produced by hvKP1 when grown under Fe-poor conditions.

Aerobactin is also the major SP secreted by the hvKP strains A1142 and A1365. To assess whether aerobactin was also the major SP secreted by other hvKP strains, conditioned medium generated by the growth of A1142 and A1365 in ascites fluid was fractionated by HPLC and assayed for SP production. HPLC analysis for both strains demonstrated a fraction 5 peak (data not shown) similar to that observed for hvKP1 and shown to contain aerobactin (Fig. 3A and C). Quantitative SP analysis of the HPLC fractions demonstrated that 96% and 95.9% of the total SP activity resided in fraction 5 for A1142 and A1365, respectively (Table 2). To further substantiate these findings, aerobactin-deficient isogenic derivatives of A1142 and A1365 were constructed, and quantitative SP production was measured in conditioned medium and normalized to 1×10^9 CFU (Fig. 4B and C). A1142 produced a median (range) of 177 (109 to 394) μg/ml in MM, 57.5 (30.8 to 196) μg/ml in ascites fluid, and undetectable (undetectable to 3.1 μg/ml) SP in LB. In contrast, A1142 Δ*iucA* produced 45.3 (31.9 to 78.7) μg/ml in MM, 16.1 (13.0 to 17.4) μg/ml in ascites fluid, and undetectable SP in LB, which represented 79.6% and 78.1% decreases, respectively, in SP production in MM and ascites fluid. A1365 produced 219 (146 to 356) μg/ml in MM, 67.1 (42.5 to 125) μg/ml in ascites fluid, and undetectable (undetectable to 1.5 μg/ml) SP in LB. In contrast, A1365 Δ*iucA* produced 10.3 (4.3 to 12.2) μg/ml in MM, 10.2 (4.7 to 11.4) μg/ml in ascites fluid, and undetectable SP in LB, which represented 95.5% and 86.8% decreases, respectively, in SP production in MM and ascites fluid. These data demonstrated that aerobactin was the dominant SP produced by other hvKP strains when grown under Fe-poor conditions.

The gene copy number for *iucA* (aerobactin) is similar to those for *entH* (enterobactin), *iroB* (salmochelin), and *irp2* (yersiniabactin). The aerobactin and salmochelin biosynthetic genes are present on large, 200- to 224-kDa plasmids in CG43, NTUH-

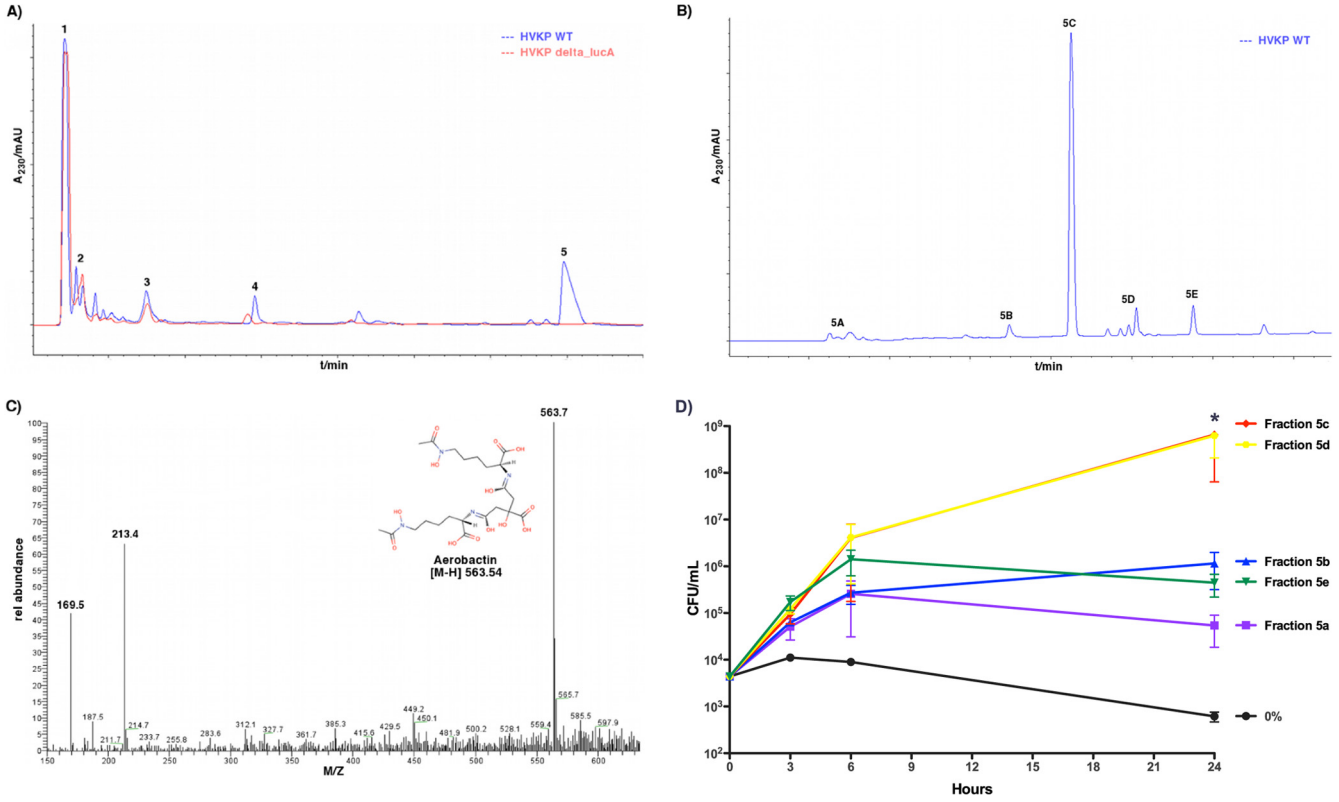

FIG 3 HPLC-mass spectrometry analysis of hvKP1-generated conditioned medium. (A) A representative HPLC profile of conditioned medium generated from the growth of hvKP1 in human ascites fluid. The fractions were designated 1 to 5. (B) Fraction 5 was further separated by HPLC into fractions 5a to 5e. (C) Mass spectrometric analysis was performed on fraction 5c and established that the species present was aerobactin. (D) The biological activities of fractions 5a to 5e were assessed by assessing the growth of hvKP1 in human ascites fluid supplemented with each fraction (5% final concentration). Supplementation with fractions 5c and 5d resulted in a significant increase in growth and/or survival for hvKP1 compared to 0% supplementation (*, $P < 0.05/5$). Data are means ± SEM; $n = 3$.

K2044, and hvKP1, the hvKP strains assessed to date (16, 31, 32). In contrast, enterobactin and yersiniabactin biosynthetic genes are chromosomally located. Quantitative PCR was performed to assess gene copy number. As expected due to the presence of 8 RNA gene clusters in *K. pneumoniae*, the quantitative PCR-calculated threshold, an inverse correlate for gene copy number, was significantly less for genes encoding 23S rRNA than for *iucA*, *entH*, *iroB*, and *irp2* under all conditions tested ($P < 0.05/4$) (Fig. 5). In contrast, the calculated threshold was similar for *iucA*, *entH*, *iroB*, and *irp2* under nearly all conditions tested (Fig. 5). There was a trend for an increase in the calculated threshold for *entH* compared to *iucA*, *iroB*, and *irp2* when 5,000 picograms of DNA was used ($P > 0.05/4$ but $P < 0.05$). However, since both *entH* and *irp2* were chromosomally located, this difference did not appear to be biologically significant (33). Likewise, the calculated threshold for *iucA* was statistically less than those for *entH* and *irp2* when 50 picograms of DNA was used. However, this difference was not observed when *iroB*, which like *iucA* is plasmid located, was compared to *entH* and *irp2* at this DNA concentration. Therefore, again these small differences did not appear to be biologically significant. Taken together, these data do not support increased copy number of the aerobactin biosynthetic genes as being responsible for its increased production.

Aerobactin enables the growth of hvKP1 and hvKP1 Δ*iucA* in human ascites fluid. To confirm that aerobactin was the primary factor in conditioned medium that enhanced the growth/survival of hvKP1 in human ascites fluid, the growth/survival of hvKP1 was assessed in human ascites fluid in the presence or absence of various growth supplements. With a starting inoculum of $<1 \times 10^5$ CFU/ml, the growth of hvKP1 in ascites fluid was limited (Fig. 6A). Likewise, the growth of hvKP1 was similarly limited when the ascites fluid was supplemented with conditioned medium deficient in aerobactin (conditioned medium generated by hvKP1 Δ*iucA*) (Fig. 6A). However, growth of hvKP1 was significantly greater ($P < 0.05/3$) in ascites fluid supplemented with purified aerobactin (460 nM; 260 μg/ml) or conditioned medium containing aerobactin (conditioned medium generated by hvKP1) (Fig. 6A). Similar results were obtained with hvKP1 Δ*iucA* and the same supplements (Fig. 6B). Importantly, hvKP1 Δ*iucA* was chemically complemented with purified aerobactin. These data confirm that aerobactin is the primary factor responsible for the phenotype of increased growth/survival of hvKP1 in human ascites fluid supplemented with conditioned medium.

The growth/survival of the wild-type strain hvKP1 and hvKP1/pFUS2 is significantly greater than that of their isogenic aerobactin-deficient derivatives hvKP1 Δ*iucA* and hvKP1 Δ*iucA*/pFUS2, respectively, in human ascites fluid *ex vivo*. To determine whether aerobactin enhanced growth/survival under clinically relevant conditions, hvKP1, hvKP1/pFUS2, hvKP1 Δ*iucA*, and hvKP1 Δ*iucA*/pFUS2 were grown in human ascites fluid *ex vivo* at starting titers of approximately 3×10^4 and 1×10^6 CFU/ml. The growth/survival of hvKP1 and hvKP1/pFUS2 was

TABLE 2 Siderophore concentrations in the different HPLC fractions

Strain/medium	Mean siderophore concn (μg/ml) ± SEM (% of total) in HPLC fraction[a]:									
	1	2	3	4	5	5a	5b	5c	5d	5e
hvKP1/MM[b]	69.1 ± 11.6 (24.9)	0.18 ± 0.18 (<0.1)	0.18 ± 0.18 (<0.1)	0.25 ± 0.25 (<0.1)	207.2 ± 22.7 (74.8)					
hvKP1 Δ*iucA*/MM	39.6 ± 0.84 (100)	0.0 ± 0.0 (0)	0.0 ± 0.0 (0)	0.0 ± 0.0 (0)	0.0 ± 0.0 (0)					
hvKP1/ascites fluid	13.1 ± 0.40 (3.6)	0.0 ± 0.0 (0)	0.0 ± 0.0 (0)	0.0 ± 0.0 (0)	350.8 ± 13.3 (96.4)					
A1142/ascites fluid	14.1 ± 0.40 (4.0)	0.0 ± 0.0 (0)	0.0 ± 0.0 (0)	0.0 ± 0.0 (0)	343.3 ± 11.8 (96.0)					
A1365/ascites fluid	13.9 ± 0.50 (4.1)	0.0 ± 0.0 (0)	0.0 ± 0.0 (0)	0.0 ± 0.0 (0)	327.6 ± 21.8 (95.9)					
hvKP1/MM						0.0 ± 0.0 (0)	0.0 ± 0.0 (0)	210.9 ± 24.1 (89.3)	25.3 ± 4.3 (10.7)	0.0 ± 0.0 (0)

[a] $n = 4$ to 6 for all measurements.
[b] MM, iron-poor M9 minimal medium.

significantly greater than that of hvKP1 Δ*iucA* and hvKP1 Δ*iucA*/pFUS2, respectively ($P < 0.05/2$) (Fig. 7A and B). The diminished growth of hvKP1 Δ*iucA* was complemented in *trans* by the plasmid pFUS2[*iucA-D*], which expressed IucA (Fig. 7A). Interestingly, when the higher starting inoculum of 1×10^6 CFU/ml was used, the difference in growth/survival between hvKP1 and hvKP1 Δ*iucA* was observed at 24 h. However, when the lower inoculum of 3×10^4 CFU/ml was used, this difference was not discerned over the first 24 h. These data demonstrated that aerobactin was needed for optimal growth/survival in a time- and inoculum-dependent fashion.

The virulence of the wild-type strain hvKP1 is significantly greater than that of its isogenic aerobactin-deficient derivative hvKP1 Δ*iucA* in both mouse s.c. and i.p. challenge models. To determine whether aerobactin contributed to the hypervirulent phenotype of hvKP1 *in vivo*, first an outbred mouse s.c. challenge model was used. Four challenge inocula were used, ranging from 3.0×10^2 to 3.5×10^5 CFU and from 2.8×10^2 to 3.6×10^5 CFU in approximately $\log_{10}$ intervals for hvKP1 and hvKP1 Δ*iucA*, respectively. The mortality of mice challenged with hvKP1 was significantly greater than that of mice challenged with hvKP1 Δ*iucA* ($P < 0.05$) (Fig. 8A and B). Generally, the timing of mortality was inversely proportional to the challenge titer. Remarkably, animals challenged with 3.0×10^2 CFU of hvKP1 experienced 100% morality, with deaths observed from 6 to 9 days postchallenge. Next, an i.p. challenge model was employed. Four challenge inocula were used, ranging from 3.2×10^1 to 3.2×10^4 CFU and from 2.4×10^1 to 2.4×10^4 CFU in $\log_{10}$ intervals for hvKP1 and hvKP1 Δ*iucA*, respectively. The mortality of mice challenged with hvKP1 was significantly greater than that of mice challenged with hvKP1 Δ*iucA* ($P < 0.05$) (Fig. 8C and D). These data demonstrated the hypervirulence of hvKP and strongly supported the importance of aerobactin in contributing to this hypervirulent phenotype.

DISCUSSION

In this study, we supported our hypotheses that hvKP strains produce more SP than cKP strains and that this trait is an important mechanism contributing to their hypervirulence. The data presented demonstrate that all 12 hvKP strains tested produced more SP than 14 cKP blood isolates under Fe-poor conditions, such as occur in the human host (Fig. 2). Further, we showed that the SP aerobactin primarily accounted for the significant increase in SP production observed with the hvKP strains hvKP1, A1142, and A1365 (Table 2; Fig. 4). In addition, we demonstrated that aerobactin was the primary factor in conditioned medium that enhanced the growth/survival of hvKP1 in human ascites fluid (Fig. 6). More importantly, hvKP1 Δ*iucA* grew/survived less well than its wild-type parent *ex vivo* in human ascites fluid (Fig. 7), and this growth defect was complemented in *trans* by the aerobactin biosynthetic genes (Fig. 7A). Lastly, hvKP1 Δ*iucA* was significantly less virulent in mouse s.c. and i.p. challenge models than its wild-type parent hvKP1 (Fig. 8). Taken together, these data directly established that under Fe-poor conditions, hvKP strains produce increased levels of SP compared to cKP strains, that aerobactin is the dominant SP produced by hvKP strains, and that aerobactin contributes to the virulence of hvKP1 *ex vivo* and *in vivo*.

The mechanism responsible for the increased aerobactin production in hvKP remains unclear. The ferric uptake regulator (Fur) has been established as an important negative regulator of Fe acquisition systems in *K. pneumoniae*, including hvKP strains

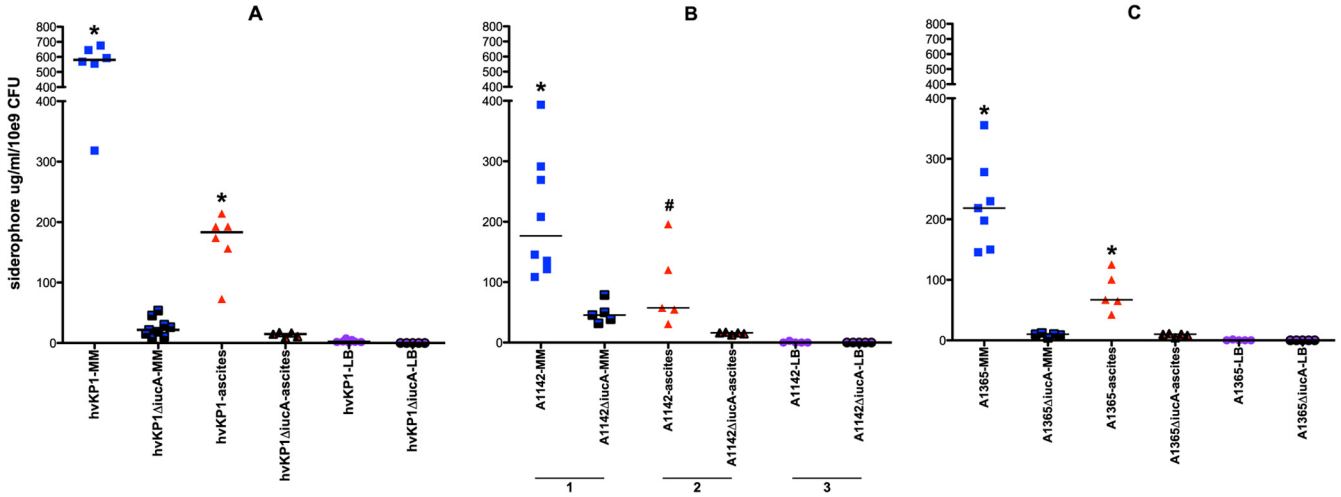

FIG 4 Quantitative measurement of siderophores (SP) in hvKP1, hvKP1 Δ*iucA*, A1142, and A1142 Δ*iucA* grown in iron-poor MM, human ascites fluid, and LB broth. Quantitative SP measurements were performed on bacterium-free supernatants harvested after overnight growth. 1, MM; 2, human ascites fluid; 3, LB. (A) hvKP1 and hvKP1 Δ*iucA*. (B) A1142 and A1142 Δ*iucA*. (C) A1365 and A1365 Δ*iucA*. The median SP concentrations for hvKP1, A1142, and A1365 compared to hvKP1 Δ*iucA*, A1142 Δ*iuc*, and A1365 Δ*iucA* when grown in MM and for hvKP1 and A1142 compared to hvKP1 Δ*iucA* and A1142 Δ*iuc* when grown in ascites fluid were significantly greater (*, $P < 0.05/3$). There was a trend for the median SP concentration of A1365 compared to A1365 Δ*iucA* when grown in ascites fluid (#, $P < 0.05$ but $> 0.05/3$). Each symbol represents the mean concentration from an independent conditioned medium measured at least in duplicate for each strain.

(34). The fact that SP production was appropriately decreased in Fe-replete LB medium (Fig. 2C) suggests that regulation is appropriate under conditions where a high concentration of Fe is present. Presumably this is mediated, at least in part, by Fur, but this has not yet been formally established for hvKP1. Since the aerobactin genes were present on a large plasmid, increased gene copy number was a consideration. However, quantitative PCR data that examined this possibility demonstrated that this was not the case. The copy numbers of the yersiniabactin and enterobactin genes (*irp2* and *entH*), which are located on the chromosome, are similar to those of the aerobactin and salmochelin genes (*iucA* and *iroB*), which are located on the plasmid (Fig. 5). Published data have shown that environmental conditions can significantly affect SP production. pH and carbon sources have been shown to modulate SP production in *Escherichia coli* (35). Optimal aerobactin production occurred at a pH of 5.6 when glycerol was used as the carbon source (as opposed to glucose). In an avian extraintestinal pathogenic *E. coli* strain (36) grown in MM, aerobactin comprised 1.9% of the total SP produced. In contrast, in a chicken infection model this proportion increased to 48% and 58.9% in pericardia and air sacs, respectively. We did not observe this discordance between MM and a more clinically relevant setting (ascites fluid in this study). Recent work on the small RNA RyhB has established that regulators beyond Fur are important for bacterial Fe homeostasis and SP production (37). Although, the mechanism(s) responsible for increased aerobactin production in hvKP1 is presently unclear and requires further study, its delineation would be important and may lend insight into potential therapeutic interventions.

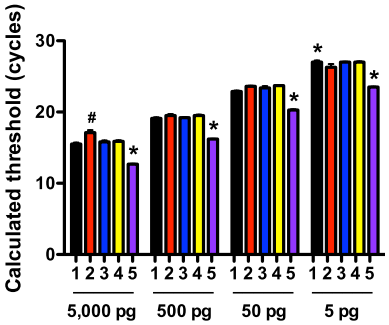

FIG 5 The gene copy numbers for *iucA*, *entH*, *iroB*, and *irp2* are similar. Quantitative PCR was performed on 4 independent concentrations of chromosomal DNA. The calculated threshold (cycles) correlates inversely with gene copy number. Black, *iucA*; red, *entH*; blue, *iroB*; yellow, *irp2*; purple, 23S RNA. *, $P < 0.05/4$ for 23S RNA compared to *iucA*, *entH*, *iroB*, and *irp2* for all DNA concentrations. #, $P > 0.05/4$ but $P < 0.1$ for *entH* compared to *iucA*, *iroB*, and *irp2* for 5,000 pg. *, $P < 0.05/4$ for *iucA* compared to *entH* and *irp2* for 50 pg. $n = 3$ for all measurements.

As discussed in the introduction, molecular epidemiologic studies were suggestive that aerobactin may be a factor that enhanced the virulence of hvKP due to its increased prevalence in hvKP strains compared to cKP strains (8, 15, 25). Older studies had demonstrated that the virulence of *E. coli* and *K. pneumoniae* was enhanced with the presence of a plasmid containing genes that encoded aerobactin (17, 38, 39). However, the presence of other virulence factors encoded on these plasmids, such as RmpA, which increased capsule production and mediated the hypermucoviscosity phenotype, was a confounding variable. More recent studies using isogenic derivatives have shown that aerobactin was the only SP needed to mediate virulence for an avian extraintestinal pathogenic *Escherichia coli* strain in a chicken infection model (40) and that in a murine urinary tract infection model the absence of the aerobactin receptor decreased fitness (41). Therefore, despite having a lower Fe association constant ($K_f = 10^{22.9}$) (42) than enterobactin ($K_f = 10^{52}$) (42), yersiniabactin ($K_f = 10^{36}$) (43), and transferrin ($K_f \sim 10^{30}$) (44), aerobactin appears to overcome this perceived disadvantage under clinically relevant conditions. Potential mechanisms for these observations include the facts that aerobactin is recycled (45) and transfers Fe from trans-

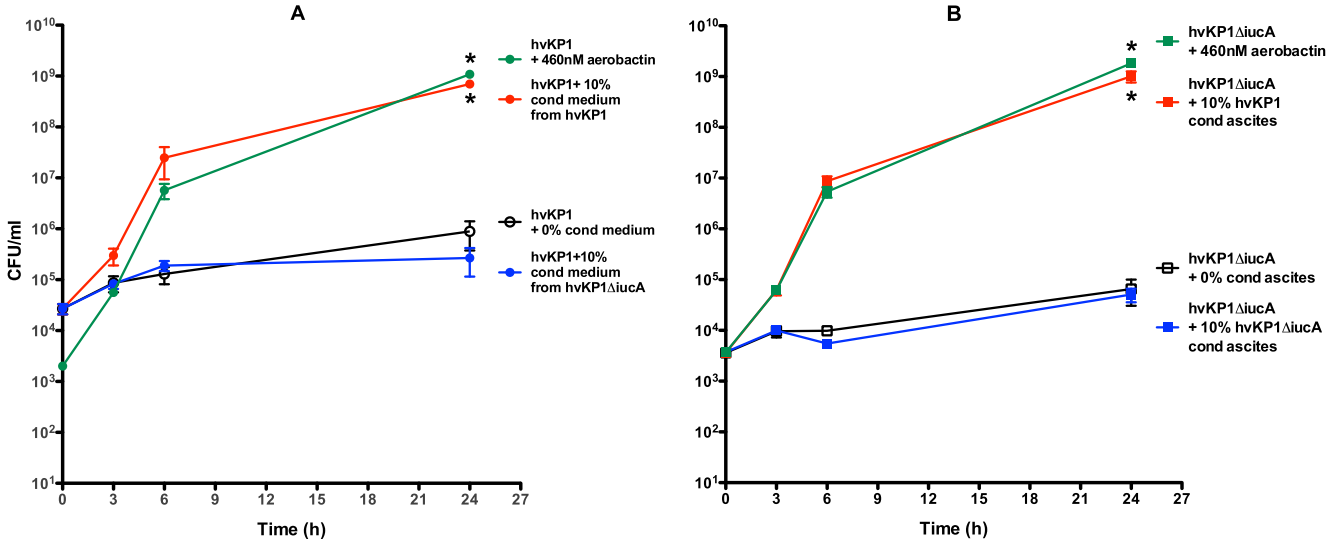

FIG 6 Growth/survival of hvKP1 and hvKP1 Δ*iucA* in human ascites fluid supplemented with purified aerobactin or conditioned medium generated by hvKP1 or hvKP1 Δ*iucA*. The growth/survival of hvKP1 and hvKP1 Δ*iucA* was assessed at 0, 3, 6, and 24 h in 100% human ascites fluid. (A) Growth/survival of hvKP1 in ascites fluid that was not supplemented (0%) or was supplemented with 10% conditioned ascites fluid generated by hvKP1 (aerobactin replete) or hvKP1 Δ*iucA* (aerobactin deficient) or purified aerobactin (460 nM; 260 μg/ml). *, $P < 0.05/3$. (B) Growth/survival of hvKP1 Δ*iucA* in ascites fluid that was not supplemented (0%) or was supplemented with 10% of conditioned ascites fluid generated by hvKP1 (aerobactin replete) or hvKP1 Δ*iucA* (aerobactin deficient) or purified aerobactin (460 nM; 260 μg/ml). *, $P < 0.05/3$. Data are means ± SEM; $n = 4$ to 6.

ferrin more efficiently than enterobactin (46) and that in contrast to the case for enterobactin, this transfer is not impeded by albumin or immunoglobulins (47). Further, aerobactin is resistant to the inhibitory effects of lipocalin 2 (48).

An increasing body of data has begun to address whether certain SP may be more efficacious in certain settings (41, 49, 50). Our *ex vivo* and *in vivo* data with human ascites fluid and mouse infection models determined that the beneficial effect of aerobactin at lower challenge titers was delayed. In contrast to enterobactin, salmochelin, and yersiniabactin, which are produced during logarithmic phase (51), aerobactin is maximally produced in late logarithmic-secondary metabolism (stationary) phase (52). Therefore, it is possible that aerobactin may contribute to the phenotype of hvKP under conditions when the host and bacterium are at a "stalemate," such as might occur with a lower challenge inoculum. The possession of a factor that enables infection

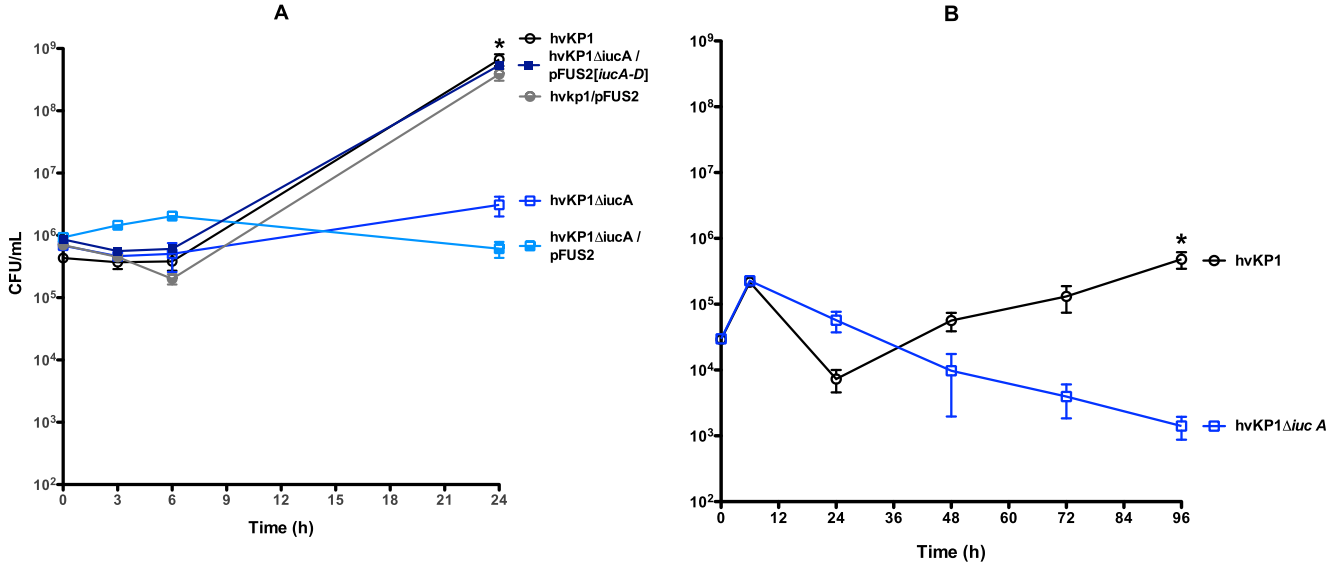

FIG 7 Growth/survival of hvKP1 and hvKP1 Δ*iucA* in human ascites fluid. The growth/survival of hvKP1, hvKP1/pFUS2, hvKP1 Δ*iucA*, hvKP1 Δ*iucA*/pFUS2, and hvKP1 Δ*iucA*/pFUS2[*iucA-D*] was assessed in 100% human ascites fluid. (A) A midlevel starting inoculum of approximately 1×10^6 CFU/ml was used, and growth/survival was assessed at 0, 3, 6, and 24 h. The growth/survival of hvKP1 and hvKP1/pFUS2 was significantly increased compared to that of hvKP1 Δ*iucA* and hvKP1 Δ*iucA*/pFUS2, respectively. *, $P < 0.05/2$. Data are means ± SEM ($n = 5$ to 8). (B) A low starting inoculum of $<1 \times 10^5$ CFU/ml was used, and growth/survival was assessed at 0, 12, 24, 48, 72, and 96 h. The growth/survival of hvKP1 was significantly increased compared to that of hvKP1 Δ*iucA*. *, $P < 0.05$. Data are means ± SEM from 3 independent experiments with $n = 3$ for each experiment.

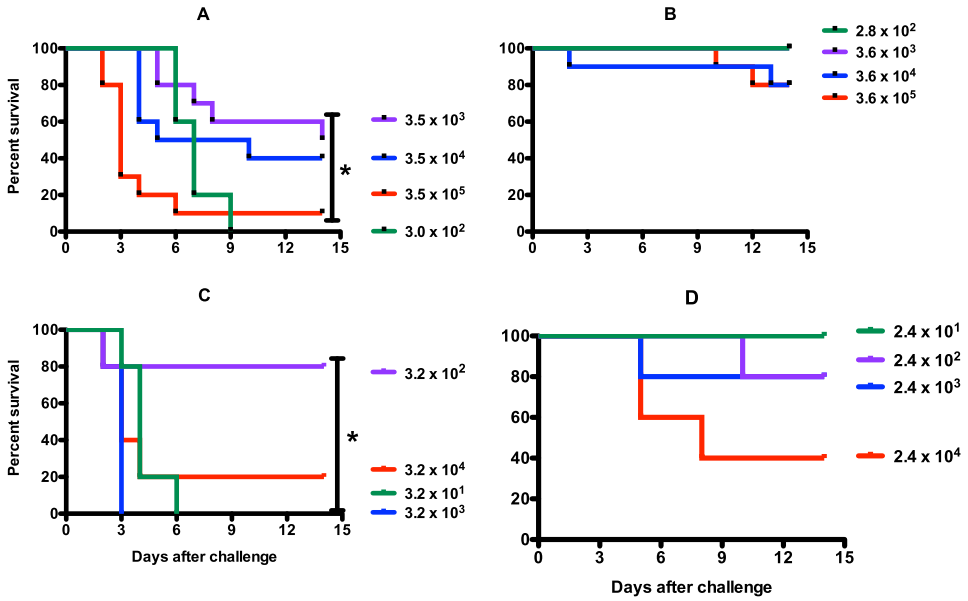

FIG 8 Survival of outbred CD1 mice after subcutaneous (s.c.) or intraperitoneal (i.p.) challenge with hvKP1 and hvKP1 Δ*iucA*. (A and B) Animals were challenged s.c. with 3.0×10^2 ($n = 5$), 3.5×10^3 ($n = 10$), 3.5×10^4 ($n = 10$), or 3.5×10^5 ($n = 10$) CFU of hvKP1 (A) or with 2.8×10^2 ($n = 5$), 3.6×10^3 ($n = 10$), 3.6×10^4 ($n = 10$), or 3.6×10^5 ($n = 10$) CFU of hvKP1 Δ*iucA* (B). (C and D) Animals were challenged i.p. with 3.2×10^1 ($n = 5$), 3.2×10^2 ($n = 5$), 3.2×10^3 ($n = 5$), or 3.5×10^4 ($n = 5$) CFU of hvKP1 (C) or with 2.4×10^1 ($n = 5$), 2.4×10^2 ($n = 5$), 2.4×10^3 ($n = 5$), or 2.4×10^4 ($n = 5$) CFU of hvKP1 Δ*iucA* (D). Strains were grown overnight in LB medium. An *in extremis* state or death was scored as nonsurvival. *, $P < 0.05$ for hvKP1 compared to hvKP1 Δ*iucA*.

with a lower inoculum would significantly enhance virulence. This characteristic may be critical for a pathogen, such as hvKP, which infects healthy ambulatory hosts who do not have an overt portal of entry (2). This is in contrast to the case for cKP, where infections are usually health care associated and often in the setting of intravascular or urinary catheters, endotracheal tubes, or open wounds.

Two challenge routes were employed to assess the role of aerobactin *in vivo*. Initially s.c. challenge was used, since hvKP strains may gain entry into the human host via this route, thereby potentially mimicking human infection (2). Further, it had been previously established that s.c. challenge with hvKP1 resulted in subsequent systemic dissemination over the next 24 to 72 h (22), making this model clinically relevant since the ability to disseminate is a defining characteristic of hvKP strains. Further and importantly, this route of infection will result in bacteria entering the bloodstream at a physiologically appropriate titer, which in turn reflects what happens during human infection and avoids a "cytokine storm" that may occur soon after bacterial challenge by other routes, such as intravenous or intraperitoneal challenge. Lastly, since aerobactin is produced during the late logarithmic-secondary metabolism phase (52), models that use metrics generated over the first 24 h may not be able to define a role for aerobactin. Further, the ability to produce aerobactin during nonlogarithmic growth may be important for growth/survival within abscesses. In contrast to our results, an isogenic aerobactin-deficient derivative of the hvKP strain NTUH-K2044 had a 50% lethal dose (LD_{50}) similar to that of its wild-type parent after i.p. and intragastric challenge in BALB/cByl mice (25). Therefore, to determine whether this contrasting observation was related to bacterial strain, challenge route, or animal breed differences, we challenged mice i.p. with hvKP1 and hvKP1 Δ*iucA*. Similar to our findings after s.c. challenge, hvKP1 was significantly more virulent than hvKP1 Δ*iucA* (Fig. 8C and D). Since our studies used outbred CD1 mice and the studies with NTUH-K2044 used an inbred BALB/c derivative, we believe that the observed difference is most likely related to the mouse strains used; however, we cannot exclude a role for differences in the bacterial strains.

The observation that hvKP strains produce more SP than cKP strains has potential implications beyond pathogenesis. Presently, since we are still establishing which factors confer hvKP strains with their unique virulence capabilities, reliable markers for differentiating cKP and hvKP pathotypes are lacking. The hypermucoviscous phenotype (mediated by RmpA/A2) as manifested by a positive string test, in combination with the clinical syndrome, are perceived to be the best markers for hvKP strains (2). However, even if the clinical microbiology laboratory considered this test, its performance can be challenging and its interpretation subjective. Further, the sensitivity and specificity of the string test for hvKP strains have not been defined, and cKP strains may also be string test positive (2). The development of a more objective diagnostic test(s) that can be employed by the clinical microbiology laboratory to reliably identify hvKP strains is requisite. An assessment of total SP production, which could be measured by a plate assay that incorporates chrome azurol S dye, may represent the solution or at least an ancillary test that could be used in conjunction with the string test and clinical features. The ability to objectively identify hvKP strains will enhance our ability to perform more comprehensive epidemiologic studies and to define the full spectrum of infectious syndromes caused by hvKP. It will also enable the incidence of infection, especially outside the Asian Pacific Rim, to be defined. Perhaps most importantly, the identification of a *K. pneumoniae* isolate as being an hvKP strain will assist the clinician in disease management. The knowledge that an hvKP strain is causing infection should prompt a search for concomitant or subsequent metastatic sites of infection, which may require drainage or

a site-driven modification of the antimicrobial regimen. It is critical to be particularly vigilant for endophthalmitis and central nervous system infection.

K. pneumoniae strains variably possess genes encoding enterobactin, salmochelin, yersiniabactin, and aerobactin. However, in contrast to hvKP strains, where most if not all strains are aerobactin positive, only 7 to 18% of putative cKP strains are aerobactin-positive (8, 15, 25). The data presented here support the concept that in an hvKP background, aerobactin is an important virulence factor and is the major contributor of high SP levels observed under Fe-poor conditions. However, due to the lack of an unequivocal definition of the hvKP pathotype, it is unclear what proportion of aerobactin-positive putative cKP strains are truly cKP, unrecognized hvKP, or of an intermediate phenotype. Further, for true cKP aerobactin-positive strains (if they exist), the contribution of aerobactin to total SP production and virulence requires assessment. In one study, for 2 stool isolates of *K. pneumoniae* grown in M63-glycerol that produced enterobactin, salmochelin, yersiniabactin, and aerobactin, aerobactin production accounted for 62% and 86% of SP production (53). However, total SP levels were not reported, and it was unclear whether these stains were cKP or hvKP isolates. Interestingly, genes that encode yersiniabactin were more prevalent in hvKP (91%) than in cKP (22%) (25), but data from this report do not support yersiniabactin as a major contributor to the high SP levels observed in hvKP strains under Fe-poor conditions.

In summary, the data presented in this report strongly support that hvKP strains produce significantly higher levels of SP than cKP strains. In the hvKP strains tested to date (hvKP1, A1141, and A1365) increased aerobactin production accounts for most if not all of this increased SP production. Further, we demonstrated that aerobactin is a major virulence determinant for hvKP1. These data have potential implications for the development of novel diagnostic tests and preventative and therapeutic strategies in the management of hvKP infection. This may be particularly important since recent data support that hvKP has the potential to be acquire significant antimicrobial resistance (54), similar to what is now occurring with cKP (55).

ACKNOWLEDGMENTS

This work was supported in part by National Institutes of Health grants 1R21AI088318-01A1 (T.A.R.) and GM-068440 (A.M.G.), by a VA Merit Review from the Department of Veterans Affairs (T.A.R.), and by Telemedicine and Advance Technical Research Center (TATRC) cooperative agreement W81XWH-11-2-0218 (A.M.G. and T.A.R.).

The funders had no role in study design, data collection and analysis, decision to publish, or preparation of the manuscript.

We thank Jin-Town Wang (Departments of Microbiology and Internal Medicine, National Taiwan University, Taipei, Taiwan, China) for providing strains from Taipei, Taiwan. We thank Alice Bergmann (University at Buffalo Chemistry Department) for performing the mass spectrometric analysis of aerobactin.

REFERENCES

1. **Shon AS, Russo TA.** 2012. Hypervirulent *Klebsiella pneumoniae*: the next superbug? Future Microbiol. **7:**669–671. http://dx.doi.org/10.2217/fmb.12.43.
2. **Shon AS, Bajwa RP, Russo TA.** 2013. Hypervirulent (hypermucoviscous) *Klebsiella pneumoniae*: a new and dangerous breed. Virulence **4:**107–118. http://dx.doi.org/10.4161/viru.22718.
3. **Liu YC, Cheng DL, Lin CL.** 1986. *Klebsiella pneumoniae* liver abscess associated with septic endophthalmitis. Arch. Intern. Med. **146:**1913–1916. http://dx.doi.org/10.1001/archinte.1986.00360220057011.
4. **Moellering RC, Jr.** 2010. NDM-1—a cause for worldwide concern. N. Engl. J. Med. **363:**2377–2379. http://dx.doi.org/10.1056/NEJMp1011715.
5. **Snitkin ES, Zelazny AM, Thomas PJ, Stock F, Henderson DK, Palmore TN, Segre JA.** 2012. Tracking a hospital outbreak of carbapenem-resistant *Klebsiella pneumoniae* with whole-genome sequencing. Sci. Transl. Med. **4:**148ra116. http://dx.doi.org/10.1126/scitranslmed.3004129.
6. **Ko WC, Paterson DL, Sagnimeni AJ, Hansen DS, Von Gottberg A, Mohapatra S, Casellas JM, Goossens H, Mulazimoglu L, Trenholme G, Klugman KP, McCormack JG, Yu VL.** 2002. Community-acquired *Klebsiella pneumoniae* bacteremia: global differences in clinical patterns. Emerg. Infect. Dis. **8:**160–166. http://dx.doi.org/10.3201/eid0802.010025.
7. **Pomakova DK, Hsiao CB, Beanan JM, Olson R, Macdonald U, Keynan Y, Russo TA.** 2012. Clinical and phenotypic differences between classic and hypervirulent *Klebsiella pneumoniae*: an emerging and underrecognized pathogenic variant. Eur. J. Clin. Microbiol. Infect. Dis. **31:**981–989. http://dx.doi.org/10.1007/s10096-011-1396-6.
8. **Jung SW, Chae HJ, Park YJ, Yu JK, Kim SY, Lee HK, Lee JH, Kahng JM, Lee SO, Lee MK, Lim JH, Lee CH, Chang SJ, Ahn JY, Lee JW, Park YG.** 2013. Microbiological and clinical characteristics of bacteraemia caused by the hypermucoviscosity phenotype of *Klebsiella pneumoniae* in Korea. Epidemiol. Infect. **141:**334–340. http://dx.doi.org/10.1017/S0950268812000933.
9. **Lee HC, Chuang YC, Yu WL, Lee NY, Chang CM, Ko NY, Wang LR, Ko WC.** 2006. Clinical implications of hypermucoviscosity phenotype in *Klebsiella pneumoniae* isolates: association with invasive syndrome in patients with community-acquired bacteraemia. J. Intern. Med. **259:**606–614. http://dx.doi.org/10.1111/j.1365-2796.2006.01641.x.
10. **Cheng NC, Yu YC, Tai HC, Hsueh PR, Chang SC, Lai SY, Yi WC, Fang CT.** 2012. Recent trend of necrotizing fasciitis in Taiwan: focus on monomicrobial *Klebsiella pneumoniae* necrotizing fasciitis. Clin. Infect. Dis. **55:**930–939. http://dx.doi.org/10.1093/cid/cis565.
11. **Kashani AH, Eliott D.** 2013. The emergence of *Klebsiella pneumoniae* endogenous endophthalmitis in the USA: basic and clinical advances. J. Ophthalmic Inflamm. Infect. **3:**28. http://dx.doi.org/10.1186/1869-5760-3-28.
12. **Chang WN, Huang CR, Lu CH, Chien CC.** 2012. Adult *Klebsiella pneumoniae* meningitis in Taiwan: an overview. Acta Neurol. Taiwan **21:**87–96.
13. **Cheng DL, Liu YC, Yen MY, Liu CY, Wang RS.** 1991. Septic metastatic lesions of pyogenic liver abscess. Their association with *Klebsiella pneumoniae* bacteremia in diabetic patients. Arch. Intern. Med. **151:**1557–1559.
14. **Wang JH, Liu YC, Lee SS, Yen MY, Chen YS, Wang JH, Wann SR, Lin HH.** 1998. Primary liver abscess due to *Klebsiella pneumoniae* in Taiwan. Clin. Infect. Dis. **26:**1434–1438. http://dx.doi.org/10.1086/516369.
15. **Yu VL, Hansen DS, Ko WC, Sagnimeni A, Klugman KP, von Gottberg A, Goossens H, Wagener MM, Benedi VJ.** 2007. Virulence characteristics of Klebsiella and clinical manifestations of *K. pneumoniae* bloodstream infections. Emerg. Infect. Dis. **13:**986–993. http://dx.doi.org/10.3201/eid1307.070187.
16. **Chen YT, Chang HY, Lai YC, Pan CC, Tsai SF, Peng HL.** 2004. Sequencing and analysis of the large virulence plasmid pLVPK of *Klebsiella pneumoniae* CG43. Gene **337:**189–198. http://dx.doi.org/10.1016/j.gene.2004.05.008.
17. **Nassif X, Sansonetti PJ.** 1986. Correlation of the virulence of *Klebsiella pneumoniae* K1 and K2 with the presence of a plasmid encoding aerobactin. Infect. Immun. **54:**603–608.
18. **Yu WL, Ko WC, Cheng KC, Lee CC, Lai CC, Chuang YC.** 2008. Comparison of prevalence of virulence factors for *Klebsiella pneumoniae* liver abscesses between isolates with capsular K1/K2 and non-K1/K2 serotypes. Diagn. Microbiol. Infect. Dis. **62:**1–6. http://dx.doi.org/10.1016/j.diagmicrobio.2008.04.007.
19. **Cheng HY, Chen YS, Wu CY, Chang HY, Lai YC, Peng HL.** 2010. RmpA regulation of capsular polysaccharide biosynthesis in *Klebsiella pneumoniae* CG43. J. Bacteriol. **192:**3144–3158. http://dx.doi.org/10.1128/JB.00031-10.
20. **Hsu CR, Lin TL, Chen YC, Chou HC, Wang JT.** 2011. The role of *Klebsiella pneumoniae rmpA* in capsular polysaccharide synthesis and virulence revisited. Microbiology **157:**3446–3457. http://dx.doi.org/10.1099/mic.0.050336-0.
21. **Lin TL, Yang FL, Yang AS, Peng HP, Li TL, Tsai MD, Wu SH, Wang JT.** 2012. Amino acid substitutions of MagA in *Klebsiella pneumoniae* affect the biosynthesis of the capsular polysaccharide. PLoS One **7:**e46783. http://dx.doi.org/10.1371/journal.pone.0046783.

22. **Russo TA, Shon AS, Beanan JM, Olson R, Macdonald U, Pomakov AO, Visitacion MP.** 2011. Hypervirulent *K. pneumoniae* secretes more and more active iron-acquisition molecules than "classical" *K. pneumoniae* thereby enhancing its virulence. PLoS One **6:**e26734. http://dx.doi.org/10.1371/journal.pone.0026734.
23. **Ward CG, Hammond JS, Bullen JJ.** 1986. Effect of iron compounds on antibacterial function of human polymorphs and plasma. Infect. Immun. **51:**723–730.
24. **Garenaux A, Caza M, Dozois CM.** 2011. The ins and outs of siderophore mediated iron uptake by extra-intestinal pathogenic *Escherichia coli*. Vet. Microbiol. **153:**89–98. http://dx.doi.org/10.1016/j.vetmic.2011.05.023.
25. **Hsieh PF, Lin TL, Lee CZ, Tsai SF, Wang JT.** 2008. Serum-induced iron-acquisition systems and TonB contribute to virulence in *Klebsiella pneumoniae* causing primary pyogenic liver abscess. J. Infect. Dis. **197:**1717–1727. http://dx.doi.org/10.1086/588383.
26. **Luke NR, Howlett AJ, Shao J, Campagnari AA.** 2004. Expression of type IV pili by *Moraxella catarrhalis* is essential for natural competence and is affected by iron limitation. Infect. Immun. **72:**6262–6270. http://dx.doi.org/10.1128/IAI.72.11.6262-6270.2004.
27. **Antoine R, Alonso S, Raze D, Coutte L, Lesjean S, Willery E, Locht C, Jacob-Dubuisson F.** 2000. New virulence-activated and virulence-repressed genes identified by systematic gene inactivation and generation of transcriptional fusions in *Bordetella pertussis*. J. Bacteriol. **182:**5902–5905. http://dx.doi.org/10.1128/JB.182.20.5902-5905.2000.
28. **Russo TA, MacDonald U, Beanan JM, Olson R, MacDonald IJ, Sauberan SL, Luke NR, Schultz LW, Umland TC.** 2009. Penicillin-binding protein 7/8 contributes to the survival of *Acinetobacter baumannii* in vitro and in vivo. J. Infect. Dis. **199:**513–521. http://dx.doi.org/10.1086/596317.
29. **Schwyn B, Neilands JB.** 1987. Universal chemical assay for the detection and determination of siderophores. Anal. Biochem. **160:**47–56. http://dx.doi.org/10.1016/0003-2697(87)90612-9.
30. **Russo T, Sharma G, Brown C, Campagnari A.** 1995. The loss of the O4 antigen moiety from the lipopolysaccharide of an extraintestinal isolate of *Escherichia coli* has only minor effects on serum sensitivity and virulence *in vivo*. Infect. Immun. **63:**1263–1269.
31. **Wu KM, Li LH, Yan JJ, Tsao N, Liao TL, Tsai HC, Fung CP, Chen HJ, Liu YM, Wang JT, Fang CT, Chang SC, Shu HY, Liu TT, Chen YT, Shiau YR, Lauderdale TL, Su IJ, Kirby R, Tsai SF.** 2009. Genome sequencing and comparative analysis of *Klebsiella pneumoniae* NTUH-K2044, a strain causing liver abscess and meningitis. J. Bacteriol. **191:**4492–4501. http://dx.doi.org/10.1128/JB.00315-09.
32. **Russo TA, Gill SR.** 2013. Draft genome sequence of the hypervirulent *Klebsiella pneumoniae* strain hvKP1, isolated in Buffalo, New York. Genome Announc. **1:**e0006513. http://dx.doi.org/10.1128/genomeA.00065-13.
33. **West CP, Dupras DM.** 2013. 5 ways statistics can fool you—tips for practicing clinicians. Vaccine **31:**1550–1552. http://dx.doi.org/10.1016/j.vaccine.2012.11.086.
34. **Lin CT, Wu CC, Chen YS, Lai YC, Chi C, Lin JC, Chen Y, Peng HL.** 2011. Fur regulation of the capsular polysaccharide biosynthesis and iron-acquisition systems in *Klebsiella pneumoniae* CG43. Microbiology **157:**419–429. http://dx.doi.org/10.1099/mic.0.044065-0.
35. **Valdebenito M, Crumbliss AL, Winkelmann G, Hantke K.** 2006. Environmental factors influence the production of enterobactin, salmochelin, aerobactin, and yersiniabactin in *Escherichia coli* strain Nissle 1917. Int. J. Med. Microbiol. **296:**513–520. http://dx.doi.org/10.1016/j.ijmm.2006.06.003.
36. **Caza M, Lepine F, Milot S, Dozois CM.** 2008. Specific roles of the *iroBCDEN* genes in virulence of an avian pathogenic *Escherichia coli* O78 strain and in production of salmochelins. Infect. Immun. **76:**3539–3549. http://dx.doi.org/10.1128/IAI.00455-08.
37. **Salvail H, Masse E.** 2012. Regulating iron storage and metabolism with RNA: an overview of posttranscriptional controls of intracellular iron homeostasis. Wiley Interdiscip. Rev. RNA **3:**26–36. http://dx.doi.org/10.1002/wrna.102.
38. **Williams PH.** 1979. Novel iron uptake system specified by ColV plasmids: an important component in the virulence of invasive strains of *Escherichia coli*. Infect. Immun. **26:**925–932.
39. **Smith HW.** 1974. A search for transmissible pathogenic characters in invasive strains of *Escherichia coli*: the discovery of a plasmid-controlled toxin and a plasmid-controlled lethal character closely associated, or identical, with colicine V. J. Gen. Microbiol. **83:**95–111. http://dx.doi.org/10.1099/00221287-83-1-95.
40. **Caza M, Lepine F, Dozois CM.** 2011. Secretion, but not overall synthesis, of catecholate siderophores contributes to virulence of extraintestinal pathogenic *Escherichia coli*. Mol. Microbiol. **80:**266–282. http://dx.doi.org/10.1111/j.1365-2958.2011.07570.x.
41. **Garcia EC, Brumbaugh AR, Mobley HL.** 2011. Redundancy and specificity of *Escherichia coli* iron acquisition systems during urinary tract infection. Infect. Immun. **79:**1225–1235. http://dx.doi.org/10.1128/IAI.01222-10.
42. **Neilands JB.** 1981. Microbial iron compounds. Annu. Rev. Biochem. **50:**715–731. http://dx.doi.org/10.1146/annurev.bi.50.070181.003435.
43. **Perry RD, Balbo PB, Jones HA, Fetherston JD, DeMoll E.** 1999. Yersiniabactin from *Yersinia pestis*: biochemical characterization of the siderophore and its role in iron transport and regulation. Microbiology **145:**1181–1190. http://dx.doi.org/10.1099/13500872-145-5-1181.
44. **Weinberg ED.** 1978. Iron and infection. Microbiol. Rev. **42:**45–66.
45. **Braun V, Brazel-Faisst C, Schneider R.** 1984. Growth stimulation of *Escherichia coli* in serum by iron(III) aerobactin. Recycling of aerobactin. FEMS Microbiol. Lett. **21:**99–103. http://dx.doi.org/10.1111/j.1574-6968.1984.tb00193.x.
46. **Konopka K, Bindereif A, Neilands JB.** 1982. Aerobactin-mediated utilization of transferrin iron. Biochemistry **21:**6503–6508. http://dx.doi.org/10.1021/bi00268a028.
47. **Konopka K, Neilands JB.** 1984. Effect of serum albumin on siderophore-mediated utilization of transferrin iron. Biochemistry **23:**2122–2127. http://dx.doi.org/10.1021/bi00305a003.
48. **Flo TH, Smith KD, Sato S, Rodriguez DJ, Holmes MA, Strong RK, Akira S, Aderem A.** 2004. Lipocalin 2 mediates an innate immune response to bacterial infection by sequestrating iron. Nature **432:**917–921. http://dx.doi.org/10.1038/nature03104.
49. **Bachman MA, Lenio S, Schmidt L, Oyler JE, Weiser JN.** 2012. Interaction of lipocalin 2, transferrin, and siderophores determines the replicative niche of *Klebsiella pneumoniae* during pneumonia. mBio **3**(6):e00224–11. http://dx.doi.org/10.1128/mBio.00224-11.
50. **Bearden SW, Perry RD.** 1999. The Yfe system of *Yersinia pestis* transports iron and manganese and is required for full virulence of plague. Mol. Microbiol. **32:**403–414. http://dx.doi.org/10.1046/j.1365-2958.1999.01360.x.
51. **Seo JH, Hong JS, Kim D, Cho BK, Huang TW, Tsai SF, Palsson BO, Charusanti P.** 2012. Multiple-omic data analysis of *Klebsiella pneumoniae* MGH 78578 reveals its transcriptional architecture and regulatory features. BMC Genomics **13:**679. http://dx.doi.org/10.1186/1471-2164-13-679.
52. **Chouikha I, Bree A, Moulin-Schouleur M, Gilot P, Germon P.** 2008. Differential expression of *iutA* and *ibeA* in the early stages of infection by extra-intestinal pathogenic *E. coli*. Microbes Infect. **10:**432–438. http://dx.doi.org/10.1016/j.micinf.2008.01.002.
53. **Bachman MA, Oyler JE, Burns SH, Caza M, Lepine F, Dozois CM, Weiser JN.** 2011. *Klebsiella pneumoniae* yersiniabactin promotes respiratory tract infection through evasion of lipocalin 2. Infect. Immun. **79:**3309–3316. http://dx.doi.org/10.1128/IAI.05114-11.
54. **Li W, Sun G, Yu Y, Li N, Chen M, Jin R, Jiao Y, Wu H.** 2014. Increasing occurrence of antimicrobial-resistant hypervirulent (hypermucoviscous) *Klebsiella pneumoniae* isolates in China. Clin. Infect. Dis. **58:**225–232. http://dx.doi.org/10.1093/cid/cit675.
55. **Centers for Disease Control and Prevention.** 2013. Vital signs: carbapenem-resistant enterobacteriaceae. MMWR Morb. Mortal. Wkly. Rep. **62:**165–170.

ACS chemical biology

Articles

pubs.acs.org/acschemicalbiology

Identification of Inhibitors of PvdQ, an Enzyme Involved in the Synthesis of the Siderophore Pyoverdine

Jacqueline M. Wurst,[†] Eric J. Drake,[‡,§] Jimmy R. Theriault,[†] Ivan T. Jewett,[†] Lynn VerPlank,[†] Jose R. Perez,[†] Sivaraman Dandapani,[†] Michelle Palmer,[†] Samuel M. Moskowitz,[∥,⊥] Stuart L. Schreiber,[†] Benito Munoz,[†] and Andrew M. Gulick*[,‡,§]

[†]The Broad Institute, Cambridge, Massachusetts 02142, United States

[‡]Hauptman−Woodward Medical Research Institute, New York 14203, United States

[§]Department of Structural Biology, University at Buffalo, Buffalo, New York 14203, United States

[∥]Department of Pediatrics, Massachusetts General Hospital, Boston, Massachusetts 02114, United States

[⊥]Department of Pediatrics, Harvard Medical School, Boston, Massachusetts 02115, United States

Supporting Information

ABSTRACT: *Pseudomonas aeruginosa* produces the peptide siderophore pyoverdine, which is used to acquire essential Fe^{3+} ions from the environment. PvdQ, an Ntn hydrolase, is required for the biosynthesis of pyoverdine. *PvdQ* knockout strains are not infectious in model systems, suggesting that disruption of siderophore production via PvdQ inhibition could be exploited as a target for novel antibacterial agents, by preventing cells from acquiring iron in the low iron environments of most biological settings. We have previously described a high-throughput screen to identify inhibitors of PvdQ that identified inhibitors with IC_{50} values of ∼100 μM. Here, we describe the discovery of ML318, a biaryl nitrile inhibitor of PvdQ acylase. ML318 inhibits PvdQ *in vitro* (IC_{50} = 20 nM) by binding in the acyl-binding site, as confirmed by the X-ray crystal structure of PvdQ bound to ML318. Additionally, the PvdQ inhibitor is active in a whole cell assay, preventing pyoverdine production and limiting the growth of *P. aeruginosa* under iron-limiting conditions.

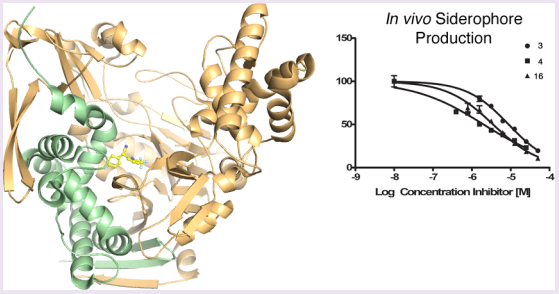

The growing prevalence of drug-resistant bacterial pathogens is of significant concern in the United States and worldwide. Of particular concern are the multidrug resistant Gram-negative bacteria including *Klebsiella pneumoniae*, *Acinetobacter* species, *Enterobacter* species, and *Pseudomonas aeruginosa*.[1,2] Gram-negative human pathogens such as *P. aeruginosa* typically require intracellular iron levels in the micromolar range for growth and infectivity.[3,4] The low abundance of iron in a typical host environment has provided a selective pressure for *P. aeruginosa* to develop a mechanism to extract iron from the extracellular milieu.

Targeting siderophore biosynthesis as a strategy to reduce virulence[5] has received much attention recently. Salicyl-AMS (5′-O-(N-salicylsulfamoyl)adenosine), a nM inhibitor of the myocobactin biosynthetic enzyme MbtA,[6−8] reduces the growth of *M. tuberculosis* in mouse lungs.[9] Importantly, this work validates the approach that preventing pathogen access to essential nutrients and demonstrates the bioavailability of the Salicyl-AMS inhibitor and the primary importance of mycobactin over other iron-acquisition pathways.

P. aeruginosa produces pyoverdine, a peptide siderophore that scavenges extracellular iron.[10] Secreted pyoverdine binds to Fe^{3+} with high affinity ($K_f \sim 10^{24}$ M^{-1} at pH 7.0) and the resulting complex is taken into the bacterial cell through a specific receptor.[11] Pyoverdine also plays a role in the regulation of other *P. aeruginosa* virulence factors[12−14] and biofilm formation.[15−17]

It has been shown that pyoverdine-deficient mutant strains are not infectious in the mouse lung,[18] plant,[19] and *C. elegans*.[20] Pyoverdine is biosynthesized by four nonribosomal peptide synthetases (NRPSs) and 10 additional modifying enzymes.[10,21] The modular NRPS enzymes contain multiple catalytic domains joined in a single protein that catalyze peptide production in an assembly line fashion. During synthesis, the nascent peptide is covalently bound to an integrated peptidyl carrier protein domain and delivered to the neighboring catalytic domains. In this modular architecture, each NRPS module catalyzes the incorporation of a single substrate into the final peptide product.[22]

Pyoverdine is composed of a conserved dihydroquinoline-type chromophore and a peptide tail that varies among different *Pseudomonas* species (Figure 1A).[11,21] Additionally, most strains produce variable pyoverdine isoforms with N-terminal succinate, succinamide, or glutamate moieties bound to the

Received: February 28, 2014
Accepted: May 13, 2014
Published: May 13, 2014

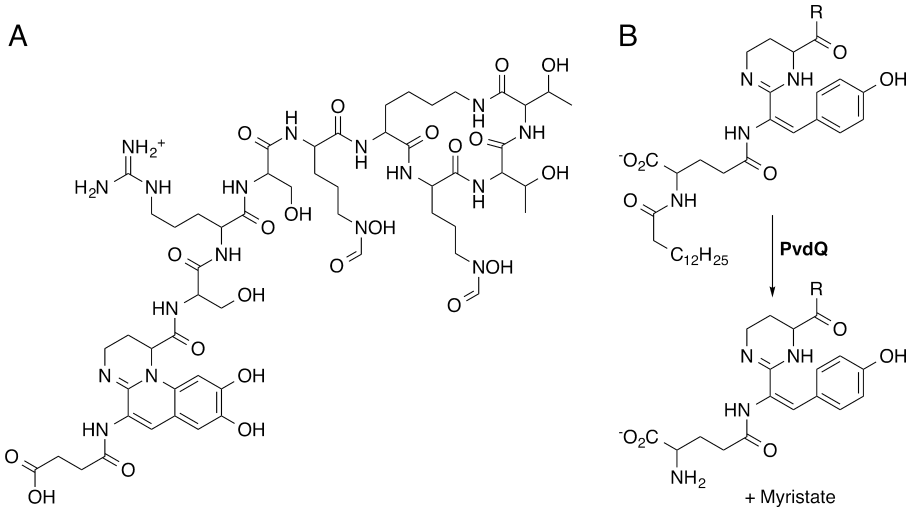

Figure 1. Structure of pyoverdine and the role of PvdQ in biosynthesis. (A) The mature pyoverdine siderophore is an undecapeptide containing an N-terminal sidearm, the chromophore, and a species-specific peptide chain. (B) PvdQ catalyzes the removal of the myristoyl group from the pyoverdine precursor.

chromophore. PvdL, the first NRPS protein of the pyoverdine pathway, is shared among all sequenced pseudomonads and generates the peptide backbone that is converted into this chromophore.[21] Interestingly, PvdL contains a N-terminal module with homology to fatty acyl-CoA ligases.[23] We recently[24] showed that this unusual NRPS architecture incorporates a myristate molecule, subsequently identified as either myristic or myristoleic acid,[25] at the N-terminus of an intermediate in pyoverdine biosynthesis. Additionally, we demonstrated that the incorporated fatty acid, which is not present on mature pyoverdine, is removed by PvdQ,[24] one of the 10 auxiliary proteins necessary for pyoverdine synthesis (Figure 1B).[10] PvdQ belongs to a family of N-terminal nucleophile (Ntn) hydrolases that catalyze the cleavage of amide bonds via an acylated enzyme intermediate.[26] PvdQ exhibits promiscuity in activity and also cleaves acyl-homoserine lactones that are involved in quorum signaling.[27,28]

To examine the role of PvdQ in pyoverdine maturation, we developed a high-throughput biochemical assay to find inhibitors of the PvdQ acylase activity.[24] The assay monitored the hydrolysis of *p*-nitrophenyl myristate (Figure 2A) and showed good reproducibility and signal-to-noise parameters, with Z′ scores of 0.7−0.9 within one plate and 0.6 overall. In this proof-of-concept study, we screened 1280 compounds, identifying aryl bromides **1** and **2** (Figure 2B), which exhibit IC_{50} values of 130 μM and 65 μM and bind in the fatty acid binding pocket.[24] This success with a small library suggested that a more thorough effort might lead to compounds with higher affinity. We therefore conducted a high-throughput screen with a larger chemical library and 4-methylumbelliferyl laurate (4-MU laurate), a fluorogenic substrate with improved signal-to-noise properties, to identify more potent scaffolds for PvdQ inhibition that can serve as tool compounds for understanding pyoverdine maturation and therapeutic leads for *P. aeruginosa* infection.

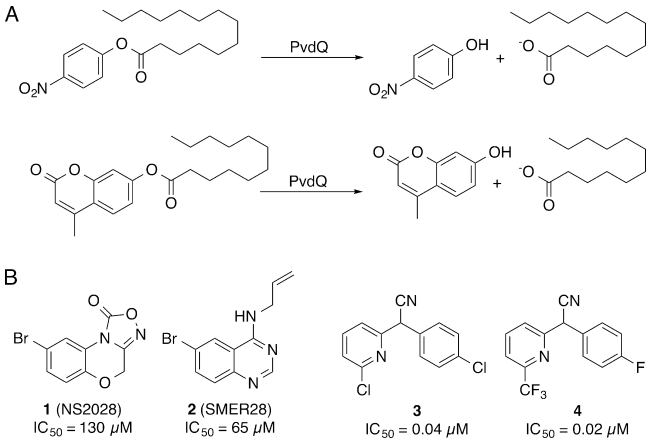

Figure 2. High-throughput screen for PvdQ inhibitors. (A) PvdQ hydrolysis of either *p*-nitrophenyl myristate or 4-MU-laurate substrates result in production of compounds that can be detected through absorbance or fluorescence. (B) Comparison of biochemical PvdQ inhibition activities of prior art compounds (**1**, **2**) to the high-throughput screening lead **3** and the optimized probe **4**.

RESULTS

High Throughput Screening of PvdQ. Our previous screening with the LOPAC1280 chemical library used the chromogenic substrate. Optimization and miniaturization of this assay resulted in improved signal-to-noise with the fluorogenic substrate 4-MU laurate. A high-throughput biochemical assay with the fluorogenic substrate was screened with the NIH MLSMR (National Institutes of Health Molecular Libraries Small Molecule Repository) collection of 337 488 compounds at 10 μM. Fluorescence measurements at 0 and 60 min were read and a total of 213 compounds were deemed active (inhibition of >20% fluorescence in both replicates) and 198 compounds were considered inconclusive (inhibition of >20% in one replicate). Of these 411 compounds, 396 were readily available and were rescreened at 9 concentrations ranging from 0.003 to 19.5 μM to assess preliminary potency. Here, 89 had IC_{50} values lower than 10 μM. The most potent inhibitors of PvdQ acylase were tested in a preliminary whole-cell *P. aeruginosa* (PAO1 strain) in the presence of metal chelator ethylenediamine-*N*,*N*′-bis(2-hydroxyphenyl-acetic acid) (EDDHA) and in a HeLa cell toxicity counter screen.[29] The whole cell assay with *P. aeruginosa* had two readouts; absorption at 600 nm was measured as a reporter

dx.doi.org/10.1021/cb5001586 | ACS Chem. Biol. 2014, 9, 1536−1544

of growth inhibition, while absorption at 405 nm was measured as a reporter of pyoverdine production.[30]

Biarylnitrile **3** was selected for further development on the basis of activity against PvdQ, activity in the whole cell assay, specificity as determined by lack of activity in other PubChem Bioassays, lack of toxicity with HeLa cells, and chemical tractability for generation of compound analogues. The hit compound **3** exhibited an IC_{50} of 40 nM against PvdQ acylase in biochemical assays (Figure 2). In preliminary growth assays, the hit compound displayed an IC_{50} of 59 μM against *P. aeruginosa* PAO1.[29] In addition, **3** was not active in any other assay submitted to PubChem at the time of analysis, including toxicity studies with other bacteria, including *M. tuberculosis* and *E. coli*.

Synthesis of Biaryl Nitrile Analogues. Based on scaffold **3**, a panel of analogues was synthesized and tested for PvdQ inhibition activity. The racemates of most analogues were conveniently synthesized via arylations of benzylacetonitriles with halopyridines[31] or alkylations with haloalkanes.[32] (We note that separation of the enantiomers was not successful due to racemization of the benzylic position at ambient temperatures and neutral conditions.) A representative example of the arylation is shown for the synthesis of biaryl nitrile **4** (Figure 3).

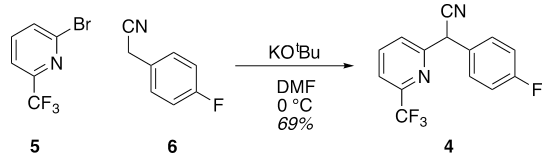

5 6 4

Figure 3. Synthesis of biaryl nitrile **4** from bromopyridine **5** and benzyl nitrile **6**.

Coupling of 2-bromo-5-trifluoromethylpyridine **5** with 4-fluorobenzyl nitrile **6** using potassium *tert*-butoxide gave the desired biaryl nitrile **4** in 69% yield. Tetrazoles were synthesized from nitriles via [3 + 2] cycloaddition and amino nitriles were synthesized from 4-chlorobenzaldehyde by a Strecker reaction (not shown).[33,34]

Structure–Activity Relationship Analysis. Modifications to the phenyl ring comprising the eastern half of lead **3** were analyzed in the biochemical assay (Table 1). Relative to the 4-chlorophenyl (**3**), the unsubstituted phenyl ring (**7**) and the addition of a hydrogen bond acceptor at the *ortho* position (**8**,**11**) led to at least 7-fold decreased *in vitro* potency. By comparison, analogues with an electron-withdrawing group at the *para* position (**9**, **10**, **12**, **13**) performed better.

Table 1. SAR Analysis of Eastern Analogues

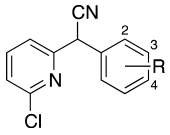

analog	R	PvdQ (*in vitro*) IC_{50}[a] (μM)
3	4-Cl	0.04 ± 0.01
7	H	0.30 ± 0.02
8	2-OCH_3	0.40 ± 0.08
9	4-F	0.07 ± 0.02
10	4-CF_3	0.39 ± 0.10
11	2-OCH_3	1.7 ± 0.6
12	2-Cl, 4-Cl	0.25 ± 0.04
13	2-F, 4-Cl	0.06 ± 0.02

[a]Average of at least three replicates ± standard deviation.

With regards to the western half of the scaffold, synthetic efforts focused on removing the potentially labile 2-chloro substituent on the pyridine ring without sacrificing potency (Table 2). Removal of the 2-chloro (**24**) resulted in a 7-fold

Table 2. SAR of Pyridine with a 4-Substituted Phenyl Ring

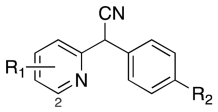

analog	R_1	R_2	PvdQ (*in vitro*) IC_{50}[a] (μM)
3	2-Cl	Cl	0.04 ± 0.01
14	3-Cl	Cl	0.13 ± 0.04
15	5-Cl	Cl	0.01 ± 0.004
16	2-CF_3	Cl	0.01 ± 0.005
17	2-CN	Cl	0.18 ± 0.05
18	2-CH_3	Cl	0.25 ± 0.04
19	3-CH_3	Cl	0.25 ± 0.09
20	3-CF_3	Cl	2.4 ± 1.2
21	2-Cl, 3-CF_3	Cl	0.62 ± 0.08
22	2-CN, 3-CH_3	Cl	0.18 ± 0.02
23	3-CN	Cl	2.5 ± 0.5
24	H	Cl	0.27 ± 0.03
4	2-CF_3	F	0.02 ± 0.01
25	2-CH	F	0.13 ± 0.02
26	2-CN, 3-CH_3	F	0.13 ± 0.07
27	2-Cl, 3-CF_3	F	0.74 ± 0.28
28	2-Cl, 3-CF_3	CF_3	2.3 ± 1.9
29	2-CF_3	CF_3	0.14 ± 0.06

[a]Average of at least three replicates ± standard deviation.

increase in IC_{50}. The 3-chloro analogue (**14**) showed reduced potency relative to lead **3**. Meanwhile, the 5-chloro analogue **15** increased potency 4-fold *in vitro* relative to **3**, as did replacement of the 2-chloro substituent on the pyridine ring with trifluoromethyl (**16**). We note that the IC_{50} of **15** and **16** were at or slightly below half the concentration of PvdQ used in the biochemical assays, indicating that these are tight-binding inhibitors. Potentially, the true binding affinity is even better for these and the most potent compounds identified than is reflected by their IC_{50} values. All other substitutions on the pyridine resulted in lower inhibitory efficiency (**17**–**23**) when the eastern aryl ring retained the 4-chlorophenyl.

Replacement of the 4-chloro substituent with 4-fluoro on the eastern phenyl ring led to a series of analogues (**4**,**25**–**27**) with similar potencies to those observed in the 4-chloro series. Notably, this 4-fluoro series included the 2-trifluoromethylpyridine analogue (**4**) with very similar potency to 2-trifluoromethylpyridine analogue (**16**) of the 4-chloro series. Substitution at carbon four on the eastern ring with trifluoromethyl was not beneficial (**28**–**29**).

Incorporation of multiple halogens into the phenyl ring (Table 3) demonstrated that fluoride is tolerated in the 2-position of the phenyl ring (**30**–**32**), and the 2-CF_3 pyridine analogue (**31**) showed improvement over the HTS lead (**3**). A 2-chloro substituent on the phenyl ring is less tolerated, as shown by the decrease in potency for 2,4-dichloro analogues (**33**–**36**) compared to the monochloride analogues described in Table 2.

dx.doi.org/10.1021/cb5001586 | *ACS Chem. Biol.* 2014, 9, 1536–1544

Table 3. SAR of Pyridine Analogues with 2,4-Halide Substituted Phenyl Ring

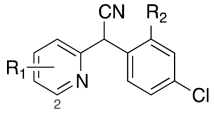

analog	R_1	R_2	PvdQ (*in vitro*) IC_{50}[a] μM
3	2-Cl	H	0.04 ± 0.01
30	2-CN	F	0.11 ± 0.01
31	2-CF3	F	0.01 ± 0.001
32	2-Cl, 3-CF3	F	0.63 ± 0.05
33	2-CN	Cl	0.29 ± 0.03
34	3-CN	Cl	1.8 ± 0.34
35	5-Cl	Cl	0.21 ± 0.03
36	2-Cl, 3-CF3	Cl	0.97 ± 0.46

[a]Average of at least three replicates ± standard deviation.

To address the chemical liability of the benzylic nitrile group and to mimic the natural, lipophilic myristate ligand of PvdQ, the pyridyl ring was removed and replaced with various hydrophobic alkyl chains (Table 4, **37**–**40**, **46**), which resulted in lower *in vitro* potency. Efforts to enhance the solubility of these alkyl analogues through the incorporation of heteroatoms in either the alkyl chain (**41**–**45**, **47**, **48**) or the aryl ring (**49**–**51**) afforded analogues that did not perform well (Table 4).

Table 4. SAR of Alkylated Nitriles

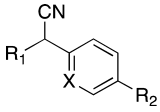

analog	R_1	R_2	X	PvdQ (*in vitro*) IC_{50}[a] μM
3	2-Cl pyridine	Cl	CH	0.04 ± 0.01
37	$(CH_2)_2CH_3$	Cl	CH	5.9 ± 1.3
38	$(CH_2)_3CH_3$	Cl	CH	1.4 ± 0.8
39	$CH_2CH(CH_3)_2$	Cl	CH	0.29 ± 0.09
40	$CH_2CH(CH_2)_2$	Cl	CH	0.54 ± 0.17
41	$(CH_2)_2OCH_3$	Cl	CH	4.8 ± 0.4
42	$((CH_2)_2O)_2CH_3$	Cl	CH	4.7 ± 3.0
43	$(CH_2)_3N(CH_3)_2$	Cl	CH	>10
44	$NH(CH_2)_2OCH_3$	Cl	CH	>10
45	1-pyrrolidine	Cl	CH	0.26 ± 0.29
46	$(CH_2)_3CH_3$	F	CH	0.32 ± 0.16
47	$(CH_2)_2OCH_3$	F	CH	0.29 ± 0.12
48	$(CH_2)_3CH_3$	CF_3	CH	>10
49	$(CH_2)_3CH_3$	Cl	N	3.8 ± 3.5
50	$(CH_2)_3CH_3$	F	N	0.37 ± 0.08
51	$(CH_2)_3CH_3$	H	N	8.4 ± 3.2

[a]Average of at least three replicates ± standard deviation.

Other compounds that were examined included analogues in which the nitrile was replaced with a tetrazole (Table 5, **52**–**53**), an analogue in which the benzylic center was quaternarized (**54**), and an analogue in which the western and eastern aromatic rings were tethered in a seven-membered ring (**55**) (Table 5). These compounds all showed significantly worse activity.

Crystal Structure Analysis. We examined the binding of the new compounds with X-ray crystallography. The initial HTS lead **3** and the fluorinated analogue **4** were selected for structural studies. The binding mode of biaryl nitriles to PvdQ was first studied by solving the structure of PvdQ bound to **3** at a resolution of 2.0 Å (Figure 4). Hit compound **3** sits in the acyl-binding site with the 4-chlorophenyl directed into the pocket away from the catalytic nucleophile (Figure 4). Hydrophobic residues Leu169, Leu269, Val374, Leu375, Trp378, and Pro401, as well as the methyl group of Thr166 surround the 4-chlorophenyl ring. The 2-chloropyridine lies in a hydrophobic pocket created by Met245, Phe248, Phe240, and His284. Leu266 fits between the two aromatic rings of and contributes to the hydrophobic cavities for both rings. Hydrophobic interactions dominate both spaces that accommodate the aromatic rings of the biarylnitrile scaffold.

Table 5. SAR of Bis-benzylic Nitrile Replacements

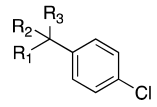

analog	R_1	R_2	R_3	PvdQ (*in vitro*) IC_{50}[a] μM
3	2-Cl pyridine	H	CN	0.04±0.01
52	2-Cl pyridine	H		3.4±2.3
53	$(CH_2)_3CH_3$	H		6.7±4.7
54	3-CF_3 pyridine	CH_3	CN	1.1±1.0
55	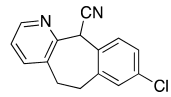			9.1±1.5

[a]Average of at least three replicates ± standard deviation.

A parallel-displaced π-stacking interaction between the 4-chlorophenyl and Trp378, and a T-shaped π-stacking interaction between the 2-chloropyridine and Phe240 could account for improved binding and the corresponding increase in potency for the biaryl nitrile analogues versus analogues containing aliphatic chains (Figure 4, Table 4). Interestingly, an overlay of the natural myristate ligand extends across the synthetic substrate with maximal overlap at the 2-position on the pyridine and the 4-position on the phenyl ring. This suggests that substitutions at these positions offer the best fit in the active site. The electrophilic 2-chloropyridine is approximately 7.4 Å from the catalytic nucleophile Ser217 and is not poised for covalent attachment. Therefore, the expectation is that nonelectrophilic substitutions will not reduce potency and these inhibitors would be competitive with substrate binding.

The nitrile moiety is directed into a ring formed by the main chain atoms of Pro401, Trp402, and Val403; the main chain amine of Trp402 hydrogen bonds to the nitrogen atom of the ligand nitrile (Figure 4). The side chains of all three of these residues contribute to this hydrophobic pocket. A π-stacking interaction between the nitrile moiety of the ligand and the indole ring of Trp402 stabilizes the binding orientation.

Co-crystallization of PvdQ with the more potent biaryl nitrile **4** offered additional insights (Figure 5). Crystals diffracted at 2.3 Å and the density of **4** was positioned in the PvdQ acyl-binding pocket analogously to **3**, allowing facile placement of the ligand. Residues Thr166, Leu266, Leu269, Val374, and

dx.doi.org/10.1021/cb5001586 | ACS Chem. Biol. 2014, 9, 1536–1544

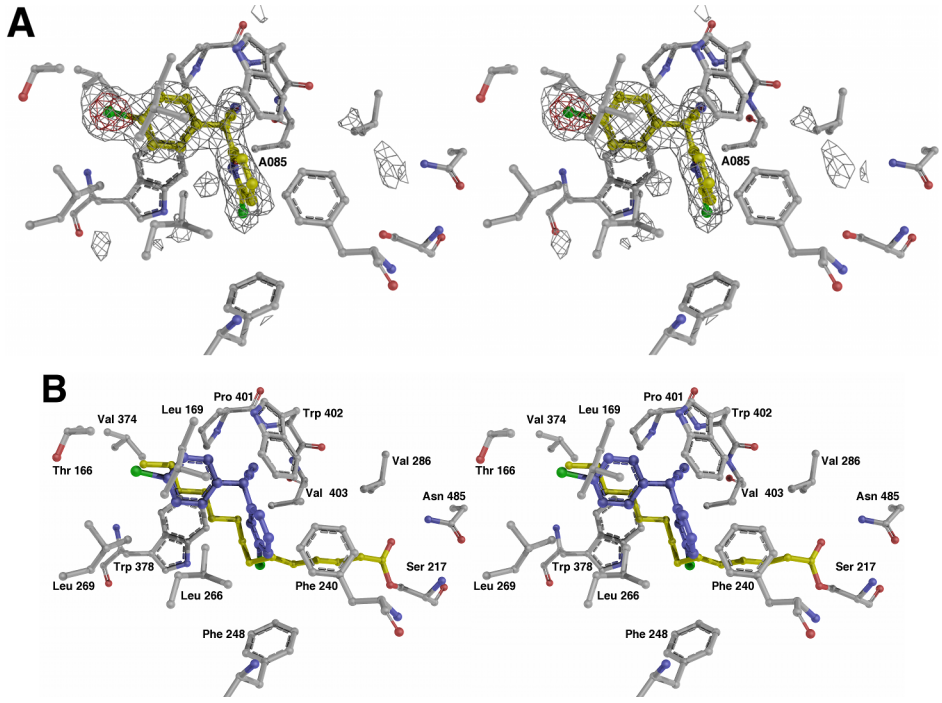

Figure 4. Structure of PvdQ bound to HTS hit compound **3**. (A) Electron density is shown, calculated with coefficients of the form Fo-Fc generated prior to building the ligand in the active site. Density is contoured at 3σ (gray) and 8σ (red). (B) Active site of the enzyme is shown of the PvdQ bound to **3**. Superposed on the structure is the fatty acid chain from covalently acylated structure from PDB 3L94.

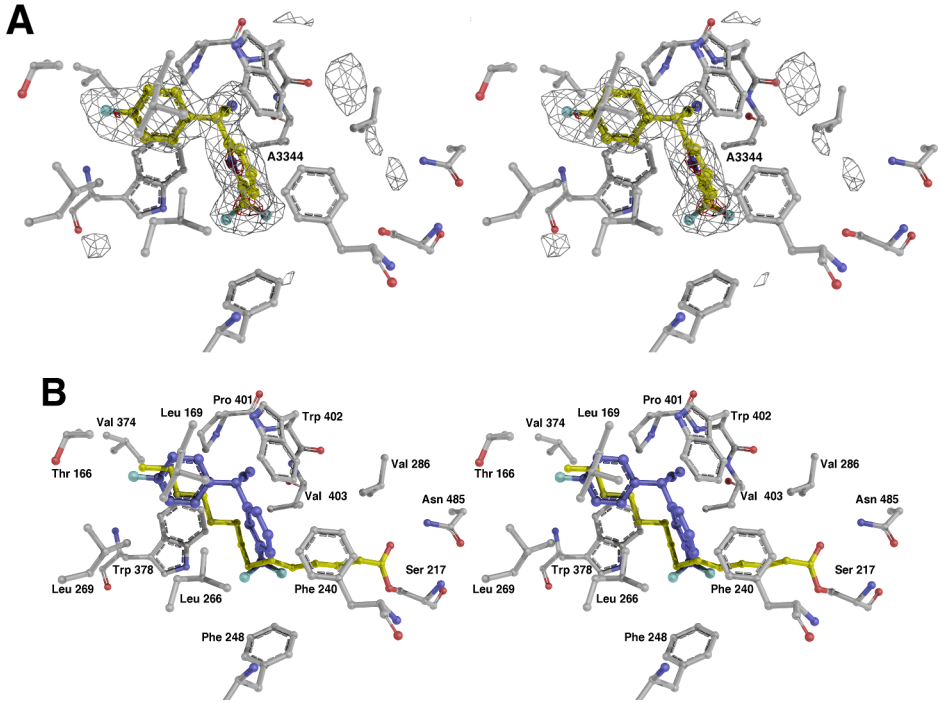

Figure 5. Structure of PvdQ bound to **4**. (A) Final probe compound ML318 is shown with electron density, calculated with coefficients of the form Fo-Fc generated prior to building the ligand in the active site, also included. Density is contoured at 3σ (gray) and 8σ (red). (B) Active site of the enzyme is shown of the PvdQ bound to **4**. As in Figure 4, the fatty acid chain from covalently acylated structure from PDB 3L94 is also shown.

Trp378 make contacts to 4-fluorophenyl as with 4-chlorophenyl of **3**. Again, the nitrile was surrounded by Pro401, Trp402, and Val403 residues, which provided key side chain and π-stacking interactions. Parallel-displaced and T-shaped π-stacking to Phe240 and Trp378, respectively, also enforced strong binding of the aromatic rings within the active site. Interestingly, the replacement of 2-chloro substituent on pyridine with trifluoromethyl provided the largest structural change between the binding of ligands **3** and **4**. Whereas the only residue within 4 Å of the pyridyl chlorine atom of **3** is His284, each fluorine atom from the CF_3 interacts with hydrophobic functionality on Phe240, Ile274, Trp378, Trp402,

dx.doi.org/10.1021/cb5001586 | *ACS Chem. Biol.* 2014, 9, 1536–1544

Table 6. Activity of Analogues in Other *P. aeruginosa* Strains and Toxicity Counter Screen

	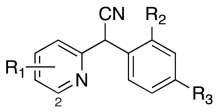			PAO1 wild type IC_{50}[a]	PAK *P. aeruginosa* IC_{50}[a]		pyoverdine production IC_{50}[a]
					wild type	pump mutant	
analog	R_1	R_2	R_3	μM[b]	μM[b,c]	μM[b]	μM[d]
4	**2-CF_3**	**H**	**F**	**19±4**	**43±18**	**1.4±0.2**	**1.9±0.2**
16	2-CF_3	H	Cl	11±3	24±10	1.8±0.3	3.5±1.3
31	2-CF_3	F	Cl	11±6	36±16	1.5±0.7	6.4±0.2
3	2-Cl	H	Cl	37±12	44±12	1.6±0.5	18±3.2
13	2-Cl	F	Cl	33±10	51±15	3.2±0.6	13±0.6
15	5-Cl	H	Cl	43±14	70±22	1.7±0.7	25±7.5

[a]Average of at least three replicates ± standard deviation. [b]405 nm wavelength measuring effect on pyoverdine production. [c]Measurement taken as $AbsAC_{-35}$ (absolute active concentration at 35% inhibition), the predetermined activity threshold chosen for comparison because not all compounds reached a plateau of activity at 50% inhibition. [d]Quantified by analysis of the isolated pyoverdine HPLC peaks present in culture media of cells treated with varying concentrations of each inhibitor.

and Val403 side chains. These hydrophobic interactions are along the same vector observed for the natural myristate ligand and these interactions could account for the increase in potency observed for **4**.

Analysis of the mostly hydrophobic fatty acid binding pocket in the context of the inhibitor-bound crystal structures informs the SAR of the analogues. The 2-chloropyridine group binds in the pocket closer to the catalytic serine while the 4-chlorophenyl group sits more deeply in the pocket. Compounds **3** and **4** both bind tightly in the pocket; except for the pyridyl nitrogen, each atom on the two aryl groups is less than 4 Å from a protein atom. While one edge of the phenyl ring points directly toward the peptide bond that joins Leu169 and Leu170, the other edge of the ring points toward a relatively large pocket that ends at Asn273. The presence of this pocket likely accommodates the variations in the C2 and C4 positions of the phenyl ring (Table 1). The 4-chlorophenyl could be replaced with a 2-fluoro-4-chlorophenyl group without a dramatic loss of activity, as in compounds **13** and **31**.

Binding at the wider side of the hydrophobic binding pocket, the pyridine ring is more accepting of substitutions. Indeed, a wide variety of pyridine analogues retained activity with IC_{50} values below 200 nM (Table 2). As a whole, the alkyl substituted analogues (Table 4) that replaced the pyridine ring with the alkyl group showed weaker activity. This suggests that the $\pi-\pi$ stacking interactions with Phe240 may be an important feature of binding the bisaryl inhibitor.

The nitrile replacements (Table 5) show the importance of the inhibitor framework to binding affinity. The replacement of the nitrile with a tetrazole in **52** and **53** increased the IC_{50} above 3 μM. The tight binding of the nitrile to the pocket formed by the peptide backbone of Pro401 through Val403 provides an explanation for this result. The ring positions shows that the geometry of binding can not accommodate the bridged seven-membered ring of **55**.

As noted above, we were unable to purify enantiopure compounds due to the racemization of the chiral carbon at ambient conditions. The structure demonstrates, however, that the enzyme bound specifically to the *S*-isomer of both **2** and **3**, which results in the nitrile positioned in the pocket formed by the main chain of Pro401-Val403 and the pyridine ring deeper in the acyl binding pocket. Given the approximate symmetry of the bisbenzylic compounds, it is possible that the *R*-isomers also could bind in the pocket with the result of switching the positions of the phenyl and pyridine rings. However, substitutions at the C3 position of the pyridyl ring result in drops of at least 10-fold in potency and indeed are some of the worst compounds identified—**20**, **23**, **28**, and **34**, for example—suggesting that substitutions *para* to the benzylic carbon are not well-accommodated and thus the *R*-enantiomer may not bind well in the PvdQ binding pocket.

Inhibitor Activity in Whole-Cell Assays. Despite exhibiting an IC_{50} of 40 nM in the biochemical assay, the primary hit compound **3** showed only μM activity in the preliminary whole cell assay.[29] We reasoned that this observation may be due partly to the nonlethality of the PvdQ knockout[14,35] and the known difficulty of small molecules to effectively permeate *P. aeruginosa*.[36] We therefore initiated a study of compound stability and the impact on pyoverdine production in whole cells.

We first screened compounds **3** and **4** for stability (Supporting Information). After 48 h in neutral PBS buffer, about 30−40% of **3** remains. After 6 h in the presence of 50 μM glutathione, about 90% remains. These values are modestly improved for the probe compound **4**, but overall the modest stability is a liability for further biological examination and the potential to develop these lead compounds for pharmaceutical activities.

Because of the limited stability of the compounds, we first developed a short-term assay to monitor the effect of several of the best inhibitors (those with IC_{50} < 0.06 μM) upon

dx.doi.org/10.1021/cb5001586 | *ACS Chem. Biol.* 2014, 9, 1536−1544

pyoverdine production in a whole cell assay. To demonstrate an on-target effect, *P. aeruginosa* (PAO1) was grown for 4 h in the presence of compounds and the amount of pyoverdine produced was directly measured using HPLC. Pyoverdine migrates as a cluster of HPLC peaks that were integrated for IC_{50} calculation (Table 6). This direct readout of pyoverdine production demonstrates the ability of these compounds to inhibit PvdQ in *P. aeruginosa.* Analogue **4** proved to be the most potent inhibitor of pyoverdine production with a whole cell IC_{50} of 1.9 μM.

We then tested these compounds against *P. aeruginosa* in 48 h growth cultures, understanding that differences in compound stability may influence the ability to rigorously compare the impact on pyoverdine production (Table 6). We first analyzed the compounds against the PA01 strain used earlier and monitored absorbance of culture media at 405 nm. The IC_{50} values for six biaryl nitriles ranged from 11 to 43 μM. We expected that the difference between the biochemical (nM) and whole cell (μM) activities are likely related to the ability of *P. aeruginosa* to export the compounds through nonspecific exporters.[37] We therefore screened the same compounds against a second *P. aeruginosa* strain (PAK) and a pump mutant (*mexAB-oprM*) of the PAK strain (Table 6). The most potent compounds retained similar activity in the PAK wild type strain and the potency of these small molecules was augmented in the pump mutant *mexAB-oprM* (Table 6). These data illustrate that these compounds are efficacious across two *P. aeruginosa* strains (PAO1 and PAK) and that the difference between the *in vitro* and *in vivo* activities is partly due to the efflux mechanisms.

Complementation with Inhibitors of Pyoverdine Synthesis Genes. Finally, we asked whether reduction in the expression of pyoverdine production enzymes such as PvdQ could further sensitize *P. aeruginosa*. Recently, a library of U.S. FDA-approved compounds were screened for molecules that block expression of pyoverdine synthetic genes.[38] These efforts identified 5-fluorocytosine (5-FC), which blocks transcription of *pvdS*, a σ-factor that is involved in activating a variety of genes in iron-depleted conditions. The effectiveness of 5-fluorocytosine was investigated *in vivo* and reduced *P. aeruginosa* growth and virulence in a mouse pulmonary infection. We therefore examined pyoverdine production in the HPLC assay for cells treated with either **4** or 5-FC alone, or with equal concentrations of **4** and 5-FC. Whereas the IC_{50} value for **4** and for 5-FC alone were 7.9 and 8.3 μM, the IC_{50} for the combined treatment was 1.7 μM. This demonstrates that reducing the expression level of the pyoverdine synthesis proteins sensitized the cells to the effects of the PvdQ inhibitor and could be an effective strategy for reducing pyoverdine production.

Despite the active nitrile moiety on the compounds identified herein, there is no evidence of a covalent interaction between PvdQ and either **3** or **4**. Recently, Fast and colleagues designed a covalent inhibitor of PvdQ using a tridecylboronic acid that binds covalently to the catalytic serine.[39] Kinetic and structural evidence show it is a competitive inhibitor that binds in the fatty acyl binding pocket. Growth of *P. aeruginosa* was inhibited by the boronic acid inhibitor when cotreated with phenylalanine-arginine-β-naphthylamide, a wide-spectrum inhibitor of multidrug resistance exporters. Given our results with the *mexA-oprM* mutant PAK strain, we are examining whether the inclusion of the exporter inhibitor may further enhance the efficacy of the biaryl nitrile inhibitors of PvdQ.

Summary. A high-throughput screen against the pyoverdine maturation enzyme PvdQ with the National Institutes of Health (NIH) MLSMR collection identified a biaryl nitrile scaffold (**3**) amenable to medicinal chemistry studies due to its modular nature. Numerous analogues were synthesized to investigate SAR at three regions of the scaffold leading to a more potent fluorinated biaryl nitrile **4**. Compound **4** was the most potent in the whole cell assays for inhibition of pyoverdine production directly measured by HPLC and has been designated as Probe Compound ML318.[29] On the pyridyl portion of the scaffold, electron-withdrawing groups, particularly in the 2-position were found in the most active analogues. On the phenyl portion, a halide in the 4-position was optimal. Crystallographic analyses of lead **3** and the optimized probe **4** in the acyl-binding pocket of PvdQ suggest a competitive binding mode for this class of biaryl nitriles. Distinctive hydrophobic, π-stacking and nitrile hydrogen bonding interactions rationalized the potent activities observed. The hit and probe compounds were shown to be active in whole cell assays, reducing the production of mature pyoverdine with IC_{50} values in the low μM range. The stability of the compounds limited effectiveness, as did the presence of *Pseudomonas* export machinery that likely explained the difference between the compounds in the whole cell vs biochemical assays. Nonetheless, the compounds confirm that targeting PvdQ specifically and siderophore synthesis proteins in general can be a suitable strategy to reduce the production of these important virulence determinants.

METHODS

High-Throughput Screening of PvdQ Activity. The enzymatic substrate 4-methylumbelliferyl (4-MU) laurate (Research Organics) solution was formulated using 1 volume isopropanol (Sigma), 0.1 volume Triton X-100 (Sigma), and 15 volumes of TNT buffer. The PvdQ protein preparation and 4-MU laurate solution were mixed together at the time of the screen using a BioRaptr FRD microfluidic workstation (Beckman Coulter) to a final concentration 0.02 μM PvdQ and 0.8 mM 4-MU laurate at RT in 1536-well high base black bar-coded square well assay plates (Aurora Biotechnologies) with compounds added previously, using an Echo acoustic liquid handler (Labcyte). The primary assay was performed with 337 488 library compounds at a concentration of 10 μM. Active compounds were rescreened at 8 concentrations of 3-fold dilutions starting at a highest concentration of 10 μM. The positive control, isopropyl dodecylfluorophosphonate (IDFP) (Cayman chemicals), was added in 24 selective wells to a final concentration of 200 μM. After the addition steps, the assay plates were first read for fluorescence at time = 0, then incubated at RT for 60 min, and then were read again at time = 60 min. Fluorescence was measured using the ViewLux uHTS Microplate Imager (PerkinElmer) with 303−367 nm excitation filter and 440−460 nm emission filter. The fluorescence generated by the enzymatic reaction was calculated as the difference between the two reads (60 min vs 0 min). Each dose response curve was normalized to a DMSO control set at 0% activity and the positive control (IDFP) set at −100% activity. The raw value attributed to each compound was converted to a percent effect based on these controls.

IC_{50} values were determined using the same fluorogenic assay with nine compound concentrations that ranged from 3 nM to 19.5 μM with PvdQ concentration of 20 nM. Additional details concerning the assay and the compounds determined to be active, as well as initial characterization of probe **4**, designated ML318, are available in the NIH Molecular Probe Report.[29]

Chemical Synthesis of Biaryl Nitriles. Biaryl nitriles were synthesized for SAR studies of inhibition of PvdQ acylase activity from phenylacetonitriles and substituted pyridines. Specific synthesis

procedures, NMR characterization, and yields are described in the Supporting Information.

Determination of the Structure of PvdQ Bound to 3 and 4. The structure determination of PvdQ bound to **3** and **4** along with diffraction and refinement statistics are presented in the Supporting Information.

***In Vivo* Inhibition of Pyoverdine Production.** Cultures of *Pseudomonas aeruginosa* PAO1 wild-type (ATCC 15692) were grown overnight (16 h) in 50 mL rich LB media. A pellet containing the bacteria was generated through centrifugation at 1725*g* for 10 min at 20 °C. The cells were washed once with 25 mL of 5% CAA media and centrifuged again at 20 °C (1725*g*, 10 min). The bacteria were resuspended in CAA media with 0.5% DMSO to calculated OD_{600} = 1.25. PAO1 wildtype and PvdQ deletion mutant cells (1 mL, OD_{600} = 0.2) were inoculated into seven serial dilutions of PvdQ small molecule inhibitors (100 μM to 1.5 μM final concentrations) in triplicate. Each bacteria and PvdQ compound inhibitor dilution/combination was grown for 4 h at 37 °C with shaking (250 rpm). An aliquot of 200 μL was transferred into a Costar clear bottom black side where the bacterial growth was measured at 600 nm. The remaining 800 μL of the bacterial culture was poured into a 1.5 mL eppendorf tube and centrifuged at 16 200 g for 5 min at 4 °C. The supernatant (500 μL) was removed and filtered through a 0.45 μM filter. The eluted solution was centrifuged under vacuum at 16 200 g at 20 °C to dryness (2 min). The dry pellet was reconstituted in 350 μL of a solution containing 2% acetonitrile, 98% H_2O, and 0.1% formic acid. The pyoverdine peaks were analyzed using the GraphPad Prism software on a transformed (x = log(x)) versus (no inhibitor = 100%). Dose response curves were calculated using a variable slope with constraints at 0 and 100. Details regarding chromatography are in the Supporting Information

***Pseudomonas aeruginosa* PAO1 Growth Delay Assay.** *Pseudomonas aeruginosa* PAO1 wild-type cells were grown overnight (16 h) in SM9 media. Prior to the addition of the bacteria, 30 μL of SM9 media with or without 2 μM (final concentration) of EDDHA was added to the 384-well black clear bottom assay plates (Aurora Biotechnologies). Compounds were added by pin tool transfer at 200 nL, to the final concentrations starting from 67 μM, with 8 concentrations at 3-fold dilutions. *P. aeruginosa* PAO1 cells (10 μL, diluted to a calculated OD_{600} = 2 × 10^{-6}) with or without 2 μM EDDHA was dispensed in the same wells. After incubation for 18−30 h at 37 °C, the absorbance at 600 and 405 nm was measured using an EnVision (PerkinElmer) plate reader. The data were reported at the concentration where the normalized dose response curve crosses a predetermined threshold since no positive control exists to set the −100% value.

***Pseudomonas aeruginosa* PAK Growth Delay Assay.** *Pseudomonas aeruginosa* PAK wild-type or pump mutant mexAB-OprM were grown overnight (16 h) in SM9 media at 37 °C. SM9 media was prepared ± 2 μM EDDHA and 20 μL was added to each well of 384-well black, clear bottom plates. Compounds (8 concentrations, 3 fold dilutions starting at 10 mM) were transferred via pin tool at 300 nL, giving final compound concentrations from 100 μM to 15 nM. *P. aeruginosa* wild-type or pump mutant *mexAB-OprM* culture (10 μL) diluted at OD_{600} = 0.05 in SM9 media (±2 μM EDDHA) was added to each well and the plates were incubated for 28 h at 30 °C, in a humidified environment. After 28 h incubation, the absorbance values were read with an EnVision plate reader at 600 nm (cell growth) and 405 nm (pyoverdine production). The data were again reported at the concentration where the normalized dose response curve crosses a predetermined threshold since no positive control exists to set the −100% value.[29] For the wild-type PAK cells, the data were reported at a slightly higher threshold since not all compounds reached 50% inhibition at the concentrations tested. This would make the impact of the *mexAB-OprM* mutation even larger.

■ ASSOCIATED CONTENT

Ⓢ Supporting Information

Detailed description of bacterial media, protein production, biological assays, analytical assays, pump mutant strain construction, NMR spectra, and crystal structures. This material is available free of charge via the Internet at http://pubs.acs.org.

Accession Codes

The final crystal structures and structure factors have been deposited in the PDB: PvdQ plus **3,** 4K2F; PvdQ plus **4**, 4K2G.

■ AUTHOR INFORMATION

Corresponding Author

*Tel.: 716 898-8619. Email: gulick@hwi.buffalo.edu.

Notes

The authors declare no competing financial interest.

■ ACKNOWLEDGMENTS

We gratefully acknowledge the National Institutes of Health (NIH) (U54HG005032 awarded to S.L.S.) for funding and the Broad Institute Analytical team, especially C. Mosher, T. Anthoine, and S. Johnston for expert mass spectral analysis and compound stability testing. We also acknowledge N. Dasgupta (Massachusetts General Hospital) and M. Brannon (University of Washington, Seattle) for bacterial strain construction. We thank C. Scherer for helpful discussions. This work was additionally supported by grants GM-068440 and MH-092076 (A.M.G.), by grant AI-067653 (S.M.M.), and TATRC cooperative agreement W81XWH-11-2-0218 (A.M.G.). Portions of this work were carried out at SSRL, which is supported by the DOE and NIGMS (including P41GM103393). S.L.S. is an Investigator with the Howard Hughes Medical Institute.

■ REFERENCES

(1) Kanj, S. S., and Kanafani, Z. A. (2011) Current concepts in antimicrobial therapy against resistant gram-negative organisms: Extended-spectrum β-lactamase-producing Enterobacteriaceae, carbapenem-resistant Enterobacteriaceae, and multidrug-resistant *Pseudomonas aeruginosa*. *Mayo Clinic Proceedings 86*, 250−259.

(2) Peterson, L. R. (2009) Bad bugs, no drugs: No ESCAPE revisited. *Clin. Infect. Dis. 49*, 992−993.

(3) Mekalanos, J. J. (1992) Environmental signals controlling expression of virulence determinants in bacteria. *J. Bacteriol. 174*, 1−7.

(4) Sandy, M., and Butler, A. (2009) Microbial iron acquisition: Marine and terrestrial siderophores. *Chem. Rev. 109*, 4580−4595.

(5) Miethke, M., and Marahiel, M. A. (2007) Siderophore-based iron acquisition and pathogen control. *Microbiol Mol. Biol. Rev. 71*, 413−451.

(6) Ferreras, J. A., Ryu, J. S., Di Lello, F., Tan, D. S., and Quadri, L. E. (2005) Small-molecule inhibition of siderophore biosynthesis in *Mycobacterium tuberculosis* and *Yersinia pestis*. *Nat. Chem. Biol. 1*, 29−32.

(7) Miethke, M., Bisseret, P., Beckering, C. L., Vignard, D., Eustache, J., and Marahiel, M. A. (2006) Inhibition of aryl acid adenylation domains involved in bacterial siderophore synthesis. *FEBS J. 273*, 409−419.

(8) Qiao, C., Gupte, A., Boshoff, H. I., Wilson, D. J., Bennett, E. M., Somu, R. V., Barry, C. E., 3rd, and Aldrich, C. C. (2007) 5′-O-[(N-Acyl)sulfamoyl]adenosines as antitubercular agents that inhibit MbtA: An adenylation enzyme required for siderophore biosynthesis of the mycobactins. *J. Med. Chem. 50*, 6080−6094.

(9) Lun, S., Guo, H., Adamson, J., Cisar, J. S., Davis, T. D., Chavadi, S. S., Warren, J. D., Quadri, L. E., Tan, D. S., and Bishai, W. R. (2013) Pharmacokinetic and *in vivo* efficacy studies of the mycobactin biosynthesis inhibitor salicyl-AMS in mice. *Antimicrob. Agents Chemother. 57*, 5138−5140.

(10) Ochsner, U. A., Wilderman, P. J., Vasil, A. I., and Vasil, M. L. (2002) GeneChip expression analysis of the iron starvation response in *Pseudomonas aeruginosa*: Identification of novel pyoverdine biosynthesis genes. *Mol. Microbiol. 45*, 1277−1287.
(11) Visca, P., Imperi, F., and Lamont, I. L. (2007) Pyoverdine siderophores: From biogenesis to biosignificance. *Trends Microbiol. 15*, 22−30.
(12) Lamont, I. L., Beare, P. A., Ochsner, U., Vasil, A. I., and Vasil, M. L. (2002) Siderophore-mediated signaling regulates virulence factor production in *Pseudomonas aeruginosa*. *Proc. Natl. Acad. Sci. U. S. A. 99*, 7072−7077.
(13) Meyer, J. M., Neely, A., Stintzi, A., Georges, C., and Holder, I. A. (1996) Pyoverdin is essential for virulence of *Pseudomonas aeruginosa*. *Infect. Immun. 64*, 518−523.
(14) Nadal Jimenez, P., Koch, G., Papaioannou, E., Wahjudi, M., Krzeslak, J., Coenye, T., Cool, R. H., and Quax, W. J. (2009) Role of PvdQ in *Pseudomonas aeruginosa* virulence under iron-limiting conditions. *Microbiology 156*, 49−59.
(15) Banin, E., Vasil, M. L., and Greenberg, E. P. (2005) Iron and *Pseudomonas aeruginosa* biofilm formation. *Proc. Natl. Acad. Sci. U.S.A. 102*, 11076−11081.
(16) Costerton, J. W., Stewart, P. S., and Greenberg, E. P. (1999) Bacterial biofilms: A common cause of persistent infections. *Science 284*, 1318−1322.
(17) Sauer, K., Cullen, M. C., Rickard, A. H., Zeef, L. A., Davies, D. G., and Gilbert, P. (2004) Characterization of nutrient-induced dispersion in *Pseudomonas aeruginosa* PAO1 biofilm. *J. Bacteriol. 186*, 7312−7326.
(18) Lehoux, D. E., Sanschagrin, F., and Levesque, R. C. (2000) Genomics of the 35-kb pvd locus and analysis of novel pvdIJK genes implicated in pyoverdine biosynthesis in *Pseudomonas aeruginosa*. *FEMS Microbiol. Lett. 190*, 141−146.
(19) Taguchi, F., Suzuki, T., Inagaki, Y., Toyoda, K., Shiraishi, T., and Ichinose, Y. (2010) The siderophore pyoverdine of *Pseudomonas syringae* pv. tabaci 6605 is an intrinsic virulence factor in host tobacco infection. *J. Bacteriol. 192*, 117−126.
(20) Papaioannou, E., Wahjudi, M., Nadal-Jimenez, P., Koch, G., Setroikromo, R., and Quax, W. J. (2009) Quorum-quenching acylase reduces the virulence of *Pseudomonas aeruginosa* in a *Caenorhabditis elegans* infection model. *Antimicrob. Agents Chemother. 53*, 4891−4897.
(21) Schalk, I. J., and Guillon, L. (2013) Pyoverdine biosynthesis and secretion in *Pseudomonas aeruginosa*: implications for metal homeostasis. *Environ. Microbiol. 15*, 1661−1673.
(22) Challis, G. L., and Naismith, J. H. (2004) Structural aspects of non-ribosomal peptide biosynthesis. *Curr. Opin Struct Biol. 14*, 748−756.
(23) Mossialos, D., Ochsner, U., Baysse, C., Chablain, P., Pirnay, J. P., Koedam, N., Budzikiewicz, H., Fernandez, D. U., Schafer, M., Ravel, J., and Cornelis, P. (2002) Identification of new, conserved, non-ribosomal peptide synthetases from fluorescent pseudomonads involved in the biosynthesis of the siderophore pyoverdine. *Mol. Microbiol. 45*, 1673−1685.
(24) Drake, E. J., and Gulick, A. M. (2011) Structural characterization and high-throughput screening of inhibitors of PvdQ, an NTN hydrolase involved in pyoverdine synthesis. *ACS Chem. Biol. 6*, 1277−1286.
(25) Hannauer, M., Schafer, M., Hoegy, F., Gizzi, P., Wehrung, P., Mislin, G. L., Budzikiewicz, H., and Schalk, I. J. (2012) Biosynthesis of the pyoverdine siderophore of *Pseudomonas aeruginosa* involves precursors with a myristic or a myristoleic acid chain. *FEBS Lett. 586*, 96−101.
(26) Artymiuk, P. J. (1995) A sting in the (N-terminal) tail. *Nat. Struct. Biol. 2*, 1035−1037.
(27) Bokhove, M., Jimenez, P. N., Quax, W. J., and Dijkstra, B. W. (2010) The quorum-quenching N-acyl homoserine lactone acylase PvdQ is an Ntn-hydrolase with an unusual substrate-binding pocket. *Proc. Natl. Acad. Sci. U.S.A. 107*, 686−691.
(28) Sio, C. F., Otten, L. G., Cool, R. H., Diggle, S. P., Braun, P. G., Bos, R., Daykin, M., Camara, M., Williams, P., and Quax, W. J. (2006) Quorum quenching by an N-acyl-homoserine lactone acylase from *Pseudomonas aeruginosa* PAO1. *Infect. Immun. 74*, 1673−1682.
(29) Theriault, J. R., Wurst, J., Jewett, I., Verplank, L., Perez, J. R., Gulick, A. M., Drake, E. J., Palmer, M., Moskowitz, S., Dasgupta, N., Brannon, M. K., Dandapani, S., Munoz, B., and Schreiber, S. (2013) Identification of a small molecule inhibitor of Pseudomonas aeruginosa PvdQ acylase, an enzyme involved in siderophore pyoverdine synthesis., In *Probe Reports from the NIH Molecular Libraries Program [Internet]*; National Center for Biotchnology Information (U.S.), Bethesda, MD.
(30) Meyer, J. M., Halle, F., Hohnadel, D., Lemanceau, P., and Ratefiarivelo, H. (1987) Siderophores of *Pseudomonas*−biological properties, In *Iron Transport in Microbes, Plants, and Animals* (Winkelmann, G., Van der Helm, D., and Neilands, J. B., Eds.), pp 189−205, VCH, Weinheim Germany.
(31) Sommer, M. B., Begtrup, M., and Bogeso, K. P. (1990) Displacement of halogen of 2-halogeno-substituted benzonitriles with carbanion. Preparation of (2-cyanoaryl)arylacetonitriles. *J. Org. Chem. 55*, 4817−4821.
(32) Hino, K., Nagai, Y., and Uno, H. (1988) Agents acting on the central nervous system. Synthesis of 3-phenyl-2-piperazinyl-1-benzazocines, 3-substituted-2-piperazinyl-1-benzazepines, and related compounds. *Chem. Pharmaceut. Bull. 36*, 2386−2400.
(33) Gutmann, B., Roduit, J. P., Roberge, D., and Kappe, C. O. (2010) Synthesis of 5-substituted 1H-tetrazoles from nitriles and hydrazoic acid by using a safe and scalable high-temperature microreactor approach. *Angew. Chem., Int. Ed. Engl. 49*, 7101−7105.
(34) Tran, V. H., Kantharaj, R., Roufogalis, B. D., and Duke, C. C. (2006) An efficient and facile synthesis of capsaicin-like compounds as agonists of the TRPV1 receptor. *Eur. J. Org. Chem. 2006*, 2970−2976.
(35) Clatworthy, A. E., Pierson, E., and Hung, D. T. (2007) Targeting virulence: A new paradigm for antimicrobial therapy. *Nat. Chem. Biol. 3*, 541−548.
(36) Lomovskaya, O., Warren, M. S., Lee, A., Galazzo, J., Fronko, R., Lee, M., Blais, J., Cho, D., Chamberland, S., Renau, T., Leger, R., Hecker, S., Watkins, W., Hoshino, K., Ishida, H., and Lee, V. J. (2001) Identification and characterization of inhibitors of multidrug resistance efflux pumps in *Pseudomonas aeruginosa*: Novel agents for combination therapy. *Antimicrob. Agents Chemother. 45*, 105−116.
(37) Pages, J. M., and Amaral, L. (2009) Mechanisms of drug efflux and strategies to combat them: Challenging the efflux pump of Gram-negative bacteria. *Biochim. Biophys. Acta 1794*, 826−833.
(38) Imperi, F., Massai, F., Facchini, M., Frangipani, E., Visaggio, D., Leoni, L., Bragonzi, A., and Visca, P. (2013) Repurposing the antimycotic drug flucytosine for suppression of *Pseudomonas aeruginosa* pathogenicity. *Proc. Natl. Acad. Sci. U.S.A. 110*, 7458−7463.
(39) Clevenger, K. D., Wu, R., Er, J. A., Liu, D., and Fast, W. (2013) Rational design of a transition state analogue with picomolar affinity for *Pseudomonas aeruginosa* PvdQ, a siderophore biosynthetic enzyme. *ACS Chem. Biol. 8*, 2192−2200.

IAI Journals.ASM.org

The K1 Capsular Polysaccharide from *Acinetobacter baumannii* Is a Potential Therapeutic Target via Passive Immunization

Thomas A. Russo,[a,d] Janet M. Beanan,[b,d] Ruth Olson,[b,d] Ulrike MacDonald,[b,d] Andrew D. Cox,[e] Frank St. Michael,[e] Evgeny V. Vinogradov,[e] Brad Spellberg,[f] Nicole R. Luke-Marshall,[c,d] Anthony A. Campagnari[c,d]

Veterans Administration Western New York Healthcare System,[a] Department of Medicine,[b] Department of Microbiology and Immunology,[c] and The Witebsky Center for Microbial Pathogenesis,[d] University at Buffalo-State University of New York, Buffalo, New York, USA; Institute for Biological Sciences, National Research Council of Canada, Ottawa, Ontario, Canada[e]; Division of General Internal Medicine, Los Angeles Biomedical Research Institute at Harbor-University of California Los Angeles Medical Center, Torrance, California, USA[f]

The emergence of extremely resistant and panresistant Gram-negative bacilli, such as *Acinetobacter baumannii*, requires consideration of nonantimicrobial therapeutic approaches. The goal of this report was to evaluate the K1 capsular polysaccharide from *A. baumannii* as a passive immunization target. Its structure was determined by a combination of mass spectrometric and nuclear magnetic resonance (NMR) techniques. Molecular mimics that might raise the concern for autoimmune disease were not identified. Immunization of CD1 mice demonstrated that the K1 capsule is immunogenic. The monoclonal antibody (MAb) 13D6, which is directed against the K1 capsule from *A. baumannii*, was used to determine the seroprevalence of the K1 capsule in a collection of 100 *A. baumannii* strains. Thirteen percent of the *A. baumannii* isolates from this collection were seroreactive to MAb 13D6. Opsonization of K1-positive strains, but not K1-negative strains, with MAb 13D6 significantly increased neutrophil-mediated bactericidal activity *in vitro* ($P < 0.05$). Lastly, treatment with MAb 13D6 3 and 24 h after bacterial challenge in a rat soft tissue infection model resulted in a significant decrease in the growth/survival of a K1-positive strain compared to that of a K1-negative strain or to treatment with a vehicle control ($P < 0.0001$). These data support the proof of principle that the K1 capsule is a potential therapeutic target via passive immunization. Other serotypes require assessment, and pragmatic challenges exist, such as the need to serotype infecting strains and utilize serotype-specific therapy. Nonetheless, this approach may become an important therapeutic option with increasing antimicrobial resistance and a diminishing number of active antimicrobials.

Acinetobacter baumannii has become a pathogen of increasing medical importance (1, 2). The majority of *A. baumannii* infections have been acquired in health care facilities (3–5). The respiratory tract, particularly in ventilated patients, the urinary tract, the bloodstream, intravascular devices, surgical sites (including sites of postneurosurgical meningitis), and decubitus or diabetic ulcers are favored sites of infection (6, 7). *A. baumannii* has also been shown to cause infections outside the health care setting, namely, severe community-acquired pneumonia (usually in alcoholics) (8–10) and infections in war-related injuries and in tsunami survivors (11, 12). Mortality rates associated with *A. baumannii* infection range from 19 to 54% (13).

Particularly worrisome is the significant degree of antimicrobial resistance demonstrated by many strains of *A. baumannii* (14, 15). The prevalence of multiresistance (resistance to three or more classes of antimicrobials), extreme resistance (resistance to all but one or two classes of antimicrobials), and panresistance (resistance to all antimicrobials) is increasing (16, 17).

Thus, treatment of infections due to *A. baumannii* has become challenging. Unfortunately, as of 2009 there were virtually no new antimicrobial agents active against Gram-negative bacilli (GNB) in the pharmaceutical pipeline (18). A 2011 update found some antimicrobials that had activity against GNB in development, but none have reached phase 3 trials (19, 20). Some combination of the development of new antimicrobial agents and nonantimicrobial approaches to treatment is needed. One approach worthy of consideration is the use of passive immunization. Historically this approach has been used primarily for toxin-mediated disease (e.g., snake or tetanus toxins) and viral infections (e.g., rabies or varicella-zoster virus) (21, 22). Although passive immunization (treatment with specific or nonspecific immunoglobulin preparations) provides only temporary immunity, it may be sufficient to clear an acute infection alone or in combination with antimicrobials that possess less than optimal efficacy. Recently, anti-OmpA antibodies were shown to confer protection against extremely antimicrobial-resistant *A. baumannii* in a mouse bloodstream infection model (23), justifying the potential of this approach for *A. baumannii*.

Capsular polysaccharides often possess the desirable characteristics of an antigenic target such as surface exposure, broad prevalence among clinical isolates, generation of a protective immune response, and a role in the pathogenesis of disease. Further, capsules have formed the basis for several successful vaccines directed against extracellular bacterial pathogens such as *Haemophilus influenzae* type b, *Streptococcus pneumoniae*, and certain serotypes of *Neisseria meningitidis* (24–27). Although not as efficacious, a vac-

Received 2 November 2012 **Returned for modification** 2 December 2012
Accepted 24 December 2012
Published ahead of print 7 January 2013
Editor: J. B. Bliska
Address correspondence to Thomas A. Russo, trusso@acsu.buffalo.edu.
Supplemental material for this article may be found at http://dx.doi.org/10.1128/IAI.01184-12.

doi:10.1128/IAI.01184-12

cine based on the Vi capsular polysaccharide is approved for *Salmonella typhi* (28). A potential limitation of active immunization with nonzwitterionic polysaccharides is the development of a T-independent response that is characterized by a poor memory response, particularly in the very young and old (29). However, the development of conjugated vaccines has for the most part overcome this drawback (30). Therefore, we hypothesized that capsular polysaccharides of *A. baumannii* would make an ideal antigenic target for protection against or treatment of infection, using either an active or passive immunization approach. Remarkably little is known about the prevalence and antigenic variation of capsular polysaccharides in *A. baumannii*. Presumably most clinical isolates possess a capsule since its loss severely decreases virulence (31); however, this has not been systematically established. Further, the number and prevalence of capsular serotypes in clinical *A. baumannii* isolates are also unknown. Studies assessing seroprevalence and evaluating specific capsular serotypes for their potential as active or passive immunization targets are needed.

Our laboratory is in the process of filling these knowledge gaps. To date, we have established that the K1 capsular polysaccharide from the *A. baumannii* strain AB307-0294 is surface exposed and is a virulence factor (31). However, no data are available on its seroprevalence, its immunogenicity, and the ability of antibodies directed against the capsular polysaccharide from *A. baumannii* to confer protection against infection. In this report those critical criteria for a vaccine candidate were assessed. Further, the structure of the K1 capsule was also delineated to determine whether any epitopes resembled human antigens. The results obtained support the hypothesis that *A. baumannii* capsular polysaccharides warrant continued evaluation as potential targets for active and/or passive immunization.

MATERIALS AND METHODS

Bacterial strains and media. *A. baumannii* strain AB307-0294 (blood isolate, sequence type 15 [ST15], clonal group 1 based on work by Ecker et al. [32]) is an encapsulated isolate from a patient hospitalized at Erie County Medical Center, Buffalo, NY, in 1994 (33). Capsule serotypes have not been defined in *A. baumannii*. Therefore, we have designated the capsular serotype present in AB307-0294 as K1. AB307.30 is an isogenic K1-negative derivative of AB307-0294 that possesses a disruption in *ptk*, which encodes a putative protein tyrosine kinase (PTK) (31). *A. baumannii* strains 693, 715, and 803 are K1 capsule positive, were obtained from the Walter Reed Army Medical Center (WRAMC, kindly provided by David Craft and Paul Scott), and were used in opsonophagocytosis studies. *A. baumannii* strain AB979 is K1 capsule negative, was also obtained from the WRAMC, and was used in the rat soft tissue infection model studies (34). The collection of 100 strains used for seroprevalence studies are listed in Table S1 in the supplemental material with their STs and sites of isolation when delineated. These *A. baumannii* strains were obtained from the WRAMC (78), Buffalo, NY (11), Los Angeles, CA (5), Chicago, IL (2), Cleveland, OH (1), and the ATCC (3). Strains were grown in Luria-Bertani (LB) medium unless stated otherwise and maintained at −80°C in 50% LB broth and 50% glycerol.

Determination of the K1 capsule structure. Polysaccharides were isolated from AB307-0294 (wild type, K1 capsule positive) and AB307.30 (isogenic derivative of AB307-0294, capsule negative) by standard phenol-water extraction (35). Structural elucidations were performed on the purified high-molecular-weight capsular polymer, isolated following anion-exchange chromatography as described previously (36). Capillary electrophoresis electrospray mass spectrometry (CE-ES-MS) and nuclear magnetic resonance (NMR) spectroscopy experiments were performed as described previously (37).

Generation and production of the MAb 13D6, which is specific for the K1 capsule expressed in AB307-0294. Monoclonal antibodies (MAbs) were developed and screened as described previously (38, 39). In brief, two BALB/c mice were injected intraperitoneally with a sublethal dose (1×10^4 CFU) of live AB307-0294 (K1 positive) without an adjuvant at 0, 2, and 4 weeks. Four days after the final immunization the mice were euthanized, their spleens were harvested, and a fusion was performed in accordance with standard methodology (40). Hybridomas that reacted to proteinase K-resistant, periodate-sensitive bacterial surface epitopes were selected for further analyses. MAb 13D6 met these criteria and was shown to be directed against the K1 capsule (31). Isotyping (Zymed Laboratories Inc.; mouse MonoAb-ID kit) established that MAb 13D6 was an IgM. The MAb 13D6 hybridoma was sent to Maine Biotechnology Services for production of purified MAb. The harvested ascites fluid had a total protein concentration of 34.92 mg/ml, 8.08% of which was immunoglobulin, resulting in an estimated 2.8 mg/ml of MAb 13D6. Since it is possible that background antibodies may be present in the ascites fluid, the actual concentration of MAb 13D6 may be lower. This preparation was used for *in vitro* and *in vivo* studies.

Generation of polyclonal K1 antisera. Capsular polysaccharide was extracted with cold 0.1 M pyridine acetate (pH 5.0) as described previously (41). The extract was dialyzed against endotoxin-free water and then treated with proteinase K, DNase I, and RNase A. Preimmunization antisera were obtained, and CD1 outbred male mice (18 to 20 g) were intramuscularly immunized with capsule purified from 150 mg (wet weight) of bacteria ($n = 6$) or with 1× phosphate-buffered saline (PBS) (pH 7.2) ($n = 6$) without adjuvant at 0, 2, and 4 weeks to generate anti-K1 immune and nonimmune antisera, respectively. Anti-K1 immune antisera, obtained at 5 weeks after initial immunization, were pooled and absorbed against AB307.30 (isogenic K1-negative derivative of AB307-0294) to remove any noncapsular antibodies that may have been generated from the presence of trace contaminants in the capsule preparation used for immunization. An immune dot assay was used to quantitate the immunogenicity of the K1 capsule. Preimmune and nonimmune antisera were nonreactive at the lowest dilution of 1:250. Anti-K1 immune antisera were reactive at a 1/25,000 dilution. These preparations were used to assess the anti-capsule IgG/IgM response via flow cytometry by comparing serum reactivities between the wild-type strain AB307-0294 and AB307.30, the difference reflecting anticapsular antibody.

Flow cytometry studies for the detection of polyclonal K1 antisera reactivity to AB307-0294 (K1 capsule positive) and AB307.30 (K1 capsule negative). Flow-cytometric assessment of antibody binding was performed as described previously (42). In brief, the appropriate strains were grown in LB medium, diluted to 1×10^6 CFU, washed in 100 μl of 1× PBS, resuspended in 100 μl of 1:100-diluted preimmune, nonimmune, or anti-K1 immune polyclonal mouse antiserum (complement inactivated by heating at 56°C for 30 min), and incubated for 60 min at 37°C with constant rotation. Preliminary experiments established that this incubation time and dilution resulted in maximal antibody binding (data not shown). Following incubation the bacteria were washed once with 0.5 ml of 1× PBS, resuspended in 100 μl of goat anti-mouse IgG/IgM–fluorescein isothiocyanate (FITC)-labeled conjugate (Caltag Laboratories), and incubated at 37°C for 30 min with constant rotation. Bacteria were washed, resuspended in 500 μl of 1× PBS, transferred to 5-ml tubes, and assayed for antibody binding by flow cytometry. Ten thousand bacterial events were gated in the forward-scatter versus side-scatter plot, discriminating them from "debris," and antibody-bound-bacterium events were assessed in the FL-1 channel and reported as percent positives or geometric mean fluorescence (GMF). Binding in the presence of the FITC-labeled conjugate alone served as the nonspecific binding control. An autofluorescence control consisted of bacteria incubated in the absence of antibody.

Colony lift immunoassays. Numbered grids were marked on the back of LB plates. Bacterial strains were assigned a number, streaked onto the designated grid, and incubated overnight at 37°C. The next day a nitrocellulose transfer membrane that was marked for orientation was placed onto the colonies, incubated at 4°C for 15 min, and then carefully removed and dried at 37°C for 1 h. The membrane was washed with Tris-buffered saline (10 mM Tris, 150 mM NaCl, pH 7.4; TBS) to remove excess bacteria, blocked while being shaken with 3% nonfat milk in TBS for 1 h at room temperature, washed again with TBS, and then incubated overnight while being shaken at 4°C with MAb 13D6 (undiluted culture supernatants). After overnight incubation, the membrane was washed with TBS and incubated for 1 h at room temperature with a 1/3,000 dilution of peroxidase-labeled goat anti-mouse IgM (μ) antibody (KPL). Subsequently the membrane was washed with TBS and developed with 4-chloro-1-naphthol (Sigma) in methanol-TBS-H_2O_2 until the desired color development. Reactions were stopped with distilled water.

PMN-mediated bactericidal assay. A neutrophil (PMN)-mediated bactericidal assay was performed essentially as described previously (43). For these studies MAb 13D6 (specific for the K1 capsule) or MAb3F7 (IgM isotype control specific for the *Moraxella catarrhalis* serotype B lipooligosaccharide [LOS] [44]) was used. In brief, 1.0×10^6 CFU of AB307-0294 (K1 capsule positive), AB307.30 (homologous capsule negative), AB797 (heterologous K1 negative), AB693 (heterologous K1 capsule positive), AB715 (heterologous K1 capsule positive), and AB803 (heterologous K1 capsule positive) were either (i) preopsonized for 50 min at 37°C in 90 μl of 1× PBS (pH 7.4) plus 10 μl of MAb (final 1:10 dilution; previously heated at 56°C for 30 min to inactivate complement [Δ56°C]) or (ii) incubated for 50 min at 37°C with 100 μl of 1× PBS in the absence of MAb. After incubation, bacteria were brought to a volume of 5 ml by adding 20% Δ56°C plasma–1× PBS (pH 7.4) (plasma-PBS), resulting in an estimated 2×10^5 CFU/ml of AB307-0294 (quantified by a subsequent titer). Five hundred microliters of opsonized or nonopsonized AB307-0294 was added to each well of a tissue culture plate (Costar 3472-clear; Corning Inc., Corning, NY) that contained either 5×10^5 human PMNs purified via a Ficoll-Hypaque gradient (Amersham) (45) in 500 μl of plasma-PBS (PMNs were allowed to adhere at room temperature for 30 min) or 500 μl of plasma-PBS alone. To expedite contact between bacteria and neutrophils, the tissue culture plate was spun at 218 × *g* for 10 min and placed at 37°C in a CO_2 incubator. After 60 min, 20 μl of saponin (from a 25-mg/ml stock solution in H_2O) was added to each well and the titer of AB307-0294 was determined. Bacterial titers were calculated as the initial log CFU minus the log CFU after 1 h of incubation at 37°C for the following conditions: (i) no antibody/PMN negative, (ii) no antibody/PMN positive, (iii) antibody/PMN negative, and (iv) antibody/PMN positive. The metric of interest for this assay was the difference between bacterial titers in the presence of PMN with or without MAb (condition ii versus iv), which reflects the effect of opsonization.

Rat soft tissue infection model. An established rat (Long-Evans) soft tissue infection model was employed as previously reported (34). The rat soft tissue infection model studies were reviewed and approved by the University at Buffalo and Veterans Administration Institutional Animal Care Committee. In brief, a subcutaneous pouch was created through the injection of 30 ml of air into the back of anesthetized male Long-Evans rats (175 to 200 g), followed by the injection of 1 ml of 1% croton oil in a filter-sterilized vegetable oil vehicle. The space is allowed to mature into an encapsulated, fluid-filled (8- to 12-ml) "pouch" over 6 to 8 days. AB307-0294 and AB979 were injected into the pouch to achieve starting titers of approximately 1×10^5 and 1×10^3 CFU/ml, respectively. In this manner, due to various *in vivo* growth characteristics, the bacterial titers in the pouch would be similar at the time of initial treatment with the K1 capsule-specific MAb 13D6. Pouch fluid was removed to enumerate bacterial counts at 1 min, 3 h, 6 h, 24 h, and 48 h postinoculation. For passive immunization studies, animals were treated via injection into the pouch with 2.35 mg of the K1 capsule-specific MAb 13D6 or a 1× PBS control at 3 and 24 h after bacterial challenge.

Statistical analyses. Continuous data were assessed for normality and presented as means ± standard errors of the means (SEM). *P* values of $0.05/n$ (n = the number of comparisons) are considered statistically significant based on the Bonferroni correction for multiple comparisons. A statistical trend was defined as a *P* value $<0.1/n$ but $>0.05/n$. *In vivo* activity of MAb 13D6 was defined as a difference in the survival and growth of the test strain in animals treated with MAb 13D6 compared to those in animals treated with buffer alone. To normalize *in vitro* and *in vivo* data, $\log_{10}$-transformed values were utilized, the area under each curve was calculated, and these areas were compared using two-tailed unpaired *t* tests (Prism 4 for MacIntosh; GraphPad Software Inc.).

RESULTS

The structure of the K1 capsule. CE-ES-MS and NMR spectroscopy structural analyses indicated that a high-molecular-weight polysaccharide polymer, consistent with capsular polysaccharide, could be identified from the AB307-0294, but not the AB307.30, polysaccharide preparations. Structural elucidations were performed on the purified high-molecular-weight polymer isolated following anion-exchange chromatography. Mass spectrometric analysis suggested that the polymer was made up of a trisaccharide repeat unit with residues of masses of 203, 217, and 228 Da. There was also evidence of an alternate trisaccharide made up of residues with masses of 203, 217, and 272 Da (Fig. 1). NMR analysis confirmed and extended this observation, revealing that the polymer was identical to that identified previously from *A. baumannii* strain 24 (46), with a trisaccharide repeat unit consisting of three residues, all in pyranose form: α-galactosaminuronic acid (A), α-*N*-acetylglucosamine (B), and 2,4-diamino-2,4,6-trideoxy-glucose (bacillosamine; C). The capsule structure is as follows: -[3-β-D-QuiNAc4NR-1-4-α-GlcNAc6OAc-1-4-α-D-GalNAcA-1-]$_n$-, where residue A is 4-α-D-GalNAcA-1, residue B is 4-α-GlcNAc6OAc-1, and residue C is 3-β-D-QuiNAc4NR-1. The O-acetylation on residue B is present in approximately 70% of the repeat units, and for residue C the amino group at the 4 position is modified such that R is either an acetyl or a 3-OH-butyrate group in an approximately 1:1 ratio. These data also demonstrate that the K1 capsule is distinct from the AB307-0294 lipopolysaccharide (47) and the extracellular polysaccharide poly-β-(1-6)-*N*-acetylglucosamine (48).

The K1 capsule is not predicted to be cross-reactive to human epitopes. The *A. baumannii* capsule might induce antibodies that are reactive to human epitopes, which would be a risk factor for the development of autoimmune disease. Importantly, structural data (see above; Fig. 1) did not identify any known cross-reactive epitopes, such as sialic acid. The K1 capsule does contain bacillosamine, a rare amino sugar, which is not present in humans (49).

The K1 capsule is immunogenic. A mandatory trait for a vaccine candidate is immunogenicity. Although the overwhelming majority of capsular serotypes are very immunogenic, some are poor immunogens (e.g., the polysialic acid K1 capsule from extraintestinal pathogenic *Escherichia coli*) (50, 51). Therefore, the immunogenicity of the *A. baumannii* K1 capsule was assessed by intramuscular injection of CD1 mice with purified capsule or with 1× PBS without adjuvant at 0, 2, and 4 weeks to generate anti-K1 immune or nonimmune antisera, respectively. Antisera, obtained at 5 weeks after the initial immunization, were used to assess the immune response against capsule by flow cytometry. These data clearly established that the K1 capsule was immunogenic (Table 1 and Fig. 2; both generated from the same data set). This was dem-

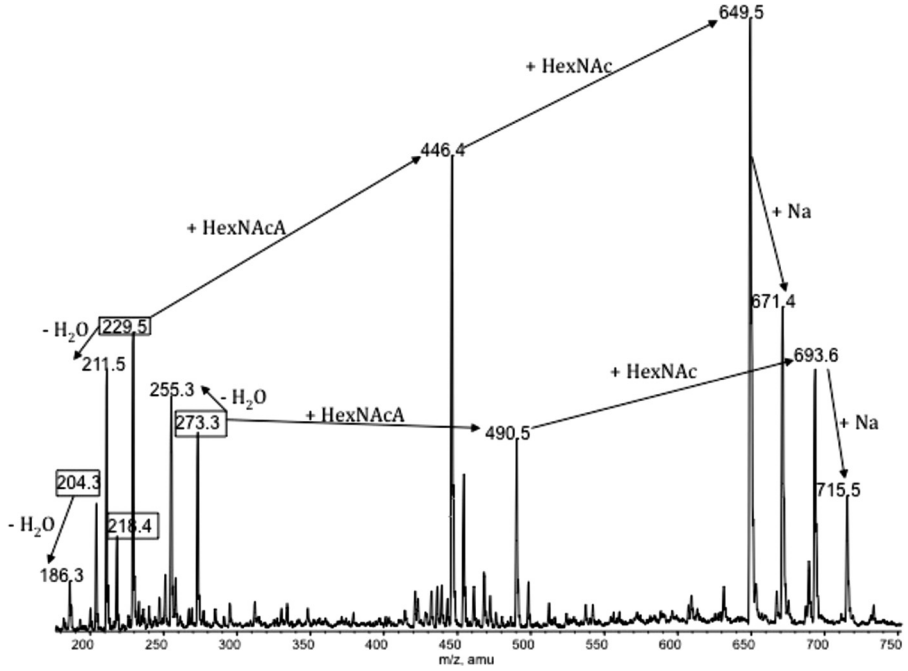

FIG 1 Positive-ion CE-ES-MS of purified capsular polysaccharide from AB307-0294. Boxed ions refer to $HexNAc^+$ (204 Da), $HexNAcA^+$ (218 Da), 6-dHexNAc4NAc$^+$ (229 Da), and 6-dHexNAc4NBu$^+$ (273 Da). Addition of HexNAc and HexNAcA to these residues is indicated with arrows, as are anhydro glycoforms ($-H_2O$) and sodiated glycoforms ($+Na$).

onstrated by the significant increase in reactivity observed with the anti-K1 immune serum against AB307-0294 (K1 capsule positive) compared to that observed with AB307.30 (K1 capsule negative) ($P < 0.05$).

Thirteen percent of *A. baumannii* strains studied possess the K1 serotype. Colony lift immunoasays were used to assess the seroprevalence of the K1 serotype in a collection of 100 *A. baumannii* strains. The ST, geographic origin, and site of isolation for all stains, when known, are listed in Table S1 in the supplemental material. The overall seroprevalence of K1-positive strains was 13%. The sites of isolation for the K1-positive strains were blood ($n = 6$), axilla ($n = 2$), wounds ($n = 1$), urine ($n = 1$), environment ($n = 1$), and unknown ($n = 2$). The known STs for the K1-positive strains were ST14 ($n = 6$), ST15 ($n = 1$), and ST16 ($n = 1$). All ST14 strains were K1 positive, but the collection contained 3 ST15 strains and one ST16 strain that were K1 negative.

TABLE 1 Binding of anti-K1 immune and nonimmune polyclonal mouse antisera to AB307-0294 (K1 capsule positive) and AB307.30 (K1 capsule negative) as assessed by flow cytometry

Parameter	Value[a] for:	
	AB307-0294	AB307.30
% bacterial cells bound with:		
Nonimmune antisera	2.2 ± 0.2	1.2 ± 0.1
Anti-K1 immune antisera	84.9 ± 1.9*	6.3 ± 0.4
Geometric mean fluorescence of cells bound with:		
Nonimmune antisera	2.8 ± 0.02	5.8 ± 0.2
Anti-K1 immune antisera	137.3 ± 12*	8.6 ± 0.2

[a] *, $P < 0.05$ (*t* test) for AB307-0294 compared to AB307.30. Values are means ± SEM for $n = 3$ or 4.

MAb 13D6 increases neutrophil-mediated bactericidal activity *in vitro*. An *in vitro* neutrophil opsonophagocytosis assay was performed to assess whether opsonization of K1-positive strains with MAb 13D6 increased bactericidal activity. The bactericidal activity of interest was reflected by the initial log CFU minus the log CFU after 1 h of incubation at 37°C in the presence of human PMNs with and without opsonization.

Opsonization with MAb 13D6 significantly increased bactericidal activity against the K1-positive strains AB307-0294, AB693, and AB803 ($P < 0.05$), and there was a trend for AB715 ($P = 0.0596$) compared to nonopsonized bacteria (Fig. 3A and D to F). By contrast, opsonization with MAb 13D6 did not significantly increase bactericidal activity against the K1-negative strains AB307.30 and AB797 compared to nonopsonized bacteria (Fig. 3B and C). Opsonization with MAb3F7, an isotype control, did not significantly increase bactericidal activity against any of the strains (data not shown). Taken together, these data demonstrate that the increased neutrophil-mediated bactericidal activity against K1-positive strains observed in the presence of MAb 13D6 is a specific effect and support the potential therapeutic utility of antibodies directed against the K1 capsule for K1-positive strains.

Passive immunization with MAb 13D6 increases clearance of the K1-positive strain AB307-0294. To test the hypothesis that passive immunization could be used therapeutically for infections due to *A. baumannii*, an established rat soft tissue infection model was used (34). This model is clinically relevant since *A. baumannii* has been recognized as a cause of a variety of soft tissue infections (6, 7). In this model a subcutaneous encapsulated, fluid-filled "pouch" was created, from which multiple fluid samplings after bacterial challenge were obtained in order to enumerate CFU. AB307-0294 (K1 positive) and AB979 (K1 negative) were injected into the pouch so that, when treatment with MAb 13D6 occurred

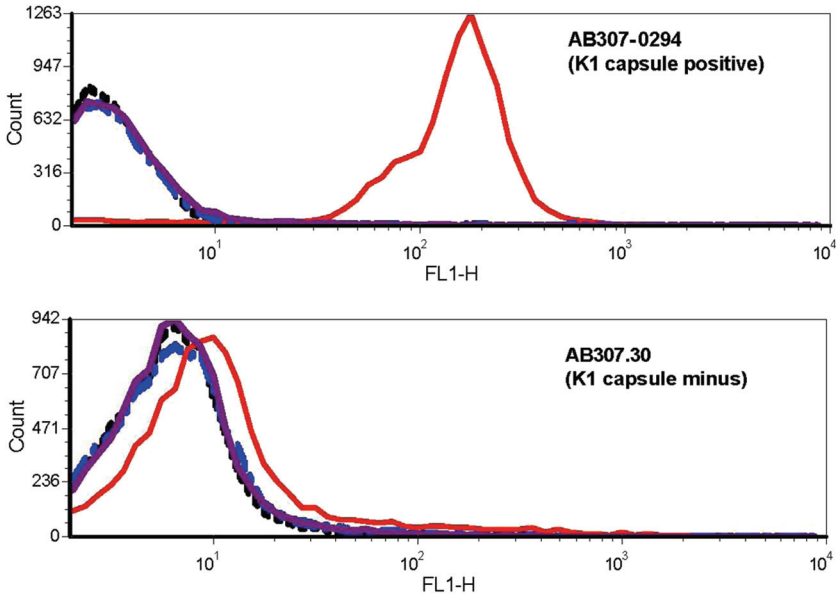

FIG 2 The K1 capsule present on AB307-0294 is immunogenic. Binding of preimmune, nonimmune, and anti-K1 immune polyclonal mouse antisera to AB307-0294 (wild type; K1 capsule positive) and AB307.30 (K1 capsule minus) was detected by goat anti-mouse IgG/IgM–fluorescein isothiocyanate (FITC)-labeled conjugate. Preimmune serum was obtained from animals prior to immunization (negative control). Nonimmune antiserum was generated by immunizing CD1 mice with 1× PBS alone (negative control). Anti-K1 immune antiserum was generated by immunizing mice with extracted K1 capsule from AB307-0294, followed by subsequent absorption against the capsule-negative derivative AB307.30. Representative curves are shown. Preimmune antiserum, black dashed lines; nonimmune antiserum, solid purple lines; anti-K1 immune antiserum, solid red lines; FITC-labeled conjugate alone (nonspecific binding control), blue dashed lines. An autofluorescence control (antibody not added) was also performed, and the curves were similar to the other negative controls (data not shown).

3 h after bacterial challenge, their titers would be similar. A second treatment with MAb 13D6 was given at 24 h (Fig. 4, arrows). Treatment with MAb 13D6 significantly decreased the growth/survival of AB307-0294 compared to treatment with 1× PBS ($P < 0.05$) (Fig. 4A). By contrast, AB979 was unaffected by treatment with MAb 13D6 (Fig. 4B). These data support the concept that treatment of infection due to *A. baumannii* with antibodies directed against capsular polysaccharide has therapeutic potential.

DISCUSSION

Given the paucity of new antimicrobial agents active against GNB in the pharmaceutical pipeline (19, 20), consideration of passive immunization as a treatment modality is warranted. In this report, we tested the hypothesis that antibodies directed against a capsular polysaccharide of *A. baumannii* have therapeutic potential via passive immunization. Previous work established that the K1 capsular polysaccharide from the *A. baumannii* strain AB307-0294 is surface exposed and is a virulence factor (31). Data reported here extend these observations. The K1 capsule is immunogenic (Table 1 and Fig. 2). Opsonization of the K1-positive strain AB307-0294 with MAb 13D6, which is directed against the K1 capsule, increases neutrophil-mediated bactericidal activity *in vitro* (Fig. 3). Lastly, treatment after the initiation of infection with MAb 13D6 increases bacterial clearance in an *in vivo* soft tissue infection model (Fig. 4). While previous studies have shown that bacterial capsules can be effective immunogens, this is the first set of data to our knowledge that supports the potential use of the capsular polysaccharide as a target for antibody-mediated therapeutics in *A. baumannii*. Additional targets which may also be useful include OmpA (23) and the noncapsular bacterial surface polysaccharide poly-β-(1-6)-*N*-acetylglucosamine (52).

Active or passive immunization raises the concern for an autoimmune response. Selected lipooligosaccharide (LOS) serotypes of *Campylobacter jejuni* that contain *N*-acetylneuraminic acid (sialic acid) are mimics of human gangliosides and have been associated with development of Guillain-Barre and the Miller Fisher variant (53, 54). The *N. meningitidis* serogroup B capsule and the *E. coli* K1 capsule are polysialic acid capsules that are potential mimics of host tissue. The neisserial serogroup B capsule can induce antibodies that are cross-reactive with the embryonic but not adult neural cell adhesion molecules (55). Further, certain *Neisseria* and *Haemophilus* LOS structures mimic glycosphingolipids and gangliosides; however, evidence that antibodies directed against these structures cause autoimmune disease in humans is not compelling (56). The delineation of the K1 capsule did not identify any mimics, such as sialic acid, of concern for cross-reactivity to human epitopes (Fig. 1). Nonetheless, formal testing would be required to support the speculation that this immunogen could be safely used in humans.

A potential limitation for the use of capsule as a target for passive or active immunization would be the existence of a large number of clinically relevant serotypes. For example, more than 80 capsular serotypes exist for *E. coli* strains (57, 58). It is not known how many capsular serotypes exist for *A. baumannii*. However, the initial seroprevalence data on K1 (13% of the strains studied) are encouraging. We appreciate that a greater and more geographically diverse number of clinical isolates require serotyping to more definitively define K1 seroprevalence. However, since K1-positive strains comprised 13% of the *A. baumannii* strains tested, this suggests that the number of capsular serotypes in *A. baumannii* may not be overwhelming. From an active-vaccination

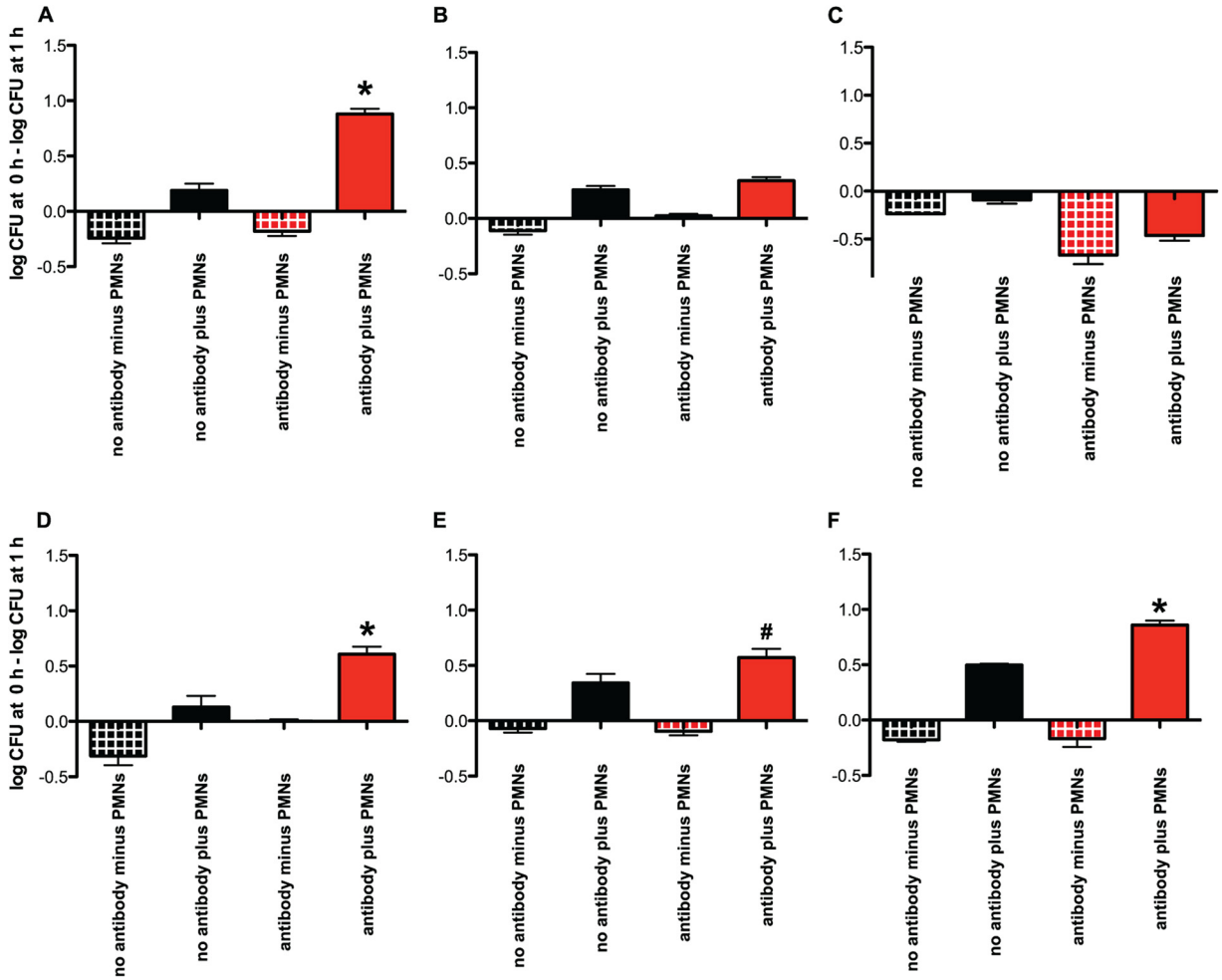

FIG 3 Opsonization with MAb 13D6 significantly increases neutrophil (PMN)-mediated bactericidal activity *in vitro* against K1-positive, but not K1-negative strains. Neutrophil-mediated bactericidal activity against opsonized (with MAb 13D6) and nonopsonized *A. baumannii* strains in the presence or absence of PMN is shown. The opsonophagocytosis assay was performed as described in Materials and Methods. (A) AB307-0294 (homologous K1 positive); (B) AB307.30 (homologous K1 negative); (C) AB797 (heterologous K1 negative); (D) AB693 (heterologous K1 positive); (E) AB715 (heterologous K1 positive); (F) AB803 (heterologous K1 positive). $n = 3$ to 6. *, $P < 0.05$; #, $P < 0.1$ but > 0.05 (two-tailed unpaired t test).

perspective, identification of 10 to 20 clinically important capsular serotypes would be encouraging since 13-valent conjugated and 23-valent nonconjugated capsular polysaccharide vaccines are already in clinical use for prevention of *S. pneumoniae* infections.

The use of anticapsular antisera as a treatment modality (passive immunization) presents a greater number of challenges. First, it would likely only be considered in the setting of defined infections caused by extremely resistant or panresistant *A. baumannii*.

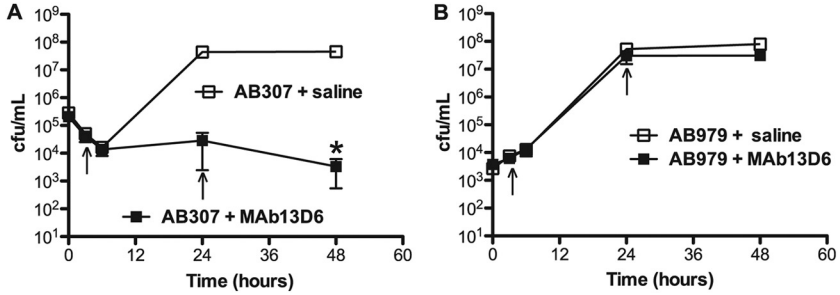

FIG 4 Passive immunization with MAb 13D6 significantly increases the *in vivo* clearance of AB307-0294 (K1 positive) but not AB979 (K1 negative). Growth/survival of *A. baumannii* strains AB307-0294 (A) and AB979 (B) in the rat soft tissue infection model with or without treatment with MAb 13D6 is shown. Details are in Materials and Methods. At 3 and 24 h after bacterial challenge the infected pouches were treated with the K1 capsule-specific MAb 13D6 or 1× PBS (arrows). AB307-0294 and AB979 were injected into the pouch to achieve bacterial titers that would be similar at the time of initial treatment with MAb 13D6. Data are means ± SEM ($n = 8$ for AB307-0294 and $n = 4$ for AB979). *, $P < 0.05$ for AB307-0294 treated with MAb 13D6 compared to AB307-0294 treated with 1× PBS.

Further, the commercial development of multiple capsule serotype-specific antisera would be needed. Another limitation would be the need for laboratory identification of the serotype, but this could be easily accomplished via a rapid immunologic or PCR-based approach. Serotype-specific capsular antisera for passive immunization would likely be optimal due to both cost and potential efficacy (concentration related) considerations. However, despite these potential challenges, unless new classes of antimicrobials active against extremely resistant or panresistant *A. baumannii* are developed, this alternative approach warrants consideration.

We demonstrated that MAb 13D6, which is directed against the K1 capsule, increased neutrophil-mediated bactericidal activity *in vitro* and could be used to increase the clearance of the K1-positive strain AB307-0294 in a soft tissue infection model. The lack of an effect of MAb 13D6 on the *in vivo* growth and/or survival of AB979, which has a non-K1 capsule, established specificity. It might seem logical to have used the isogenic K1-negative derivative AB307.30 instead of AB979 for these studies. Unfortunately this was not possible because AB307.30 is readily cleared in this infection model, likely due to an increased sensitivity to complement-mediated bactericidal activity (31). The goal of this set of studies was to establish capsule as a potential therapeutic target via passive immunization. We appreciate that MAb 13D6 may not optimize clearance of K1 *A. baumannii* strains. The development of alternative antibodies with enhanced affinity and/or an alternative isotype would likely confer an even greater degree of efficacy. We also appreciate that the efficacy of passive immunization as a treatment modality needs to be assessed in other infection models. However, the fact that we were able to achieve a 4-log decrease in bacterial CFU compared to no treatment in a model of closed-space infections, which are notoriously difficult to cure in the absence of drainage, is encouraging and establishes proof of principle. A strength of this study was that animals were treated with MAb 13D6 after infection was established. Pretreatment or simultaneous treatment at the time of bacterial challenge is a far less rigorous approach for establishing efficacy and is clinically less relevant. Further, the use of passive immunization to prevent *A. baumannii* infection would be impractical.

In summary, data are presented that support the proof of principle that the *A. baumannii* K1 capsular polysaccharide is a viable therapeutic target via passive immunization. Future studies will need to establish the number and prevalence of non-K1 capsular polysaccharides from *A. baumannii* and determine whether these serotypes are also amenable to an antibody-based therapeutic intervention.

ACKNOWLEDGMENTS

This work was supported in part by a VA Merit Review from the Department of Veterans Affairs (T.A.R.), by a Telemedicine and Advance Technical Research Center Cooperative Agreement W23RYX1055N607 (T.A.R.), and by National Institutes of Health grants 1R21AI088318-01A1 (T.A.R.) and 1R21 AI101426-01 (A.A.C.).

The funders had no role in study design, data collection and analysis, decision to publish, or preparation of the manuscript.

We thank Jacek Stupak for mass spectrometry and Bruce Davidson for assistance in analyzing flow cytometry data.

REFERENCES

1. **Perez F, Endimiani A, Bonomo RA.** 2008. Why are we afraid of Acinetobacter baumannii? Expert Rev. Anti Infect. Ther. **6**:269–271.
2. **Perez F, Hujer AM, Hujer KM, Decker BK, Rather PN, Bonomo RA.** 2007.Global challenge of multidrug-resistant Acinetobacter baumannii. Antimicrob. Agents Chemother. **51**:3471–3484.
3. **Fournier PE, Richet H.** 2006.The epidemiology and control of Acinetobacter baumannii in health care facilities. Clin. Infect. Dis. **42**:692–699.
4. **van Dessel H, Kamp-Hopmans TE, Fluit AC, Brisse S, de Smet AM, Dijkshoorn L, Troelstra A, Verhoef J, Mascini EM.** 2002. Outbreak of a susceptible strain of Acinetobacter species 13 (sensu Tjernberg and Ursing) in an adult neurosurgical intensive care unit. J. Hosp. Infect. **51**:89–95.
5. **Richet H, Fournier PE.** 2006. Nosocomial infections caused by Acinetobacter baumannii: a major threat worldwide. Infect. Control Hosp. Epidemiol. **27**:645–646.
6. **Falagas ME, Karveli EA.** 2007. The changing global epidemiology of Acinetobacter baumannii infections: a development with major public health implications. Clin. Microbiol. Infect. **13**:117–119.
7. **Peleg AY, Seifert H, Paterson DL.** 2008. Acinetobacter baumannii: emergence of a successful pathogen. Clin. Microbiol. Rev. **21**:538–582.
8. **Anstey NM, Currie BJ, Hassell M, Palmer D, Dwyer B, Seifert H.** 2002. Community-acquired bacteremic Acinetobacter pneumonia in tropical Australia is caused by diverse strains of Acinetobacter baumannii, with carriage in the throat in at-risk groups. J. Clin. Microbiol. **40**:685–686.
9. **Anstey NM, Currie BJ, Withnall KM.** 1992. Community-acquired Acinetobacter pneumonia in the Northern Territory of Australia. Clin. Infect. Dis. **14**:83–91.
10. **Chen MZ, Hsueh PR, Lee LN, Yu CJ, Yang PC, Luh KT.** 2001. Severe community-acquired pneumonia due to Acinetobacter baumannii. Chest **120**:1072–1077.
11. **Garzoni C, Emonet S, Legout L, Benedict R, Hoffmeyer P, Bernard L, Garbino J.** 2005. Atypical infections in tsunami survivors. Emerg. Infect. Dis. **11**:1591–1593.
12. **Maegele M, Gregor S, Steinhausen E, Bouillon B, Heiss MM, Perbix W, Wappler F, Rixen D, Geisen J, Berger-Schreck B, Schwarz R.** 2005. The long-distance tertiary air transfer and care of tsunami victims: injury pattern and microbiological and psychological aspects. Crit. Care Med. **33**:1136–1140.
13. **Gaynes R, Edwards JR.** 2005. Overview of nosocomial infections caused by gram-negative bacilli. Clin. Infect. Dis. **41**:848–854.
14. **Roca I, Espinal P, Vila-Farres X, Vila J.** 2012. The Acinetobacter baumannii oxymoron: commensal hospital dweller turned pan-drug-resistant menace. Front. Microbiol. **3**:148.
15. **Fishbain J, Peleg AY.** 2010. Treatment of Acinetobacter infections. Clin. Infect. Dis. **51**:79–84.
16. **Magiorakos AP, Srinivasan A, Carey RB, Carmeli Y, Falagas ME, Giske CG, Harbarth S, Hindler JF, Kahlmeter G, Olsson-Liljequist B, Paterson DL, Rice LB, Stelling J, Struelens MJ, Vatopoulos A, Weber JT, Monnet DL.** 2012. Multidrug-resistant, extensively drug-resistant and pandrug-resistant bacteria: an international expert proposal for interim standard definitions for acquired resistance. Clin. Microbiol. Infect. **18**:268–281.
17. **Howard A, O'Donoghue M, Feeney A, Sleator RD.** 2012. Acinetobacter baumannii: an emerging opportunistic pathogen. Virulence. **3**:243–250.
18. **Boucher HW, Talbot GH, Bradley JS, Edwards JE, Gilbert D, Rice LB, Scheld M, Spellberg B, Bartlett J.** 2009. Bad bugs, no drugs: no ESKAPE! An update from the Infectious Diseases Society of America. Clin. Infect. Dis. **48**:1–12.
19. **Boucher, H., Gilbert D, Benjamin D, Bradley J., Murray B, Spellberg B, Talbot G.** 2011. 10 x '20 progress: development of new drugs active against resistant Gram-negative bacilli, abstr. LB-27. Abstr. 49th Annu. Meet. Infect. Dis. Soc. Am., Boston, MA.
20. **Butler MS, Cooper MA.** 2011. Antibiotics in the clinical pipeline in 2011. J. Antibiot. **64**:413–425.
21. **Hsu JL, Safdar N.** 2011. Polyclonal immunoglobulins and hyperimmune globulins in prevention and management of infectious diseases. Infect. Dis. Clin. North Am. **25**:773–788.
22. **Both L, Banyard AC, van Dolleweerd C, Horton DL, Ma JK, Fooks AR.** 2012. Passive immunity in the prevention of rabies. Lancet Infect. Dis. **12**:397–407.
23. **Luo G, Lin L, Ibrahim AS, Baquir B, Pantapalangkoor P, Bonomo RA, Doi Y, Adams MD, Russo TA, Spellberg B.** 2012. Active and passive immunization protects against lethal, extreme drug resistant-Acinetobacter baumannii infection. PLoS One **7**:e29446. doi:10.1371/journal.pone.0029446.

24. **Fedson DS, Nicolas-Spony L, Klemets P, van der Linden M, Marques A, Salleras L, Samson SI.** 2011. Pneumococcal polysaccharide vaccination for adults: new perspectives for Europe. Expert Rev. Vaccines **10**:1143–1167.
25. **O'Loughlin RE, Edmond K, Mangtani P, Cohen AL, Shetty S, Hajjeh R, Mulholland K.** 2010. Methodology and measurement of the effectiveness of Haemophilus influenzae type b vaccine: systematic review. Vaccine **28**:6128–6136.
26. **Safadi MA, McIntosh ED.** 2011. Epidemiology and prevention of meningococcal disease: a critical appraisal of vaccine policies. Expert Rev. Vaccines **10**:1717–1730.
27. **Bryant KA, Marshall GS.** 2011. Haemophilus influenzae type b-Neisseria meningitidis serogroups C and Y tetanus toxoid conjugate vaccine for infants and toddlers. Expert Rev. Vaccines **10**:941–950.
28. **Engels EA, Lau J.** 2000. Vaccines for preventing typhoid fever. Cochrane Database Syst. Rev. CD001261. doi:10.1002/14651858.CD001261.
29. **Avci FY, Kasper DL.** 2010. How bacterial carbohydrates influence the adaptive immune system. Annu. Rev. Immunol. **28**:107–130.
30. **Blanchard-Rohner G, Pollard AJ.** 2011. Long-term protection after immunization with protein-polysaccharide conjugate vaccines in infancy. Expert Rev. Vaccines **10**:673–684.
31. **Russo TA, Luke NR, Beanan JM, Olson R, Sauberan SL, MacDonald U, Schultz LW, Umland TC, Campagnari AA.** 2010. The K1 capsular polysaccharide of Acinetobacter baumannii strain 307-0294 is a major virulence factor. Infect. Immun. **78**:3993–4000.
32. **Ecker JA, Massire C, Hall TA, Ranken R, Pennella TT, Agasino Ivy C, Blyn LB, Hofstadler SA, Endy TP, Scott PT, Lindler L, Hamilton T, Gaddy C, Snow K, Pe M, Fishbain J, Craft D, Deye G, Riddell S, Milstrey E, Petruccelli B, Brisse S, Harpin V, Schink A, Ecker DJ, Sampath R, Eshoo MW.** 2006. Identification of Acinetobacter species and genotyping of Acinetobacter baumannii by multilocus PCR and mass spectrometry. J. Clin. Microbiol. **44**:2921–2932.
33. **Russo TA, MacDonald U, Beanan JM, Olson R, MacDonald IJ, Sauberan SL, Luke NR, Schultz LW, Umland TC.** 2009. Penicillin-binding protein 7/8 contributes to the survival of Acinetobacter baumannii in vitro and in vivo. J. Infect. Dis. **199**:513–521.
34. **Russo TA, Beanan JM, Olson R, MacDonald U, Luke NR, Gill SR, Campagnari AA.** 2008. Rat pneumonia and soft-tissue infection models for the study of Acinetobacter baumannii biology. Infect. Immun. **76**:3577–3586.
35. **Westphal O, Jann K.** 1965. Bacterial lipopolysaccharide. Methods Carbohydr. Chem. **5**:88–91.
36. **Vinogradov EV, Van Der Drift K, Thomas-Oates JE, Meshkov S, Brade H, Holst O.** 1999. The structures of the carbohydrate backbones of the lipopolysaccharides from Escherichia coli rough mutants F470 (R1 core type) and F576 (R2 core type). Eur. J. Biochem. **261**:629–639.
37. **St Michael F, Li J, Vinogradov E, Larocque S, Harper M, Cox AD.** 2005. Structural analysis of the lipopolysaccharide of Pasteurella multocida strain VP161: identification of both Kdo-P and Kdo-Kdo species in the lipopolysaccharide. Carbohydr. Res. **340**:59–68.
38. **Campagnari AA, Ducey TF, Rebmann CA.** 1996. Outer membrane protein B1, an iron-repressible protein conserved in the outer membrane of Moraxella (Branhamella) catarrhalis, binds human transferrin. Infect. Immun. **64**:3920–3924.
39. **Loehfelm TW, Luke NR, Campagnari AA.** 2008. Identification and characterization of an Acinetobacter baumannii biofilm-associated protein. J. Bacteriol. **190**:1036–1044.
40. **Haase EM, Campagnari AA, Sarwar J, Shero M, Wirth M, Cumming CU, Murphy TF.** 1991. Strain-specific and immunodominant surface epitopes of the P2 porin protein of nontypeable Haemophilus influenzae. Infect. Immun. **59**:1278–1284.
41. **Russo T, Guenther J, Wenderoth S, Frank M.** 1993. Generation of isogenic K54 capsule-deficient *Escherichia coli* strains through Tn*phoA*-mediated gene disruption. Mol. Microbiol. **9**:357–364.
42. **Russo TA, Beanan JM, Olson R, Genagon SA, Macdonald U, Cope JJ, Davidson BA, Johnston B, Johnson JR.** 2007. A killed, genetically engineered derivative of a wild-type extraintestinal pathogenic E. coli strain is a vaccine candidate. Vaccine **25**:3859–3870.
43. **Russo TA, Beanan JM, Olson R, Macdonald U, Cope JJ.** 2009. Capsular polysaccharide and the O-specific antigen impede antibody binding: a potential obstacle for the successful development of an extraintestinal pathogenic Escherichia coli vaccine. Vaccine **27**:388–395.
44. **Edwards KJ, Allen S, Gibson BW, Campagnari AA.** 2005. Characterization of a cluster of three glycosyltransferase enzymes essential for Moraxella catarrhalis lipooligosaccharide assembly. J. Bacteriol. **187**:2939–2947.
45. **Russo, TA, Davidson BA,, Genagon SA, Warholic NM, Macdonald U, Pawlicki PD, Beanan JM, Olson R, Holm BA, Knight PR, III.** 2005. E. coli virulence factor hemolysin induces neutrophil apoptosis and necrosis/lysis in vitro and necrosis/lysis and lung injury in a rat pneumonia model. Am. J. Physiol. Lung Cell. Mol. Physiol. **289**:L207–L216.
46. **Vinogradov EV, Brade L, Brade H, Holst O.** 2003. Structural and serological characterisation of the O-antigenic polysaccharide of the lipopolysaccharide from Acinetobacter baumannii strain 24. Carbohydr. Res. **338**:2751–2756.
47. **Luke NR, Sauberan SL, Russo TA, Beanan JM, Olson R, Loehfelm TW, Cox AD, St. Michael F, Vinogradov EV, Campagnari AA.** 2010. Identification and characterization of a glycosyltransferase involved in Acinetobacter baumannii lipopolysaccharide core biosynthesis. Infect. Immun. **78**:2017–2023.
48. **Choi AH, Slamti L, Avci FY, Pier GB, Maira-Litran T.** 2009. The pgaABCD locus of Acinetobacter baumannii encodes the production of poly-beta-1-6-N-acetylglucosamine, which is critical for biofilm formation. J. Bacteriol. **191**:5953–5963.
49. **Sharon N.** 2007. Celebrating the golden anniversary of the discovery of bacillosamine, the diamino sugar of a bacillus. Glycobiology **17**:1150–1155.
50. **Wyle FA, Artenstein MS, Brandt BL, Tramont EC, Kasper DL, Altieri PL, Berman SL, Lowenthal JP.** 1972. Immunologic response of man to group B meningococcal polysaccharide vaccines. J. Infect. Dis. **126**:514–521.
51. **Finne J, Leinonen M, Makela PH.** 1983. Antigenic similarities between brain components and bacteria causing meningitis. Implications for vaccine development and pathogenesis. Lancet **ii**:355–357.
52. **Skurnik D, Davis MR, Jr, Benedetti D, Moravec KL, Cywes-Bentley C, Roux D, Traficante DC, Walsh RL, Maira-Litran T, Cassidy SK, Hermos CR, Martin TR, Thakkallapalli EL, Vargas SO, McAdam AJ, Lieberman TD, Kishony R, Lipuma JJ, Pier GB, Goldberg JB, Priebe GP.** 2012. Targeting pan-resistant bacteria with antibodies to a broadly conserved surface polysaccharide expressed during infection. J. Infect. Dis. **205**:1709–1718.
53. **Prendergast MM, Moran AP.** 2000. Lipopolysaccharides in the development of the Guillain-Barre syndrome and Miller Fisher syndrome forms of acute inflammatory peripheral neuropathies. J. Endotoxin Res. **6**:341–359.
54. **Yuki N, Hartung HP.** 2012. Guillain-Barre syndrome. N. Engl. J. Med. **366**:2294–2304.
55. **Moe GR, Tan S, Granoff DM.** 1999. Molecular mimetics of polysaccharide epitopes as vaccine candidates for prevention of Neisseria meningitidis serogroup B disease. FEMS Immunol. Med. Microbiol. **26**:209–226.
56. **Harvey HA, Swords WE, Apicella MA.** 2001. The mimicry of human glycolipids and glycosphingolipids by the lipooligosaccharides of pathogenic neisseria and haemophilus. J. Autoimmun. **16**:257–262.
57. **Jann B, Jann K.** 1990. Structure and biosynthesis of the capsular antigens of Escherichia coli. Curr. Top. Microbiol. Immunol. **150**:19–42.
58. **Orskov F, Orskov I, Jann B, Jann K.** 1977. Serology, chemistry, and genetics of O and K antigens of Escherichia coli. Bacteriol. Rev. **41**:667–710.

RESEARCH ARTICLE

In Vivo-Validated Essential Genes Identified in *Acinetobacter baumannii* by Using Human Ascites Overlap Poorly with Essential Genes Detected on Laboratory Media

Timothy C. Umland,[a,b] L. Wayne Schultz,[a,b] Ulrike MacDonald,[c,d,e] Janet M. Beanan,[c,d,e] Ruth Olson,[c,d,e] and Thomas A. Russo[c,d,e,f]

Hauptman-Woodward Medical Research Institute, Buffalo, New York, USA[a]; Departments of Structural Biology,[b] Medicine,[c] and Microbiology and Immunology[d] and the Witebsky Center for Microbial Pathogenesis,[e] University at Buffalo, State University of New York, Buffalo, New York, USA; and Veterans Administration Western New York Healthcare System, Buffalo, New York, USA[f]

ABSTRACT **A critical feature of a potential antimicrobial target is the characteristic of being essential for growth and survival during host infection. For bacteria, genome-wide essentiality screens are usually performed on rich laboratory media. This study addressed whether genes detected in that manner were optimal for the identification of antimicrobial targets since the *in vivo* milieu is fundamentally different. Mutant derivatives of a clinical isolate of *Acinetobacter baumannii* were screened for growth on human ascites, an *ex vivo* medium that reflects the infection environment. A subset of 34 mutants with unique gene disruptions that demonstrated little to no growth on ascites underwent evaluation in a rat subcutaneous abscess model, establishing 18 (53%) of these genes as *in vivo* essential. The putative gene products all had annotated biological functions, represented unrecognized or underexploited antimicrobial targets, and could be grouped into five functional categories: metabolic, two-component signaling systems, DNA/RNA synthesis and regulation, protein transport, and structural. These *A. baumannii in vivo* essential genes overlapped poorly with the sets of essential genes from other Gram-negative bacteria catalogued in the Database of Essential Genes (DEG), including those of *Acinetobacter baylyi*, a closely related species. However, this finding was not due to the absence of orthologs. None of the 18 *in vivo* essential genes identified in this study, or their putative gene products, were targets of FDA-approved drugs or drugs in the developmental pipeline, indicating that a significant portion of the available target space within pathogenic Gram-negative bacteria is currently neglected.**

IMPORTANCE **The human pathogen *Acinetobacter baumannii* is of increasing clinical importance, and a growing proportion of isolates are multiantimicrobial-resistant, pan-antimicrobial-resistant, or extremely resistant strains. This scenario is reflective of the general problem of a critical lack of antimicrobials effective against antimicrobial-resistant Gram-negative bacteria, such as *Pseudomonas aeruginosa*, *Klebsiella pneumoniae*, *Enterobacter* sp., and *Escherichia coli*. This study identified a set of *A. baumannii* genes that are essential for growth and survival during infection and demonstrated the importance of using clinically relevant media and *in vivo* validation while screening for essential genes for the purpose of developing new antimicrobials. Furthermore, it established that if a gene is absent from the Database of Essential Genes, it should not be excluded as a potential antimicrobial target. Lastly, a new set of high-value potential antimicrobial targets for pathogenic Gram-negative bacteria has been identified.**

Received 11 April 2012 **Accepted** 23 July 2012 **Published** 21 August 2012

Citation Umland TC, et al. 2012. *In vivo*-validated essential genes identified in *Acinetobacter baumannii* by using human ascites overlap poorly with essential genes detected on laboratory media. mBio 3(4):e00113-12. doi:10.1128/mBio.00113-12.

Editor George Drusano, University of Florida—Albany

Address correspondence to Timothy C. Umland, umland@hwi.buffalo.edu, or Thomas A. Russo, trusso@buffalo.edu.

The identification of bacterial essential genes (i.e., genes required for growth and/or survival) has been an important tool for dissecting biological pathways and functions, identifying evolutionary relationships, promoting synthetic biology, and predicting antimicrobial targets. An essential gene is often considered a member of the minimal gene set required for growth of a specific organism under optimal conditions (i.e., nutrient-rich media and absence of environmental stress) (1). This definition integrates with the practical consideration of using standard laboratory *in vitro* growth conditions. Despite this seemingly simple definition of "essential gene," in practice a number of experimental subtleties exist that may influence the identification of these genes (e.g., genetic variation across strains, random versus systematic mutagenesis protocols, growth condition differences, clonal versus mixed populations, and the working definition used to designate a gene as essential) (1–4). These complexities are exemplified by comparison of genome-wide essentiality screens conducted upon the same species using different methodologies. In the case of *Escherichia coli*, the Keio collection identified 303 essential genes (5), an earlier screen identified 620 essential genes (6), and Ecogene has reannotated the Keio collection as representing 289 essential genes by using more stringent criteria (7). Expanding the comparison across species to include additional Gram-negative bacteria (GNB) or more distantly related Gram-positive bacteria

(GPB) further emphasizes the disparity between experimentally determined bacterial essential gene sets. For example, a comparison of *Helicobacter pylori* essential genes to *E. coli*, *Haemophilus influenzae*, or *Mycobacterium tuberculosis* indicated that 55% were essential in at least one of these species, but only 11% were essential in all considered species (8).

Gene essentiality is increasingly being viewed as contextual, with decreased nutrient levels, changes in carbon sources, or environmental stress (e.g., change of temperature) altering the set of genes required for growth (1, 9–11). A recent study testing yeast deletion mutants against a multitude of small molecules and environmental stresses concluded that up to 97% of its genes contribute to wild-type growth in the presence of one or more chemicals or environmental conditions (12), compared to ~20% of its genes annotated as essential under optimal laboratory growth conditions. A similar chemical genetics approach in *E. coli* identified 116 genes, unique from those present in the Keio collection, that were essential in rich laboratory media when stressed by a 324-chemical screen (13). These studies underscore the fact that microorganisms infrequently encounter ideal growth conditions except in the lab, and so they have evolved to grow and survive in multiple changing environments. For example, a pathogenic bacterium encounters a very different environment during infection of a host (nutrient poor, host defenses) than during growth on lab media (nutrient rich).

Whole-genome essentiality screening requires considerable resources, and bacterial species selected for such screens are largely important model systems (e.g., *E. coli*) or human pathogens. The Database of Essential Genes (DEG; version 6.8) contains genome-scale essentiality data for 17 unique bacterial species obtained from 20 published screens (14). For the majority of bacterial species, experimental data establishing gene essentiality are sparse, and so an annotation of "essential" for most bacterial genes is a prediction based on homology to experimentally established essential genes. Given the modest overlap of experimentally determined whole-genome essentiality screens (pairwise bacterial species comparisons typically exhibit 50 to 70% overlap, which rapidly decreases as more species are compared [8, 15–17]), confidence levels for *in silico* essentiality predictions may vary widely and in many cases have not been quantified. Bioinformatic selection strategies for target-based antimicrobial discovery rely heavily upon essentiality annotations (18–20), and so an evaluation of the accuracy of essential and nonessential gene predictions is of practical importance.

Essential genes hold the promise of being potential new drug targets. We are at risk for entering a postantibiotic era, due to the evolution of multidrug, extreme drug, and pan-drug (MDR, XDR, PDR) resistance in GNB. Identification of new drug targets will lead to the development of new antimicrobials, which are urgently needed. *Acinetobacter baumannii* is the poster child for this emerging threat (21), with both the incidence of infections and those due to XDR and PDR strains increasing (22–29). Treatment of infections due to *Acinetobacter* has become challenging, and the need to identify new antimicrobial targets is more pressing than ever. Unfortunately, as of 2009 there were virtually no new antimicrobial agents active against GNB in the pharmaceutical pipeline (21). A 2011 update found several antimicrobials in development that had activity against GNB, but none have reached phase 3 trials (30, 31).

Given the urgent need for new classes of antimicrobial therapeutics effective against *A. baumannii* and MDR, XDR, or PDR GNB in general, we employed a previously utilized experimental approach (32) for the identification of unrecognized or underexploited antimicrobial targets. This approach has the potential to effectively promote the development of new small-molecule antimicrobial therapeutics through novel targets and thereby circumvent current resistance mechanisms (33). This strategy was designed to efficiently identify *A. baumannii* genes essential for growth and survival during infection in a rat subcutaneous abscess model (i.e., *in vivo* essential genes) but not essential *in vitro* on rich laboratory media (34, 35). Here, we report 18 verified *in vivo* essential genes that form a set of putative antimicrobial targets, representing a largely new set of antimicrobial targets based upon evaluation against two drug target databases. These *A. baumannii* genes were compared to bacterial genes annotated as essential in DEG, revealing that 89% could not be readily predicted as *in vivo* essential. Data are presented that support the concept that the genes identified and catalogued as essential in DEG need to be interpreted within the context of their method of identification. Our review of the literature revealed that most screens were conducted using rich laboratory media, and none were performed using a clinically relevant medium, demonstrating a limitation of the data currently in DEG. This highlights that the cataloguing of essential genes is incomplete, and that although labor and cost intensive, experimental establishment of *in vivo* essential genes within an appropriate environmental context is needed. An understanding of this limitation within DEG is critical since it is often used as part of the decision process assessing the validity of potential drug targets. Consideration of potential drug targets within a clinically relevant context has enabled antimicrobial target space to be expanded, as well as enabled the refinement of bioinformatic methods used to prioritize antimicrobial targets.

RESULTS

Identification of *A. baumannii* genes essential for growth in human ascites *ex vivo*. *A. baumannii* strain 307-0294 (AB307-0294) was randomly mutagenized using the transposon EZ-Tn*5*<kan-2>. Mutants (2,934 total) were isolated on Mueller-Hinton (MH) kanamycin plates and subsequently gridded onto ascites plates containing kanamycin (40 μg/ml). Mutant derivatives (224 total; 7.6%) of AB307-0294 were identified that displayed significantly decreased or absent growth on ascites plates. Chromosomal sequencing using primers from the ends of EZ-Tn*5*<kan-2> was performed on all 224 mutants, enabling the location of the transposon insertion sites to be identified. Analysis of these data revealed a set of 90 unique genes where the loss of function due to transposon-mediated gene disruption resulted in the phenotype of near wild-type growth on rich laboratory (MH) medium plates but decreased or absent growth on ascites plates. This phenotype is likely to be predictive of AB307-0294 genes dispensable for *in vitro* growth under optimal conditions (rich laboratory medium, which does not reflect the *in vivo* environment) but essential for growth and survival during systemic infection of the human host (i.e., essential *in vivo*), since human ascites is similar to the exudative inflammatory fluid environment that extracellular bacterial pathogens encounter during human infection. This simple concept is the strength of this approach, which has not generally been used in screens for essential genes. Based upon a bioinformatic filter, 34 of the 90 *A. baumannii* genes were selected, primarily

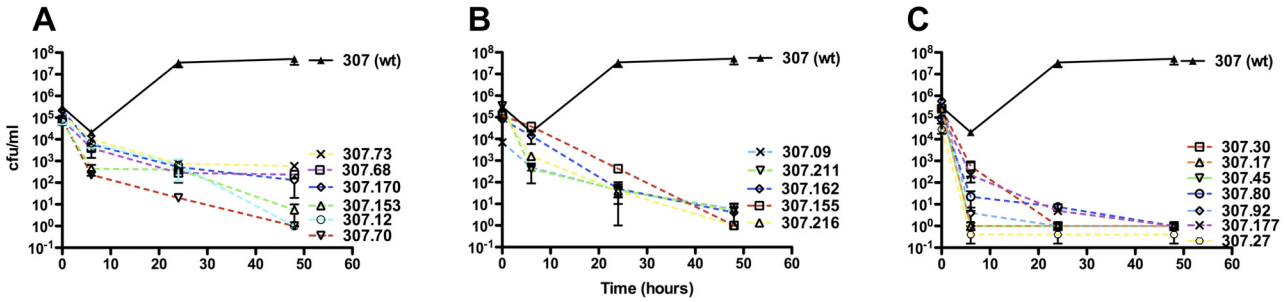

FIG 1 Growth/clearance of AB307-0294 wild type (wt) and mutant derivatives in the rat subcutaneous abscess infection model. (A) Comparison of wild type (AB307-0294) and mutants with disruptions in metabolic pathway and two-component signaling genes. AB307.12 (*carA*$^-$), AB307.68 (*aroA*$^-$), AB307.70 (*rstA*$^-$), AB307.73 (*aceE*$^-$), AB307.153 (*envZ*$^-$), AB307.170 (*aroC*$^-$). (B) Comparison of wild type and mutants with disruptions in DNA/RNA synthesis or regulation and protein transport genes. AB307.09 (*pyrC*$^-$), AB307.155 (*rpmA*$^-$), AB307.162 (*trmD*$^-$), AB307.211 (*secE*$^-$), AB307.216 (*relA*$^-$). (C) Comparison of wild type and mutants with disruptions in structural genes. AB307.17 (*ompF*$^-$), AB307.27 (*pbpG*$^-$), AB307.30 (*ptk*$^-$), AB307.45 (*epsA*$^-$), AB307.80 (*uppP*$^-$), AB307.92 (*spsC*$^-$), AB307.177 (*ostA*$^-$). Data are means ± SEM for 3 to 4 experiments for each time point.

based upon lack of homology to human genes, for verification of *in vivo* essentiality.

Fifty-three percent of AB307-0294 mutant derivatives with decreased growth in human ascites were essential in a rat subcutaneous abscess model. Thirty-four unique AB307-0294 mutant strains were tested in a well-established rat subcutaneous abscess model that has been validated for use with *A. baumannii* (36). Importantly, multiple host defense factors, including complement, professional phagocytes, and antimicrobial peptides, are present in this model. This critical step verifies *in vivo* essentiality via monitoring of the quantitative growth and survival of specific mutant strains over time. The use of an *in vivo* infection model (i.e., infection within a host) subjects the *A. baumannii* mutants to a range of conditions, including restricted nutrients and immune responses, difficult or impossible to completely replicate outside a host.

This *in vivo* assessment revealed that 18 of the 34 (53%) mutated genes were essential *in vivo* (Fig. 1; Table 1). The criterion used to classify a gene as *in vivo* essential was a $\geq$2 $\log_{10}$ reduction from the original bacterial titer within 48 h postinfection (hpi). Impressively, 10 of the 18 mutant strains exhibiting a significant *in vivo* growth defect had a $\geq$5 $\log_{10}$ reduction and/or complete kill within 48 hpi (Fig. 1). Furthermore, at 48 hpi, all of the mutant strains exhibited a $\geq$5 $\log_{10}$ reduction compared to the corresponding titer of the wild-type AB307-0294 control. Mutations that resulted in bacteriostatic or mildly decreased growth over the test period were not classified as *in vivo* essential genes. All of the 18 *in vivo* essential genes had annotated biological functions and were grouped into five functional categories (metabolic, two-component signaling [TCS] systems, DNA/RNA synthesis and regulation, protein transport, and structural). These data demonstrate that the genes disrupted in mutants with decreased or no growth in human ascites are likely to be essential *in vivo*.

Genes identified to be essential for growth and/or survival under clinically relevant conditions are not essential in rich laboratory medium. Importantly, all 18 mutants grew in the rich

TABLE 1 AB307-0294 *in vivo* essential genes and gene products

Ab307-0294 gene locus	Gene	Mutation no.[a]	Annotation	UniProt no.	OMA no.	Polar effect exclusion
ABBFA_000154	*aceE*	73	Pyruvate dehydrogenase E1 component	B7GV82	ACIB300151	RT-PCR amplicon
ABBFA_000285	*envZ*	153	Osmolarity sensor protein EnvZ	B7GVK9	ACIB300278	RT-PCR amplicon
ABBFA_000350	*trmD*	162	tRNA (guanine-1)-methyltransferase	B7GVS0	ACIB300339	RT-PCR amplicon
ABBFA_000621	*ompF*	17	Outer membrane porin F precursor	B7GWT4	ACIB300599	Genome organization
ABBFA_000700	*uppP*	80	Undecaprenyl-diphosphatase UppP	B7GXE2	ACIB300672	RT-PCR amplicon
ABBFA_000738	*rpmA*	155	Ribosomal protein L27	B7GXH9	ACIB300709	RT-PCR amplicon
ABBFA_000787	*carA*	12	Carbamoyl-phosphate synthase small chain	B7GY14	ACIB300758	RT-PCR amplicon
ABBFA_001168	*aroA*	68	3-Phosphoshikimate 1-carboxyvinyltransferase	B7GZU8	ACIB301129	RT-PCR amplicon
ABBFA_001801	*aroC*	170	Chorismate synthase	B7H3A6	ACIB301758	Genome organization
ABBFA_001929	*ostA*	177	Organic solvent tolerance protein OstA	B7H3N4	ACIB301886	RT-PCR amplicon
ABBFA_002478	*pyrC*	9	Dihydroorotase, type II	B7GX48	ACIB302431	Complementation
ABBFA_002866	*rstA*	70	Transcriptional regulatory protein RstA	B7GZC5	ACIB302811	Downstream gene—identical signal path
ABBFA_002981	*relA*	216	GTP pyrophosphokinase	B7H017	ACIB302919	Genome organization
ABBFA_003254	*secE*	211	Preprotein translocase, SecE subunit	B7H1K4	ACIB303187	RT-PCR amplicon
ABBFA_003295	*pbpG*	27	Penicillin-binding protein 7/8 (PBP7/8)	B7H1P0	ACIB303223	Complementation
ABBFA_003451	*spsC*	92	Perosamine synthase	B7H2H8	ACIB303374	RT-PCR amplicon
ABBFA_003459	*epsA*	45	EPS I polysaccharide export outer membrane protein EpsA precursor	B7H2I6	ACIB303382	Complementation
ABBFA_003461	*ptk*	30	Tyrosine-protein kinase Ptk	B7H2I8	ACIB303384	Complementation

[a] Mutation number assigned to a specific AB307-0294 transposon mutant.

TABLE 2 Growth characteristics of *A. baumannii in vivo* essential gene mutants

AB307-0294 gene	Function	Growth[a]		
		LB	Ascites	*In vivo*
aceE	Carbohydrate and amino acid metabolism	+2	+1	−2
envZ	Two-component system signaling	+2	0	−2
trmD	tRNA modification	+2	0	−2
ompF	Outer membrane porin	+2	−2	−2
uppP	Peptidoglycan synthesis	+2	−2	−2
rpmA	Ribosome assembly and translation	+2	0	−2
carA	Pyrimidine metabolism	+1	−2	−2
aroA	Chorismate and aromatic amino acid metabolism	+2	0	−2
aroC	Chorismate metabolism	+2	0	−2
ostA	Outer membrane LPS assembly	+2	−2	−2
pyrC	Pyrimidine metabolism	+2	0	−2
rstA	Two-component system signaling	+2	0	−2
relA	Nucleotide metabolism; stringent response	+2	0	−2
secE	Protein transport	+2	0	−2
pbpG	Peptidoglycan synthesis/modification	+2	−2	−2
spsC	LPS synthesis/modification	+2	−1	−2
epsA	Capsule transport, outer membrane	+2	−1	−2
ptk	Capsule synthesis	+2	−1	−2

[a] Growth of mutant strain compared to that of the wild type in LB-rich laboratory medium, human ascites, or *in vivo* in a rat subcutaneous abscess infection model. Growth scale: +2, wild type; +1, less than wild type; 0, neither growth nor kill; −1, modest kill; −2, significant kill.

Luria-Bertani (LB) laboratory medium, with all but the *carA*$^-$ mutant displaying growth at or near wild-type levels (Table 2). The optimal density at 600 nm (OD_{600}) of the *carA*$^-$ mutant culture was ~66% of the corresponding wild-type culture after 24 h. Although these mutant growth results on LB medium were expected, based on the design of our essentiality screen, they emphasize a fundamental difference from most other screens that define essentiality as a lack of growth in rich laboratory medium. In contrast, we further screened the set of mutants that survived in LB medium in human ascites. This point is critical since these genes, which have been shown to be essential for the growth and/or survival of *A. baumannii ex vivo* in human ascites and *in vivo* in a rat infection model, would not have been identified by a rich laboratory medium screen. Since the human host is a modified minimal medium (e.g., iron depleted) that contains host defense factors, the clinical relevance of essential genes identified on rich laboratory medium may be uncertain or misleading.

The correlation of experimentally identified AB307-0294 *in vivo* essential genes compared to those present in DEG was poor. The results of our AB307-0294 *in vivo* essentiality screen were compared to the bacterial genes annotated as essential within DEG (version 6.8) (14). DEG contains the results of 20 genome-wide essentiality screens across 17 unique bacterial species (see Table S1 and Fig. S1 in the supplemental material).

DEG was searched for orthologs to the 18 identified *A. baumannii in vivo* essential genes. The ortholog match criterion was selected to maximize the likelihood that the *A. baumannii* to DEG matches possessed identical or highly similar biological functions (37–39), a practice followed by others (40, 41). This is especially important for large superfamilies, where subfamilies may have distinct functional differences. DEG ortholog matches were then separated into GNB only; GNB only, excluding *A. baylyi*; non-GNB (i.e., GPB, mycobacteria, and mycoplasma); and all bacteria species (Fig. 2). The majority of *A. baumannii in vivo* essential

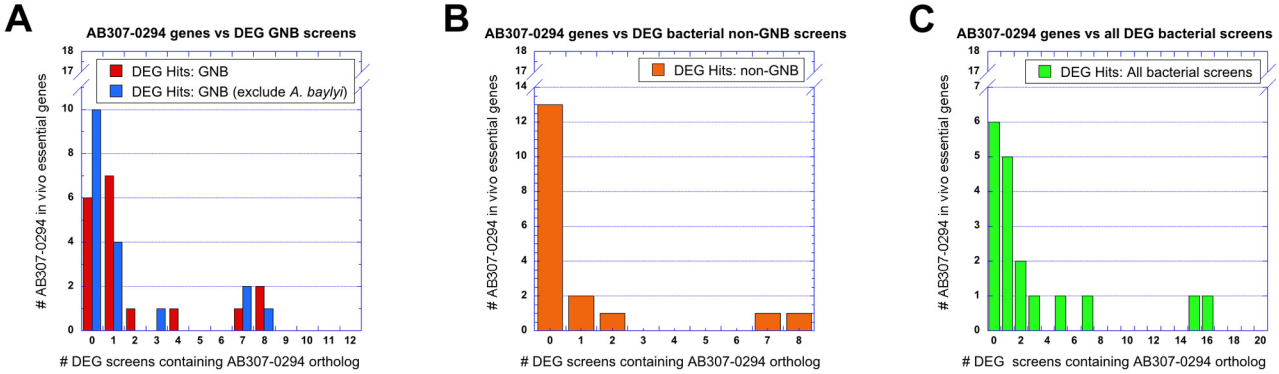

FIG 2 Histograms of the occurrence of orthologs to the 18 AB307-0294 *in vivo* essential genes identified in this study within the bacterial genome-wide essentiality screen data compiled in DEG. Columns at the left side of each histogram indicate AB307-0294 *in vivo* essential genes having few or no orthologs annotated as essential within DEG. (A) Comparison to all 12 GNB data sets within DEG (red columns) and to the same set excluding *A. baylyi* (blue columns); (B) comparison to the 8 non-GNB data sets (includes GPB, mycobacterium, and mycoplasma species) within DEG; (C) comparison to all 20 bacterial data sets present within DEG.

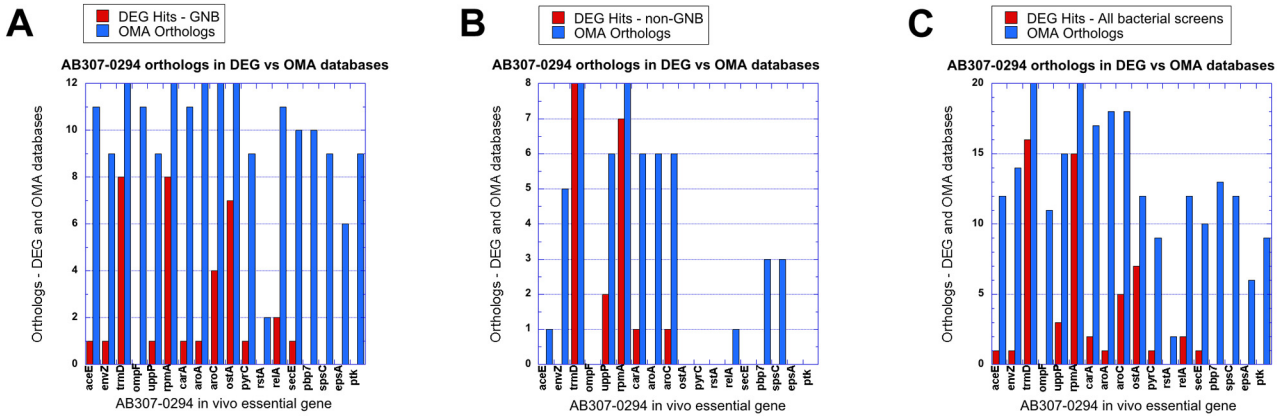

FIG 3 The occurrence of orthologs to each of the 18 AB307-0294 *in vivo* essential genes identified in this study within the bacterial genome-wide essentiality screen data compiled in DEG (red columns) and within the genomes of the same bacterial species (blue columns). (A) Comparison the 12 GNB data sets within DEG; (B) comparison to the 8 non-GNB bacterial data sets (includes GPB, mycobacterium, and mycoplasma species) within DEG; (C) comparison to all 20 bacterial data sets present within DEG.

genes/gene products had few or no bacterial orthologs annotated within DEG as essential. The distribution of DEG ortholog matches is skewed slightly toward a greater frequency when only the DEG GNB data are considered, with 13/18 (72%) genes with ≤1 ortholog and 6/18 (33%) with no matches (Fig. 2A). This observation may be expected, as generally the DEG GNB species are more closely related to *A. baumannii* than DEG's non-GNB species, for which 15/18 (83%) genes had ≤1 ortholog and 13/18 (72%) genes had no matches (Fig. 2B). Likewise, excluding consideration of the most closely related species, *A. baylyi*, shifts the distribution toward a lower occurrence of orthologs to *A. baumannii in vivo* essential genes within DEG's GNB set (14/18 [77%] with ≤1 ortholog and 10/18 [56%] with no matches) (Fig. 2A). Therefore, the fact that an ortholog is not listed as essential in DEG or that it has been identified as essential in only a few species by no means excludes it as being essential *in vivo*. This has obvious implications given that the data within DEG is typically heavily weighted during decisions on the validity of gene products being potential antimicrobial targets for a given genera or species.

It is noteworthy that even the *A. baumannii in vivo* essential genes that have many ortholog hits within DEG possess an important phenotypical difference from those matches. All bacterial essentiality screens within DEG, with the exception of the *A. baylyi* screen, were conducted on rich laboratory media. Hence, genes annotated as essential within those screens indicate that the respective gene disruption mutants were nonviable in rich media. However, all 18 of the *A. baumannii in vivo* essential genes identified in this study grew at or near wild-type levels in rich media (Table 2). Thus, all 18 *A. baumannii* genes form a set unique from the essential genes in DEG.

The poor correlation of experimentally identified AB307-0294 *in vivo* essential genes compared to those annotated in DEG was not due to the absence of orthologs. A potential reason why few *A. baumannii in vivo* essential gene orthologs were present in DEG may be that the 17 bacterial species annotated in DEG simply lack orthologous genes (i.e., a gene cannot be annotated as essential if that gene is not present in the genome of the wild-type organism). The OMA ortholog database was searched to confirm that for most of the 18 *A. baumannii* genes, orthologous genes were prevalent in the bacterial species contained in DEG (Fig. 3). Over 70% (13/18) of the *A. baumannii* genes have orthologs in >50% of the bacterial species annotated in DEG. Furthermore, only one of the *A. baumannii* genes, *rstA*, has an ortholog in <25% of the DEG bacterial species and so may be classified as unique to *Acinetobacter*. Orthologs are more frequently present in the DEG GNB species (Fig. 3A) versus the DEG non-GNB species (Fig. 3B), which is not unexpected. While the 18 *A. baumannii in vivo* essential genes are not universally conserved across bacteria, most are widely distributed across species, especially across other GNB. Thus, their general absence from being annotated as essential in DEG is not due to these genes being unique to *Acinetobacter*.

The growth environment used for the essentiality screen appears to be critical. The fact that AB307-0294 and mutant derivatives with disruptions in genes essential for growth and/or survival *in vivo* were identified using a screen with human ascites likely explains the poor correlation to genes annotated as essential in DEG. Nearly all of the screens used to identify genes in DEG were performed in rich laboratory medium. A single genome-wide essentiality screen within DEG was conducted against a defined minimal medium, which is a better representation of the nutrient levels available in the human growth environment. The organism screened belonged to the same genus (*Acinetobacter baylyi*), yet only seven of the 18 identified essential genes were in common (42) (Table 3). The Keio collection of *E. coli* genome-wide-directed single gene mutants, excluding mutants nonviable in rich media, has also been evaluated for growth characteristics in a defined minimal medium (10). This study detected four *E. coli* genes essential in minimal media in addition to the three *E. coli* genes essential on rich media that are orthologous to *A. baumannii in vivo* essential genes. The results of these two studies were compared to the 18 *A. baumannii in vivo* essential genes to determine if the *E. coli* and *A. baylyi* ortholog mutants' growth phenotypes in minimal media correlated to *in vivo* growth and survival phenotypes in *A. baumannii*. Only 3 of 18 of the *A. baumannii in vivo* essential genes unambiguously correlated to the minimal medium growth phenotype of mutations in orthologous genes in both *E. coli* and *A. baylyi*. While definitive conclusions cannot be drawn, these results suggest that minimal medium may be an improved screening environment compared to rich laboratory medium because it more closely represents the *in vivo* environment.

TABLE 3 *A. baumannii in vivo* essential genes versus essentiality in minimal medium

AB307-0294 gene	Minimal medium study result[a]		Prediction *in vivo*[b]
	E. coli	*A. baylyi*	
aceE	N	N	NE
envZ	N	Y	?
trmD	NT	Y	EE
ompF	N	N	NE
uppP	N	N	NE
rpmA	NT	N	?
carA	Y	Y	E
aroA	Y	N	?
aroC	Y	Y	E
ostA	NT	N	?
pyrC	Y	Y	E
rstA	No ortho	N	NE
relA	N	Y	?
secE	No ortho	Y	?
pbpG	N	N	NE
spsC	No ortho	N	NE
epsA	N	N	NE
ptk	N	N	NE

[a] Keio Collection growth study of *E. coli* mutants in defined minimal MOPS (morpholinepropanesulfonic acid) medium (10) and *A. baylyi* essentiality study performed in defined minimal MA medium (42). N, gene not essential in minimal medium; Y, gene essential in minimal medium; No ortho, absence of orthologous gene; NT (*E. coli* only), not tested in minimal medium, as gene was essential in rich medium.
[b] Prediction that an AB307-0294 gene would be *in vivo* essential based upon minimal medium studies for *E. coli* and *A. baylyi*. E, predicted *in vivo* essential, no growth in minimal medium for both *E. coli* and *A. baylyi* ortholog mutants; EE, predicted essential under some condition (i.e., rich or minimal medium); NE, predicted as not *in vivo* essential, as growth occurs in minimal medium for both *E. coli* and *A. baylyi* ortholog mutants; ?, prediction of *in vivo* essentiality ambiguous due to different results in the *E. coli* and *A. baylyi* minimal medium screens.

TABLE 4 *A. baumannii in vivo* essential genes as antimicrobial targets

Gene	UR/UE[a]	Rank[b]
aceE	++	H
envZ	++	M
trmD	++	M
ompF	+++	L
uppP	+++	H
rpmA	++	M
carA	++	H
aroA	+	H
aroC	++	H
ostA	+++	L
pyrC	++	H
rstA	+++	L
relA	++	M
secE	+++	L
pbpG	+	H
spsC	+++	H
epsA	+++	M
ptk	+++	M

[a] UR/UE, unrecognized/underexploited drug target as evaluated by comparison to entries within DrugBank (56) and the Therapeutic Target Database (57). +++, no ortholog present; ++, ortholog entry present, listed inhibitor(s) classified as experimental (i.e., prior to preclinical studies) and nondrug like; +, no ortholog entry present but a related protein class is targeted by an approved drug or a chemical inhibitor in commercial use.
[b] Evaluation of potential as an antimicrobial drug target: H, high; M, medium; L, low.

However, it does not serve as an optimal surrogate for an *in vivo* growth environment for GNB. A partial explanation for this may be that *in vivo* conditions possess host defense factors that have bactericidal activity and that are not present in laboratory medium. In contrast, the use of human ascites likely enhanced our identification of genes essential for growth and/or survival *in vivo* because it contains active complement.

Further, a recent genome-wide chemical genetics *E. coli* study was designed to identify genes essential under specific chemical or environmental stresses (13). Few of the conditionally essential genes identified overlapped with the *A. baumannii in vivo* essential genes identified in our study, suggesting that extensive chemical genetics screens are not a replacement for *in vivo* studies.

The majority of the identified AB307-0294 *in vivo* essential genes are unrecognized or underexploited antimicrobial targets. Bioinformatic selection of putative antimicrobial drug targets typically requires that a gene or an ortholog has been annotated as essential (18, 40). The lack of significant numbers of orthologs annotated as essential in DEG for most of the identified *A. baumannii in vivo* essential genes suggested that few of these genes would have been selected as possible drug targets through a bioinformatic screen. In order to determine if orthologs to any of these genes have received serious attention as an antimicrobial target, both DrugBank and the Therapeutic Target Database (TTD) were searched (Table 4). This analysis revealed that none of the 18 *A. baumannii* genes identified in this study, or orthologs to these genes, were targets of FDA-approved drugs or drugs in the developmental pipeline. Almost half lacked an entry in these drug target databases.

Two genes (*aroA* and *pbpG*) lacked an entry for an ortholog, but entries did exist for related protein families that were targets of drug or drug-like small molecules. In these two cases, the attention that these related proteins received as antimicrobial targets was due largely to spillover from more extensive efforts on nonbacterial targets. In plants, the gene product of *aroA*, 3-phosphoshikimate 1-carboxyvinyltransferase (PSCVT), is the target of the broad-spectrum herbicide glyphosate (Roundup). However, while plant PSCVTs are glyphosate sensitive (class I), bacterial PSCVT enzymes may belong to either class I or class II (glyphosate resistant). Additionally, in previous bacterial genome-wide essentiality screens, an *aroA* ortholog was detected as essential in only *Caulobacter crescentus* (Table 5). Supporting data exist indicating the *in vivo* importance of *aroA* in other pathogenic GNB. *Salmonella enterica aroA* mutants yield highly attenuated strains due to both the inability to produce aromatic metabolites and cell wall and outer membrane defects that reduce resistance to innate immune responses (43). The gene *pbpG* encodes penicillin-binding protein 7/8 (PBP-7/8), a low-molecular-weight (LMW) PBP. The high-molecular-weight (HMW) PBPs are heavily exploited antibacterial targets, but previous to the demonstration that *A. baumannii* PBP-7/8 was *in vivo* essential (35), LMW PBPs were not recognized as contributing to bacterial survival and hence were largely neglected as targets. *E. coli* LMW PBPs were recently reported to provide intrinsic resistance against β-lactams, further underscoring the previously unappreciated roles for these proteins during infection and antimicrobial treatment (44). A third gene, *pryC*, encoding dihydroorotase (DHOase), is noteworthy because the human and *Plasmodium* genes encoding this function have received attention as potential anticancer and antimalarial targets, respectively. However, the *Plasmodium* and human enzymes belong to a different DHOase

TABLE 5 Ortholog distribution of AB307-0294 *in vivo* essential genes in bacterial species annotated in DEG[a]

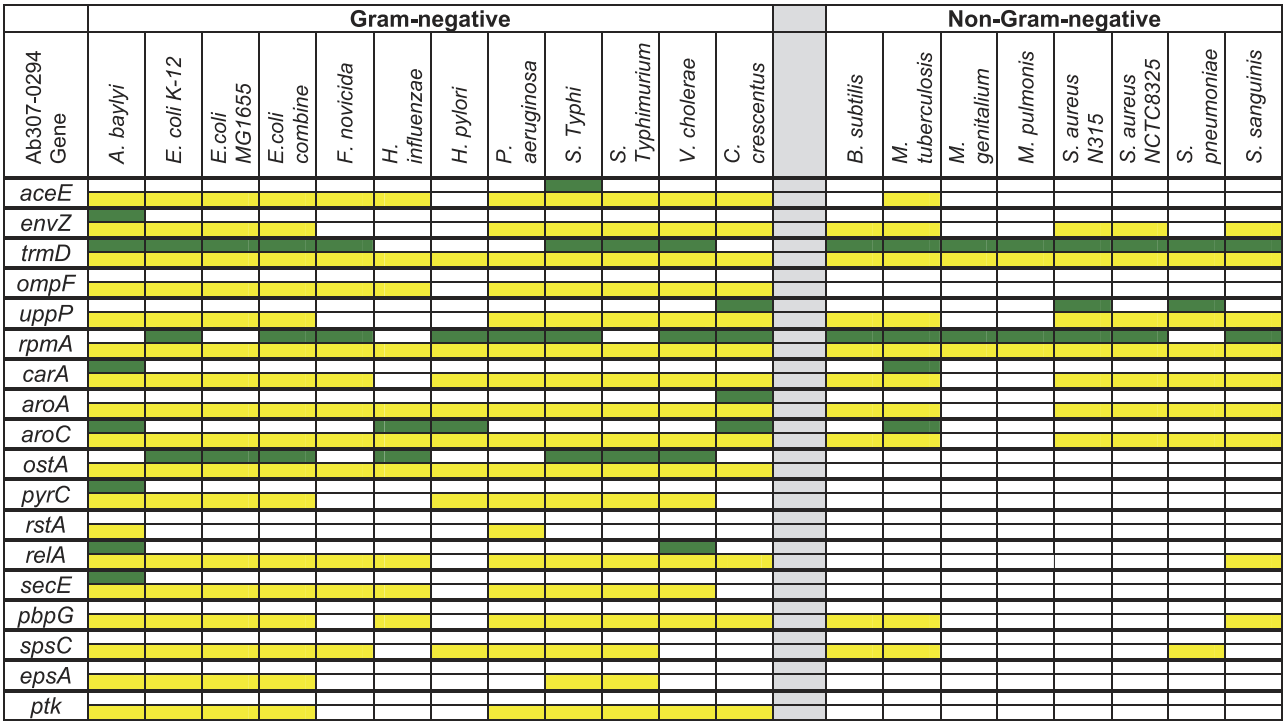

[a] Green indicates the presence of an ortholog to an AB307-0294 *in vivo* essential gene annotated as essential in a bacterial species present within DEG version 6.8. Yellow indicates the presence of an ortholog of any type (essential or nonessential) to an AB307-0294 *in vivo* essential gene.

class than that found in the majority of bacteria, including exhibiting different active-site architectures.

Given our identification of these 18 *A. baumannii* genes as *in vivo* essential, we evaluated their likelihood of serving as potential anti-GNB targets by criteria commonly used in the bioinformatic selection of targets. This analysis revealed that many of the identified *A. baumannii* genes possess significant potential as therapeutic targets within GNB despite being previously overlooked (Table 4). Therefore, within the context of identifying essential genes for the purpose of developing new classes of antimicrobials for human infections, the growth medium/environment used for the essentiality screen is critical.

DISCUSSION

This study identified a unique set of *A. baumannii* genes representing high-value, unrecognized or underexploited, potential antimicrobial targets for pathogenic GNB. Further, this report established that if a gene is not in DEG, it should not be excluded from consideration as a potential drug target. Lastly, the data demonstrated the importance of using clinically relevant media and *in vivo* validation when screening for essential genes for the purpose of developing new classes of antimicrobials for human infections.

The strategy used for identifying *in vivo* essential genes within *A. baumannii* is not only efficient, it is also capable of identifying genes involved in multiple pathways and functions and enhances the understanding of pathogen biology. The putative products of three *in vivo* essential genes participate in metabolic pathways (Fig. 1A). The genes *aroA* and *aroC* encode 3-phosphoshikimate 1-carboxyvinyltransferase and chorismate synthase, respectively, which catalyze the final two steps of chorismate biosynthesis. This is an example of our screen identifying functionally related genes that participate in the same pathway but are not contained within the same operon. The *A. baumannii aroA* gene additionally encodes prephenate dehydrogenase (PD) activity, yielding an unusual fusion protein. Typically, these two activities are present as separate proteins in bacteria (45). PD is a member of the aromatic amino acid biosynthesis pathway, which uses a derivative of chorismate as its initial substrate. The third metabolic gene was identified as *aceE*, putatively encoding the pyruvate dehydrogenase E1 component. This protein participates in the conversion of pyruvate to acetyl coenzyme A (acetyl-CoA), which then feeds into the citric acid cycle and other metabolic pathways. Two genes participating in separate TCS systems, *envZ* and *rstA*, were identified as *in vivo* essential (Fig. 1A). The gene *envZ* putatively encodes the osmolarity sensor protein, a trans-inner membrane sensor protein that propagates its signal through a cytoplasmic histidine kinase domain. This protein participates in osmoregulation, responding to environmental stimuli. The *rstA* gene putatively encodes a response regulator protein, RstA, which propagates the signal from its corresponding sensor protein RstB by acting as a transcriptional regulator. The environmental stimulus that the RstA/RstB TCS system responds to is unknown. DNA/RNA synthesis and regulation forms a third group containing five *in vivo* essential genes (Fig. 1B). This group may be subdivided into tRNA modification [*trmD*, which putatively encodes tRNA (guanine-1)-methyltransferase], ribosome assembly and translation (*rmpA*, which putatively encodes ribosomal protein L27), pyrimidine me-

tabolism (*carA*, which putatively encodes carbamoyl-phosphate synthase small chain; *pyrC*, which encodes a type II dihydroorotase), and pppGpp synthesis for signaling the stringent response that modulates transcription profiles and decreases tRNA and rRNA synthesis under stress conditions (*relA*, which putatively encodes GTP pyrophosphokinase). Both carbamoyl phosphate synthase small subunit and DHOase are key enzymes in the pyrimidine biosynthesis pathway. Identification of genes participating in the same metabolic pathway but distantly located within *A. baumannii*'s genome increased confidence in the screening results. One of the identified genes, *secE*, has a predicted protein transport function (Fig. 1B). It putatively encodes a component of the SecYEG translocon. This is an integral membrane protein complex spanning the inner membrane that actively translocates proteins into the periplasm. Seven of the identified *in vivo* essential genes possess annotated functions that are predicted to affect structural integrity: the outer membrane (*ompF*, which putatively encodes outer membrane porin F; *ostA*, which putatively encodes organic solvent tolerance protein), peptidoglycan synthesis and modification (*uppP*, which putatively encodes undecaprenyl-diphosphatase; *pbpG*, which putatively encodes PBP-7/8), capsule synthesis and transport (*ptk*, which putatively encodes tyrosine-protein kinase; *epsA*, which putatively encodes EPS I polysaccharide export outer membrane protein), and lipopolysaccharide synthesis and modification (*spsC*, which putatively encodes perosamine synthase) (Fig. 1C). Their structural role is reinforced by the results of quantitative growth studies of these mutants in human serum, demonstrating extreme sensitivity to the bactericidal activity of complement (34, 35) (data not shown). It was noteworthy that *pbpG* was identified in our screen (36). PBP-7/8 belongs to the LMW class of PBPs. LMW PBPs have been largely neglected because they were not recognized as essential using *in vitro* assays, unlike the HMW PBPs that are well-known targets of β-lactam antibiotics. These results strongly suggest that the mechanism of action of β-lactam antibiotics may be partially due to inactivation of LMW PBPs.

The strategy to identify *in vivo* essential genes in this study should be applicable to other bacterial species that can be cultured and subjected to gene disruption by random mutagenesis. Critical to the strategy is the approach of screening in a clinically relevant medium, in this case human ascites, which is an *ex vivo* medium reflective of inflammatory extracellular fluid. This simple innovation is critical for the efficiency of our approach. By selecting for transposon mutants on laboratory medium and then screening for essentiality on ascites plates, we are able to identify, in one step, genes (targets) that are both likely essential and expressed *in vivo*. The strength of this approach is that it is unbiased and highly efficient. We do not select the targets but allow the genetic screen, designed to identify the phenotype of *in vivo* essentially, to dictate the choices. This approach has a ~50% success rate for selecting genes later verified as essential in a rat abscess infection model. Target validation in an appropriate animal model(s) is a strong predictor of efficacy in humans (46) and is a critical step, since target essentiality *in vitro* or even *ex vivo* may not translate into the *in vivo* environment (47).

The results of this study also demonstrated that a set of *A. baumannii* genes that were initially identified on ascites plates and subsequently established to be *in vivo* essential is largely distinct from ortholog sets that are essential for growth in rich laboratory media. Broadly, this difference in essential gene sets can be attributed to differences in the growth environment used during the process of essential gene identification. While conceptually this difference is easy to understand, it often is not fully appreciated when interpreting results of essential gene screens or extrapolating from these results to computationally select antimicrobial drug targets or predict essential genes in other species. This concept is also applicable for the identification of virulence factors that may also serve as antimicrobial targets or vaccine candidates. DEG is a repository of publically released genome-wide essentiality screens and serves as a common source for bioinformatic methods requiring essentiality data. Overall, the data contained within DEG are of high quality when considered within the context of how they were generated. For all bacterial species in DEG, genome-wide screening was conducted *in vitro* using laboratory media, and all but one used rich media. Genes annotated as nonessential by such screens cannot be excluded *a priori* as having an essential role *in vivo*. These screens were not designed to replicate physiological conditions that may be encountered by a pathogen during infection. All 18 *A. baumannii in vivo* essential genes identified in this study carry the annotation of nonessential under *in vitro* conditions used in nearly all genome-wide screens published to date. It is important that the growth conditions used to identify essential genes should be concordant with the project's goal. The human host environment is deficient in selected requisite nutrients and possesses host defense factors. For example, certain purines, pyrimidines, and amino acids are variably present in various human body fluids, including plasma (48, 49). Based solely on concentration measurements, it is unclear whether their bioavailability is sufficient to support the growth of a corresponding auxotrophic bacterial strain. However, numerous biological studies have demonstrated that a pathogen's ability to synthesize or uptake certain noniron nutritional factors, such as purines, pyrimidines, and amino acids, is critical for virulence within the host (50). This study further supports the concept that human body fluids are a modified minimal medium beyond iron limitation. A number of the AB307-0294 mutants identified by the phenotype of being unable to grow in human ascites possessed gene disruptions in pyrimidine or amino acid metabolic pathways. Therefore, if the objective is to identify potential antimicrobial targets, it is important that essential genes are identified in a clinically relevant medium or environment. Likewise, the use of genome-wide chemical genetic screening in rich laboratory media may fail to detect a significant percentage of *in vivo* essential genes. Findings from this report demonstrate that the pool of potential antimicrobial targets with *A. baumannii* can be expanded and refined based on the use of a more clinically relevant definition of gene essentiality. This strategy is applicable to other human microbial pathogens.

The number of bacterial species with experimentally determined genome-wide essentiality is small (i.e., 20 total screens of 17 unique species in DEG version 6.8), and conducting such screens is resource intensive. This set of circumstances has naturally led to the extrapolation of the data within DEG to predict essential genes in other organisms. Cross-species prediction of gene essentiality has been recognized as difficult, and even ortholog conservation across multiple species is not necessarily a marker of essentiality (11). Analysis of the *A. baumannii* results against the bacterial entries in DEG was in agreement with the difficulty of inferring essentiality cross-species. The majority of *A. baumannii* genes verified as *in vivo* essential could not be readily predicted with a high confidence level based on comparison to DEG (Fig. 2; Table 5).

Although differences in screening methods likely account for a significant amount of the variation between *A. baumannii in vivo* essential genes identified in this study and the essential genes catalogued within DEG, it has been shown that genes identified in one species in a defined environment are not necessarily essential in another species or genera under the same conditions (8).

Conversely, although not experimentally established in this report, the presence of a gene or an ortholog to that gene in DEG is not a guarantee of that gene being essential *in vivo*. Many of the elements of the type II fatty acid biosynthesis (FASII) pathway (i.e., *fab* gene cluster) in a number of bacteria have been annotated as essential, forming the basis of the development of antimicrobials targeting this pathway (51, 52). However, it has recently been demonstrated that this pathway may not be essential to GPB during infection. Specifically, the inhibited or genetically disrupted GPB FASII pathway can be compensated by fatty acids present in serum (47, 53). Thus, *in vitro* essentiality data obtained using rich laboratory medium failed to accurately reflect the genes required, and not required, for the promotion of infection in clinically relevant environments.

Several limitations should be noted regarding our strategy for identifying essential genes. First, it does not identify genes essential in rich laboratory media. However, it is likely that many of the genes that would be identified as essential on rich laboratory media will encode proteins that are already targeted by the present antimicrobial armamentarium, such as those involved with cell wall or protein synthesis. Second, genes identified as *in vivo* essential in one bacterial species (e.g., *A. baumannii*) are not certain to be *in vivo* essential in other genera or even species, but this is a problem present in all essentiality screening methods. Redundant or alternative metabolic or biosynthetic pathways may exist; therefore, conclusive proof of essentiality requires experimental confirmation under appropriate conditions. Additional research is required to determine if the level of conservation of the essentiality phenotype across species varies significantly between genes identified *in vitro* using rich laboratory media and those identified *in vivo*. Lastly, the *A. baumannii* genetic screen was designed to examine essentiality in extracellular inflammatory fluid. Bacterial infections occur in other physiological environments that ascites and the rat abscess model may mimic poorly. An interesting future research direction will be to test our results in one or more different infection models. It is likely that at least some variation will be observed for *in vivo* essentiality based on the site of infection and/or the animal species used. That said, we have previously tested several of our *A. baumannii* mutants in a rat pneumonia model, and in all cases significant decreases in bacterial titers were observed (35). It is also possible that bacterial genes found to be *in vivo* essential in a rat will not be *in vivo* essential in humans, or vice versa, due to specific pathogen-host interactions. For example, *Neisseria* species obtain iron from host transferrin and lactoferrin proteins. *Neisseria*'s receptors for these proteins have evolved to be specific for only these proteins from the human and closely related primates (54, 55). Pathogen-host specificity is a recognized issue for any animal model system and not solely a problem with our strategy.

The results presented here expand antimicrobial target space and increase awareness that the environment during infection may differ significantly from laboratory *in vitro* growth conditions. Furthermore, these results emphasize the need to incorporate appropriate *in vitro* screens and clinically relevant *in vivo* studies (i.e., animal infection models) early in the process of evaluating potential antimicrobial targets. Neglecting to do so may have significantly skewed past selection of targets. Antimicrobial drug development in general, and especially against GNB, is challenging for a variety of reasons. A successful antimicrobial drug must have characteristics beyond simple inhibition of the target's function. Features include permeability properties that enable target site access, resistance to degradation and efflux, favorable pharmacokinetic and pharmacodynamic properties, and acceptable toxicity. These and other necessary or desired features are often at odds with one another chemically, requiring multiple rounds of optimization (56). Expansion of target space allows for the exploration of different regions of chemical space, increasing the probability that appropriate lead molecules will be identified that can be developed into new classes of antimicrobials.

The identification of *in vivo* essential genes increases the understanding of the *in vivo* physiology of *A. baumannii* growth, which is an important initial step for target-based drug development strategies and may facilitate the understanding of the mechanism of action. A number of high-throughput screening (HTS) campaigns, designed to identify drug leads targeting essential genes as part of a target-based approach, have not, as of yet, come to fruition (46). However, one of the important points of this study is that many of these previous screens may not have been optimally designed with respect to target selection. Retrospective analyses of failed target-based HTS campaigns have identified problems in the HTS design, especially the use of chemical libraries of limited chemical diversity primarily designed for eukaryotic targets (33, 57). Multiple approaches may be used for the identification of lead compounds effective against specific targets, which can be subsequently validated using a combination of appropriate bacterial constructs in clinically relevant *in vitro* and *in vivo* models. Structurally enabled fragment-based lead discovery (FBLD) methods differ significantly in methodology and philosophy from HTS. Importantly, FBLD allows a much more efficient and larger sampling of chemical space while simultaneously allowing greater freedom for medicinal chemistry to engineer desired properties during the optimization of initial drug lead compounds towards therapeutics suitable for clinical testing (58, 59). Although the concept of an antimicrobial being active against multiple independent targets is appealing, particularly for durability, this is not a necessary requirement for an effective antimicrobial. Several strategies are compatible with leveraging our results toward drug development: single pharmacophore/multitarget compounds, hybrids of two pharmacophores, combinations of single-target inhibitors to avoid resistance development, and structure-based drug design to create multiple intramolecular drug–target interactions (60). Lastly, our results will allow the (re)examination of these genes. For example, it is possible that screening hits against several of the genes/gene products may have been identified in the past but never pursued because the targets were previously considered to be nonessential.

In summary, this study demonstrates the underappreciated concept that decisions on the potential validity of antimicrobial targets by investigators and pharmaceutical companies need to be made within the environmental context (e.g., rich laboratory medium versus infection model) of how a gene was identified as essential. The absence of a database that catalogues clinically relevant essential genes has impeded a fuller definition of the antimicrobial target space.

MATERIALS AND METHODS

AB307-0294 is a clinical blood isolate representative of *A. baumannii*. *A. baumannii* strain 307-0294 (AB307-0294) (blood isolate from Buffalo, NY, sequence type [ST] 15, clonal group 1 based on Ecker et al. [61]) was selected as our model strain for these studies. We have previously used this strain in related studies (34–36). The genome of AB307-0294 has been fully sequenced, containing 3.76 Mbp and 3,531 predicted open reading frames (ORFs) (62). Compared with the five genomes in the public domain (ATCC 17978, 0057, AYE, ACICU, SDF) and three additional isolates (900 [perineal isolate], 853 [blood isolate from Iraq], and 979 [environmental isolate from Iraq]) sequenced by T. A. Russo, A. Campagnari, and S. Gill (unpublished data), available at the time of the initiation of these studies, AB307-0294 shared ~3 Mbp. AB307-0294 is relatively drug susceptible, enabling the performance of genetic manipulations. It is closely related to *A. baumannii* strains 0057 and AYE, with only approximately 3% of AB307-0294's genome differing from these strains, virtually all of which are two prophage clusters. Taken together, these data support AB307-0294 as being both clinically appropriate, representative of contemporary *A. baumannii* strains, and an ideal background to identify new or unrecognized antimicrobial targets of interest.

Identification of AB307-0294 genes essential for growth in human ascites *ex vivo*. The experimental approach was a modification of the method previously used to identify virulence factors in extraintestinal pathogenic *E. coli* (32) and was subsequently applied to *A. baumannii* (34, 35). Briefly, the EZ-Tn*5*<kan-2> transposome (EPICENTRE Biotechnologies) was electroporated into AB307-0294 to create random mutants. Mutagenized bacteria were selected on MH plates containing kanamycin (40 μg/ml), a nutrient-rich laboratory medium. Mutants were then gridded onto plates comprised solely from human exudative ascites, kanamycin (40 μg/ml), and agar (ascites plates). Human ascites was collected from deidentified patients who were undergoing therapeutic paracentesis for symptoms due to abdominal distension. These individuals were not being treated with antimicrobials and were not infected with human immunodeficiency, hepatitis B, or hepatitis C virus. The ascites was cultured to confirm sterility, divided into aliquots, and stored at −80°C. The procedures for obtaining human ascites were reviewed and approved by the Western New York Veterans Administration Institutional Review Board. Informed consent was used to obtain human blood for the preparation of serum (approval ID 00063). The Western New York Veterans Administration Institutional Review Board for the process of obtaining ascites waived informed consent (approval ID 00098). An expedited review was performed, because the ascites was collected from deidentified patients who were undergoing therapeutic paracentesis for symptoms due to abdominal distension. Mutants exhibiting no or minimal growth on ascites plates had their sites of transposon insertion identified by chromosomal sequencing using previously described methods (35), and each interrupted ORF was identified by comparison to the annotated AB307-0294 genomic sequence (GenBank no. CP001172). Note that saturation mutagenesis was not achieved. Depending on the method of estimation, the predicted number of mutants required to reach 95% saturation of the AB307-0294 genome would be 12,000 to 42,000 (63). Further, transposon-mediated mutagenesis is more likely to interrupt longer genes, and so our data set may be biased against short genes. However, given the objective of evaluating the growth phenotype on ascites plates as predictive of *in vivo* essentiality rather than identifying all *in vivo* essential genes, this lack of saturation mutagenesis was acceptable.

Quantitative *in vitro* growth analyses. Mutant derivatives of AB307-0294 that demonstrated decreased or absent growth on ascites plates underwent quantitative growth assessment in rich laboratory medium (LB) and human ascites as described (35, 36).

Exclusion of polar effects in mutant derivatives of AB307-0294. Potential transposon-mediated polar effects on downstream genes were evaluated. For 10 of the mutants, reverse transcription-PCR (RT-PCR) was performed on the gene immediately downstream that was in the same transcriptional orientation, and an amplicon of the expected size was successfully generated (data not shown). For these RT-PCR studies, RNA was isolated from each mutant strain using the RNeasy Protect minikit (Qiagen Inc., Valencia, CA). Samples were treated with DNase I twice to completely digest contaminating chromosomal DNA. Absence of contaminating DNA was confirmed by testing all RNA samples prior to RT-PCR analysis using the appropriate primer pair and GoTaq Green master mix (Promega, Madison, WI). The Qiagen OneStep RT-PCR kit was used for subsequent RT-PCR analyses of all samples. Primers were designed to amplify 100 to 500 bp of the RNA transcript being assessed. Primers are listed in Table S2 in the supplemental material. A positive control that amplified the RNA transcript from the single-stranded binding protein (SSB) was run concurrently with all samples tested.

Four of the AB307-0294 mutants were complemented *in trans* using the *A. baumannii* cloning vector pNLAC1 with restoration of the phenotype of being able to grow and survive in human ascites (34, 35) (data not shown for *pyrC*). For one mutant derivative, a polar effect was excluded because the downstream gene was part of the same multisubunit two-component regulatory system. In three of the mutants, the downstream gene was in a reversed transcriptional orientation, excluding polar effects. Results are summarized in Table 1.

Assessment of AB307-0294 mutant derivatives with decreased growth in human ascites in a rat subcutaneous abscess model. The University at Buffalo and Veterans Administration Institutional Animal Care Committees approved the rat subcutaneous abscess model. This study was carried out in strict accordance with the recommendations in the Guide for the Care and Use of Laboratory Animals of the National Institutes of Health, and all efforts were made to minimize suffering. Mutants exhibiting significantly decreased or absent growth in human ascites were evaluated in an established rat soft-tissue infection model for *in vivo* growth/survival (36). Briefly, a subcutaneous space is created through the injection of 30 ml of air into the back of anesthetized Long-Evans rats (200 to 225 g), followed by the injection of 1 ml of 1% croton oil in a filter-sterilized vegetable oil vehicle. The space was allowed to mature into an encapsulated, fluid-filled (8- to 12-ml) pouch over 6 to 8 days. Neutrophils would have migrated into the abscess in response to appropriate chemotactic signals. The abscess' subcutaneous location enabled multiple injections and samplings to be performed over time. AB307-0294 or mutant derivatives were injected alone into the abscess of an anesthetized animal, resulting in an estimated starting abscess concentration of 1×10^5 CFU/ml. Within 1 min after the bacteria were injected into the abscess, 0.5 ml of abscess fluid was removed to measure the actual starting bacterial titer. Fluid aliquots (0.5 ml) were subsequently obtained from anesthetized animals 3, 6, 24, and 48 h after the initial bacterial challenge, and bacterial titers were enumerated. *In vivo* data are presented as means ± standard errors of the means (SEM). To normalize *in vivo* data, $\log_{10}$ transformed values were utilized, the area under each curve was calculated, and these areas were compared using two-tailed unpaired *t* tests (Prism 4 for Macintosh, GraphPad Software Inc.).

Prioritization of genes identified by *in vitro* ascites screen for *in vivo* evaluation. Genes were analyzed for conservation across five additional *A. baumannii* strains possessing sequenced genomes (AB0057, ACICU, ATCC 17978, AYE, SDF) at the initiation of this study and for the lack of close human homologues using BLAST (64). The identified genes were conserved across *A. baumannii* strains but exhibited a wide range of similarity to human genes. This filtering process was performed to reduce the number of mutant strains and animals used, with the current study focusing on those potential targets with little to no homology to human genes.

Comparison of *A. baumannii in vivo* essential genes to DEG. Putative protein sequences were generated from the DNA sequences of the 18 AB307-0294 genes experimentally established to be essential *in vivo*. These proteins were compared to bacterial genome-wide essentiality screen data available in the Database of Essential Genes, version 6.8 (14), by BLASTp (64). Significant DEG BLASTp hits (E values of <1e−10 and coverage of >75% of the AB307-0294 protein) were then evaluated using the OMA

Browser to determine orthologs (i.e., OMA ortholog and close ortholog groups) to *A. baumannii* targets (65).

Comparison to known drug targets. Similarly, two drug target databases (Therapeutic Targets Database [TTD] and DrugBank) (66, 67) were searched using BLASTp for proteins similar to *A. baumannii* targets, and significant matches were confirmed as orthologs with the OMA browser. The putative protein products derived from the *A. baumannii* genes experimentally established *in vivo* as being essential were evaluated for their potential as antimicrobial targets. Criteria were similar in concept to other published methods (18, 40) modified for GNB. In addition to the absolute criterion that the genes were verified as *in vivo* essential in *A. baumannii*, other factors considered included conservation across *A. baumannii* strains and multiple clinically important GNB, a knowledge of the biological role to aid understanding inhibitor/drug lead mechanisms of action, a defined druggable site on the protein, the availability of an activity assay, the feasibility of biochemical and biophysical experimental study, and the lack of closely related proteins in humans.

SUPPLEMENTAL MATERIAL

Supplemental material for this article may be found at http://mbio.asm.org/lookup/suppl/doi:10.1128/mBio.00113-12/-/DCSupplemental.

Figure S1, TIF file, 2.5 MB.
Table S1, PDF file, 0.1 MB.
Table S2, PDF file, 0.1 MB.

ACKNOWLEDGMENTS

This work was support in part by a Telemedicine and Advance Technical Research Center (TATRC) cooperative agreement W23RYX1055N607, an interdisciplinary grant from the University at Buffalo (L.W.S., T.A.R., and T.C.U.), and a VA Merit Review grant from the Department of Veterans Affairs (T.A.R.).

REFERENCES

1. **D'Elia MA, Pereira MP, Brown ED.** 2009. Are essential genes really essential? Trends Microbiol. **17**:433–438.
2. **Dowell RD, et al.** 2010. Genotype to phenotype: a complex problem. Science **328**:469.
3. **Grenov AI, Gerdes SY.** 2008. Modeling competitive outgrowth of mutant populations: why do essentiality screens yield divergent results? Methods Mol. Biol. **416**:361–367.
4. **Osterman AL, Gerdes SY.** 2008. Comparative approach to analysis of gene essentiality. Methods Mol. Biol. **416**:459–466.
5. **Baba T, et al.** 2006. Construction of *Escherichia coli* K-12 in-frame, single-gene knockout mutants: the Keio collection. Mol. Syst. Biol. **2**:2006.0008.
6. **Gerdes SY, et al.** 2003. Experimental determination and system level analysis of essential genes in *Escherichia coli* MG1655. J. Bacteriol. **185**: 5673–5684.
7. **Rudd KE.** 2000. EcoGene: a genome sequence database for *Escherichia coli* K-12. Nucleic Acids Res. **28**:60–64.
8. **Salama NR, Shepherd B, Falkow S.** 2004. Global transposon mutagenesis and essential gene analysis of *Helicobacter pylori*. J. Bacteriol. **186**: 7926–7935.
9. **Dammel CS, Noller HF.** 1995. Suppression of a cold-sensitive mutation in 16S rRNA by overexpression of a novel ribosome-binding factor, RbfA. Genes Dev. **9**:626–637.
10. **Joyce AR, et al.** 2006. Experimental and computational assessment of conditionally essential genes in *Escherichia coli*. J. Bacteriol. **188**: 8259–8271.
11. **Zalacain M, et al.** 2003. A global approach to identify novel broad-spectrum antibacterial targets among proteins of unknown function. J. Mol. Microbiol. Biotechnol. **6**:109–126.
12. **Hillenmeyer ME, et al.** 2008. The chemical genomic portrait of yeast: uncovering a phenotype for all genes. Science **320**:362–365.
13. **Nichols RJ, et al.** 2011. Phenotypic landscape of a bacterial cell. Cell **144**:143–156.
14. **Zhang R, Lin Y.** 2009. DEG 5.0, a database of essential genes in both prokaryotes and eukaryotes. Nucleic Acids Res. **37**:D455–D458.
15. **Cameron DE, Urbach JM, Mekalanos JJ.** 2008. A defined transposon mutant library and its use in identifying motility genes in *Vibrio cholerae*. Proc. Natl. Acad. Sci. U. S. A. **105**:8736–8741.
16. **Gallagher LA, et al.** 2007. A comprehensive transposon mutant library of *Francisella novicida*, a bioweapon surrogate. Proc. Natl. Acad. Sci. U. S. A. **104**:1009–1014.
17. **Langridge GC, et al.** 2009. Simultaneous assay of every *Salmonella typhi* gene using one million transposon mutants. Genome Res. **19**:2308–2316.
18. **Crowther GJ, et al.** 2010. Identification of attractive drug targets in neglected-disease pathogens using an *in silico* approach. PLoS Negl. Trop. Dis. **4**:e804.
19. **Payne DJ, Gwynn MN, Holmes DJ, Rosenberg M.** 2004. Genomic approaches to antibacterial discovery. Methods Mol. Biol. **266**:231–259.
20. **Shen Y, et al.** 2010. Blueprint for antimicrobial hit discovery targeting metabolic networks. Proc. Natl. Acad. Sci. U. S. A. **107**:1082–1087.
21. **Boucher HW, et al.** 2009. Bad bugs, no drugs: no ESKAPE! An update from the infectious Diseases Society of America. Clin. Infect. Dis. **48**:1–12.
22. **Garnacho-Montero J, Amaya-Villar R.** 2010. Multiresistant *Acinetobacter baumannii* infections: epidemiology and management. Curr. Opin. Infect. Dis. **23**:332–339.
23. **Manchanda V, Sanchaita S, Singh N.** 2010. Multidrug resistant Acinetobacter. J. Global Infect. Dis. **2**:291–304.
24. **Kim BN, et al.** 2009. Management of meningitis due to antibiotic-resistant Acinetobacter species. Lancet Infect. Dis. **9**:245–255.
25. **Snitkin ES, et al.** 2011. Genome-wide recombination drives diversification of epidemic strains of *Acinetobacter baumannii*. Proc. Natl. Acad. Sci. U. S. A. **108**:13758–13763.
26. **Towner KJ.** 2009. Acinetobacter: an old friend, but a new enemy. J. Hosp. Infect. **73**:355–363.
27. **Sengstock DM, et al.** 2010. Multidrug-resistant *Acinetobacter baumannii*: an emerging pathogen among older adults in community hospitals and nursing homes. Clin. Infect. Dis. **50**:1611–1616.
28. **Perez F, et al.** 2007. Global challenge of multidrug-resistant *Acinetobacter baumannii*. Antimicrob. Agents Chemother. **51**:3471–3484.
29. **Fishbain J, Peleg AY.** 2010. Treatment of Acinetobacter infections. Clin. Infect. Dis. **51**:79–84.
30. **Boucher H, et al.** 2011. 10 × '20 progress: development of new drugs active against resistant 687 Gram-negative bacilli, abstr LB-27. Abstr. 49th Ann. Meet. Infect. Disease Soc. Am. IDSA, Boston, MA.
31. **Butler MS, Cooper MA.** 2011. Antibiotics in the clinical pipeline in 2011. J. Antibiot. **64**:413–425.
32. **Russo TA, Carlino UB, Mong A, Jodush ST.** 1999. Identification of genes in an extraintestinal isolate of *Escherichia coli* with increased expression after exposure to human urine. Infect. Immun. **67**:5306–5314.
33. **Gwynn MN, Portnoy A, Rittenhouse SF, Payne DJ.** 2010. Challenges of antibacterial discovery revisited. Ann. N. Y. Acad. Sci. **1213**:5–19.
34. **Russo TA, et al.** 2010. The K1 capsular polysaccharide of *Acinetobacter baumannii* strain 307-0294 is a major virulence factor. Infect. Immun. **78**:3993–4000.
35. **Russo TA, et al.** 2009. Penicillin-binding protein 7/8 contributes to the survival of *Acinetobacter baumannii in vitro* and *in vivo*. J. Infect. Dis. **199**:513–521.
36. **Russo TA, et al.** 2008. Rat pneumonia and soft-tissue infection models for the study of *Acinetobacter baumannii* biology. Infect. Immun. **76**: 3577–3586.
37. **Altenhoff AM, Dessimoz C.** 2009. Phylogenetic and functional assessment of orthologs inference projects and methods. PLoS Comput. Biol. **5**:e1000262.
38. **Fitch WM.** 1970. Distinguishing homologous from analogous proteins. Syst. Zool. **19**:99–113.
39. **Koonin EV.** 2005. Orthologs, paralogs, and evolutionary genomics. Annu. Rev. Genet. **39**:309–338.
40. **Agüero F, et al.** 2008. Genomic-scale prioritization of drug targets: the TDR targets database. Nat. Rev. Drug Discov. **7**:900–907.
41. **Doyle MA, Gasser RB, Woodcroft BJ, Hall RS, Ralph SA.** 2010. Drug target prediction and prioritization: using orthology to predict essentiality in parasite genomes. BMC Genomics **11**:222.
42. **de Berardinis V, et al.** 2008. A complete collection of single-gene deletion mutants of *Acinetobacter baylyi* ADP1. Mol. Syst. Biol. **4**:174.
43. **Sebkova A, Karasova D, Crhanova M, Budinska E, Rychlik I.** 2008. *aro* mutations in *Salmonella enterica* cause defects in cell wall and outer membrane integrity. J. Bacteriol. **190**:3155–3160.
44. **Sarkar SK, Dutta M, Chowdhury C, Kumar A, Ghosh AS.** 2011. PBP5,

PBP6 and DacD play different roles in intrinsic beta-lactam resistance of *Escherichia coli*. Microbiology **157**:2702–2707.
45. **Song J, Bonner CA, Wolinsky M, Jensen RA.** 2005. The TyrA family of aromatic-pathway dehydrogenases in phylogenetic context. BMC Biol. **3**:13.
46. **Payne DJ, Gwynn MN, Holmes DJ, Pompliano DL.** 2007. Drugs for bad bugs: confronting the challenges of antibacterial discovery. Nat. Rev. Drug Discov. **6**:29–40.
47. **Brinster S, et al.** 2009. Type II fatty acid synthesis is not a suitable antibiotic target for Gram-positive pathogens. Nature **458**:83–86.
48. **Simmonds HA, Duley JA, Davies PM.** 1991. Analysis of purine samples and pyrimidines in blood, urine, and other physiologic fluids, p 397–424. *In* Hommes F (ed), Techniques in diagnostic human biochemical genetics. A laboratory manual. Wiley-Liss, New York, NY..
49. **Slocum RH, Cummings JG.** 1991. Amino acid analysis of physiologic samples, p 87–126. *In* Hommes F (ed), Techniques in diagnostic human biochemical genetics. A laboratory manual. Wiley-Liss, New York, NY..
50. **Russo TA, Jodush ST, Brown JJ, Johnson JR.** 1996. Identification of two previously unrecognized genes (*guaA*, and *argC*) important for uropathogenesis. Mol. Microbiol. **22**:217–229.
51. **Altabe S, Lopez P, de Mendoza D.** 2007. Isolation and characterization of unsaturated fatty acid auxotrophs of *Streptococcus pneumoniae* and *Streptococcus mutans*. J. Bacteriol. **189**:8139–8144.
52. **Zhang YM, White SW, Rock CO.** 2006. Inhibiting bacterial fatty acid synthesis. J. Biol. Chem. **281**:17541–17544.
53. **Brinster S, et al.** 2010. Reply: essentiality of FASII pathway for *Staphylococcus aureus*. Nature **463**:E4–E5.
54. **Lee BC, Schryvers AB.** 1988. Specificity of the lactoferrin and transferrin receptors in *Neisseria gonorrhoeae*. Mol. Microbiol. **2**:827–829.
55. **Perkins-Balding D, Ratliff-Griffin M, Stojiljkovic I.** 2004. Iron transport systems in *Neisseria meningitidis*. Microbiol. Mol. Biol. Rev. **68**:154–171.
56. **Hughes D.** 2003. Exploiting genomics, genetics and chemistry to combat antibiotic resistance. Nat. Rev. Genet. **4**:432–441.
57. **Silver LL.** 2011. Challenges of antibacterial discovery. Clin. Microbiol. Rev. **24**:71–109.
58. **Murray CW, Blundell TL.** 2010. Structural biology in fragment-based drug design. Curr. Opin. Struct. Biol. **20**:497–507.
59. **Scott DE, Coyne AG, Hudson SA, Abell C.** 2012. Fragment-based approaches in drug discovery and chemical biology. Biochemistry **51**:4990–5003.
60. **Silver LL.** 2007. Multi-targeting by monotherapeutic antibacterials. Nat. Rev. Drug Discov. **6**:41–55.
61. **Ecker JA, et al.** 2006. Identification of Acinetobacter species and genotyping of *Acinetobacter baumannii* by multilocus PCR and mass spectrometry. J. Clin. Microbiol. **44**:2921–2932.
62. **Adams MD, et al.** 2008. Comparative genome sequence analysis of multidrug-resistant *Acinetobacter baumannii*. J. Bacteriol. **190**:8053–8064.
63. **Phogat SK, Gupta R, Burma PK, Sen K, Pental D.** 2001. On the estimation of number of events required for saturation mutagenesis of large genomes. Curr. Sci. **80**:823–824.
64. **Johnson M, et al.** 2008. NCBI BLAST: a better web interface. Nucleic Acids Res. **36**:W5–W9.
65. **Altenhoff AM, Schneider A, Gonnet GH, Dessimoz C.** 2011. OMA 2011: orthology inference among 1000 complete genomes. Nucleic Acids Res. **39**:D289–D294.
66. **Knox C, et al.** 2011. DrugBank 3.0: a comprehensive resource for "omics" research on drugs. Nucleic Acids Res. **39**:D1035–D1041.
67. **Zhu F, et al.** 2012. Therapeutic target database update 2012: a resource for facilitating target-oriented drug discovery. Nucleic Acids Res. **40**:D1128–D1136.